

**Supramolecular polymer additives to improve the
crystallization behavior and optical properties of
polybutylene terephthalate and polyamides**

Dissertation

for the award of the academic degree of

Doctor of Natural Science (Dr. rer. nat.)

from the Faculty of Biology, Chemistry, and Geoscience

University of Bayreuth

submitted by

Florian Richter

born in Lichtenfels

Bayreuth, 2012

The thesis was carried out between August 2008 and February 2012 at the *Chair Macromolecular Chemistry I*, University of Bayreuth.

The work was supervised by Prof. Dr. Hans-Werner Schmidt.

Date of submission:

Date of defense:

Dean: Prof. Dr. Beate Lohnert

Board of examiners:

Chairman: Prof. Dr.

First Examiner: Prof. Dr. Hans-Werner Schmidt

Second Examiner: Prof. Dr.

Third Examiner: Prof. Dr.

Acknowledgement

First of all I thank Prof. Dr. Hans-Werner Schmidt for supervising and giving me the opportunity to join his research group at the Chair Macromolecular Chemistry I. I would like to thank him for the highly interesting research topic, which allowed me to gain deep insights into fundamental as well as applied research. Furthermore I am thankful for the scientific independence that was granted and continuous support that was given. Beyond that I am really grateful for the creative discussions and the enjoyable atmosphere at his chair.

I gratefully acknowledge Prof. Dr. Volker Altstädt and Michaela Kersch (Polymer Engineering, University Bayreuth) for fruitful discussions and the collaboration within the project of the SFB 840. Likewise I would like to thank Dr. Rebekka von Benten for her support and input on the laser transparency of PBT and Dr. Claus Gabriel with respect to the work on bisureas in polyamides.

Special thanks go to Jutta Failner and Sandra Ganzleben (technicians at Macromolecular Chemistry I) and to Cathrin Müller (graduate student) for their great support in additive synthesis and help in polymer processing. Also I would like to thank Martina Heider (BIMF) for carrying out the scanning electron microscopy measurements. For numerous productive discussions on trisamide chemistry, properties and applications I would like to thank the following colleagues at Macromolecular Chemistry I: Roman Kress, Dr. Reiner Giesa, Dr. Frank Abraham, Dr. Andreas Bernet and Andreas Timme. Moreover I thank my direct laboratory colleagues Dr. Klaus Kreger, Andreas Haedler, Christian Probst, Johannes Heigl, Roland Walker and Christina Löffler for scientific discussions and the enjoyable and cheerful atmosphere. Likewise I want to thank Petra Weiss for her administrative support.

I gratefully acknowledge the funding of the research on benzenetrisamide based supramolecular polymer additives by the German Research Foundation within the SFB 840 (project B4). In addition I would like to acknowledge funding from BASF SE for the research on the bisurea based additives and the support with respect to the laser transparency measurements.

Finally my kind gratitude goes to my parents who always supported me during my studies and my doctoral thesis.

Table of Contents

1.	Introduction	1
1.1.	Nucleating agents	1
1.1.1.	Nucleating agents for isotactic polypropylene.....	4
1.1.2.	Supramolecular nucleating agents	5
1.2.	Visual appearance of transparent polymers.....	15
1.3.	Laser transparency of polymers.....	18
2.	Objectives and scope of this thesis	21
3.	Methods and procedures	24
3.1.	Compounding.....	25
3.2.	Injection molding	28
3.3.	Thermal analysis.....	29
3.4.	Polarized optical microscopy	31
3.5.	Additive screening method.....	31
3.6.	Optical properties	32
3.7.	Laser transparency measurements.....	32
3.8.	Wide angle X-ray diffraction	33
3.9.	Scanning electron microscopy	33
4.	Nucleation of polybutylene terephthalate.....	34
4.1.	Introduction	34
4.2.	Results and discussion	36
4.2.1.	Chemical structures and thermal properties of the investigated 1,3,5-benzenetrisamides.....	36
4.2.2.	Nucleation properties.....	40
4.2.3.	Nucleation efficiency	55
4.2.4.	Morphology of 1,3,5-benzenetrisamides	58
4.2.5.	Laser transparency.....	64
5.	Nucleation and clarification of polyamides.....	67
5.1.	Introduction	67
5.2.	1,3,5-Benzenetrisamides as nucleating agents for polyamides	71
5.3.	Bisamides as nucleating agents for polyamides	75
5.4.	Bisureas as nucleating agents and clarifiers for polyamides.....	77

5.4.1.	Synthesis and Characterization.....	79
5.4.2.	Thermal properties	86
5.4.3.	Nucleation and optical properties of PA6.....	93
5.4.4.	Nucleation efficiency and optical properties in comparison to talc.....	115
5.4.5.	Stability of nucleation effect.....	118
5.4.6.	Influence of the mold temperature on optical properties	121
5.4.7.	Influence of sample thickness on optical properties.....	123
5.4.8.	Laser transparency.....	125
5.4.9.	Morphology of injection molded samples.....	127
5.4.10.	Crystal modification of PA6.....	131
5.4.11.	Nucleation and optical properties of PA66 and PA12 homopolymers and polyamide copolymers.....	138
6.	Summary	147
7.	Zusammenfassung	150
8.	Experimental part	153
8.1.	Materials and equipment.....	153
8.2.	Polymers.....	155
8.3.	Synthesis and characterization	156
8.3.1.	General synthetic route to trans-1,4-cyclohexyl-bisurea derivatives	156
8.3.2.	General synthetic route to cis-1,4-cyclohexyl-bisurea derivatives.....	164
8.3.3.	General synthetic route to asymmetric substituted trans-1,4-cyclohexyl-bisurea derivatives.....	167
9.	Literature	170

1. Introduction

1.1. Nucleating agents

As a result of their wide range of applications combined with their low costs, polymeric materials have nowadays become indispensable in our daily life. The use of additives open up new application areas, is essential for polymer processing and ensures the specific property profile for the end consumer. The stability of polymers, their mechanical, electrical and optical properties can be effectively enhanced by the addition of specific additives. Examples for major classes of additives include antioxidants, UV-stabilizers, processing aids, flame retardants, optical brighteners, colorants, acid scavengers and nucleating agents. The latter play an important role in semi crystalline polymers.^[1]

Nucleating agents can increase the crystallization temperature and thus reduce cycle times during melt processing^[2, 3], affect the physical properties and can in some cases improve the optical properties (clarity and haze).^[3, 4, 5-9] In heterogeneous nucleation the amount of crystal nuclei increases drastically having a strong influence on the macroscopic properties of the polymer solid state.^[1, 10] As the growth rate of the spherulites remains constant an increase in nuclei density **decreases the crystal size**, which enhances the elongation at break and the impact resistance.^[1, 11] The influence of nucleation on the morphology of neat isotactic polypropylene (iPP) and iPP comprising 0.15 wt% of the sorbitol based additive bis(3,4-dimethylbenzylidene)sorbitol (DMDBS) is shown in Figure 1. The spherulite size is strongly reduced by the addition of DMDBS compared to neat iPP shown in the right micrograph of Figure 1.

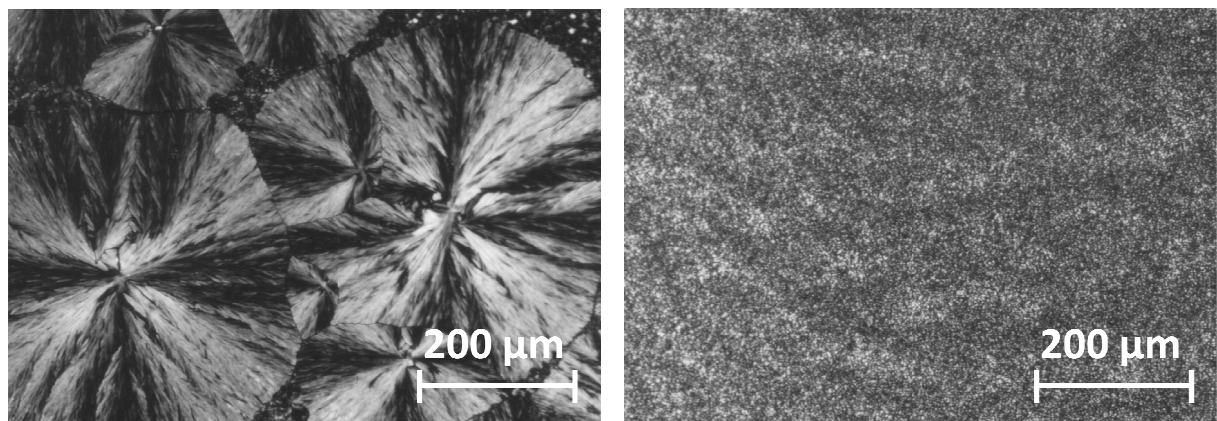


Figure 1. Polarized optical micrographs of isotactic polypropylene without additive (left) and comprising 0.15 wt% of DMDBS (right) after cooling from the melt to room temperature at 10 K/min.^[12]

Typically in low molar mass compounds crystallization upon cooling occurs rather fast, whereas the crystallization of polymeric materials requires a much larger undercooling and time. The required undercooling to initiate crystallization is shortened by the addition of a nucleating agent. Usually the undercooling is determined by non-isothermal differential scanning calorimetry (DSC).^[13] Here the **peak crystallization temperatures** of the exothermic polymer crystallization peak at a defined cooling rate is shifted to higher temperatures by the incorporation of a nucleating agent compared to the neat polymer. In Figure 2 the effect of different concentrations of a commercial nucleating agent on the peak crystallization temperatures ($T_{c,p}$) of iPP is shown. Neat iPP crystallizes at 110°C whereas upon the addition of a nucleating agent the crystallization temperature of iPP is distinctly increased. For lower additive concentrations the $T_{c,p}$ values decrease approaching the values for neat iPP. Here it is important to note, that with a few exceptions^[14, 4] the degree of crystallinity remains constant upon additivation.

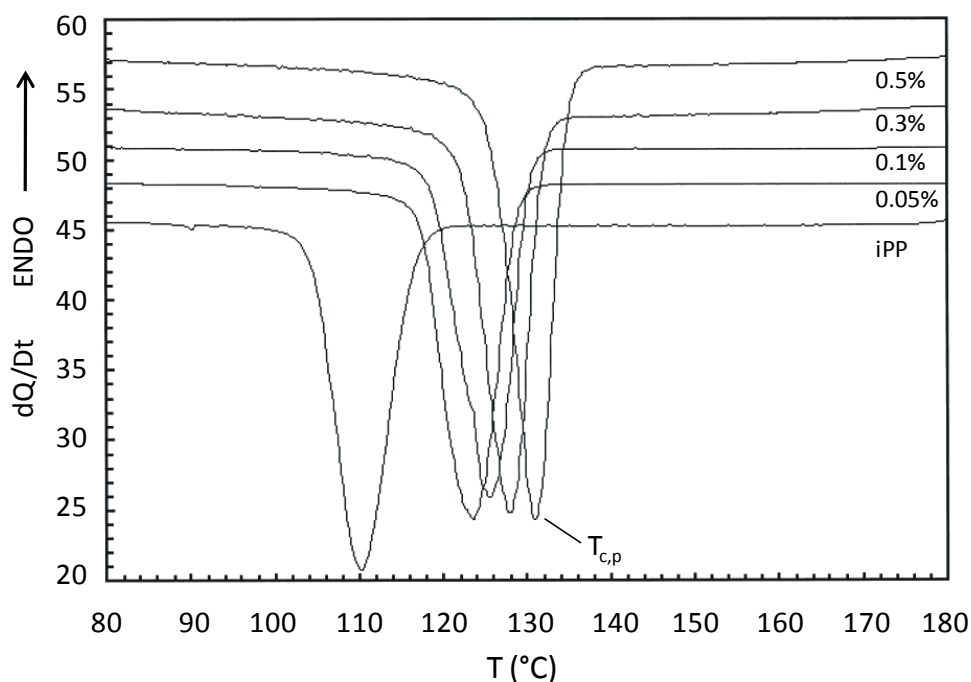


Figure 2. Differential scanning thermographs of neat iPP and iPP comprising different concentrations of the commercial nucleating agent NA 11 at a cooling rate of 10 K/min.^[15]

The **nucleation efficiency** of an additive can be calculated by comparing the increase in crystallization temperature induced by a nucleating agent to a sample nucleated by its own crystal fragments.^[16, 17] This involves the partial melting of the polymer. Upon cooling the remaining crystal fragments act as perfect nuclei for the crystallization of the polymer. The nucleation efficiency (NE) is calculated by:

$$NE (\%) = 100(\Delta T_{c,p} / \Delta T_{c,p \text{ max}}) = 100(T_{c,p \text{ nucl}} - T_{c,p \text{ neat}}) / (T_{c,p \text{ theo}} - T_{c,p \text{ neat}})$$

with $T_{c,p \text{ nucl}}$ being the crystallization temperature of the polymer induced by a nucleating agent, $T_{c,p \text{ neat}}$ being the crystallization temperature of the neat polymer and $T_{c,p \text{ theo}}$ being the maximum crystallization temperature obtained by self nucleation experiments. According to Lotz et. al. four thermal steps are necessary to determine the highest theoretical crystallization temperature of a polymer:^[16]

- The first step involves the complete *erasure of the thermal history* of the polymer. Therefore the polymer is heated well above the equilibrium melting temperature for 5 min to exclude the nucleation by unmolten self nuclei upon cooling.
- An *initial standard state* is created by cooling the “erased” melt at a defined cooling rate. This step is important to easily obtain reproducible starting material for the partial melting of the polymer.
- The next step involves the partial *melting of the polymer* at a temperature T_s between the maximum and the offset of the endothermic melting peak to create stable crystal fragments in the polymer melt.
- Subsequent cooling of the melt induces *self-nucleation* and increases the crystallization temperature of the polymer.

By repeating the four steps for different T_s values, the value for the maximum crystallization temperature ($T_{c,p \text{ theo}}$) is obtained at the peak minimum from the highest temperature exotherm.

1.1.1. Nucleating agents for isotactic polypropylene

Isotactic polypropylene combines slow crystal growth rates with a high degree of undercooling making it a perfect system to study controlled heterogeneous nucleation.^[18, 19] Due to its high commercial interest a vast number of substances have been investigated as potential nucleating agents for iPP. First research was conducted on inorganic salts such as alkaline earth metal oxides, titan dioxide, potassium and sodium phosphates or minerals such as talc, kaolin and silica.^[20–22] However these compounds exhibit the drawback of being insoluble in the polymer matrix and thus have to be finely distributed during melt processing.^[7, 23] In addition organic pigments such as γ -quinacridone, anthracinone or perylene^[21, 22, 24] and polymers like for example polyethylene terephthalate, polycyclopentene and polyethylene have been found to promote the crystallization of iPP.^[25] Apart from talcum, commercially applied nucleating agents comprise salts of organic compounds. Examples are organic salts with aluminium and alkali metals such as sodium benzoate, sodium 2,2'-methylene-bis-(4,6-di-tert-butylphenyl)phosphate (NA 11, Asahi-Denka Chemical Company)^[26] and disodium bicyclo[2.2.1]heptane-2,3-dicarboxylate, (Hyperform HPN 68, Milliken Chemical).^[27] The chemical structures of the latter two nucleating agents based on organic salts are shown in Figure 3.

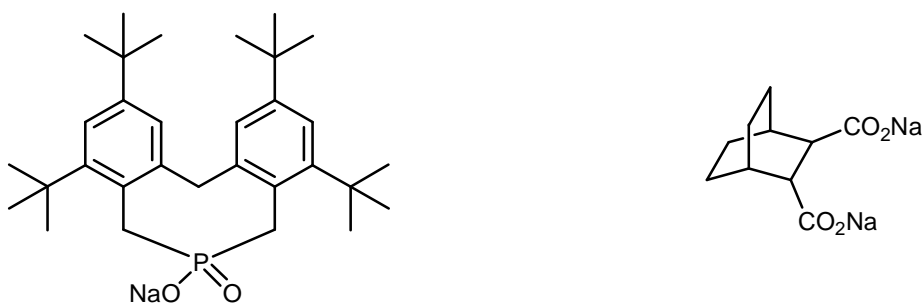


Figure 3. Chemical structures of important commercial nucleating agents for iPP; α -nucleating agent, NA 11, Asahi-Denka Chemical Company (left) and γ -nucleating agent, Hyperform HPN 68, Milliken Chemical (right).

1.1.2. Supramolecular nucleating agents

An efficient heterogeneous nucleating agent has to provide a preferably large epitaxial surface to the polymer and thus has to be finely distributed within the polymer matrix. Recently, organic nucleating agents that are soluble in the polymer melt eliminating the dispersion issues gained growing interest. Upon cooling from the melt these additives crystallize prior to the polymer into fine pronounced objects, usually in the nanometer scale. These additives are called supramolecular polymer additives. The formed supramolecular aggregates provide an extremely high density of nucleation sites due to their high surface-to-volume ratio thus maximizing the epitaxial surface.^[28] Concerning the tailored design of new supramolecular additives some general requirements have to be met:^[1, 6, 29]

- Additive should bear structural moieties to allow supramolecular aggregation by intermolecular forces.
- Additive should be soluble at the processing conditions achieving an optimal distribution in the polymer melt.
- Additive becomes insoluble above the crystallization temperature of the neat polymer upon cooling from the melt.
- Additive has an appropriate surface for the epitaxial crystallization of a particular polymer.

The nucleation ability of supramolecular polymer additives is strongly dependent on their self-assembly behavior, which is among others determined by the processing conditions, the individual chemical structure and concentration of the additive.^[6, 30]

A general scheme for the self-assembly concept of supramolecular nucleating agents is presented in Figure 4. The characteristic of supramolecular polymer additives is their solubility in the corresponding media polymer melt not necessary on a molecular level (Figure 4 A). Upon cooling the additive molecules self organize into so-called pre-aggregates due to intermolecular forces (B). Upon further cooling these aggregates assemble to form larger nano-objects (C), which are capable of providing an appropriate surface for the nucleation of the polymer (D).

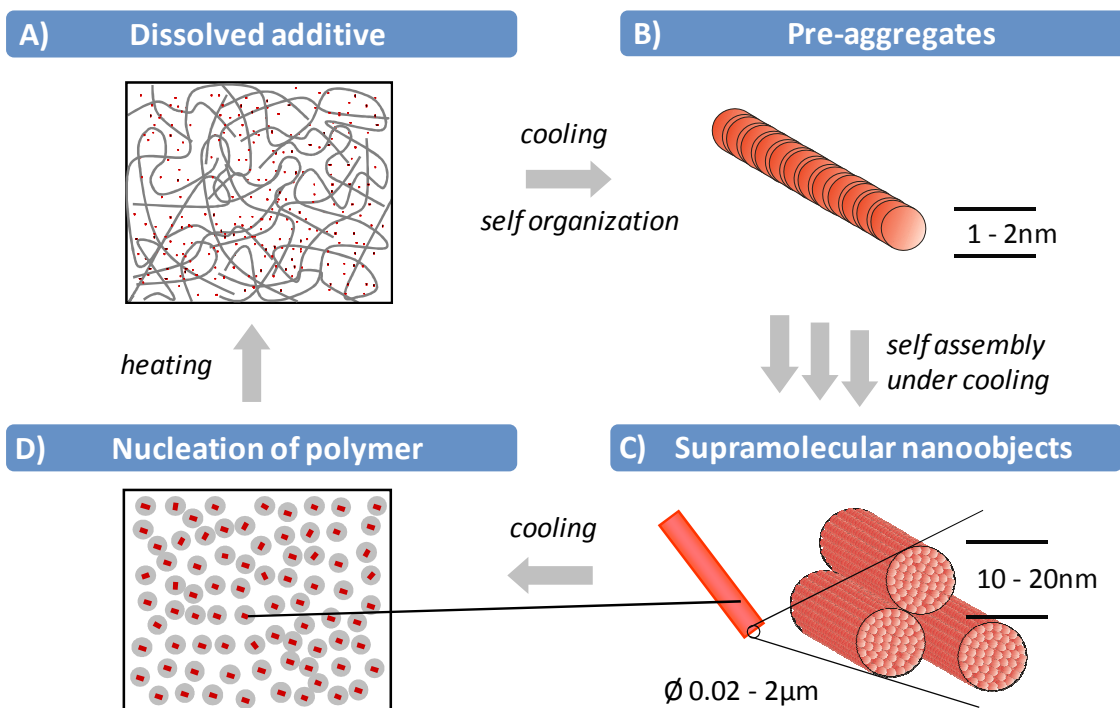


Figure 4. Thermoreversible self-assembly process of supramolecular nucleating agents.

The formation of such supramolecular structures is very sensitive towards the processing conditions, the additive concentration, and the type of polymer. Accordingly for the molecular design of new supramolecular additives several factors have to be taken into account.^[6, 31] For the one thing the strength of the intermolecular interactions governed by the symmetry of the molecule and the amount and type of hydrogen bonding units. On the other hand the choice of the peripheral substituents that influence the solubility in the particular polymer and fine tunes the additive morphology and crystallographic order. In the following developments in the field of supramolecular nucleating agents will be presented.

1.1.2.1. Sorbitol based supramolecular additives

Dibenzylidene sorbitol derivatives represent a commercially interesting and versatile class of supramolecular additives that was particularly developed with regard to the nucleation and clarification of isotactic polypropylene.^[4, 5, 32] The most important sorbitol-based nucleating agents for the α -phase of iPP are 1,3:2,4-dibenzylidenesorbitol (DBS, Millad 3905, Milliken Chemical and Irgaclear D, Ciba Speciality Chemicals), 1,3:2,4-bis(p-methylbenzylidene) sorbitol (MDBS, Millad 3940, Milliken Chemical and Irgaclear DM, Ciba Speciality Chemicals), bis(3,4-dimethylbenzylidene)sorbitol (DMDBS, Millad 3988, Milliken Chemical) and the latest generation clarifier 1,2,3-trideoxy-4,6:5,7-bis-O-[(4-propylphenyl)methylene]-nonitol

(TBPMN, Millad NX8000, Milliken Chemical). Owing to their excellent solubility in the polypropylene melt at different temperatures they bypass the dispersion issues associated with inorganic particles. Upon cooling a three-dimensional fibrillar nano network is formed, providing a high surface area for nucleation of the polymer.^[4, 33] Despite its commercial interest, sugar based (i.e. sorbitol or nonitol) nucleating agents have severe drawbacks, such as limited chemical and thermal resistance, the latter excluding their use as additives for other high melting semi crystalline polymers.^[34] Figure 5 presents the chemical structures of important commercial nucleating agents based on sorbitol or nonitol derivatives.

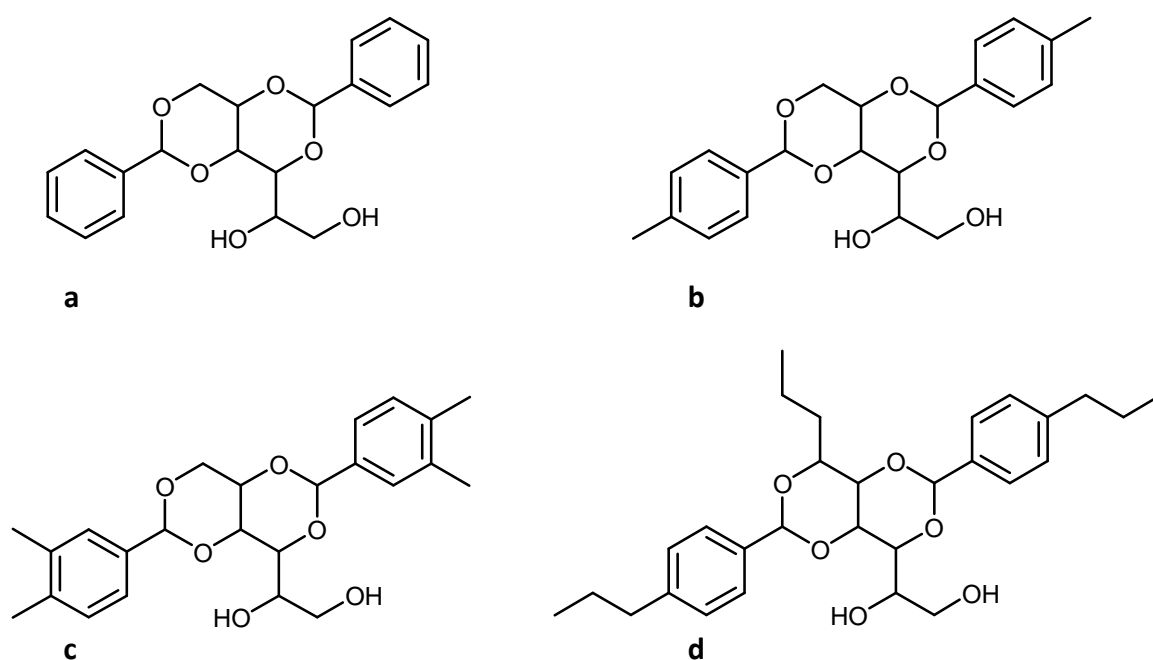


Figure 5. Chemical structures of important sorbitol based nucleating agents for iPP; α -nucleating agents 1,3:2,4-dibenzylidenesorbitol, DBS, Millad 3905 (a), 1,3:2,4-bis(p-methylbenzylidene)sorbitol, MDBS, Millad 3940 (b), bis(3,4-dimethylbenzylidene)sorbitol, DMDBS, Millad 3988 (c) and 1,2,3-trideoxy-4,6:5,7-bis-O-[(4-propylphenyl)methylene]-nonitol, TBPMN, NX8000, all from Miliken Chemical (d).

1.1.2.2. Trisamide based supramolecular additives

1,3,5-benzenetrisamide derivatives represent a recently developed class of nucleating agents that solve the aforementioned issues of sorbitol derivatives, showing remarkable nucleation properties in iPP^[6, 9, 35-37] and polyvinylidene fluoride (PVDF)^[38]. Besides their use as nucleating agents, these compounds can, depending on their structural details, be applied in electret materials based on iPP to improve their charge storage behavior^[39] or as processing aids to improve the flow properties of the polymer melt.^[40] Additionally selected 1,3,5-benzenetrisamide derivatives exhibit liquid crystalline behavior^[41] and can act as gelators for various organic solvents^[42] or water^[43]. The schematic structure of 1,3,5-benzenetrisamide derivatives is shown in Figure 6. These compounds consist of a central core with 1,3,5 substitution, moieties that are able to form intermolecular hydrogen bonds and nonpolar peripheral substituents, being responsible for the crystallographic order and the dissolution behavior in the polymer melt. Owing to their amide moieties these compounds can establish intermolecular forces via hydrogen bonds and ensure one-dimensional columnar self-assembly. By contrast to sorbitol acetal derivatives, 1,3,5-benzenetrisamides combine excellent chemical resistance with high thermal stability and thus can also be applied in high melting technical thermoplastics such as polyamides or polyesters.

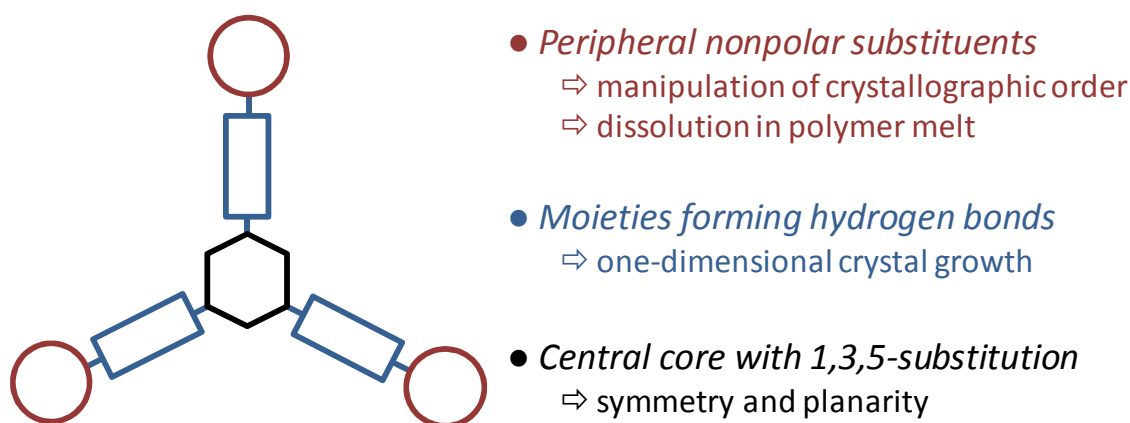


Figure 6. Schematic structure of 1,3,5 benzenetrisamide derivatives.

By this structural concept a new family of supramolecular nucleating agents for iPP and PVDF was developed over the past decade (Figure 7). So far the following cores were investigated: 1,3,5-benzene tricarboxylic acid **(a)**^[6, 12, 35, 37, 44], 5-amino isophthalic acid **(b)**^[6, 12, 44], 3,5-

diamino benzoic acid **(c)**^[6, 12, 44], 1,3,5-triamino benzene **(d)**^[6, 36, 44], cis,cis-1,3,5-cyclohexane tricarboxylic acid **(e)**^[45] and trisamides based on the melamine core **(f)**^[46]

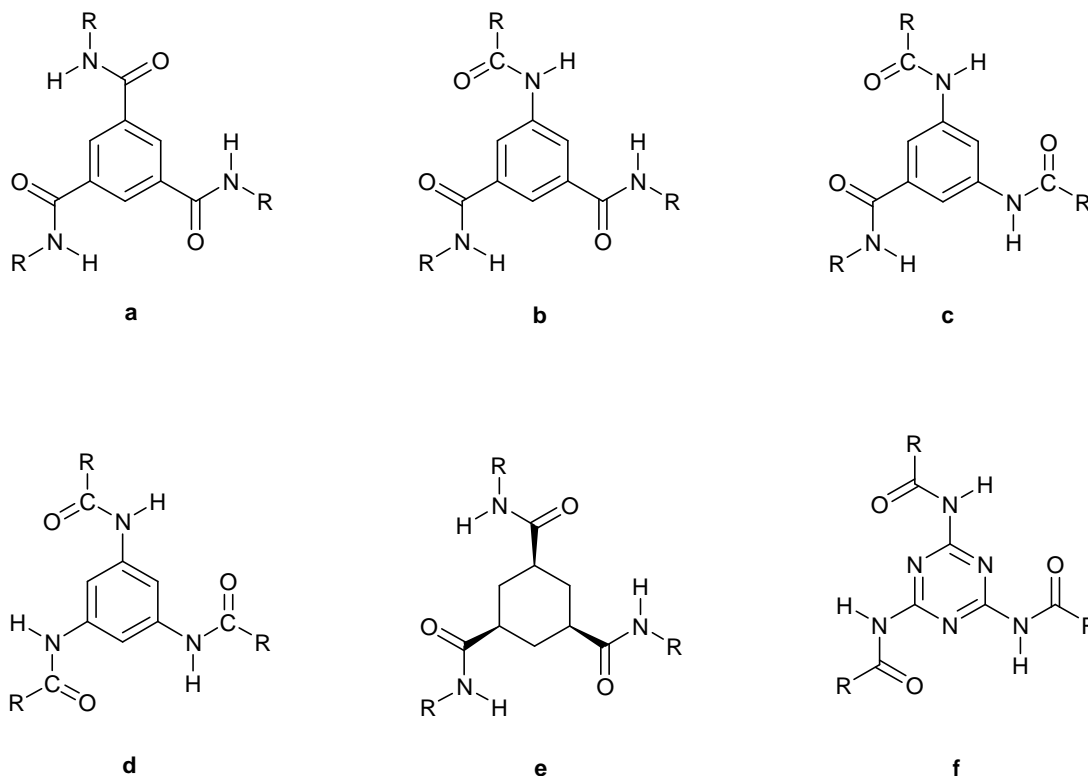


Figure 7. Basic structures of nucleating agents based on the motive of C3-symmetrical trisamides; 1,3,5-benzenetrisamide **(a)**, 5-amino isophthalic acid **(b)**, 3,5-diamino benzoic acid **(c)**, 1,3,5-triamino benzene **(d)**, cis,cis-1,3,5-cyclohexane tricarboxylic acid **(e)** and trisamides based on the melamine core **(f)**.

Out of the numerous compounds synthesized and investigated only selected derivatives are capable to induce the α or β crystal structure within iPP, or enhance the optical properties of iPP. Blomenhofer et al. reported on the use of substituted 1,3,5-benzenetrisamides as highly efficient nucleating and clarifying agents in iPP.^[6] The additives were, depending on their chemical structure, found to selectively induce the α -phase of iPP and enhance the optical properties even at very low concentrations. Based on these structural motifs the latest generation clarifying agent “IRGACLEAR[®] XT 386” was introduced by Ciba Holding SA in the year 2004.^[47] In 2009 Abraham et. al were the first to study the effect of 1,3,5-benzenetrisamides on the nucleation of PVDF as another semi-crystalline polymer.^[38] The polymer crystallization temperature and the dissolution and crystallization behavior of the additive in the PVDF melt was investigated as function of the concentration (Figure 8). As shown in Figure 8 the temperature composition diagrams are divided into three regions. In region I the additive is soluble in the polymer melt and does not crystallize upon cooling. In region II the additive is soluble at the processing temperature and crystallizes upon cooling

in fibrillar nano-objects that provide a surface for epitaxial crystallization of the polymer and induce nucleation. In region III the additive is not completely soluble under the applied temperature and nucleation both takes place on the surface of the crystallized supramolecular structures as well as on the surface of the not dissolved additive. It was found that certain 1,3,5-benzenetrisamides were soluble in the PVDF melt and self assembled prior to the polymer upon cooling promoting nucleation of PVDF.

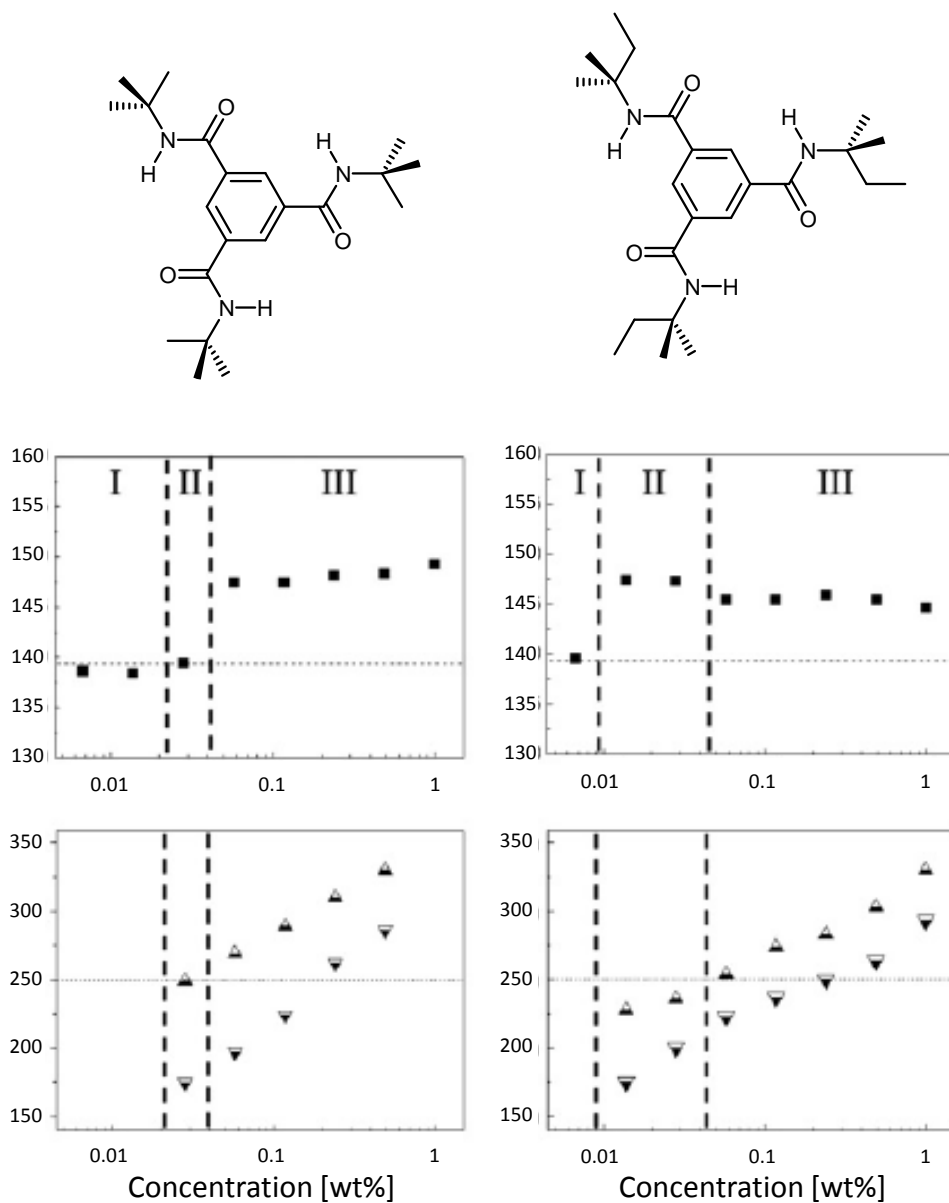


Figure 8. Crystallization temperature of PVDF (top graphs) and the dissolution temperature of the additive in the PVDF melt (triangles up) and crystallization temperature of the additive from the PVDF melt (triangles down) (bottom graphs) as function of the additive concentration. The dashed line in the top graphs represents the crystallization temperature of extruded neat PVDF $T_{c,p} = 139.3$ °C. The dotted line in the bottom graphs represents the maximum temperature (250 °C) during DSC measurements.

Lightfoot et al. were first to study the crystal structure of 1,3,5-benzenetrisamides. As example 1,3,5-tris(2,2-dimethylpropionylamino)benzene was investigated.^[48] The crystal structure reported was composed of infinite π -stacked rods supported by a triple helical network of hydrogen bonds (Figure 9 A). Due to the conjugation of the amide linkages with the aromatic core, the amide bonds are not arranged perpendicular to the benzene core, but tilted resulting in a staggered arrangement of the benzenetrisamide molecules.

The directional orientation of substituted 1,3,5-benzenetrisamides was discussed by Kristiansen et al. who examined the stacking based on the tert-butyl substituted derivative N,N',N'' -tris(tert-butyl)benzene 1,3,5-tricarboxamide (Figure 9 B).^[44, 49] It was found that the linear aggregates can possess two different helical hands, depending on the c-direction of the amide moieties (Figure 9 C). In addition, the repeat distance in the arrangement was given, which is in close proximity to the spacing of the two methyl groups in iPP, thus favoring epitaxial growth.

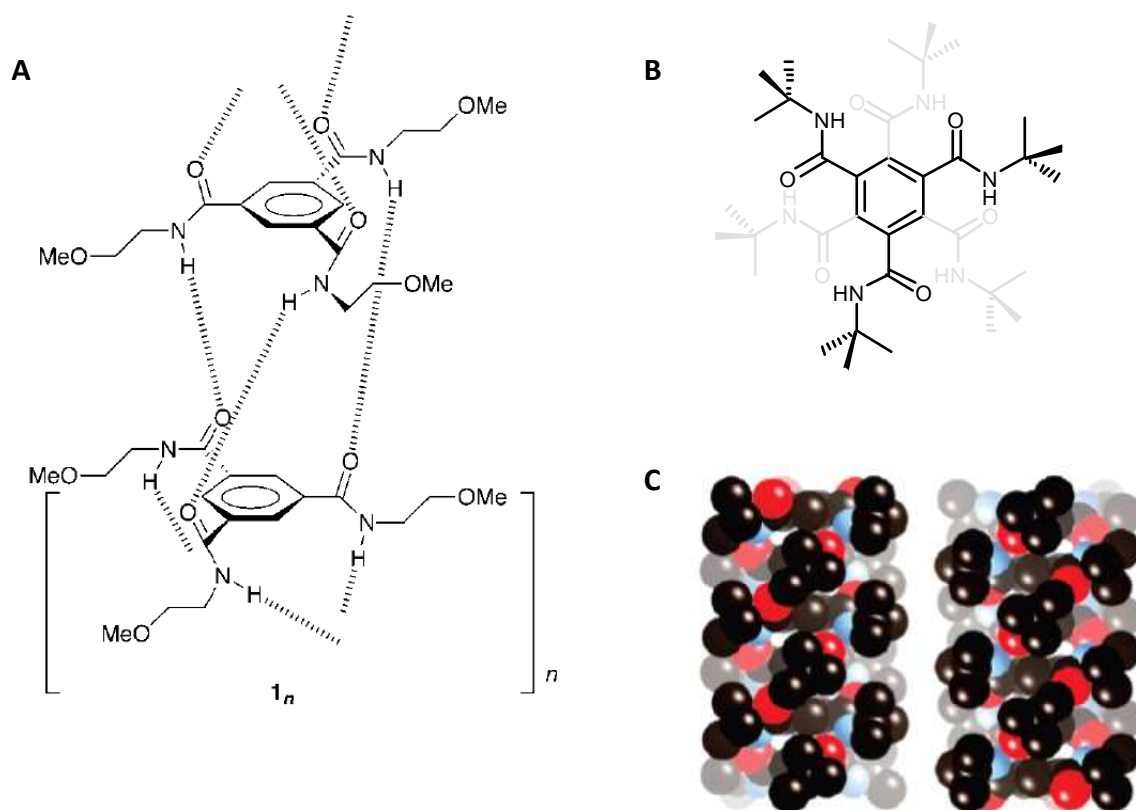


Figure 9. (A) Crystal structure of N,N',N'' -tris(2-methoxyethyl)benzene 1,3,5-tricarboxamide composed of infinite π -stacked rods supported by a triple helical network of hydrogen bonds^[48]; (B) staggered arrangement of N,N',N'' -tris(tert-butyl)benzene 1,3,5-tricarboxamide; (C) Possible configurations of N,N',N'' -tris(tert-butyl)benzene 1,3,5-tricarboxamide with the direction of the helical bonding patterns showing up (left) and down (right).^[49]

1.1.2.3. Bisamide based supramolecular polymer additives

Examples of supramolecular structures based on bisamides, bisureas and amide-ureas have been described in the literature.^[50–52] These molecules usually comprise a linear structure containing amid- and/or urea-groups. Here self assembly occurs generally into a sheet-like supramolecular structure. In most cases these compounds were investigated as organogelators^[53]. Their application in the field of supramolecular nucleating agents for iPP has also been reported.^[54, 55] Furthermore these compounds were investigated to improve the charge storage properties of iPP.^[55]

The schematic structure of linear molecules with two units capable for hydrogen bonding is shown in Figure 10. The molecules consist of a central unit being substituted symmetrically with hydrogen bonding units to promote sheet-like self assembly. By varying the peripheral substituents, the packing of the molecules and thus their dissolution properties in the polymer melt can be adjusted specifically to the polymer. Furthermore these substituents allow a fine tuning of crystallographic order and surface morphology of the additives. In addition the substituents control the distance between the individual layers.

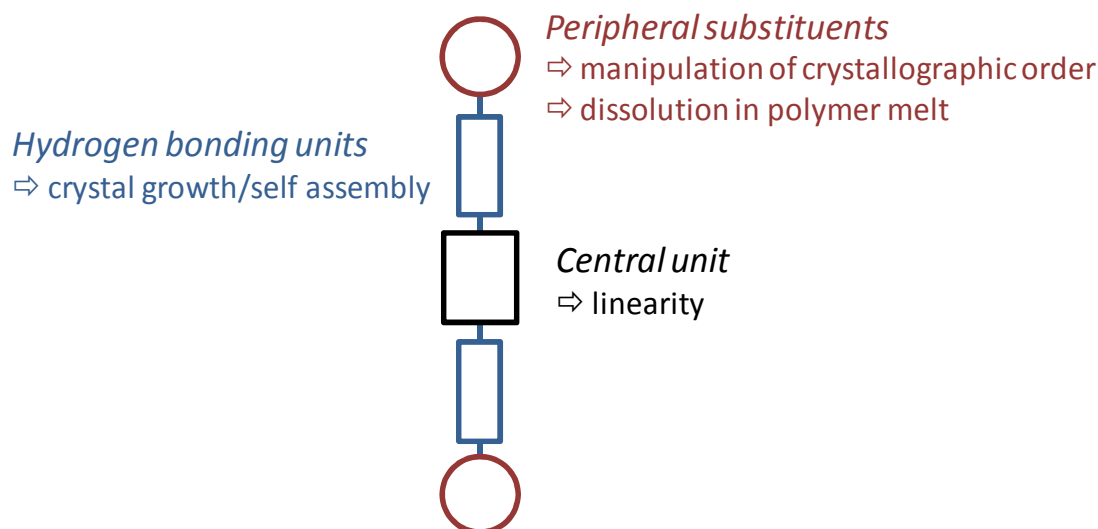


Figure 10. Schematic structure of linear additives consisting of a central unit, two hydrogen bonding units, and peripheral substituents.

Based on this schematic structure, Mohmeyer et al. studied the effect of low molecular-weight 1,4-phenylene-bisamides as nucleating agents for iPP.^[55] The solubility behavior of the additives, the nucleation efficiency and the ratio of the α - to the β -phase was

investigated with symmetrical and asymmetrical substituted bisamides, also as function of the concentration (Figure 11).

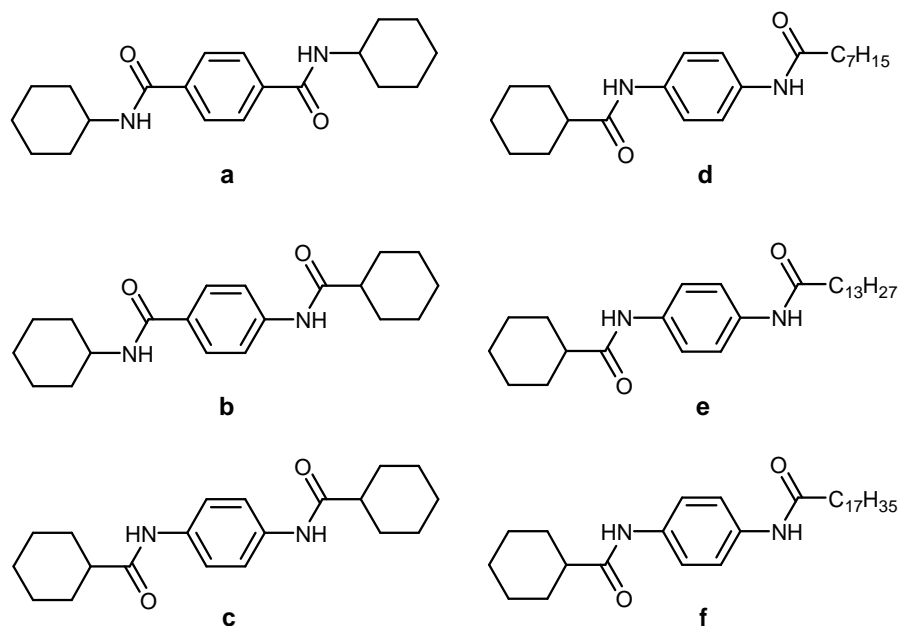


Figure 11. Chemical structures of selected additives: isomers of dicyclohexyl-substituted 1,4-phenylene bisamides **1-3** and cyclohexyl/n-alkyl-substituted 1,4-phenylene bisamides with a variation of the length of the alkyl chain **4-6**.^[55]

Above a critical concentration, the additives were found to induce the β -polymorph of iPP that exhibits enhanced mechanical properties.^[56] Nucleated iPP with the β -phase strongly scatters light. The haze is about 100 % for a 1.1 mm sample. The highest amount of β -phase was observed for the symmetrically substituted bisamides. However subtle changes in the chemical structures had significant influence on the nucleation efficiency. As seen from the wide angle X-ray patterns in Figure 12, the inversion of one amide group from compound **b** to **c** resulted in a distinct increase in β -content.

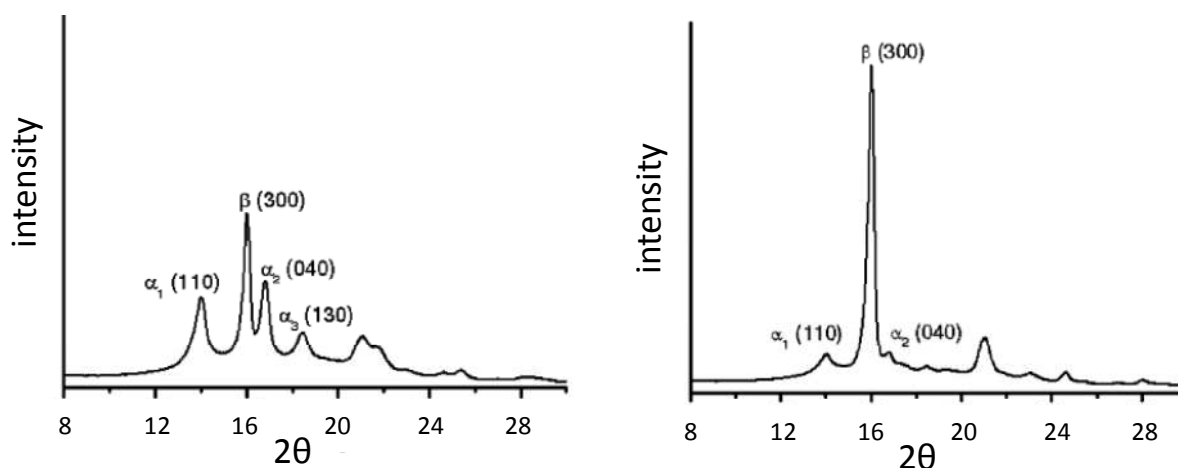


Figure 12. Wide-angle X-ray diffraction patterns of injection molded iPP plaques (1.1 mm thickness) comprising the dicyclohexyl-substituted 1,4-phenylene bisamides **b** (left) and **c** (right) at a concentration of 0.13 wt%.^[55]

Similar studies were conducted by Lu et al. who investigated the effect of eight *N,N'*-diphenyl bisamides on the formation of the β -crystalline form in iPP.^[57] Here *N,N'*-diphenyl succinamide and *N,N'*-diphenyl glutaramide were found to be the most efficient β -nucleators. New Japan Chemical investigated dicarboxylic acid derivatives for the use as β -nucleating agents in iPP. The *N,N*-dicyclohexyl-2,6-naphthalene dicarboxamide was commercialized under the trade name NJ STAR NU-100 (New Japan Chemical/Rika International, Figure 13)^[7]. The additive was found to be one of the most efficient β -nucleating agents.

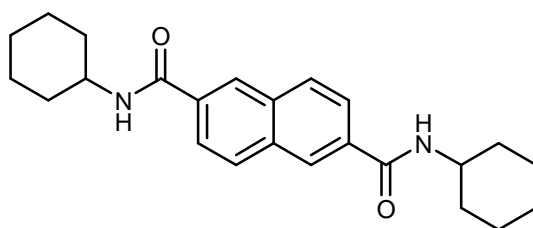


Figure 13. Chemical structure of the β -nucleating agent NJ STAR NU-100, New Japan Chemical/Rika International.

1.2. Visual appearance of transparent polymers

The appearance of a transparent object in the visible spectrum mainly derives from the transmitted light that is passing through a sample as schematically shown in Figure 14.^[58] As already mentioned above, the optical properties such as gloss, transmission, haze and clarity can be improved by the addition of the so-called “clarifying agents”. According to ASTM D 1003 the latter two parameters haze and clarity are defined through the diffuse component of the total transmitted light in the visible spectral range. The amount of light that is scattered in angles larger than 2.5° is referred to as “haze” and is a measure of the cloudiness of a sample, where high haze values cause a decrease in contrast.^[59] Plastics with a haze of 100 % strongly scatter light and appear optically opaque whereas plastics with a haze of 0 % appear “water clear”.

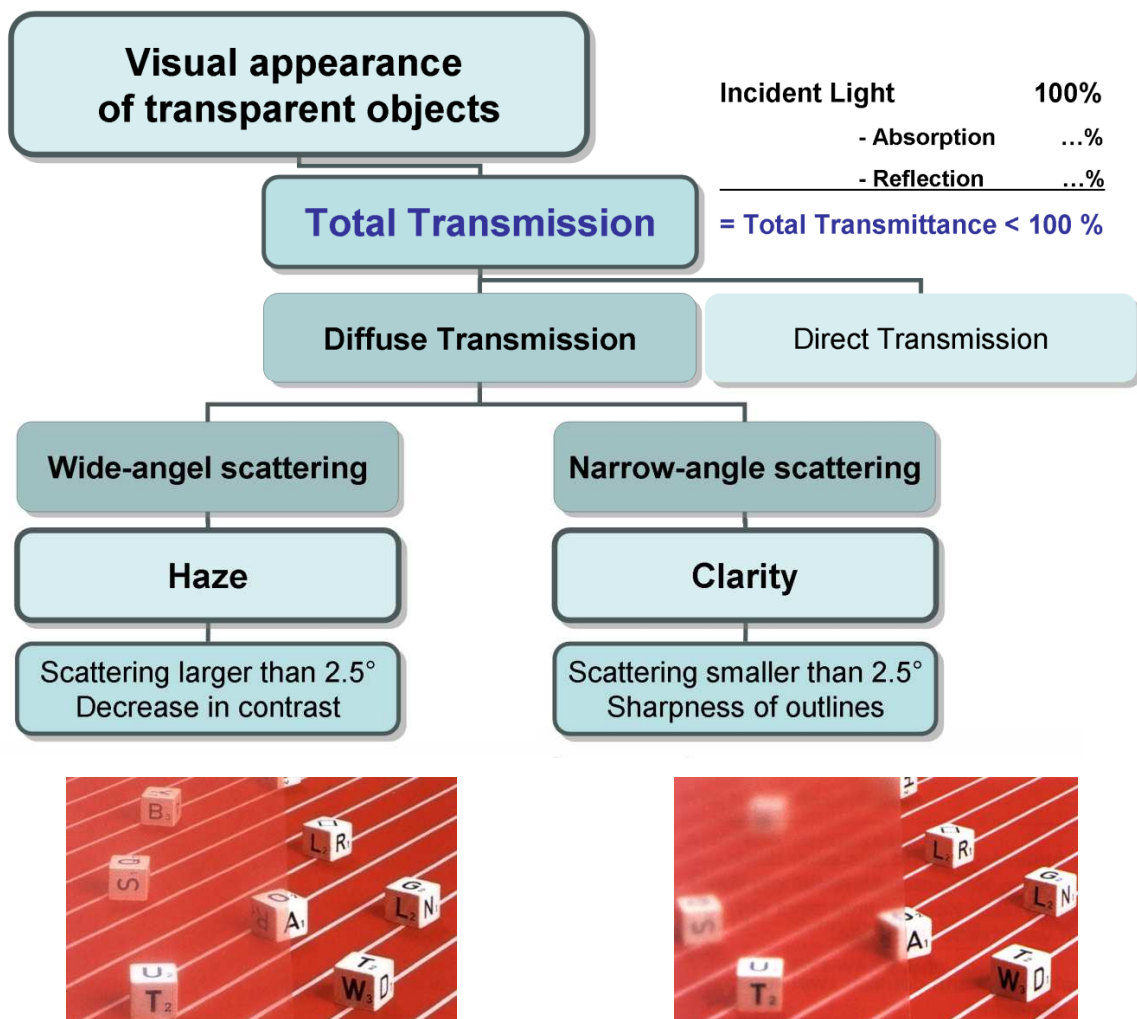


Figure 14. Parameters of the visual appearance of transparent objects (top) and influence of haze (bottom left) and clarity (bottom right) on an image.^[58]

Clarity is defined by the amount of light that is scattered in angles smaller than 2.5° , where low clarity values cause a loss in sharpness of an image. Clarity of 0 % would mean a total loss in sharpness, whereas sheet glass exhibits clarity values of 100 %. The influence of haze and clarity on the visual appearance of image is illustrated in Figure 14 (bottom). In semi-crystalline polymers differences in refractive indices of the crystalline and amorphous phase leads to scattering which reduces the optical transparency of a sample. Furthermore, scattering on anisotropic structures (i.e. spherulites) plays an important role in the optical appearance of a material. The total amount of scattered light can be decreased by reducing the spherulites size or by preventing spherulite structures to be formed.^[3, 7, 60, 61] However, a reduction in crystallite size alone by the addition of a nucleating agent cannot be regarded as only one reason for the improvements in optical properties.^[6, 9] In 2009 Bernland et al. studied the solid-state structures of nucleated and clarified iPP by means of small-angle light scattering (SALS). It was found that an efficient clarifying agent for iPP has to be capable of preventing the formation of spherulite structures but induce rod- or shish-kebab like crystalline entities.^[61]

In Figure 15 the optical appearance of injection molded iPP platelets are presented as function of the additive concentration for 1,3,5-tris(2,2-dimethylpropionylamino)benzene. The optical properties haze and clarity critically depend on the composition of the mixture. Usually in these kind of diagrams an “optimum” concentration for minimum haze can be observed, that coincides with the solubility limit of the additive at the processing conditions.^[6, 9] At the optimum concentration at around 200 – 300 ppm the best optical performance in haze and clarity is found (middle). At lower concentrations a modest reduction in haze can be observed presumably due to less available nucleation sites. Here the optical properties deteriorate approaching the values for neat iPP (left). However if the amount of additive exceeds the “optimum” concentration, scattering on undissolved additive particles increases the haze and reduces clarity (right).

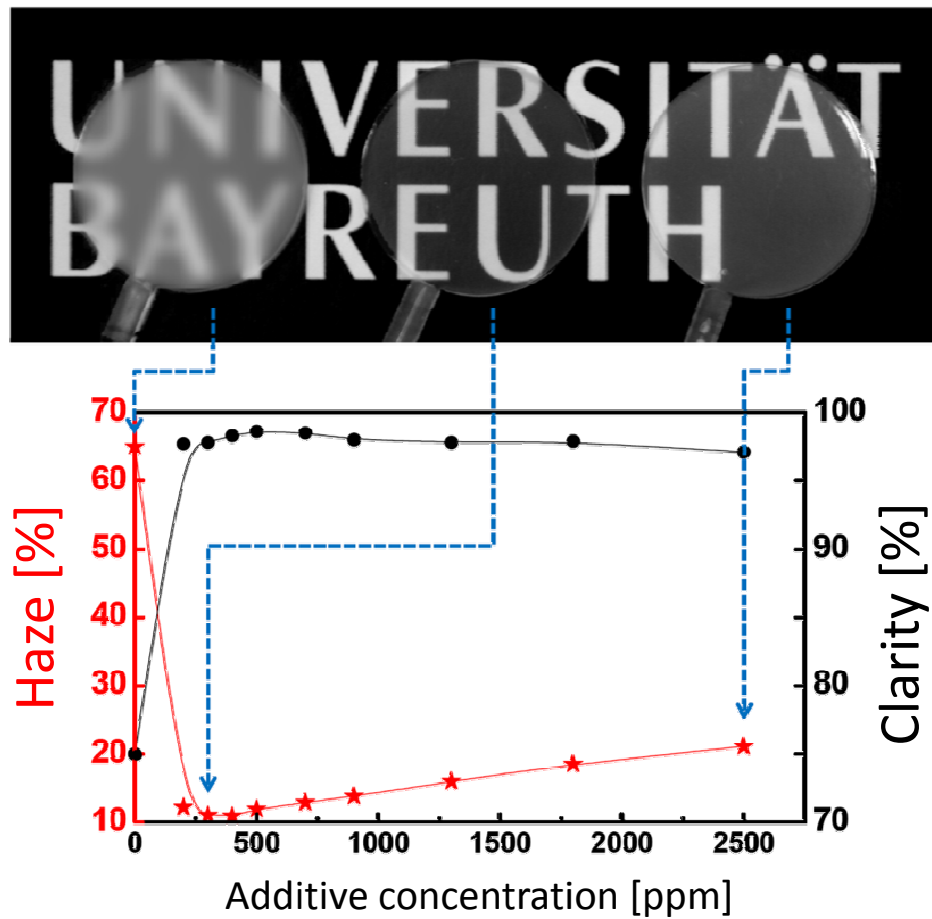


Figure 15. Optical properties (haze ★, and clarity ●) of iPP (thickness 1.1 mm) comprising different amounts of 1,3,5-tris(2,2-dimethylpropionylamino)benzene; left: neat iPP; middle: iPP with optimum additive concentration; right: iPP with 0.25 wt% of additive exceeding the optimum concentration.

1.3. Laser transparency of polymers

The steady progress in the development of polymeric products increases the demand for more complex and sophisticated components. The demands on the complex geometries, especially in small parts, can only be hardly satisfied by classical joining technologies, such as adhesive bonding or mechanical joining. Were these conventional procedures come up against their limits, welding processes can fulfill the requested requirements.^[62] Commonly the conjunction of two components by the influence of heat is referred to as welding. The required energy can either be supplied by convection, conduction, friction or radiation. In case of laser beam welding the energy is applied by radiation in the near infrared range (NIR) absorbed in the bulk material.^[63]

In this connection, two main techniques are of commercially applied. Firstly the butt welding process, where the junction occurs temporally separated to the plasticization of the polymer. Second, the more commonly applied transmission laser beam welding. In this process the two joining partners are brought in contact and held together with a moderate clamping force. The upper part has to be preferably transparent to the wave length of the irradiating laser, the lower part being absorbent. The absorption of the transmitted beam results in heating at the interfaces and melting of both parts due to thermal conduction (Figure 16).^[64]

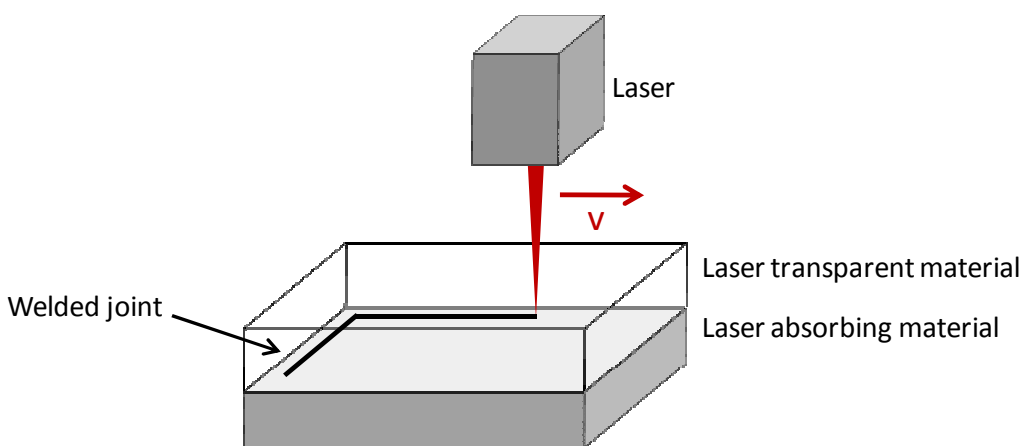


Figure 16. Schematic representation of the transmission laser beam welding process of a laser-transparent (top) and a laser-absorbing (bottom) polymer.^[63, 65]

In spite its procedural advantages and the ability to join different materials, transmission welding of polymers exhibits limitations given by the laser transparency of the base material that varies strongly for different polymers. Figure 17 shows the transmission spectra for

injection molded samples with a thickness of 2 mm of polyamide 66 (PA66), polyamide 6 (PA6) and polybutylene terephthalate (PBT).^[64] The transmittance for light in the near infrared range is considerably lower for PBT compared to the polyamides. The use of PBT as laser transparent material especially in thick parts is therefore limited.

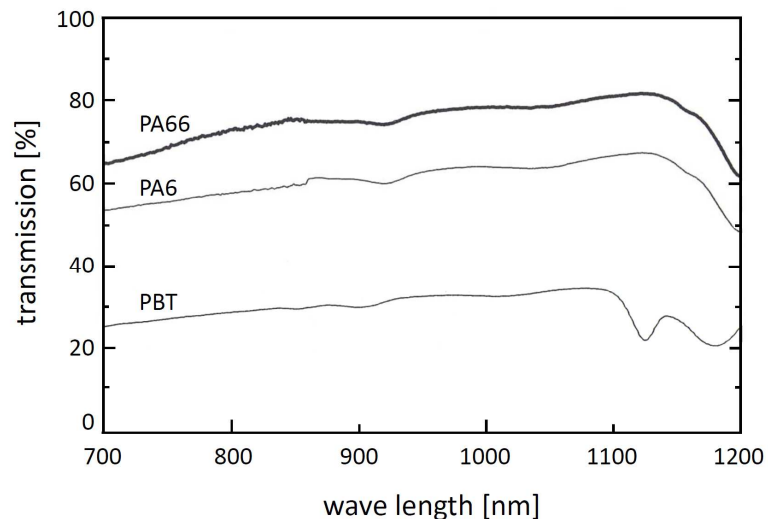


Figure 17. Transmission spectrum of PBT (Ultradur B4520), PA6 (Ultramid B3K) and PA66 (Ultramid A3k) measured on injection molded samples with a thickness of 2 mm.^[64]

The interactions of electromagnetic radiation with polymeric materials can be described by the three parameters “Transmission” (T), “Absorption” (A) and “Reflection” (R) (Figure 18). As light strikes the surface of a polymer a small amount of the incoming light is reflected. The transmitted portion of light gets partly absorbed by the polymer molecules or possible inhomogenities. The remaining fractions are either transmitted directly (specular transmission) or after being scattered on the polymer spherulites (diffuse transmission). These spherulites usually cause back-scattering associated with a loss in transmitted energy or a broadening of the laser beam.^[66] As demonstrated in Figure 17 these phenomena play a strong role in the laser transmittance of polybutylene terephthalate (PBT) limiting its usability for transmission welding techniques.^[64, 66]

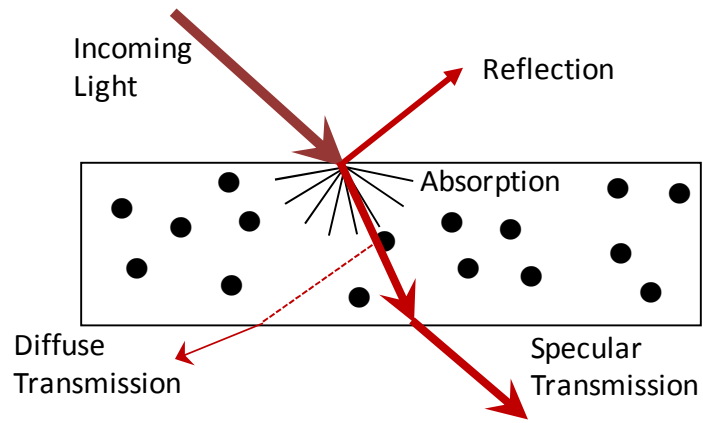


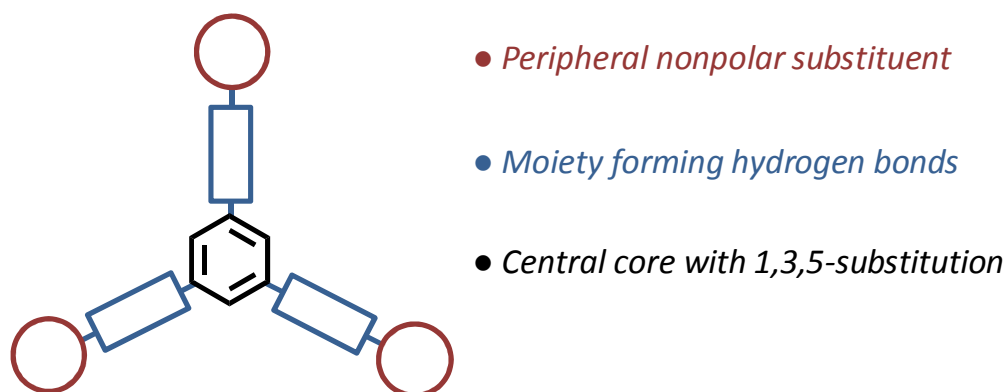
Figure 18. Interactions of electromagnetic radiation with polymers.

2. Objectives and scope of this thesis

The objectives and scope of this thesis is to explore for the first time supramolecular nucleating agents for the technical important semi-crystalline polymers polybutylene terephthalate and polyamides. The principle aim is to increase the polymer crystallization behavior, to control the polymer morphology and to improve the optical properties.

Supramolecular polymer additives based on 1,3,5-benzenetrisamides

The first part of this thesis is dedicated to the nucleation of PBT and semi-crystalline polyamides with supramolecular nucleating agents based on 1,3,5-benzenetrisamides. The schematic structure of the investigated trisamides is shown in the following.



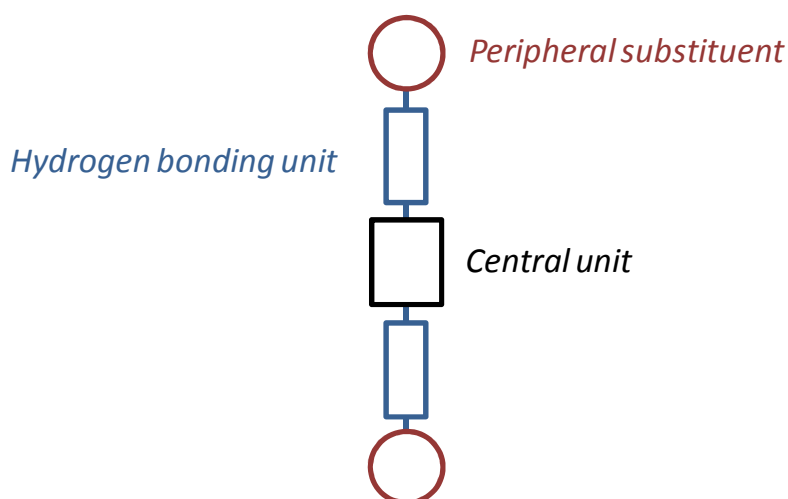
Given the current state of the art, a prediction of the nucleation properties based on the molecular structure of the additive is not possible. In order to achieve the aim to identify suitable nucleating agents and improve the crystallization behavior and optical properties of PBT and polyamides the following issues have to be addressed:

- As the individual chemical structure of the additives is crucial for the self-assembly/nucleation behavior, the core and peripheral substituents have to be systematically varied to establish *structure property relations*.
- A large number of *1,3,5-benzenetrisamide derivatives* have to be tested with respect to their nucleation potential in PBT and polyamides.
- In order to evaluate the nucleation ability of the large number of additives, a rapid and reliable *screening method* is of advantage. In this work a screening process developed at the Chair Macromolecular Chemistry I utilizing temperature dependent polarized light microscopy has to be adapted to PBT and polyamides.

- To explore the nucleation properties in more detail for selected compounds, the *additive dissolution and crystallization behavior* in the melt and the *crystallization temperature of the polymers* as function of the additive concentration have to be investigated. The additive dissolution and crystallization temperatures in the melt are determined by polarized optical microscopy and the polymer crystallization temperature is determined by DSC.
- Another aim of this thesis is to obtain more insight in the *morphology and size* of the *supramolecular nano-structures* which are formed upon cooling within the polymer melt. Experiments have to be developed to selectively remove the polymer matrix, in order to reveal the supramolecular structures. To visualize the supramolecular nano-structures scanning electron microscopy is applied.
- Finally the capability of 1,3,5-benzenetrisamides to increase the laser transparency of PBT is evaluated in collaboration with the BASF SE.

Supramolecular polymer additives based on bisureas

The aim of the second part is the synthesis and characterization of a new class of supramolecular nucleating agents, tailored to semi-crystalline polyamides. The objective is to improve the crystallization behavior and the optical properties. The linear molecules consist of a central unit being substituted symmetrically with two hydrogen bonding units to favor a sheet-like self-assembly.



To vary the self-assembly properties in the polyamide melt additives with amide and urea moieties are investigated. An additional structural variation of fundamental interest is the introduction of trans-1,4-cyclohexane and cis-1,4-cyclohexane as central unit to vary the linearity of the additives.

- Based on the schematic structure the *synthesis* of novel bisamide and bisurea derivatives has to be carried out.
- Standard characterization methods such as NMR-spectroscopy, mass spectroscopy, thermogravimetry and differential thermal analysis are applied for *characterization of the compounds*.
- To establish *structure property relations* concerning the *nucleation and clarification of semi-crystalline polyamides*, the peripheral substituents are systematically varied in length and degree of branching. The polymer crystallization temperature is determined by DSC. The optical properties are measured on injection molded samples with a standard ASTM procedure.
- To obtain a more detailed insight in the *solid state morphology* the *spherulite size* and the *crystal morphology* of the polyamides have to be investigated on injection molded specimens. As main methods, polarized optical microscopy and wide angle x-ray scattering are applied.
- The *effect of cooling rate and sample thickness on the optical properties* is studied in detail by varying mold temperature and mold thickness during the injection molding process.
- Finally the capability to increase the laser transmittance of PA6 is evaluated and compared to the commercially available nucleating agent talc.

3. Methods and procedures

The main focus of this work is on the investigation of the nucleation and clarification ability of supramolecular polymer additives in semi-crystalline polymers. The basic molecular characterization was carried out by standard techniques such as NMR- and mass spectroscopy, thermogravimetric analysis and differential thermal analysis. In order to evaluate the nucleating and clarifying potential of the supramolecular additives in various semi-crystalline polymers, efficient and reliable methods and procedures were adapted and optimized. Most of the procedures presented in the following have already been established by coworkers from the Chair Macromolecular Chemistry I for iPP^[12, 46, 31], and PVDF^[30] and were specifically adjusted to suit the specific conditions of PBT and polyamides. The advantage of these procedures resides in the possibility to obtain significant information with only small amounts of material. The polymer crystallization and melting temperatures were characterized by differential scanning calorimetry after microscale polymer processing. From injection molded platelets the optical characteristics (transmission, haze, clarity, laser transparency) were obtained and the polymer morphology was investigated. Optical and electron microscopy permit a deeper insight into the self-assembly of the supramolecular additives.

In the following the applied techniques and conditions will be briefly summarized particularly in view of the specifics of PBT and polyamides:

- Compounding
- Injection molding
- Thermal analysis
- Polarized optical microscopy
- Additive screening method
- Optical characterization
- Laser transparency measurements
- Wide angle X-ray diffraction
- Scanning electron microscopy

3.1. Compounding

To ensure a preferably homogenous distribution of the additives, the polymer granulate was first pulverized in a freezer mill. The obtained powder was blended with the additive powder. A glass bottle with the polymer powder comprising the initial additive concentration was clamped in a tumble mixer and blended for 24 h at 40 - 45 rpm (Figure 19).



Figure 19. Tumble mixer for the preparation of polymer powder/additive powder blends.

The so obtained powder mixtures were compounded in a co-rotating twin-screw compounder (DSM Xplore 15 mL) under nitrogen atmosphere (Figure 20).

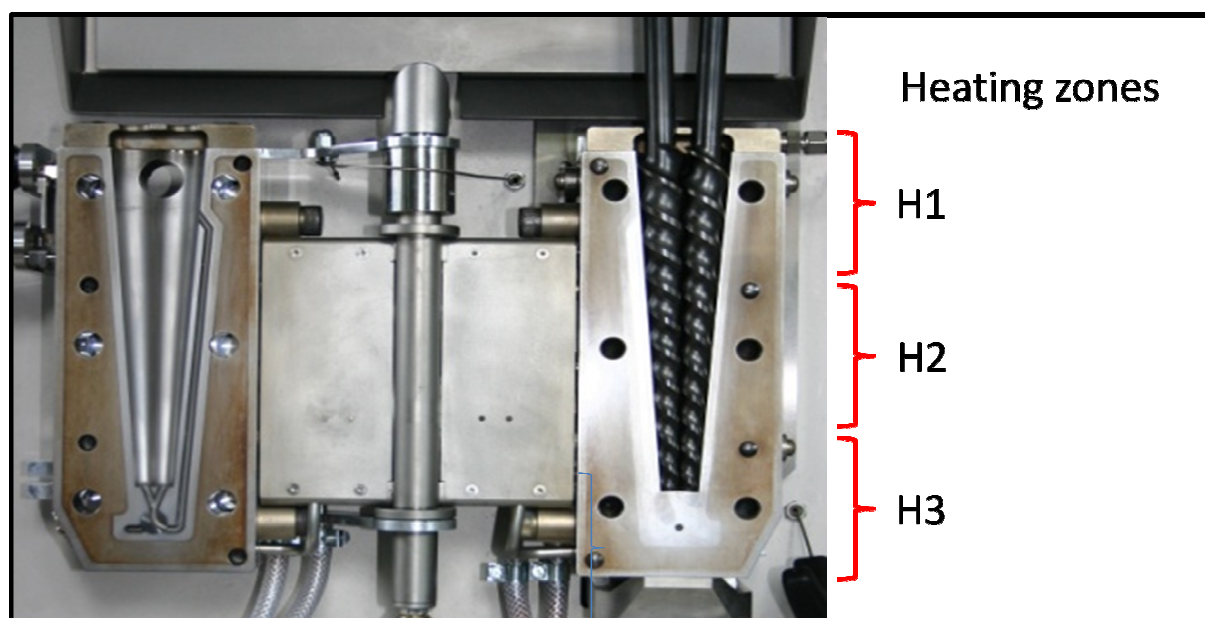


Figure 20: DSM Xplore 15 mL micro-compounder with the marked heating zones H1, H2, and H3.

The processing parameters had to be adjusted to the respective polymer and are presented in Table 1. In order to prevent the material from partial melting and adhesion to the feeding hopper, the temperature in the first heating zone (H1) was lower compared to the melting temperature of the polymer. After compounding the melt was discharged and collected either as polymer string or directly filled into the injection molding unit. Different additive concentrations were prepared by successively diluting the initial concentration with defined amounts of neat material. The neat polymer was treated in the same way to obtain blank control which was extruded. Within the thesis the values reported for the crystallization temperatures of PBT and polyamides are an average of the extruded blank control.

Table 1: Processing parameters for the investigated polymers and their measured melt temperatures.

Polymer	Temperature profile (H1-H2-H3) [°C]	Measured melt temperature [°C]	Compounding Time [min]	Rotational speed [rpm]
PBT	230-270-270	255	4	40
PA6	230-260-260	250	5	50
PA66	260-300-300	280	5	50
PA6/66	230-250-250	245	5	50
PA66/6	230-260-260	250	5	50
PA6/12	230-250-250	245	5	50
PA12	180-240-240	210	5	50

The preparation of a concentration series is exemplarily shown for PA6 in Table 2. For two cleaning runs and the first sample run a polymer/additive powder blend with a concentration of 1.5 wt% was used. For the following runs the initial additive concentration was diluted with a mixture of the polymer/additive powder blend and neat PA6 as shown in Table 2. After determining the dead volume of the compounder, the exact additive concentration in the extrudate could be calculated as follows:

With a dead volume of 5.4 g (for PA6) and an initial additive concentration of 1.5 wt%, the amount of additive within the dead volume is 0.081 g. In the first dilution run 6.8 g of the initial powder mixture with 1.5 wt% of additive and 1.8 g of neat PA6 are added. The amount of additive in 6.8 g of the initial powder mixture is 0.102 g. Thus the total amount of additive within the compounder in the first dilution runs is 0.183 g. The exact additive concentration can be calculated from the total amount of additive divided by the amount of polymer:

$$((0.081 \text{ g} + 0.102 \text{ g}) / (5.4 \text{ g} + 6.8 \text{ g} + 1.8 \text{ g})) * 100 \% = (0.183 \text{ g} / 14 \text{ g}) * 100 \% = 1.307 \%$$

Table 2. Initial weights and additive concentration for a concentration series in PA6.

Run	Comment	$m_{\text{powder mixture}}$ [g]	$m_{\text{neat polymer}}$ [g]	C_{Additive} [wt%]
1	cleaning	14.0	-	1.500
2	cleaning	8.6	-	1.500
3	1. sample	8.6	-	1.500
4	2. dilution	6.8	1.8	1.307
5	3. dilution	4.6	4.0	0.997
6	4. dilution	3.9	4.7	0.802
7	5. dilution	2.7	5.9	0.599
8	6. dilution	1.6	7.0	0.402
9	7. dilution	0.4	8.2	0.198
10	8. dilution	0.3	8.3	0.109
11	9. dilution	0.1	8.5	0.053
12	10. dilution	0.0	8.6	0.020

3.2. Injection molding

Platelets for optical characterization were prepared by injection molding the compounded blends using a micro-injection molding machine (DSM Xplore 12 mL) under nitrogen, yielding specimens with a diameter of 25 mm and different thicknesses (0.5 mm, 1 mm, 2 mm, 3 mm, 5 mm). The molds for the different thicknesses and the corresponding injection molded specimens are presented in Figure 21.

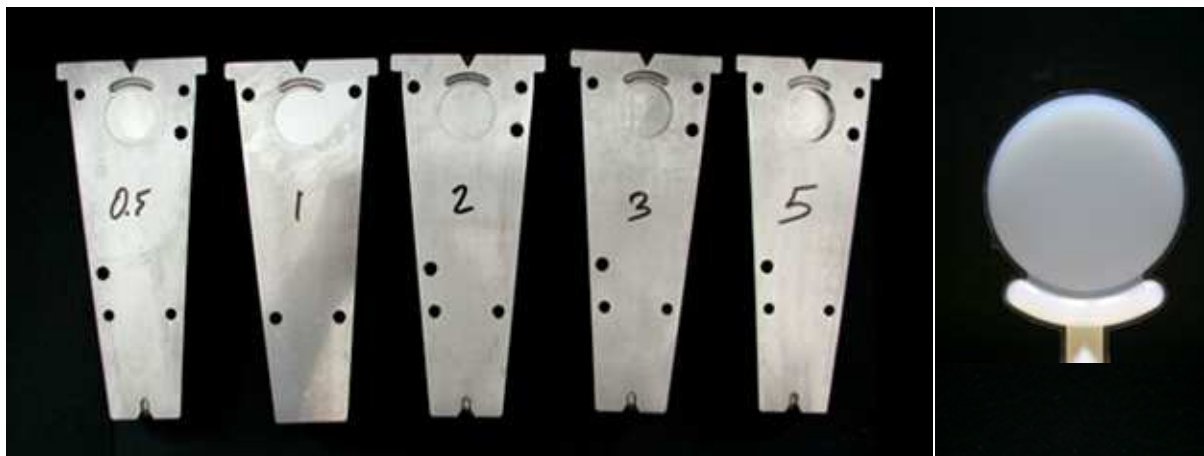


Figure 21. Injection molds with different thicknesses (0.5 mm, 1 mm, 2 mm, 3 mm and 5 mm)(left) and injection molded specimen with a diameter of 25 mm and a thickness of 1 mm (right).

The injection unit was directly filled with the polymer melt, discharged from the twin-screw compounder. The injection molding conditions for the different polymers are listed in Table 3.

Table 3: Injection molding conditions of the investigated polymers.

Polymer	Barrel temperature [°C]	Mold temperature [°C]	Injection pressure [bar]	Injection time [sec]	Holding time [sec]
PBT	250	80	6	10	10
PA6	250	100	6	10	10
PA66	260	100	6	10	10
PA6/66	240	60	8	10	10
PA66/6	250	60	8	10	10
PA6/12	240	60	6	10	10
PA12	230	60	6	10	10

3.3. Thermal analysis

DSC (differential scanning calorimetry) measurements for the determination of the polymer melting and crystallization temperatures were conducted on a Perkin Elmer Diamond DSC and a Mettler Toledo DSC/SDTA 821e under nitrogen at standard heating and cooling rates of 10 K/min. To erase the thermal history, samples were heated well above the equilibrium melting temperature for 5 min before each cooling run. For each sample two heating and cooling scans were performed. The starting and end temperatures of the polymers used in the frame of this work are presented in Table 4. Values for the polymer crystallization temperature ($T_{c,p}$) were determined at the exothermic peak minimum in the second cooling scan. Melting temperatures (T_m) were determined at the maximum of the endothermic peak of the second heating scan. Thermogravimetric analyses (TGA) of the additives were performed on a Mettler Toledo TGA/SDTA851e under nitrogen blanket at a heating rate of 10 K/min. Melting temperatures of the additives were determined by simultaneous differential thermal analysis (DTA).

Table 4. Starting and end temperatures for the DSC measurements of the investigated polymers. For each sample two heating and cooling scans were performed under nitrogen at 10 K/min. Samples were held at the end temperature for 5 min before each cooling run.

Polymer	Starting temperature [°C]	End temperature [°C]
PBT	50	260
PA6	30	250
PA66	30	280
PA6/66	30	240
PA66/6	30	250
PA6/12	30	240
PA12	30	230

To determine the nucleation efficiency of the additives, self-seeding experiments according to Lotz et al.^[9, 6] were adapted for PBT and polyamides at standard heating and cooling rates of 10 K/min. The nucleation efficiency scale is calculated by:

$$NE (\%) = 100(\Delta T_{c,p} / \Delta T_{c,p \max}) = 100(T_{c,p \text{ nucl}} - T_{c,p \text{ neat}}) / (T_{c,p \text{ theo}} - T_{c,p \text{ neat}}) \quad (1)$$

The crystallization temperature of neat melt-processed polymer ($T_{c,p \text{ neat}}$) was determined at the exothermic peak minimum upon cooling from the melt after the thermal history was erased above the equilibrium melting temperature. After partial melting for 5 min at a

temperature T_s between the maximum and the offset of the endothermic melting peak, the remaining crystal fragments act as perfect nuclei for the crystallization of the polymer and increase the crystallization temperature upon cooling. The value for the highest theoretical polymer crystallization temperature ($T_{c,p \text{ theo}}$) is obtained at the exothermic peak minimum upon cooling from T_s . The increased polymer crystallization temperature by the addition of a nucleating agent is described as $T_{c,p \text{ nucl}}$.

3.4. Polarized optical microscopy

Polarized light microscopy was performed using an optical microscope (Nikon, DIAPHOT 300) equipped with a hot stage (Mettler, FP82HT). Optical micrographs were recorded by a Nikon ACT-1 software using a digital camera (Nikon, DMX1200). The crystallization ($T_{c,a}$) and dissolution temperatures ($T_{d,a}$) of the additives were determined at the disappearance and reappearance of birefringent structures in compounded polymer samples at a heating and cooling rate of 5 K/min. The morphology of the injection molded platelets was determined on thin sections with a thickness of 10 μm . Sections were cut on a Leica RM 2255 rotary microtome parallel to the flow direction as indicated in Figure 22.

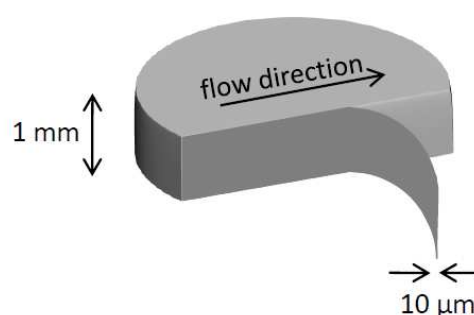


Figure 22. Thin section (10 μm thick) from injection molded specimen cut parallel to the flow direction.

3.5. Additive screening method

In order to evaluate the nucleation ability of a large number of compounds a rapid and reliable screening method is of great interest. In this work we utilized an additive screening process established by Abraham et. al.^[4] to identify suitable compounds for the use as nucleating agents. For this purpose a compression molded polymer film was placed on a microscopic slide. A small amount of additive was positioned in the middle of the film and the whole setup was covered and positioned in a hot stage under a polarized optical microscope. The samples were heated well above the melting temperature of the polymer for 5 min whereas the additives partly dissolve and diffuse into the surrounding polymer melt. The setup was slowly cooled at 10 K/min to monitor the crystallization processes of both the additives and the polymer. Optical micrographs of the screening process were recorded by a Nikon ACT-1 software using a digital camera (Nikon, DMX1200).

3.6. Optical properties

The optical properties Transmission, Haze, and Clarity were determined according to ASTM D-1003 on injection molded platelets using a Haze-Gard Plus instrument (BYK Gardner GmbH, Germany). All reported values are an arithmetic average of at least three measured specimens. The optical properties of the samples were measured 24 h after their preparation.

3.7. Laser transparency measurements

Laser transparency (LT) measurements were conducted at the BASF SE using a FOBA DP50 Nd:YAG laser marking system. The irradiating laser wave length was 1064 nm with a power output of 2 W. For determination of the laser transmittance the beam was divided into two discrete rays that were detected separately by a reference sensor (signal 1) and a measurement sensor (signal 2) after passing the polymer sample. All measurements were conducted in the middle of the injection molded specimens on at least three samples per additive and concentration. The LT values were calculated according to the following formula, as the ratio from signal 2 and signal 1:^[66]

$$Transmission [\%] = \frac{signal\ 2}{signal\ 1} * 100 \quad (2)$$

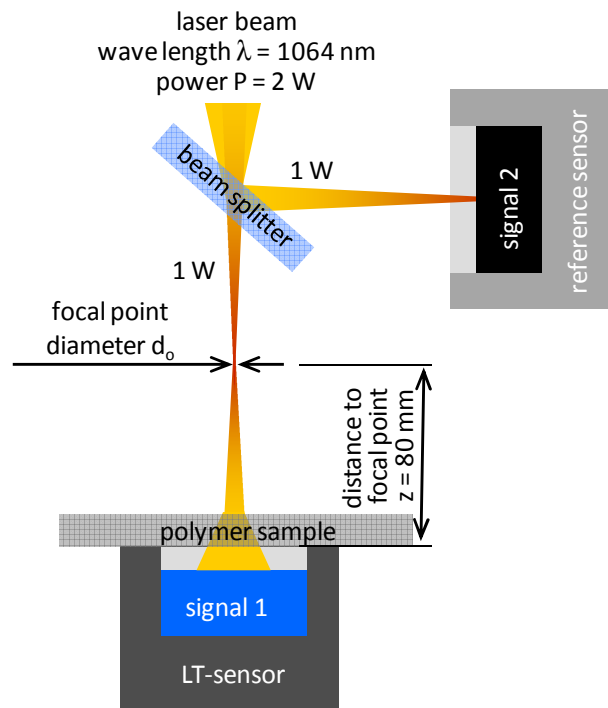


Figure 23. Schematic representation of the measurement set-up for determining the laser transparency of polymers. The laser passes through a beam splitter and the separate rays are detected by a reference sensor and a LT-sensor after penetrating the sample.

3.8. Wide angle X-ray diffraction

The crystal morphology of injection molded polyamide samples (thickness of 1.1 mm) was determined by wide angle X-ray diffraction. Measurements were performed with a Bruker D8 Advance X-ray diffractometer using CuK α radiation ($\lambda = 1.54\text{\AA}$). Data was recorded in the range of 5-45° (2θ) with a step size of 0.025° and a step time of 10 sec. The crystalline peak and the amorphous halo were separated according to a method described by Murthy et. al.^[67] using amorphous templates with Origin8G software. After profile analysis of the diffraction scans the content of α - and γ -crystal modification was calculated by

$$CI_{\alpha}(\%) = \frac{\sum A_{\alpha\text{-form}}}{\sum (A_{\alpha\text{-form}} + A_{\gamma\text{-form}}) + A_{\delta\text{-form}}} \quad (3)$$

$$CI_{\gamma}(\%) = \frac{\sum A_{\gamma\text{-form}}}{\sum (A_{\alpha\text{-form}} + A_{\gamma\text{-form}}) + A_{\delta\text{-form}}} \quad (4)$$

$$CI(\%) = CI_{\alpha} + CI_{\gamma} \quad (5)$$

with $A_{\alpha\text{-form}}$ and $A_{\gamma\text{-form}}$ being the area under the crystalline peaks of the α - and γ -modification, respectively and $A_{\delta\text{-form}}$ being the area under the amorphous halo.

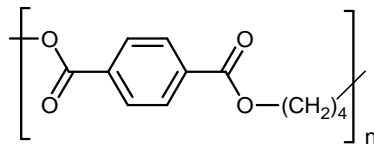
3.9. Scanning electron microscopy

Samples for the morphological studies were prepared by melting PBT comprising different concentrations of trisamide in DSC pans under nitrogen at 280°C. To ensure complete dissolution and distribution of the trisamides the samples were held for 5 min at this temperature. The samples were cooled to room temperature with defined linear cooling rates of 10, 40, 80, and 110 K/min. After removal of the solid samples from the DSC pans, the surface was hydrolyzed in a carefully stirred solution of 20 wt% sodium hydroxide in water for 2.5 h at 110 °C. Residual NaOH was removed by carefully stirring the specimens in water. The dried samples were sputtered with platinum (0.8 nm) by a Cressington Sputter Coater 208HR. Scanning electron micrographs were recorded using a Zeiss 1530 FESEM (SEM imaging). Histograms were obtained by measuring the lateral dimensions of at least 250 objects with Zeiss AxioVision LE software. The size distribution is a mean value from the lateral dimensions of all measured objects.

4. Nucleation of polybutylene terephthalate

4.1. Introduction

Polybutylene terephthalate (PBT) ranks among the semi-crystalline engineering thermoplastics and is distinguished by its good mechanical properties including high strength, rigidity, and toughness.^[68]



PBT

Its wide continuous service temperature and high chemical resistance combined with excellent electrical properties qualifies PBT for applications in electronics, automotive engineering and mechanical engineering.^[69] However PET dominates the market of fiber, film, and bottle molding applications by far, whereas PBT is mostly used for injection molding applications due to its high crystallization rate.^[68] For PBT, two crystal modifications can be formed, the triclinic α -phase and the also triclinic β -phase.^[70, 71] While the molecular packing of both modifications are very similar, differences in the fiber identity period were observed that can be attributed to conformational changes in the four-methylene group sequence (G^-G^-TTGG , α -phase and $TSTS^-T$, β -phase) as shown in Figure 24.^[71]

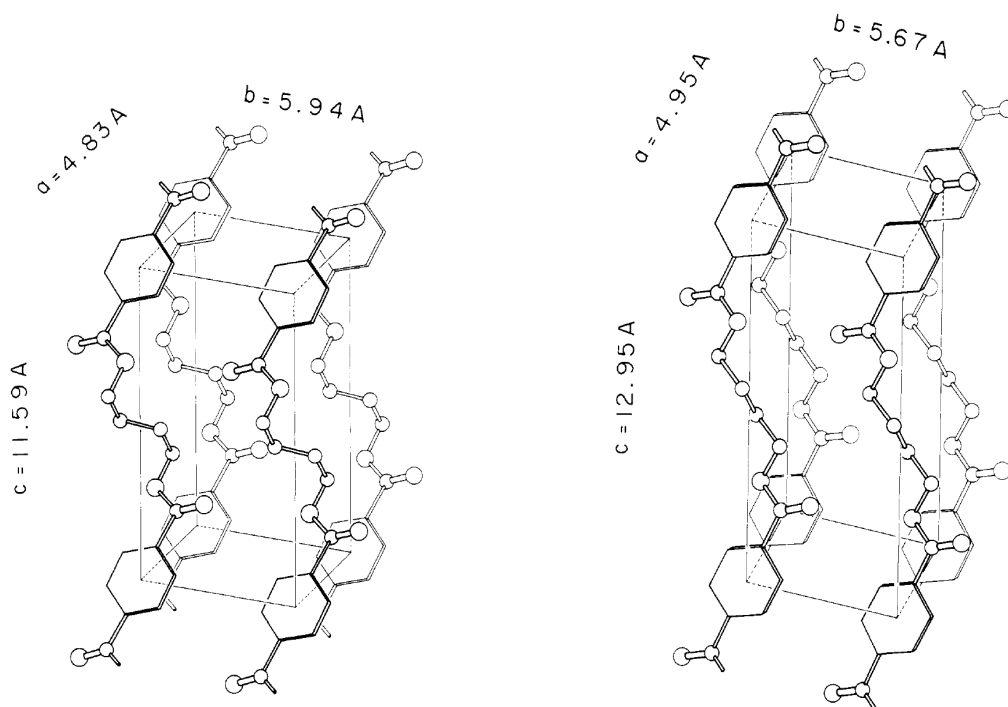


Figure 24. Triclinic unit cell and the corresponding cell dimensions of the α -form (left) and β -form (right) of PBT in the projection along the 010 plane as reported by Yokouchi.^[71]

The α -polymorph is commonly obtained by cooling from the melt whereas the β -phase occurs under strain and stress. By mechanical deformation and relaxation, the transition between the two polymorphs takes place reversibly.^[71]

Depending on the crystallization conditions different types of spherulites can be found (Figure 25).^[72, 73] A 45° maltese cross pattern is obtained upon fast cooling from the polymer melt. In contrast to this unusual type of spherulites, the 90° pattern (usual type) develops most likely from solution for example with a mixture of tetrafluoro acetic acid (TFA) in CCl₄. Isothermal crystallization at temperatures above 180°C or slowly cooled material yields a mixture of both types of spherulites.

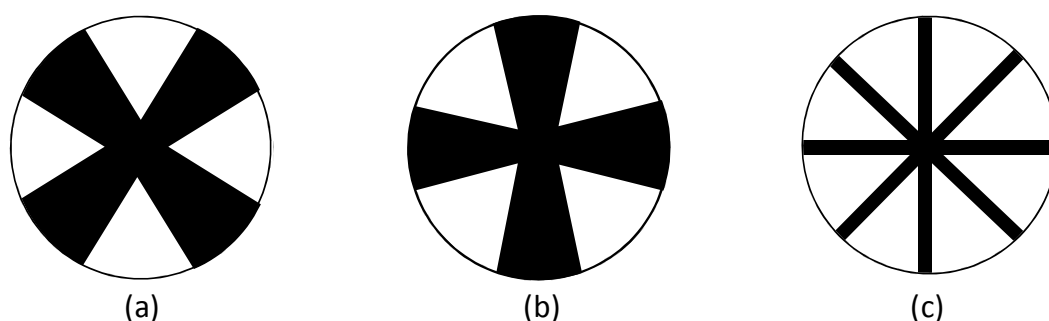


Figure 25. Types of spherulites formed at different crystallization conditions: (a) Unusual type from crystallization at low temperatures; (b) Usual type formed from solution; (c) Mixed type from isothermal crystallization above 180 °C.^[73]

In the literature only few examples for the application of nucleating agents in polybutylene terephthalate could be found. Heuseveldt et al.^[74] reported on a mixture consisting of PBT and a nucleating agent, e.g. talc, carbon black and certain inorganic phosphates. Zhang et al.^[75] studied the effect of elastomer-modified nano-SiO₂ [SiO₂-(E-MA-GMA)], a commercial nucleating agent (Bruggolen® P 250), and talc on the non-isothermal crystallization at different cooling rates. It was observed that all three compounds acted as heterogenous nuclei for the crystallization of PBT. The influence of pigments and mineral fillers on the non-isothermal crystallization behavior was investigated by Pillin et al.^[76] Generally a nucleating effect with 0.1% (w/w) pigment content was observed. Phthalocyanine Green showed the strongest influence on the crystallization of PBT. Soluble supramolecular nucleating agents for PBT have not been reported yet.

4.2. Results and discussion

In this chapter we report on 1,3,5 benzenetrisamides as supramolecular nucleating agents for PBT. To evaluate structurally different 1,3,5 benzenetrisamides as potential nucleating agents, a screening method described by Abraham et al.^[4] for PVDF was adapted for PBT. Promising compounds were investigated in a concentration range from 0.006 wt% (60 ppm) to 0.8 wt% (8000 ppm) and compared with respect to their dissolution and crystallization behavior of the additive in the PBT melt and the crystallization temperature of PBT. To obtain more insight in the morphology and size of the formed nano-objects, the PBT matrix was carefully hydrolyzed in alkaline solution. The supramolecular objects were examined and the average size was analyzed by scanning electron microscopy (SEM).

4.2.1. Chemical structures and thermal properties of the investigated 1,3,5-benzenetrisamides

43 derivatives of 1,3,5 benzenetrisamides were screened with respect to the nucleation of PBT. In order to find nucleating agents for PBT the central core and peripheral substituents were systematically varied. The additives are based on four different central cores, 1,3,5 benzenetricarboxylic acid, 1,3,5-triaminobenzene, 2,4,6-trimethyl-1,3,5-trisaminobenzene and 1,3,5-trisaminotoluene. The peripheral substituents were selected from branched aliphatic, cycloaliphatic and aromatic moieties. The chemical structures of the substituted 1,3,5-benzenetrisamides, their melting temperatures and temperatures at 10 % weight loss ($T_{-10 \text{ wt\%}}$) are summarized in Table 5.

The investigated compounds comprise for all four cores short aliphatic (**1-6**, **19-22**, **28-31**, **37**, **38**), cycloaliphatic (**7**, **8**, **23**, **24**, **32**, **39**) or aromatic moieties (**9-11**, **25**, **26**, **33-35**, **40-42**). Additionally 1,3,5-benzenetrisamide derivatives with adamantyl (**12**, **13**, **27**, **36**, **43**) or polar carboxylic acid- or amino-groups as well as their salts (**14-18**) have been investigated. Due to their stable amid linkage, all investigated compounds exhibit excellent thermal stability reflected by high melting and weight loss temperatures. The thermal behavior was obtained from TGA measurements, reported as the temperature at a weight loss of 10 % ($T_{-10 \text{ wt\%}}$). The additive melting temperatures were simultaneously determined by DTA. Owing to the formation of strong intermolecular hydrogen bonds, a large number of the investigated 1,3,5 benzenetrisamides sublime completely without melting, indicated also by a weight loss of 100 %. As example the compounds **1-5** with short branched aliphatic substituents exhibit no

melting endotherm and show direct sublimation with a 100 % weight loss. The $T_{-10 \text{ wt\%}}$ ranged between 350°C and 380°C. Increasing the number of C atoms resulted in derivatives which showed melting behavior and simultaneous evaporation from the liquid phase. Compounds **6-8** have melting temperatures between 315 and 419°C. The derivatives **9-11** with aromatic substituents showed similar melting behavior with melting temperatures between 377 and 403°C. It is interesting to note that all compounds with adamantyl substituents (**12, 13, 27, 36, 43**) sublimed directly and showed an even higher thermal stability ($T_{-10 \text{ wt\%}}$) above 440°C. A classification of the 1,3,5 benzenetrisamides **14-18** with polar substituents according to their thermal properties is difficult due to their high water uptake at ambient conditions. Therefore only the values for the melting temperatures are reported in Table 5.

Inversion of the amide linkages in the central core unit has an influence on the melting temperature of the 1,3,5 benzenetrisamides. For example the cyclohexyl derivative **23** showed a melting transition about 85°C lower compared to the corresponding compound **7** based on a 1,3,5 benzenetricarboxylic acid core. Comparing the iso-propyl substituted derivatives **1** and **19**, the compound based on 1,3,5-triaminobenzene (**19**) melted at 290°C whereas **1** sublimed. The aromatic derivatives **25** and **26** showed a melting endotherm at 278 and 304°C.

The 1,3,5-benzenetrisamides **29** and **30** with methyl substitution at the core in 2,4,6-position showed comparably low melting temperatures of 288°C and 280°C, whereas their corresponding derivatives **20** and **21** sublimed directly. Out of the nine derivatives based on 2,4,6-trimethyl-1,3,5-trisaminobenzene, seven sublimed without melting. It is interesting to note that the aromatic compounds **33-35** sublimed directly whereas the aromatic derivatives based on a 1,3,5-benzenetricarboxylic acid and a 1,3,5-triaminobenzene core exhibit a melting transition.

From the seven compounds based on the 1,3,5-trisaminotoluene core the derivatives **40-42** with aromatic substituent melted at temperatures between 332 and 353°C, whereas the remaining compounds sublimed and exhibit no melting endotherm.

Table 5. Chemical structures of the screened 1,3,5-benzenetrisamides, their melting temperatures T_m (DTA) and temperatures at 10 % weight loss $T_{-10 \text{ wt\%}}$ (TGA, N_2 atmosphere). The results on the nucleation ability of PBT were obtained by a screening method with polarized optical microscopy.

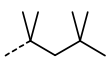
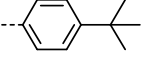
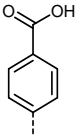
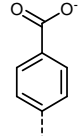
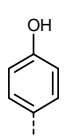
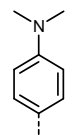
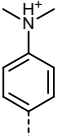
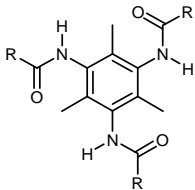
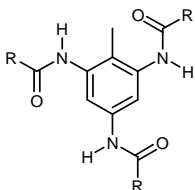
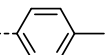
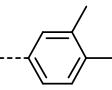
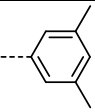
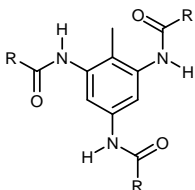
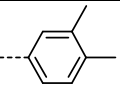
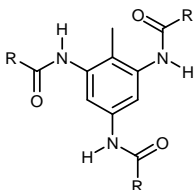
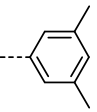
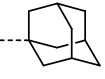
	Abbr.	1	2	3	4	5
	Substituent (R)					
	T_m [°C]	subl. ^{a)}	subl.	subl.	subl.	subl.
	$T_{-10 \text{ wt\%}}$ [°C]	353	380	358	350	362
	PBT nucleation	+ ^{b)}	+	+	+	+
Abbr.	6	7	8	9	10	
Substituent (R)						
T_m [°C]	315	371	419	377	403	
$T_{-10 \text{ wt\%}}$ [°C]	342	380	420	402	418	
PBT nucleation	- ^{c)}	+	+	+	+	
Abbr.	11	12	13			
Substituent (R)						
T_m [°C]	334	subl.	subl.			
$T_{-10 \text{ wt\%}}$ [°C]	393	448	455			
PBT nucleation	+	+	+			
Abbr.	14	15	16	17	18	
Substituent (R)						
T_m [°C]	329	394	395	374	390	
$T_{-10 \text{ wt\%}}$ [°C]	-	-	-	-	-	
PBT nucleation	n.d. ^{d)}	n.d.	n.d.	n.d.	n.d.	
Abbr.	19	20	21	22	23	
Substituent (R)						
T_m [°C]	290	subl.	subl.	subl.	286	
$T_{-10 \text{ wt\%}}$ [°C]	320	374	372	344	402	
PBT nucleation	-	+	+	+	+	
Abbr.	24	25	26	27		
Substituent (R)						
T_m [°C]	285	278	304	subl.		
$T_{-10 \text{ wt\%}}$ [°C]	378	424	424	474		
PBT nucleation	-	-	-	+		

Table 5 (continued). Chemical structures of the screened 1,3,5-benzenetrisamides, their melting temperatures T_m (DTA) and temperatures at 10 % weight loss $T_{-10 \text{ wt\%}}$ (TGA, N_2 atmosphere). The results on the nucleation ability of PBT were obtained by a screening method with polarized optical microscopy.

	Abbr.	28	29	30	31	32
	Substituent (R)					
	T_m [°C]	subl.	288	280	subl.	subl.
	$T_{-10 \text{ wt\%}}$ [°C]	418	368	335	430	438
	PBT nucleation	+	-	-	+	+
	Abbr.	33	34	35	36	
	Substituent (R)					
	T_m [°C]	subl.	subl.	subl.	subl.	
	$T_{-10 \text{ wt\%}}$ [°C]	418	439	453	440	
	PBT nucleation	+	-	+	+	
	Abbr.	37	38	39	40	41
	Substituent (R)					
	T_m [°C]	subl.	subl.	subl.	337	353
	$T_{-10 \text{ wt\%}}$ [°C]	365	362	405	408	423
	PBT nucleation	-	+	-	-	-
	Abbr.	42	43			
	Substituent (R)					
	T_m [°C]	332	subl.			
	$T_{-10 \text{ wt\%}}$ [°C]	421	450			
PBT nucleation	+	+				

a) subl.: sublimation; b) nucleation of PBT (+); c) no nucleation of PBT (-); d) n.d.: not determined due to the hygroscopicity of the compound;

4.2.2. Nucleation properties

In order to evaluate the nucleation ability of the large number of 1,3,5-benzenetrisamides investigated, a rapid and reliable screening method is of an advantage. In this work we adapted a screening process described by Abraham et al.^[38] utilizing temperature dependent polarized light microscopy. For this purpose a compression molded film of PBT was placed on a microscopic slide (Figure 26). A small amount of additive was positioned in the middle of the film and the whole setup was covered and placed in a hot stage under a polarized optical microscope. The samples were held at 280°C for 5 min whereas the 1,3,5-benzenetrisamide derivatives partly dissolve and diffuse into the surrounding polymer melt. The setup was then slowly cooled at 10 K/min to monitor the self-assembly process of the dissolved additive molecules into supramolecular nano-objects. The crystallization processes of both the additives and the polymer were recorded by a digital camera attached to the polarized optical microscope.

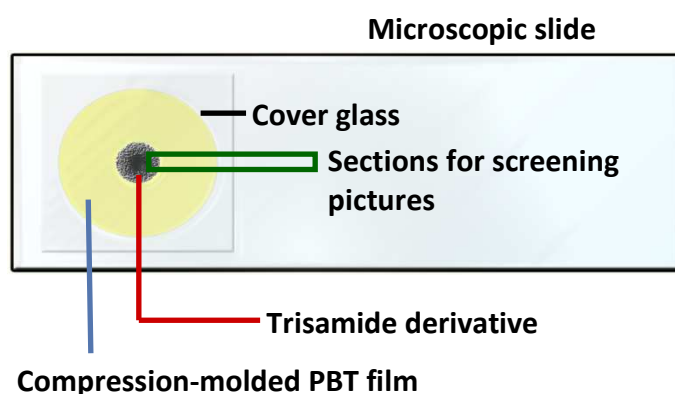


Figure 26. Setup for the screening process as established by Abraham et. al.^[38]

Figure 27 compares as an example for compound **6** and **21** micrographs recorded between crossed polarizers at different temperatures. Both micrographs at 280°C show on the right the birefringent undissolved additive in the PBT melt. The black region corresponds to the optical isotropic melt of PBT. Upon cooling to 230°C, both trisamides crystallize into fine needles. This starts from the region of the non dissolved additive. In case of **21** at 200°C the nucleation of PBT is induced on the surface of the additive needles and adjacent in the PBT melt. This indicates that very fine supramolecular structures of **21** are present, which are not visible by optical light microscopy, but capable to nucleate PBT. At lower temperature of 195°C, the PBT crystallization in the region of the additive is completed and first crystallites of PBT are formed in the remaining additive free melt. Derivative **6** is a trisamide which does

not nucleate PBT. At 230°C the trisamide crystallizes in form of fine needles, which continue to grow upon lowering the temperature (200°C). The needles do not act as nucleation sites for the crystallization of PBT. At 195°C the PBT nucleation occurs simultaneously in the additive free PBT melt and in between the needles.

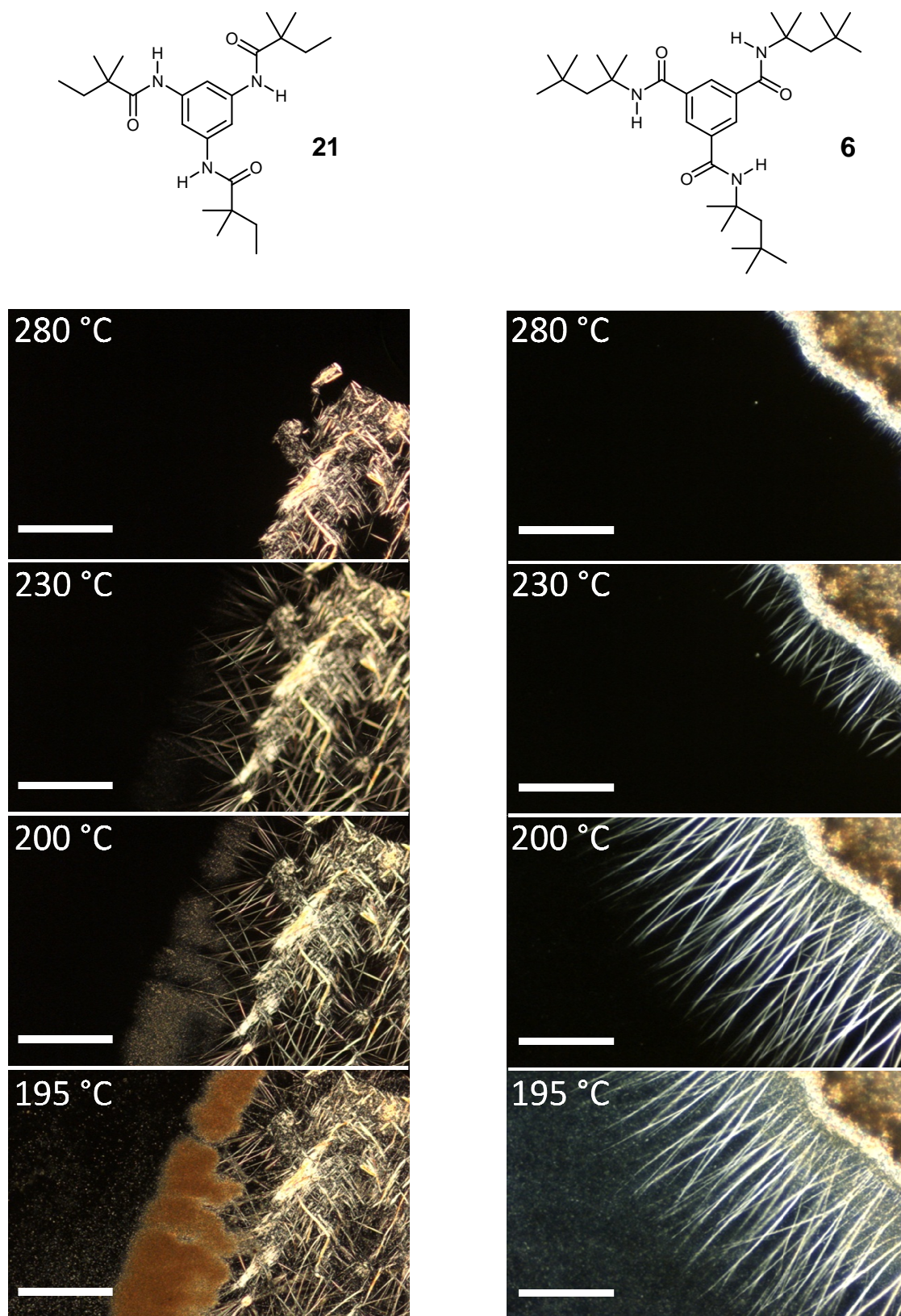


Figure 27. Optical micrographs from polarized light microscopy of the 1,3,5-benzenetrisamides **21** and **6** (scale bar 200 μm). Samples were heated, kept at 280°C for 5 minutes, cooled with a rate of 10 K/min and observed at different temperatures. The additive is visible in the isotropic PBT melt (black) on the right. The non-dissolved additive diffuses into the PBT melt and crystallizes upon cooling into fine needles. In the case of **21** nucleation of PBT is induced on the surface of the additive, whereas **6** is not capable to nucleate.

The screening results for the 1,3,5-benzenetrisamides **1-43** are also presented in Table 5. Nucleation of PBT is denoted with (+) and no visible nucleation with (-). With exception of compound **6** all compounds based on the 1,3,5-benzenetricarboxylic acid core were found to be capable of nucleating PBT. Regarding the derivatives **19** to **27** based on the 1,3,5-triaminobenzene core, five out of nine compounds showed nucleation of PBT. Usually derivatives based on 1,3,5-triaminobenzene are better soluble than their corresponding analogues from the first additive series.^[77] Therefore **19** and the compounds **24-26** were too good soluble and showed no nucleation effect in PBT. From the investigated derivatives based on the 2,4,6-trimethyl-1,3,5-trisaminobenzene core six out of nine nucleate PBT. It is interesting to note that the derivatives **29** and **30** based on 2,4,6-trimethyl-1,3,5-trisaminobenzene do not nucleate, whereas trisamides **2** and **3** based on the 1,3,5-benzenetricarboxylic acid core and **20** and **21** based on the 1,3,5-triaminobenzene core bearing the same substituent do nucleate PBT. Due to their asymmetric structure the mono-substituted 1,3,5-benzenetrisamides **37-43** can only establish weaker hydrogen bonds and should be more soluble in the polymer melt. This reflects in lower nucleation ability as only three out of seven screened derivatives were capable to nucleate PBT (**38, 42, 43**). Beside the compounds with nonpolar aliphatic or aromatic moieties, further 1,3,5-benzenetrisamides derivatives bearing polar carboxylic acid- or amino-groups as well as their salts have been investigated. As the 1,3,5-benzenetrisamides with nonpolar substituents have been tailored with respect to the nucleation of the also nonpolar iPP, the aim was to offer an appropriate surface to the more polar PBT for the epitaxial crystallization on the surface of the additive. The selected compounds **14-18** are shown in Table 5. Compounds **14, 16,** and **17** bearing polar carboxylic acid- or amino substituents exhibited excellent solubility in the polymer melt and hence were not capable to nucleate PBT. Sodium or chloride salts of these derivatives were nearly insoluble but also showed no nucleation effect in PBT.

The nucleation efficiency depends also on the additive concentration. Therefore selected 1,3,5-benzenetrisamides were investigated in a concentration range from 0.006 wt% (60 ppm) to 0.8 wt% (8000 ppm). The different concentrations were prepared by subsequently diluting the initial concentration of 0.8 wt% in the melt with neat PBT. By this dilution process the following concentrations of 0.4 wt%, 0.2 wt%, 0.1 wt%, 0.05 wt%, 0.025 wt%, 0.0125 wt% and 0.006 wt% were obtained. From each concentration the additive

dissolution and crystallization temperatures in the melt were determined by polarized optical microscopy and the crystallization temperature of PBT was determined by DSC. The crystallization temperature of melt processed neat PBT was determined at 188.5°C.

In Figure 28 the DSC cooling curves of neat PBT and PBT comprising 0.2 wt% and 0.4 wt% of **3** are shown. Due to the presence of nuclei at higher temperatures the crystallization temperature of PBT is distinctly increased upon addition of **3**. As less nucleation sites are available at lower concentrations, the $T_{c,p}$ values decrease with the amount of additive added. The crystallization temperatures reported in the following section were determined from the exothermic peak minimum of the second cooling scan.

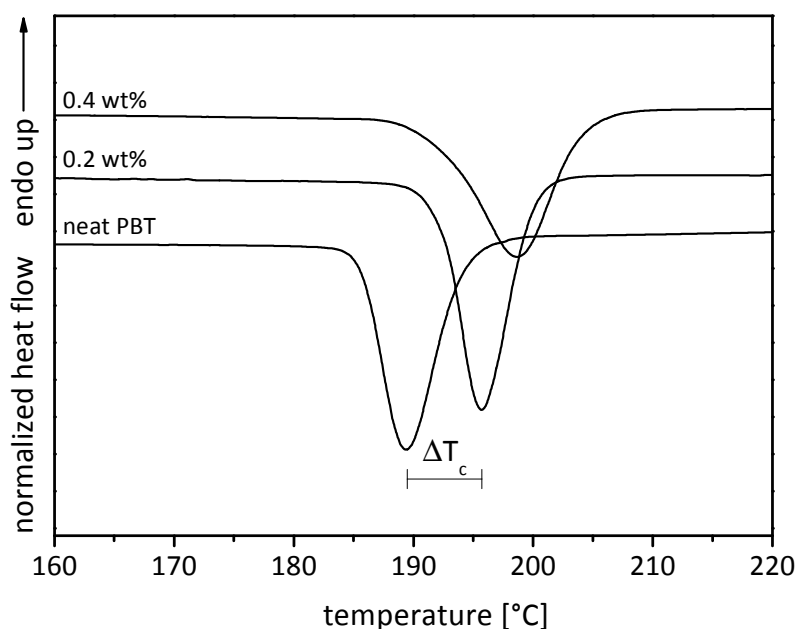


Figure 28. DSC cooling scans of neat PBT and PBT comprising 0.2 wt% of **3**.

In the following, three sets of selected compounds will be compared to discuss structure-property relations as function of the concentration. The first set compares the influence of different substituents of four trisamides based on the 1,3,5-benzenetricarboxylic acid core. The second set compares trisamides with the same substituents based on the 1,3,5-triaminobenzene core. The third set is based on the 2,4,6-trimethyl-1,3,5-triaminobenzene as core. The top row of figures 2-4 shows the crystallization temperature ($T_{c,p}$; dots) of PBT as function of the additive concentration. The dashed horizontal line indicates the $T_{c,p}$ of neat PBT as reference. The temperature composition diagrams of the binary mixtures can be divided into three regions. Region I represents the concentration range where the additive is soluble in the polymer melt and does not crystallize upon

cooling. In these cases no birefringence is observed in the melt. It should be pointed out that the lack of birefringence in the polarized optical microscope does not necessarily mean a molecular solution. Small aggregates of trisamide molecules may still be present in the melt, similar to amphiphilic molecules in optically isotropic micellar solutions. In region II the additive is soluble at the processing temperature and crystallizes upon cooling in fibrillar nano-objects, visible as birefringent structures in the melt. These supramolecular structures provide a surface for epitaxial crystallization of the polymer and induce nucleation. In region III the additive is not completely soluble under the applied temperature. Therefore nucleation both takes place on the surface of the crystallized supramolecular structures as well as on the surface of the not dissolved additive. The bottom graphs show the additive dissolution ($T_{d,a}$, triangles up) and crystallization temperature ($T_{c,a}$, triangles down) as determined by polarized light microscopy. In the bottom graphs the dashed horizontal line indicates the processing temperature of the mixing process at 260°C.

In the following, sets of selected compounds will be compared to reveal structure property relations and to investigate the concentration dependence. The first set compares the influence of different substituents of four trisamides based on the 1,3,5-benzenetricarboxylic acid core. The second and third set compares four trisamides with the same substituents based on the 1,3,5-triaminobenzene core and the 2,4,6-trimethyl-1,3,5-triaminobenzene core respectively. For each compound the top row of Figure 29, Figure 31 and Figure 33 show the crystallization temperature ($T_{c,p}$, dots) of PBT as function of the additive concentration. The dashed horizontal line indicates the $T_{c,p}$ of neat PBT as reference. The bottom graphs show the dissolution ($T_{d,a}$, triangles up) and crystallization temperature ($T_{c,a}$, triangles down) of the additive. Here, the dashed horizontal line indicates the processing temperature of 260°C.

The temperature composition diagram of a binary mixture of a polymer and an additive that is soluble in the polymer melt can be divided into three concentration regions. Region I represents the concentration range where the additive is soluble in the polymer melt and does not crystallize upon cooling prior to the polymer as determined by polarized optical microscopy. In these cases no birefringence is observed in the melt. It should be pointed out that the lack of birefringence does not mean a molecular solution because very small aggregates of trisamide molecules can be present, similar to optically isotropic micellar solutions. In region II the additive is again soluble at the processing temperature but

crystallizes in fibrillar nano-objects upon cooling from the melt. These supramolecular structures provide a surface for the epitaxial crystallization of the polymer and thus induce nucleation. In region III the additive is only partly soluble in the processing range and nucleation can both take place on the surface of the crystallized additive whiskers as well as the undissolved additive moieties.

Figure 29 compares the data of the first set of additives based on the 1,3,5-benzenetricarboxylic acid core with the substituents iso-propyl **1**, tert-butyl **2**, 1,1-dimethylpropyl **3** and cyclohexyl **7**. In agreement with the observations from the screening test, additive **1** with iso-propyl substituent is readily soluble in the PBT melt. In the concentration range from 0.006 - 0.4 wt% (I) the additive is soluble and does not crystallize prior to the polymer. Consequently no nucleation of PBT occurs. At the concentration of 0.8 wt% and the processing temperature of 260°C additive **1** is to the largest extent soluble in the PBT melt. Only a small fraction is insoluble as indicated by a weak birefringence. Upon cooling the dissolved fraction of the additive crystallizes prior to the polymer and nucleation takes place mainly at the formed supramolecular structures, but also at the not dissolved additive. The crystallization temperature of PBT is increased by 9.2°C from 188.5°C to 198.2°C. The small change in the chemical structure of the peripheral substituent from iso-propyl to tert-butyl results in a less soluble compound. Only up to 0.1 wt% additive **2** is soluble and does not crystallize upon cooling and no increase in $T_{c,p}$ is observed. In the concentration range from 0.2 - 0.8 wt% the additive is partially soluble and nucleates PBT with a $T_{c,p}$ of 192.9°C at only 0.2 wt%. Additive **3** with 1,1-dimethylpropyl substituent is slightly better soluble than **2** indicated by comparably lower $T_{d,a}$ and $T_{c,a}$ values in the range from 0.2 - 0.8 wt%. At 0.2 wt% (II) the additive is soluble at the processing temperature and crystallizes prior to the polymer. Consequently nucleation takes place only at the formed supramolecular structures with a $T_{c,p}$ of 195.7°C. At higher concentrations (III) the maximum $T_{c,p}$ of additive **3** was found to be 198.0°C at a concentration of 0.8 wt%. The cyclohexyl substituted derivative **7** is completely soluble over the entire investigated concentration range, does not crystallize prior to the polymer and consequently is not capable to nucleate PBT.

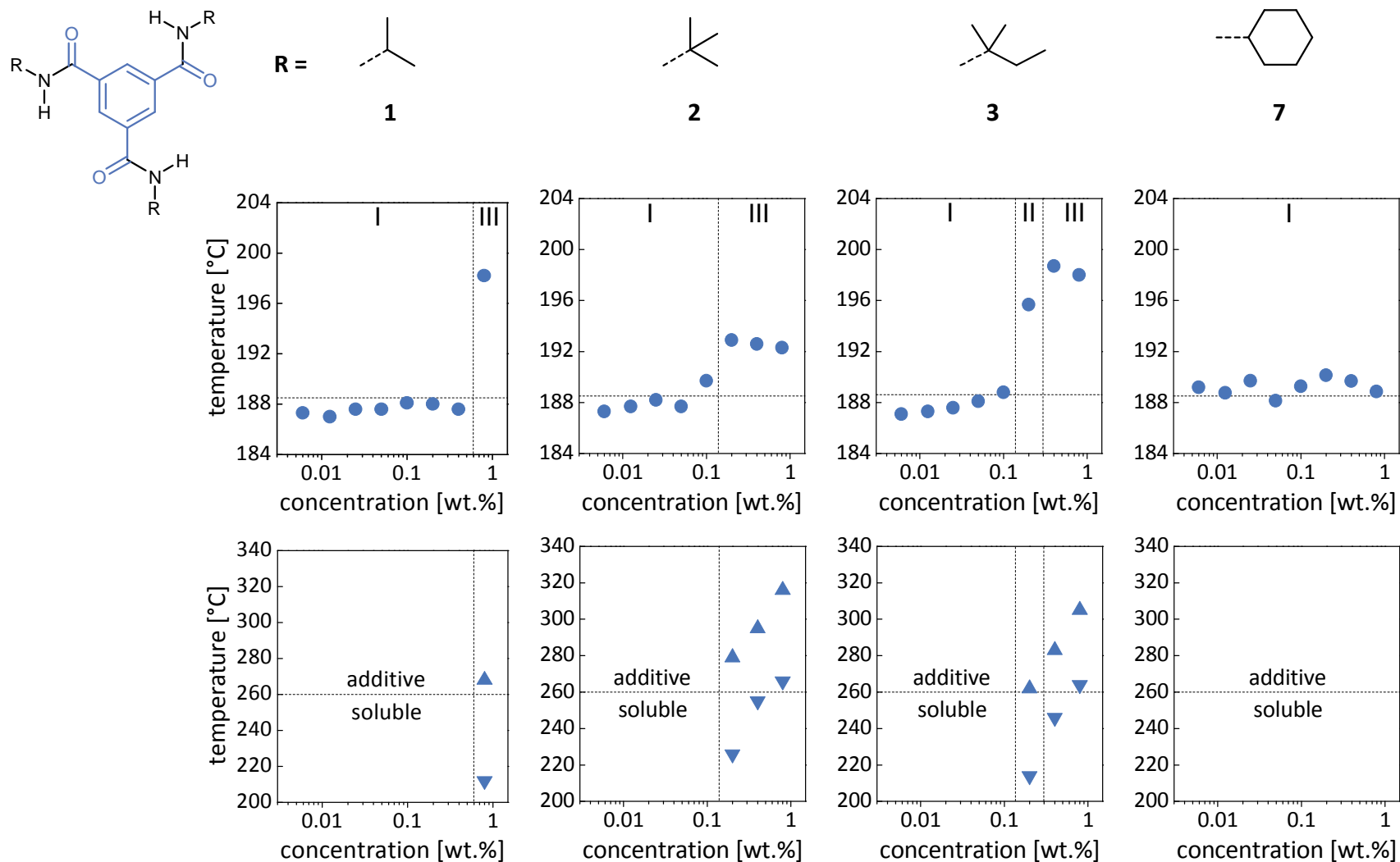


Figure 29. Crystallization temperatures of PBT ($T_{c,p}$ ●) containing the 1,3,5-benzenetrisamide derivatives **1**, **2**, **3** and **7** (top graphs) and additive dissolution ($T_{d,a}$ ▲) and crystallization temperatures ($T_{c,a}$ ▼)(bottom graphs) as function of the additive concentration. The dashed lines at 188.5°C in the top graphs represent the crystallization temperature of neat PBT. The dashed lines in the bottom graphs at 260°C indicate the processing temperature.

The structure and appearance of the supramolecular entities within the polymer matrix is strongly dependent on the individual chemical structure of the additive. At high concentrations compounds **1-3** based on 1,3,5-benzenetricarboxylic acid all showed fibrillar structures in the polymer melt upon cooling from the dissolved state as shown exemplarily for **3** in Figure 30. Here at 280°C the additive is fully soluble in the polymer melt and visible crystallization in form of fine filaments can be observed at 235°C. Upon further cooling the supramolecular structures grow larger and later act as nuclei for the polymer crystallization at temperatures below 200°C. However no conclusions can be drawn from the appearance of the fibrillar structures on the nucleation ability in the polymer.

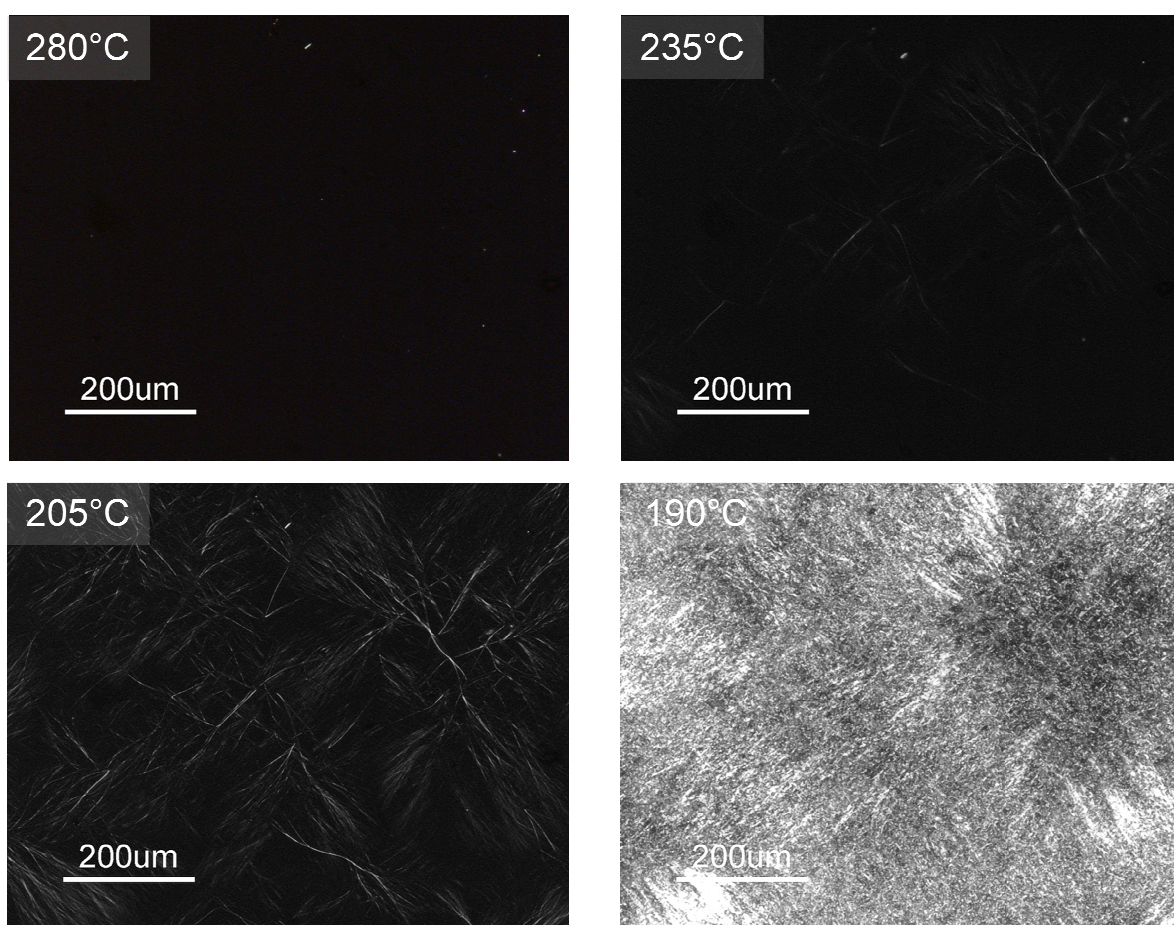


Figure 30. Polarized optical micrographs of PBT comprising 0.4 wt% of **3** cooled at 10 K/min at different stages of the cooling process.

Figure 31 presents the results of the 1,3,5-benzotrisamide derivatives **19-21** and **23** based on the 1,3,5-triaminobenzene core with the same substituents as the compounds in the first set. Inversion of the amide linkages has a pronounced influence on the solubility in the polymer melt. Trisamides based on the 1,3,5-triaminobenzene core are generally more soluble. Hence the $T_{d,a}$ and $T_{c,a}$ of the additives are shifted towards lower temperature values. This observation was also made for trisamide based nucleating agents of similar structure in isotactic polypropylene [78, 79] and polyvinylidene fluoride [4]. Compared to compound **1**, which is not soluble at the concentration of 0.8 wt%, compound **19** based on the 1,3,5-triaminobenzene core is soluble over the entire investigated concentration range. Although no birefringent structures are visible in polarized optical microscopy, a slight increase in $T_{c,p}$ of 2°C up to 190.5°C was observed at a concentration of 0.8 wt%. This indicates that very fine supramolecular nano-structures are present capable to induce nucleation. Also compound **20** based on the 1,3,5-triaminobenzene core with tert-butyl substituents is much more soluble compared to compound **2**. Only at a concentration of 0.4 wt% additive **20** self assembles upon cooling prior to PBT. But only a marginal increase of $T_{c,p}$ was observed. At a concentration of 0.8 wt% the additive is not completely soluble and an increase in $T_{c,p}$ to 193.2°C was found. Also compound **21** with 1,1-dimethylpropyl substituent is much more soluble than compound **3**. Up to a concentration of 0.4 wt% the additive remains soluble. At a concentration of 0.8 wt% **21** is soluble at the processing conditions, self assembles upon cooling and nucleates PBT very efficiently with a $T_{c,p}$ of 199.1°C, which corresponds to an increase of 10.6°C. This is the highest $T_{c,p}$ value found in this study. Compound **23** with the cyclohexane substituent is soluble over the entire investigated concentration range similar to compound **7**.

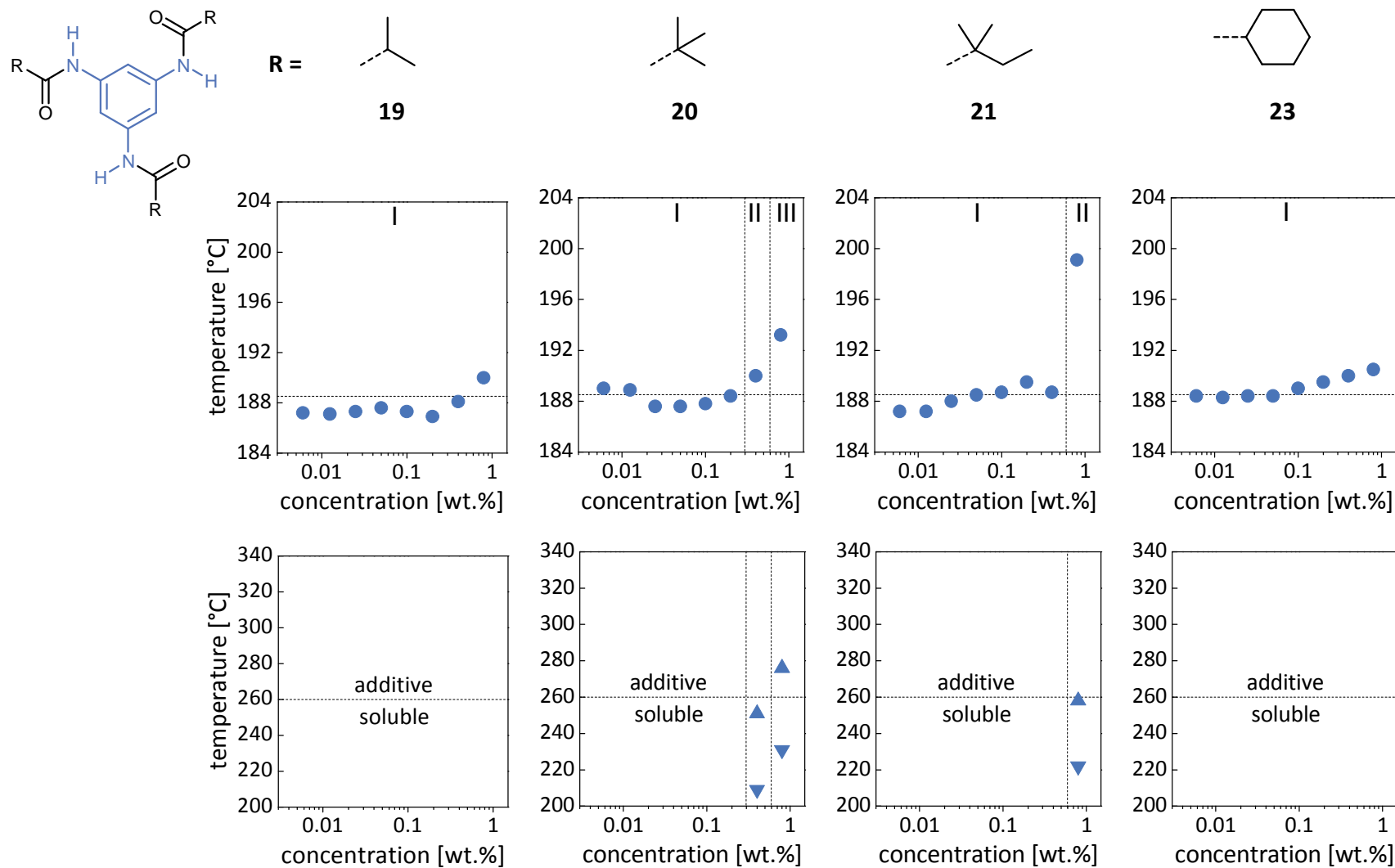


Figure 31. Crystallization temperatures of PBT (T_{cp} ●) containing the 1,3,5-benzenetrisamide derivatives **19**, **20**, **21** and **23** (top graphs) and additive dissolution ($T_{d,a}$ ▲) and crystallization temperatures ($T_{c,a}$ ▼)(bottom graphs) as function of the additive concentration. The dashed lines at 188.5°C in the top graphs represent the crystallization temperature of neat PBT. The dashed lines in the bottom graphs at 260°C indicate the processing temperature.

The additive crystallization process for the compounds based on 1,3,5-triaminobenzene is exemplarily shown for **21** in Figure 32. At 210°C the additive forms finely distributed structures that are only faintly visible in polarized optical microscopy. Although **21** is present at a higher concentration compared to **3** in Figure 30 the onset for the additive crystallization is considerably lower than for the corresponding derivative based on a 1,3,5-benzenetricarboxylic acid core.

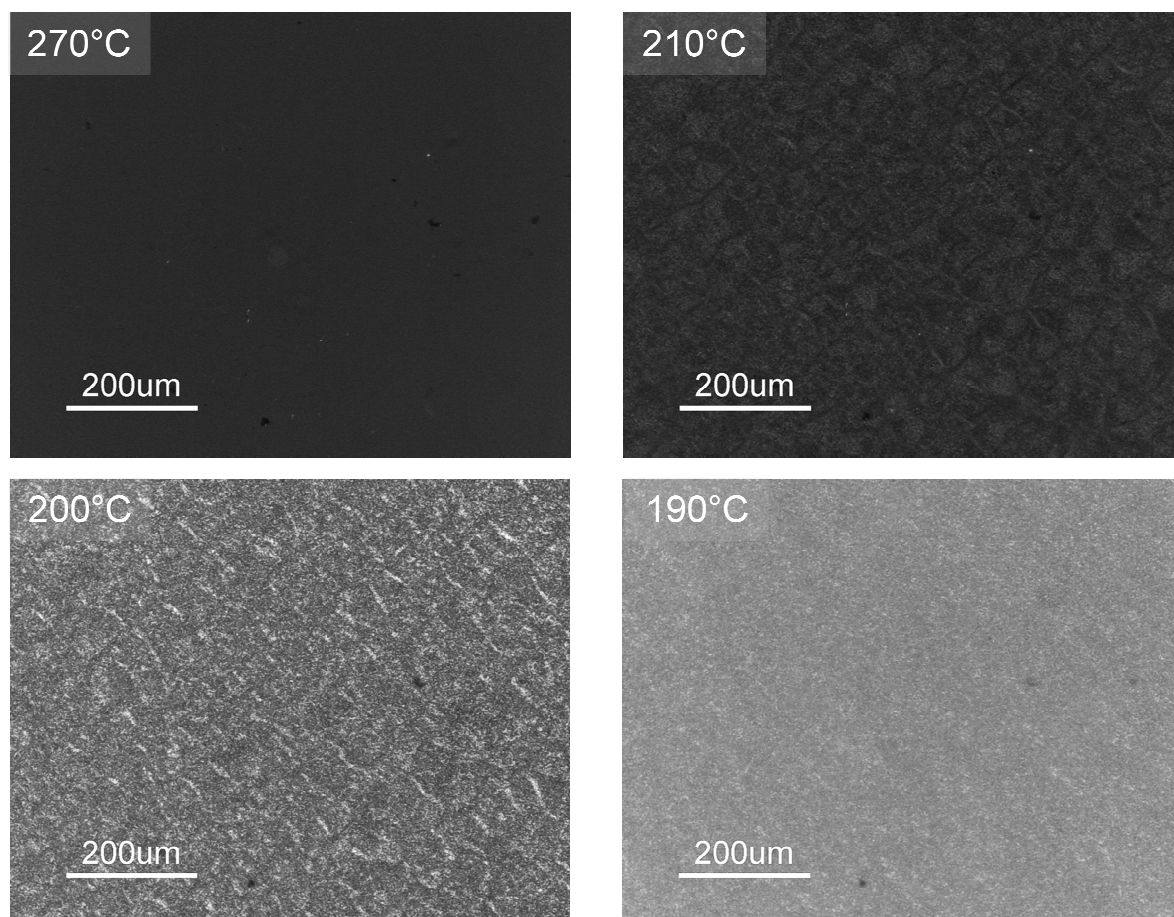


Figure 32. Polarized optical micrographs of PBT comprising 0.8 wt% of **21** cooled at 10 K/min at different stages of the cooling process.

Figure 33 compares the nucleation properties of the trisamides **28** – **30** and **32** based on the 2,4,6-trimethyl-1,3,5-trisaminobenzene core. This core was initially selected with the intention to reduce the solubility in PBT, by the addition of three additional methyl groups. This is the case if compound **28** is compared to compound **1** and **19**. Compound **28** with additional core substitution in 2,4,6-position is indeed only soluble in concentrations up to 0.05 wt% and nucleation is observed down to a concentration of 0.0125 wt%. In the concentration range from 0.1 – 0.8 wt% the additive is partially soluble and nucleates PBT with a $T_{c,p}$ of 194.8°C at 0.8 wt%. In contrast **1** and **19** are soluble almost over the entire investigated concentration range. Surprisingly, compounds **29** and **30** are soluble, where the before discussed structural analogues are much less soluble and showed the best nucleation properties. Surprisingly compounds **7** and **23** with cyclohexyl substituents are soluble over the entire concentration range compound **32** based on the 2,4,6-trimethyl-1,3,5-trisaminobenzene core is only soluble in the range from 0.006 – 0.1 wt%. The nucleation properties are very similar to compound **28**.

The above discussion on structure property relations with respect to the nucleation clearly shows that a prediction based on just the chemical structure is not possible. It is not the individual molecule, rather the structure of the supramolecular assembly, which determines the nucleation properties.

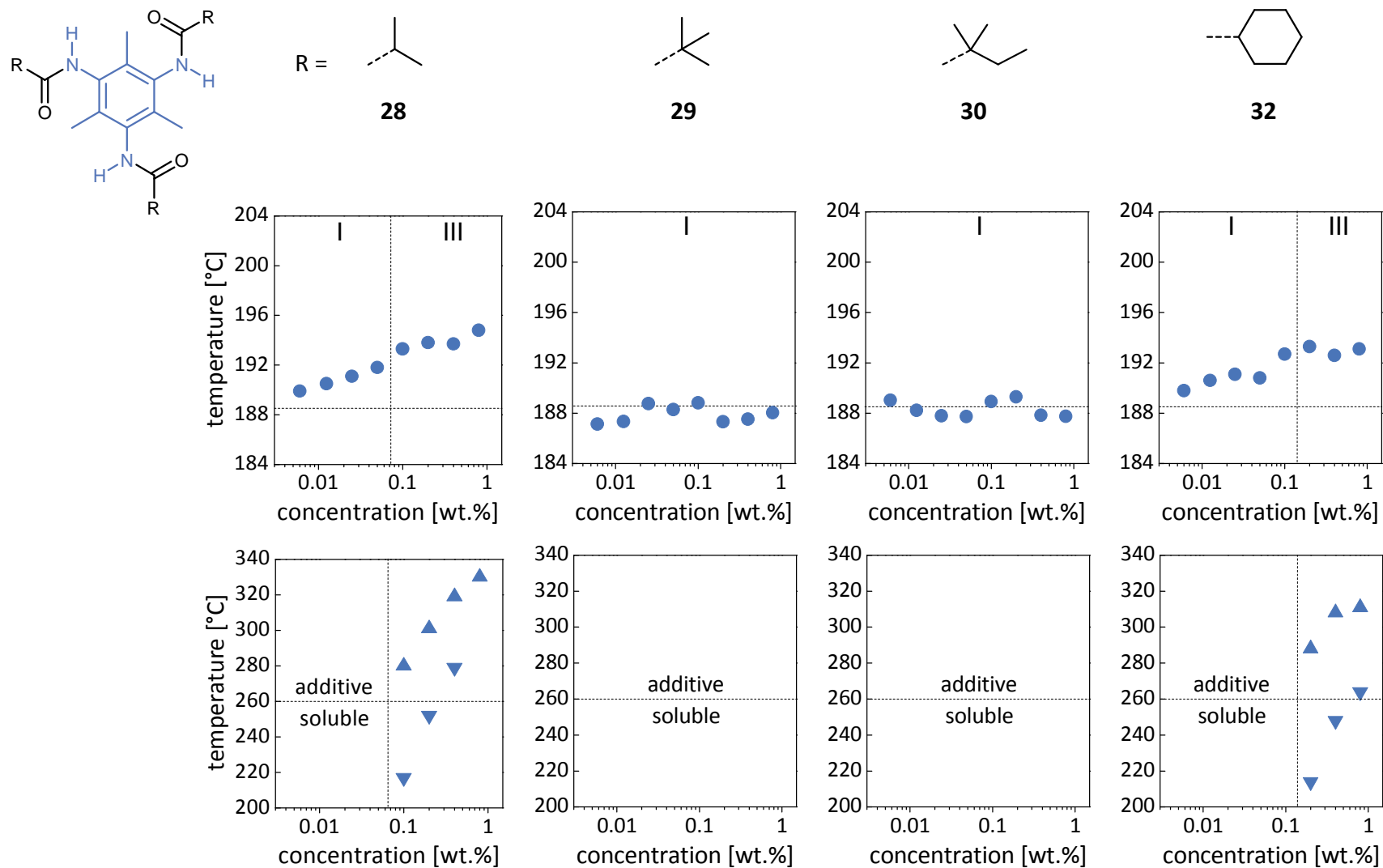


Figure 33. Crystallization temperatures of PBT (T_{cp} ●) containing the 1,3,5-benzenetrisamide derivatives **28**, **29**, **30** and **32** (top graphs) and additive dissolution ($T_{d,a}$ ▲) and crystallization temperatures (T_{ca} ▼)(bottom graphs) as function of the additive concentration. The dashed lines at 188.5°C in the top graphs represent the crystallization temperature of neat PBT. The dashed lines in the bottom graphs at 260°C indicate the processing temperature.

The formation of supramolecular structures is exemplarily shown for **28** in Figure 34. Although **28** is only soluble at high temperatures above 300°C first additive structures become visible at considerably low temperatures of 235°C.

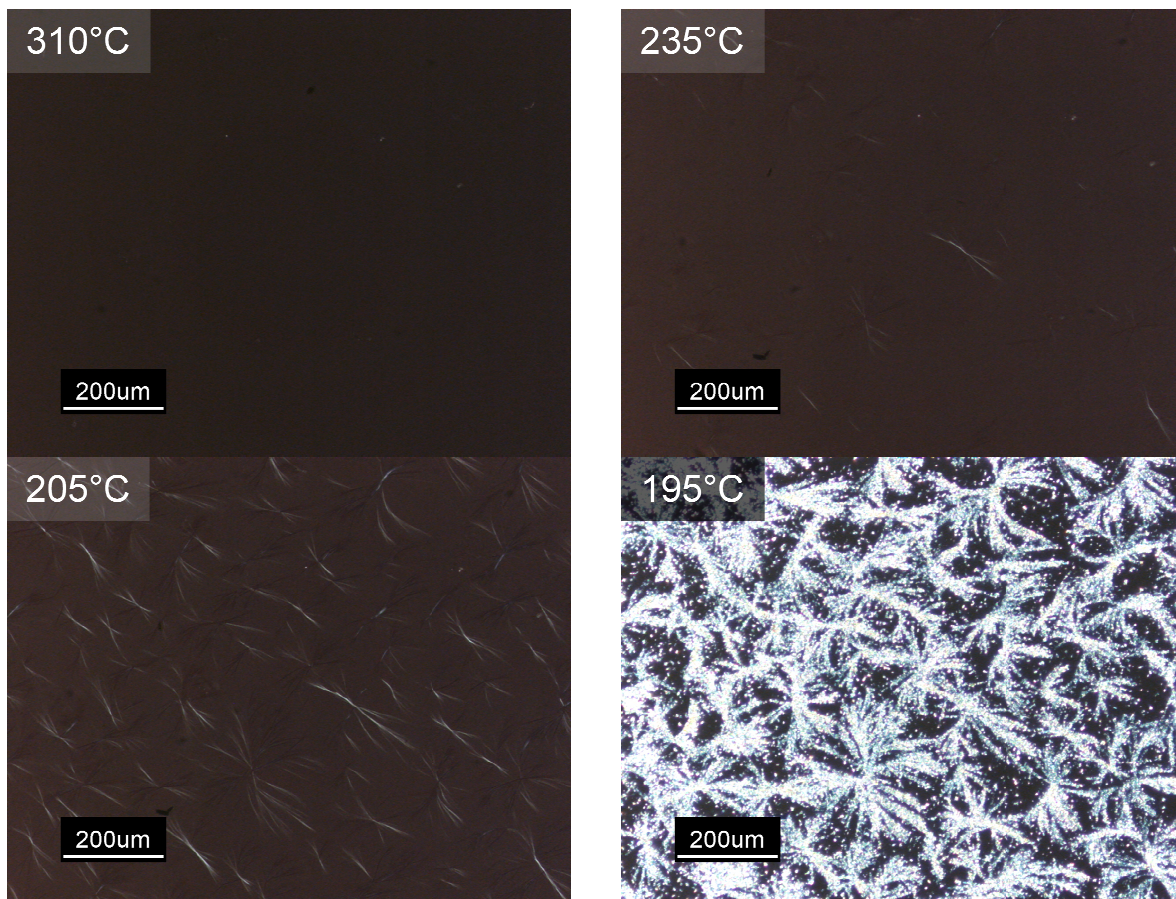


Figure 34. Polarized optical micrographs of PBT comprising 0.2 wt% of **28** cooled at 10 K/min at different stages of the cooling process.

4.2.3. Nucleation efficiency

To determine the nucleation efficiency of the 1,3,5-benzenetrisamides in PBT, self-seeding experiments as established by Lotz et al.^[6] for polypropylene were performed. This involves the partial melting of the polymer at a temperature T_s between the maximum of the endothermic melting peak and its offset, where upon cooling the remaining crystal fragments act as perfect nuclei for the crystallization of PBT and increase the crystallization temperature. The value for the highest theoretical polymer crystallization temperature ($T_{c,p\ theo}$) is obtained at the exothermic peak minimum upon cooling from T_s . The increased polymer crystallization temperature by the addition of a nucleating agent is described as $T_{c,p\ nucl}$.

The nucleation efficiency scale is calculated by:

$$NE (\%) = 100(\Delta T_{c,p} / \Delta T_{c,p\ max}) = 100(T_{c,p\ nucl} - T_{c,p\ neat}) / (T_{c,p\ theo} - T_{c,p\ neat})$$

The crystallization exotherms of neat melt processed PBT for various T_s values are shown in Figure 35. Maximum self nucleation of PBT was induced after melting for 5 min at 229.0°C yielding a maximum polymer crystallization temperature $T_{c,p\ theo}$ of 211.0°C.

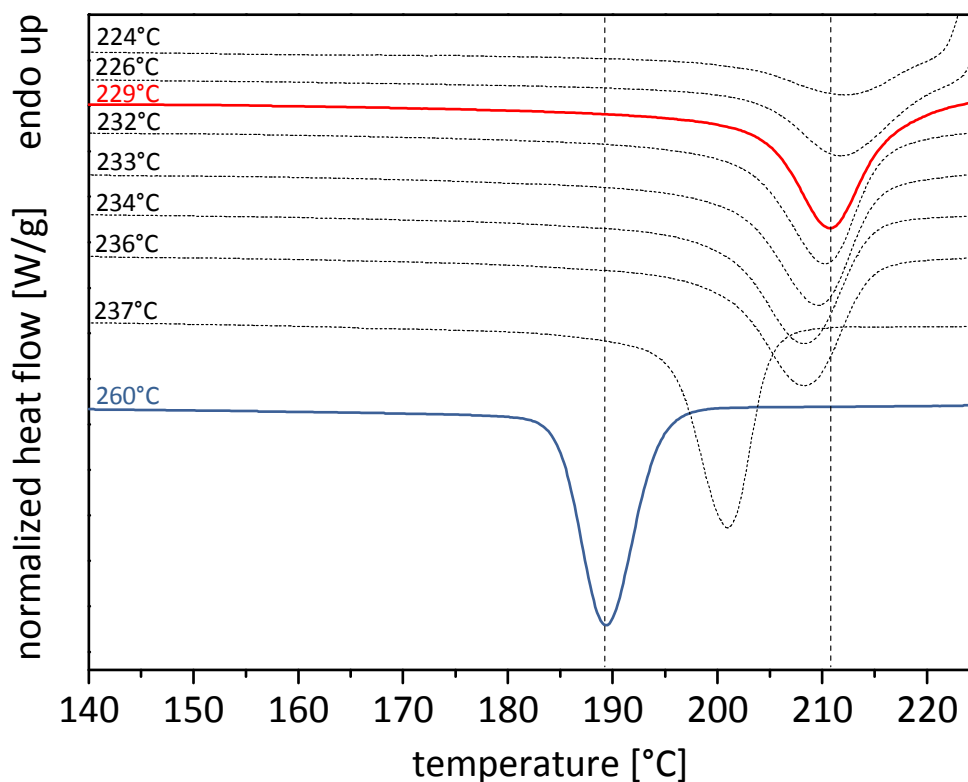


Figure 35. Crystallization exotherms of neat melt processed PBT for different T_s values.

In the following the efficiencies of the best additives from the three additive series will be compared with the reference compound talc. As presented in Figure 36 talc shows remarkable nucleation behavior over the entire concentration range with a maximum crystallization temperature of 199.7°C at 0.8 wt% (NE = 49.8 %). In comparison, compound **1** (NE = 42.2 %, $T_{c,p \text{ nucl}} = 198.0^\circ\text{C}$ at 0.8 wt%), compound **3** (NE = 45.3 %, $T_{c,p \text{ nucl}} = 198.7^\circ\text{C}$ at 0.4 wt%), and compound **21** (NE = 47.1 %, $T_{c,p \text{ nucl}} = 199.1^\circ\text{C}$ at 0.8 wt%) were found to be the most efficient nucleating agents from the investigated 1,3,5-benzenetrisamide derivatives. Even though **3** and **21** corresponds with the nucleation efficiency of the reference compound at the same concentration, benzenetrisamide derivatives only considerably affect the crystallization of the polymer when present at high additive contents.

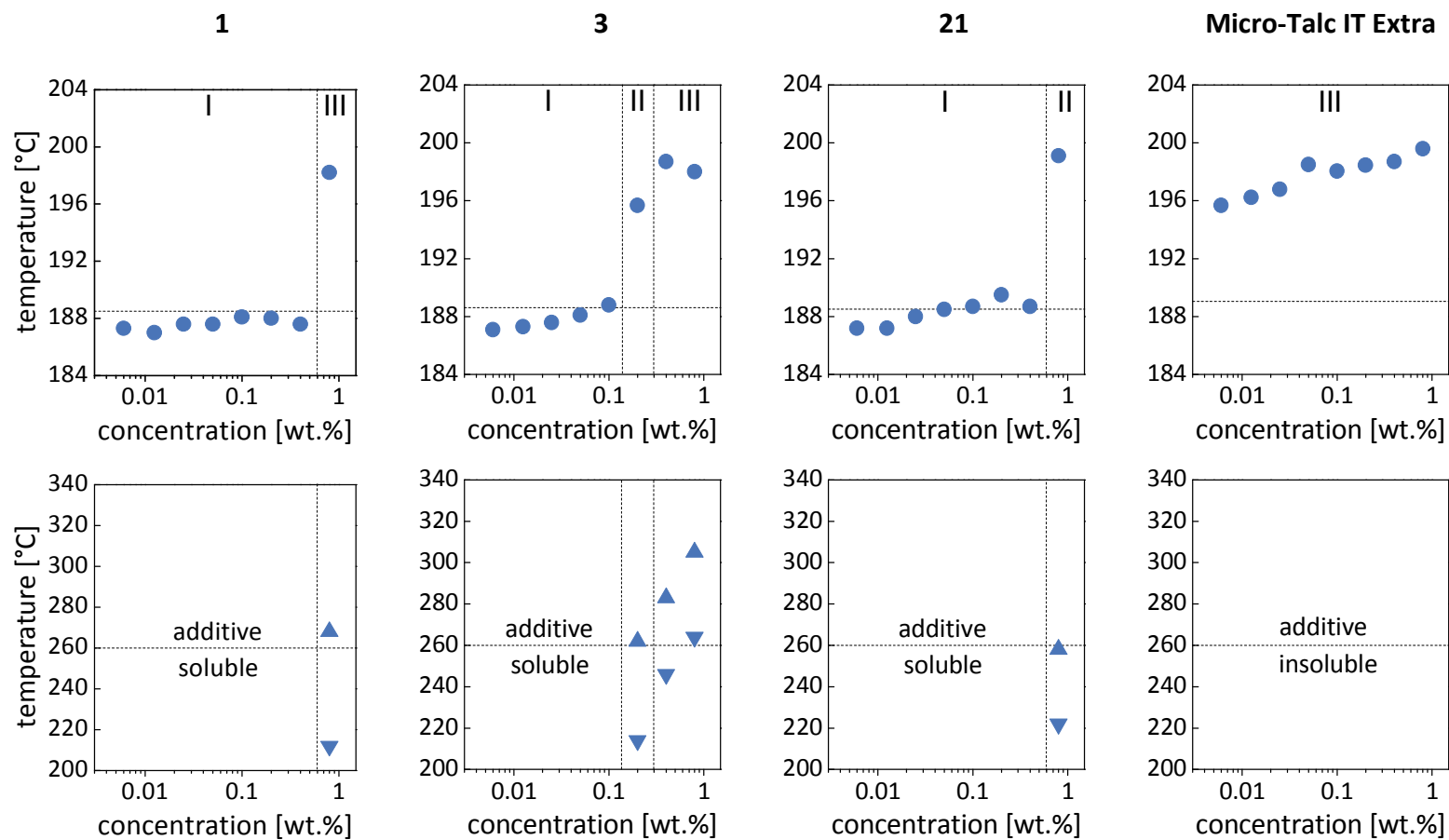


Figure 36. Crystallization temperatures of PBT ($T_{cr,p}$ ●) comprising **talcum** (top) and additive dissolution ($T_{d,a}$ ▲) and crystallization temperatures ($T_{c,a}$ ▼)(bottom) as function of the additive concentration in comparison to the three most efficient 1,3,5-benzenetrisamide nucleating agents **1**, **3**, and **21**. The dashed line at 188.5°C in the top graphs represents the crystallization temperature of neat PBT and the line in the bottom graphs at 260°C indicates the processing temperature.

4.2.4. Morphology of 1,3,5-benzenetrisamides

To obtain more insight in the morphology and size of the formed supramolecular nano structures which are formed upon cooling within PBT, experiments were conducted to hydrolyze PBT. It was possible to selectively hydrolyze the PBT matrix in alkaline solution without affecting the formed supramolecular structures. Due to the nonpolar character of the surface and in particular to the fibrillar structure, hydrolysis can only occur at both ends. Therefore the self assembled trisamides are very resistant to hydrolysis. Samples for the morphological studies were prepared by melting compositions containing 0.1 wt%, 0.2 wt% and 0.4 wt% of the 1,1-dimethyl propyl substituted trisamide **3** in DSC pans under nitrogen at 280°C. To ensure complete dissolution and distribution of the trisamides the samples were held for 5 min at this temperature. The samples were cooled to room temperature with four defined linear cooling rates of 10 K/min, 40 K/min, 80 K/min and 110 K/min. After removal of the solid samples from the DSC pans, the surface was carefully hydrolyzed in alkaline solution. Scanning electron microscopy was used to investigate the fibrillar supramolecular nano-structures. Figure 37 compares SEM micrographs of the formed supramolecular nano-structures and shows the corresponding histograms of the lateral size distribution. The first series of experiments was carried out at a concentration of 0.4 wt%. At a cooling rate of 10 K/min and after hydrolysis very long fibrillar structures, with average lateral dimensions of 142 ± 49 nm were observed. Upon increasing the cooling rate to 40 K/min at the same concentration of 0.4 wt%, a few long objects with lateral dimensions around 200 nm and numerous shorter assemblies between 25 and 65 nm are present. The average lateral dimension is with 72 ± 53 nm by a factor of two smaller. At faster cooling rates of 80 K/min and 110 K/min the fraction of long objects decreases further in favor of shorter and smaller assemblies. The average lateral dimensions are 56 ± 31 nm at 80 K/min and 50 ± 24 nm at 110 K/min.

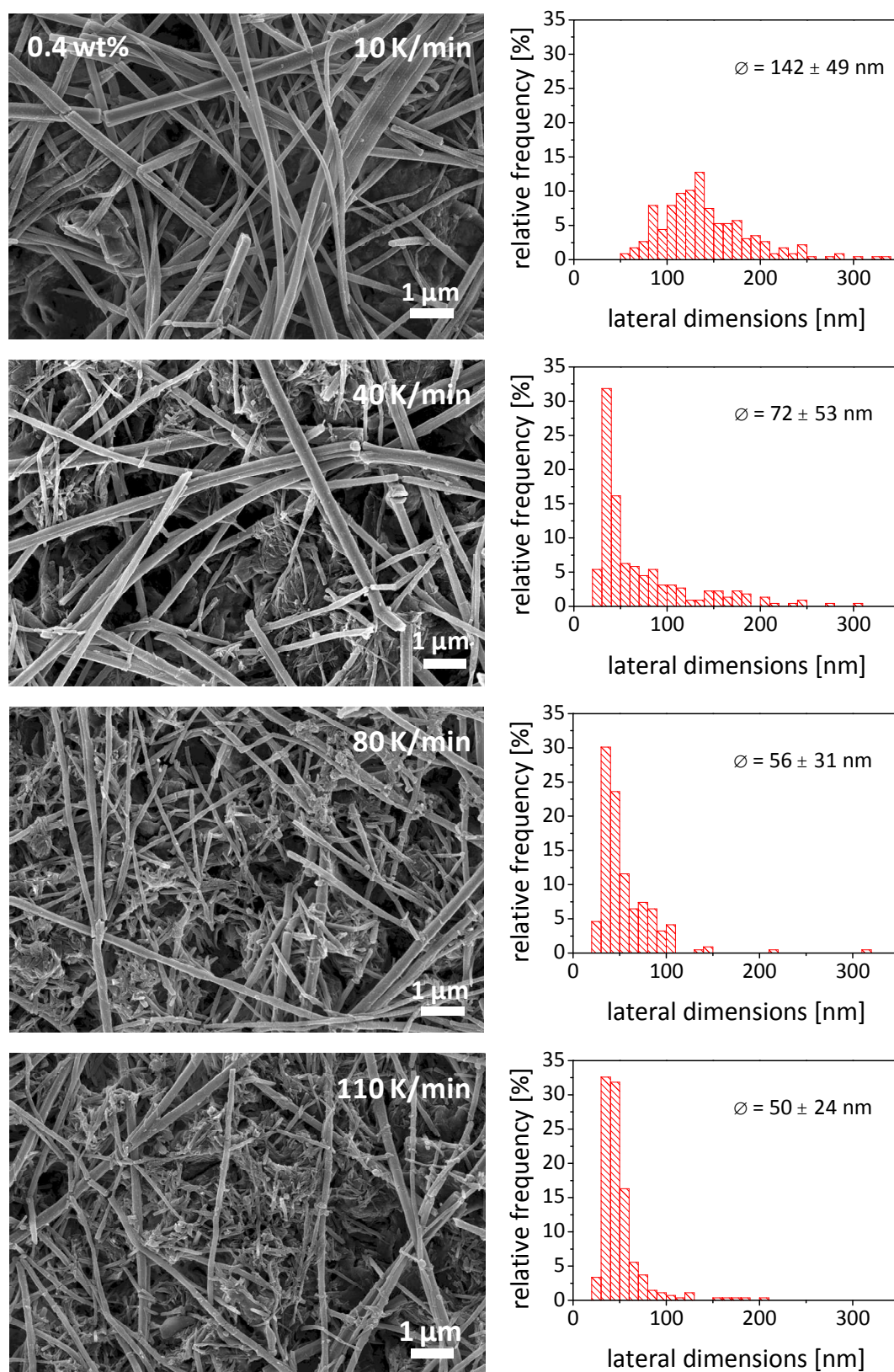


Figure 37. SEM images of supramolecular structures of **3** at a concentration of 0.4 wt% after hydrolysis of PBT and corresponding histograms of the lateral dimensions. Samples were prepared at different cooling rates of 10 K/min, 40 K/min, 80 K/min and 110 K/min.

In the second series of experiments the concentration of **3** was lowered to 0.2 wt% (Figure 38). At a cooling rate of 10 K/min, compared to the higher concentration of 0.4 wt%, lowering the concentration leads to by a factor of two smaller assemblies with narrower distribution (average lateral dimensions of 70 ± 25 nm). Increasing the cooling rate to 40 K/min at 0.2 wt% results in shorter assemblies with a narrower size distribution, similar to the observations made for 0.4 wt%. Here the average lateral dimensions are 48 ± 12 nm. Further increase in cooling rate to 80 K/min and 110 K/min results in very fine homogeneous nano-objects (sticks) with a very narrow size distribution (37 ± 6 nm). Compared to the cooling rate of 10 K/min the assemblies are by a factor of two smaller. It is interesting to note that the dimensions of the formed supramolecular structures for the highest two cooling rates are similar, featuring almost the same values for the average lateral dimensions.

In conclusion the formation of supramolecular nano-objects in a polymer melt is influenced by cooling rate and additive concentration but can be controlled. Remarkably well-defined supramolecular nano-objects can be formed.

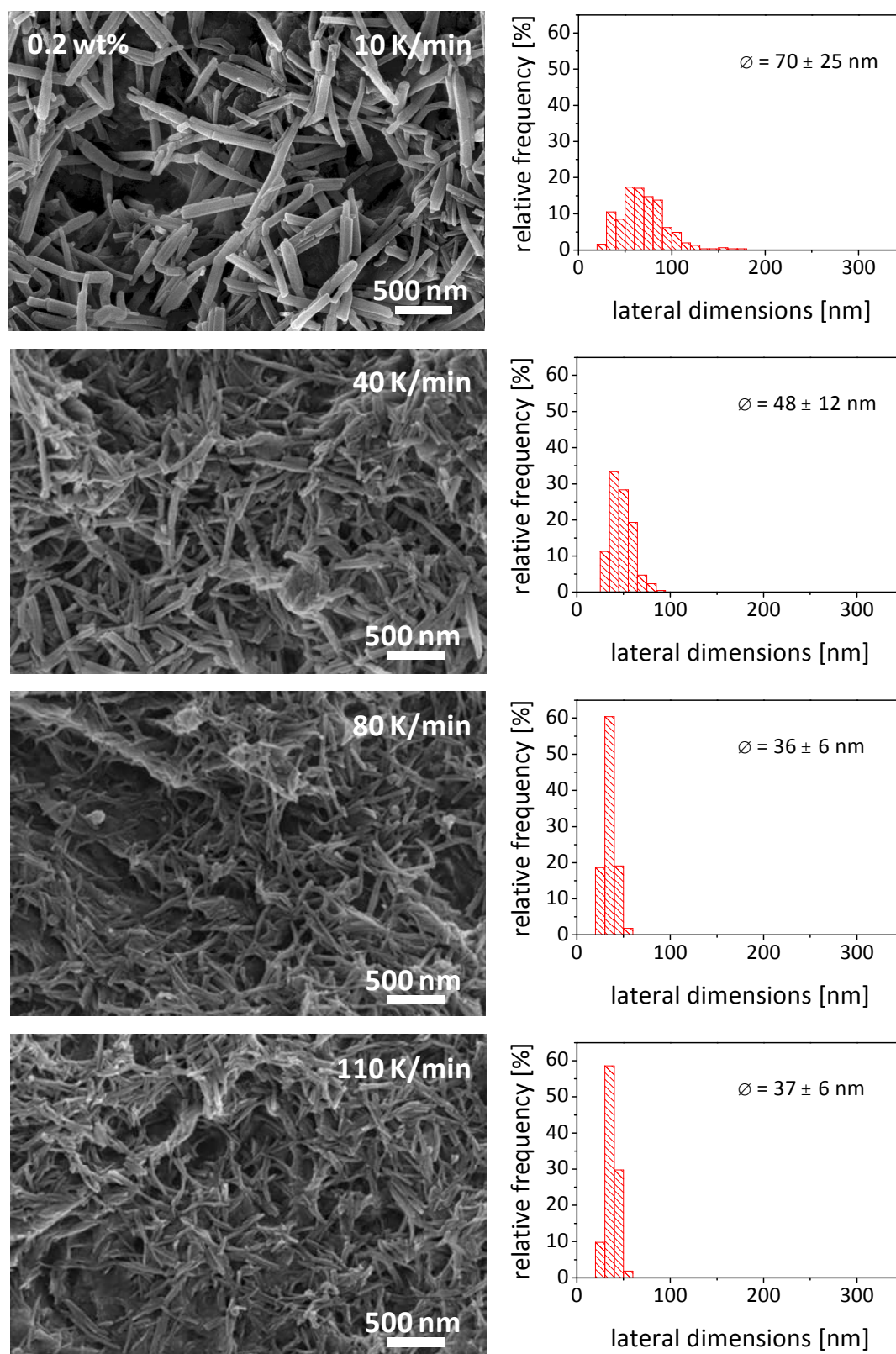


Figure 38. SEM images of supramolecular structures of **3** at a concentration of 0.2 wt% after hydrolysis of PBT and corresponding histograms of the lateral dimensions. Samples were prepared at different cooling rates of 10 K/min, 40 K/min, 80 K/min and 110 K/min.

The third series of experiments compares SEM micrographs of the formed supramolecular nano-structures at a concentration of 0.1 wt% (Figure 39). For all cooling rates very short and pronounced supramolecular nano-objects are observed. The average lateral dimensions are in the range of 40 nm and surprisingly are independent from the applied cooling conditions. Interestingly at a concentration of 0.1 wt% no nucleation of PBT is observed as indicated by the DSC measurements presented in 4.2.2. This indicates that the observed supramolecular structures are either too small to induce the nucleation of PBT or are not present in the PBT melt prior to the crystallization of the polymer.

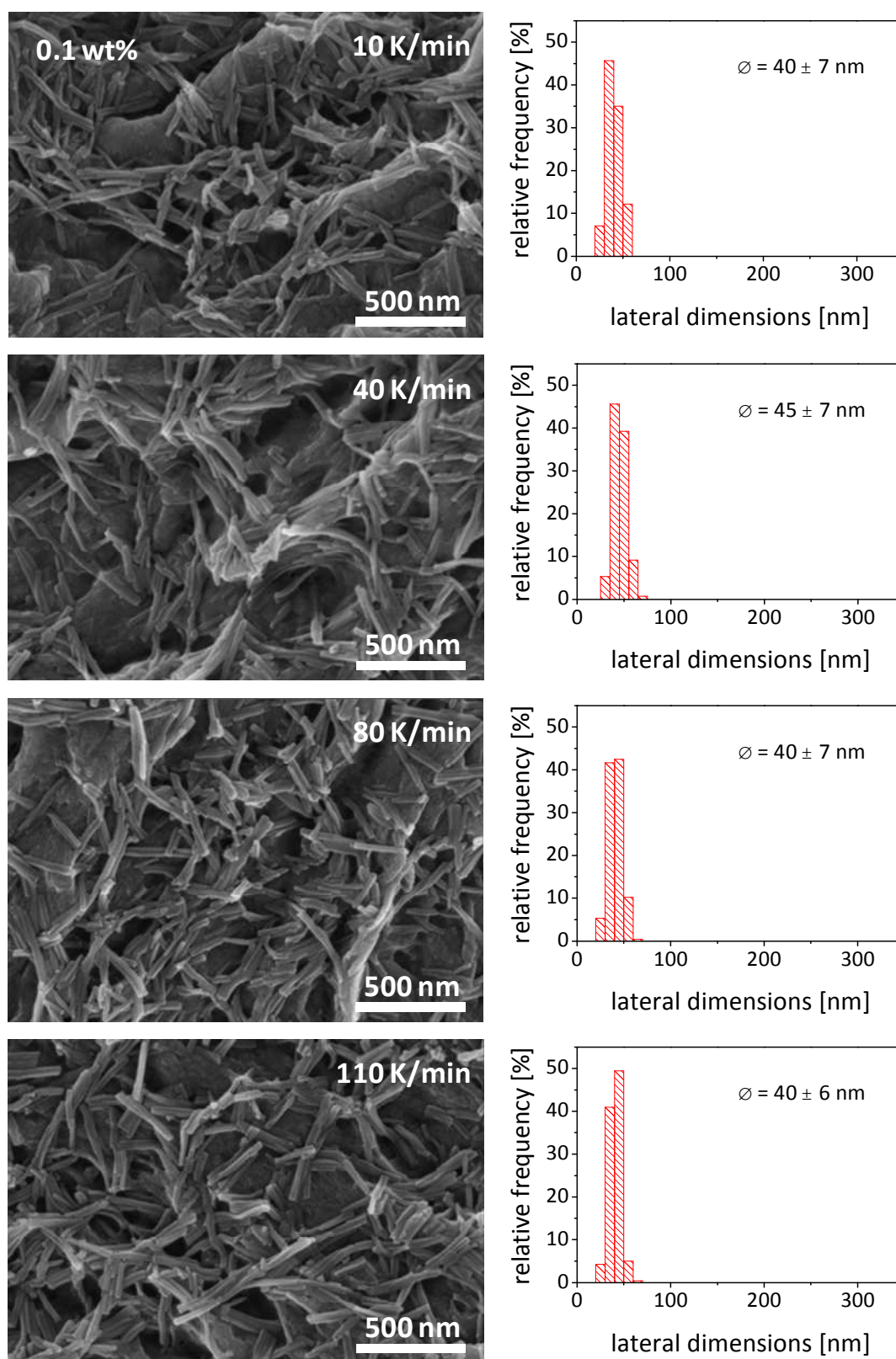


Figure 39. SEM images of supramolecular structures of **3** at a concentration of 0.1 wt% after hydrolysis of PBT and corresponding histograms of the lateral dimensions. Samples were prepared at different cooling rates of 10 K/min, 40 K/min, 80 K/min and 110 K/min.

4.2.5. Laser transparency

The transparency of a visible object is mainly governed by the amount of transmitted light. Scattering on spherulites in semi-crystalline polymers decreases the portion of specular transmitted light accompanied by an increase in diffuse transmission. This phenomenon is strongly pronounced in PBT that, even in thin parts, appears fully opaque. The use of PBT in applications such as laser transmission welding is therefore only possible to a limited extent.

^[66] As the transparency of polymers for light in the near infrared range should be dependent and capable of being influenced by its morphology, we investigated the influence of nucleation on the laser transparency of injection molded samples. In the course of this work two different PBT batches from the same polymer grade (Ultradur[®] B4500) (hereinafter referred to as “**batch1**” and “**batch2**”) were used. The reference value for the laser transparency of **batch1** was found to be $48.2 \% \pm 0.4 \%$ and thus considerably higher in comparison to **batch2** ($41.8 \% \pm 0.3 \%$). The origin of the reproducible higher values for **batch1** is not due to differences in molecular weight or spherulite size and could not be explained up to now.

The LT values at a wave length of 1064 nm of PBT comprising selected 1,3,5-benzenetrisamides that showed promising nucleation behavior in polarized optical microscopy are presented in Figure 40 and Figure 41. Laser transparency was determined at a concentration of 0.1 wt% and 0.8 wt% on injection molded specimens with a thickness of 1.1 mm. Figure 40 shows the results of the laser transparency measurements of PBT (**batch2**) comprising 0.1 wt% of additive. While all compounds showed positive nucleation behavior in the screening test none of additives were capable to improve the laser transmittance. A very similar trend was observed regarding **batch1**. All transmission values are mainly within the range of the reference material (Figure 41). Lower LT values occurring for several additives in both batches can be attributed to scattering on undissolved additive particles.

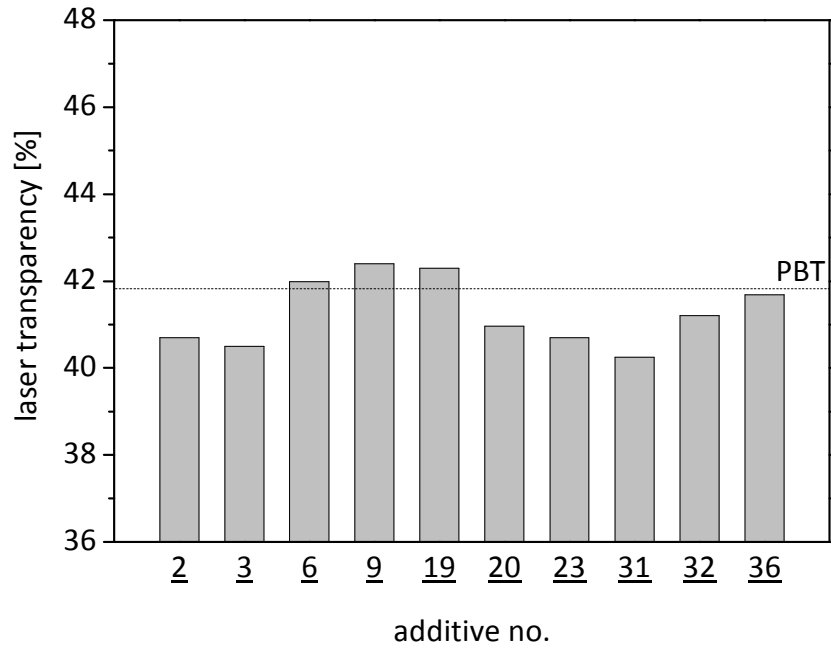


Figure 40. Laser transparency of PBT **batch1** comprising selected 1,3,5-benzenetrisamides at a concentration of 0.1 wt%.

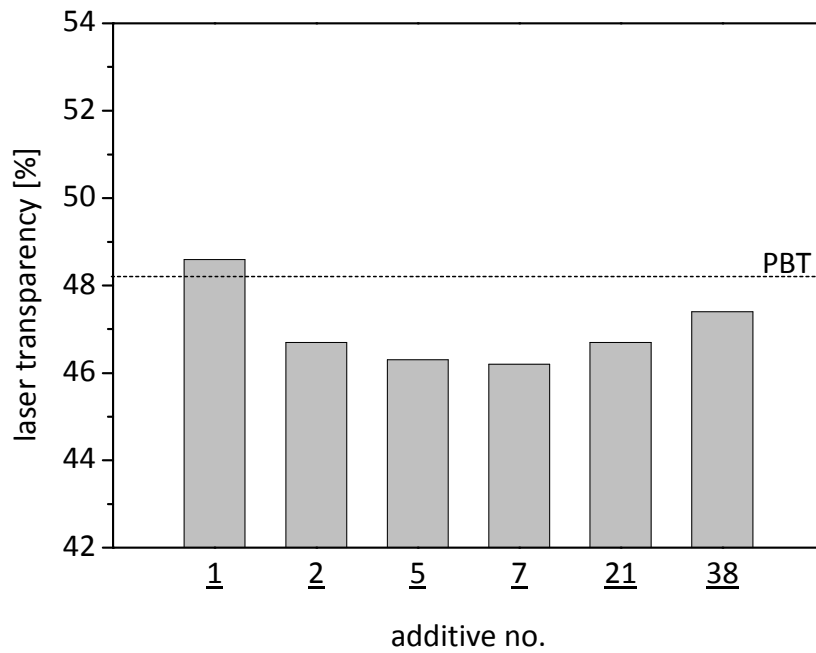


Figure 41. Laser transparency of PBT **batch2** comprising selected 1,3,5-benzenetrisamides at a concentration of 0.1 wt%.

In view of the excellent solubility of the 1,3,5-benzenetrisamides in the PBT melt, few derivatives were investigated at concentrations as high as 0.8 wt%. In spite of the high amount of additive no improvements in transmittance could be achieved (Figure 42). Taking these results into account, 1,3,5-benzenetrisamides do not, despite their ability to promote the nucleation of PBT, improve the laser transparency of PBT.

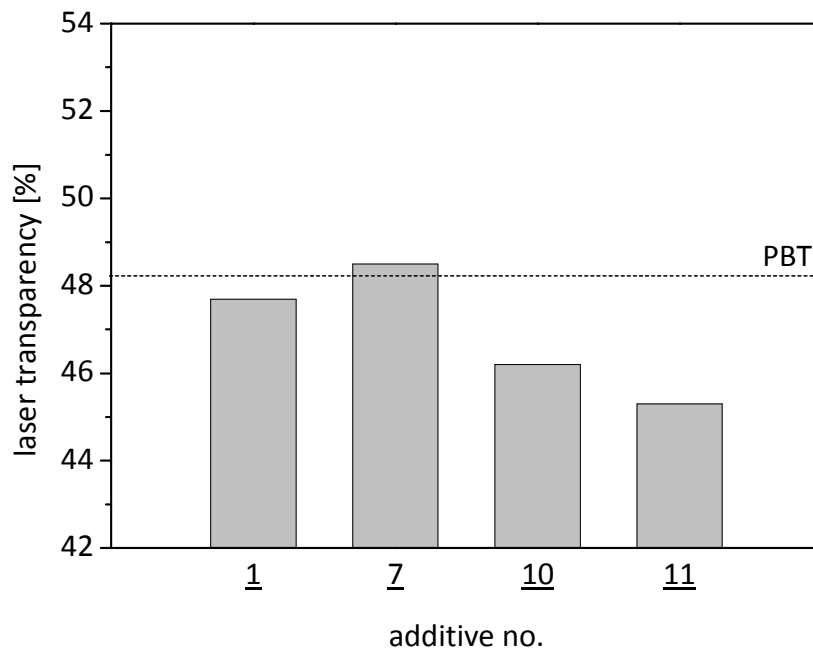
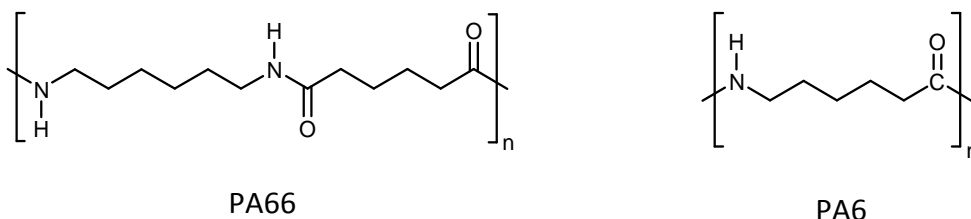


Figure 42. Laser transparency of PBT **batch2** comprising selected 1,3,5-benzenetrisamides at a concentration of 0.8 wt%.

5. Nucleation and clarification of polyamides

5.1. Introduction

Long before the first synthesis of polyamides, Carothers and his coworkers paved the way for modern polymer science with their studies on polycondensation reactions in 1929.^[80] In search of new high melting polymer analogues for aliphatic polyesters, polyamides gained growing interest over the years, leading to the invention of PA66 in 1935 and PA6 in 1938.^[81]



Both polyamides were primarily used as fibers, due to their excellent mechanical strength and temperature resistant properties. Resistance to heat, solvents, wear and abrasion opened up areas of applications as metal replacement materials for gears, bearings and coil forms among others.^[82] The capacity of polyamides for modifications such as facile copolymerization reactions and the multitude of available monomers have been important factors for the large growth of nylon resins up to now. Polyamides have become an important class of engineering thermoplastics. Among all polyamide types, PA6 and PA66 are the two most commonly used nylon resins accounting for more than a 90 % share along with special polyamide resins like PA11 and PA12 (7 %).^[82]

Depending on the crystallization conditions, PA6 crystallizes into three main polymorphs, the monoclinic α -phase, the monoclinic or pseudo-hexagonal γ -phase and the metastable hexagonal β -phase.^[78, 79, 83] Crystallization from the melt usually leads to the α - or γ -form, whereas β -crystals are formed after high-temperature annealing under vacuum.^[84]

The unit cell of the α -modification of PA6 is shown in Figure 43. The molecules are in the fully extended zig-zag conformation and form planar H-bonded sheets. The chains in these planes are orientated antiparallel allowing all hydrogen bonds to be developed perfectly.

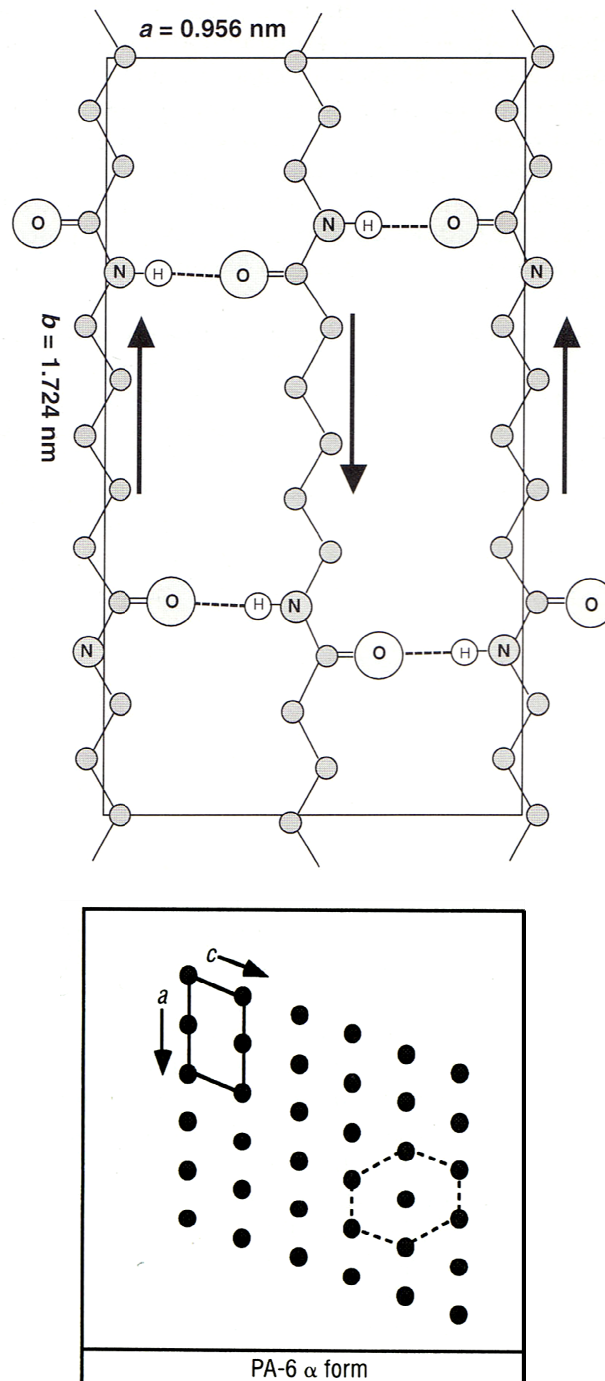


Figure 43. Monoclinic unit cell of the α -phase of PA6 in the projection along the c direction (top) and cross section of the chain positions (bottom). Images reprinted from Kohen et al.^[82]

In contrast, PA6 crystallized in the monoclinic γ -phase is composed of sheets of parallel chains that deviate from the fully planar conformation. H-bonds in this polymorph can be formed without any strain due to a 30° tilt of the amide with respect to the chain axes.

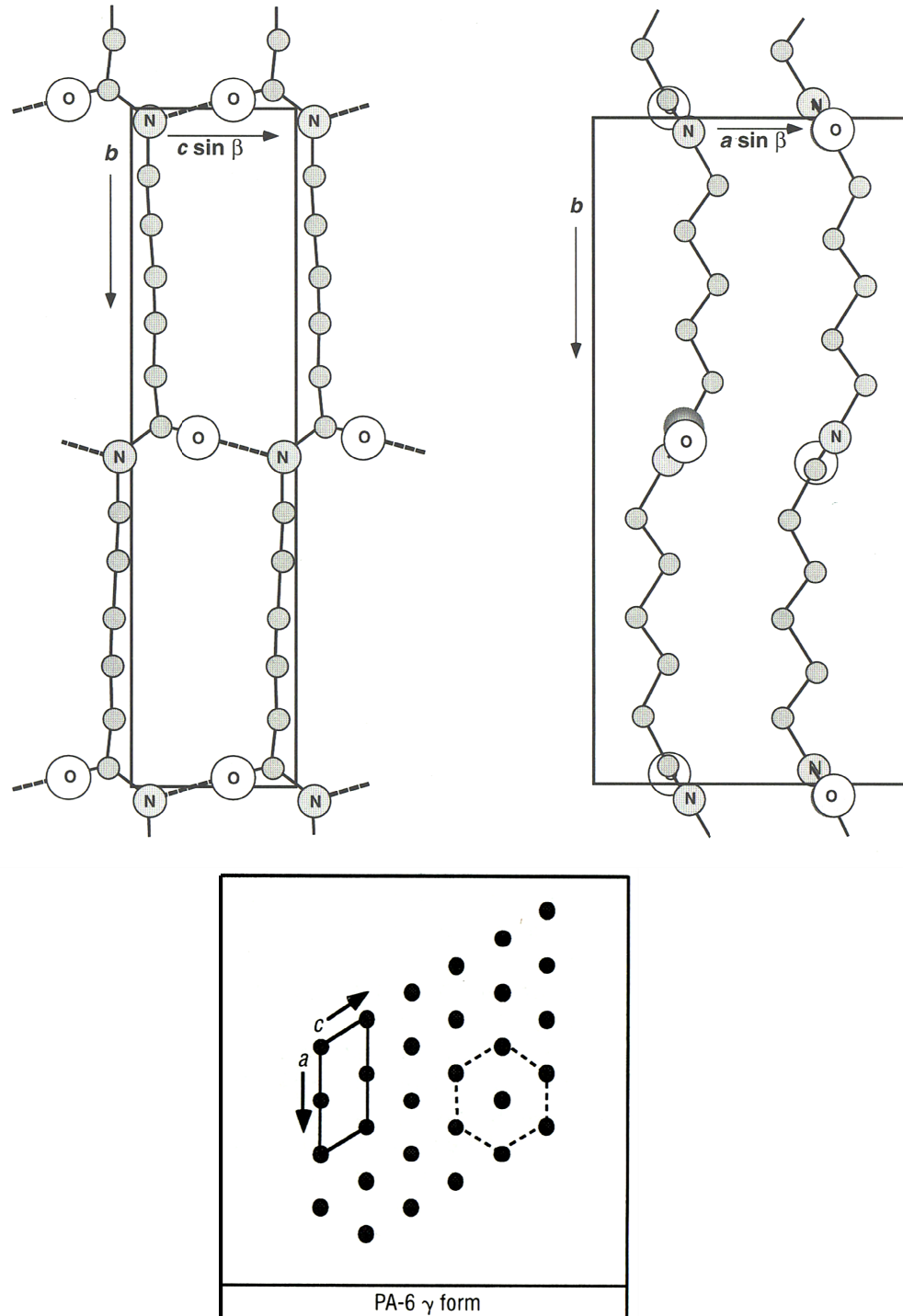


Figure 44. Monoclinic or pseudo-hexagonal unit cell of the γ -phase of PA6 in the projection along the a direction (top left) and projection along the c direction (top right) and cross section of the chain positions (bottom). Images reprinted from Kohen et al.^[82]

Both polymorphs can be converted into each other by treatment with aqueous solutions of I_2 and KI (α -phase into γ -phase) or by annealing at high temperatures (γ -phase into α -phase). Due to the arrangement of hydrogen bonds the α -phase is thermally more stable (higher melting temperature and enthalpy) compared to the γ -form. The γ -modification in turn exhibits higher fracture toughness with lower elastic modulus.^[85] The different phases and their relative amounts can be characterized using wide-angle X-ray diffractometry. Diffractograms of the two main crystal forms of PA6 α and γ are shown in Figure 45.

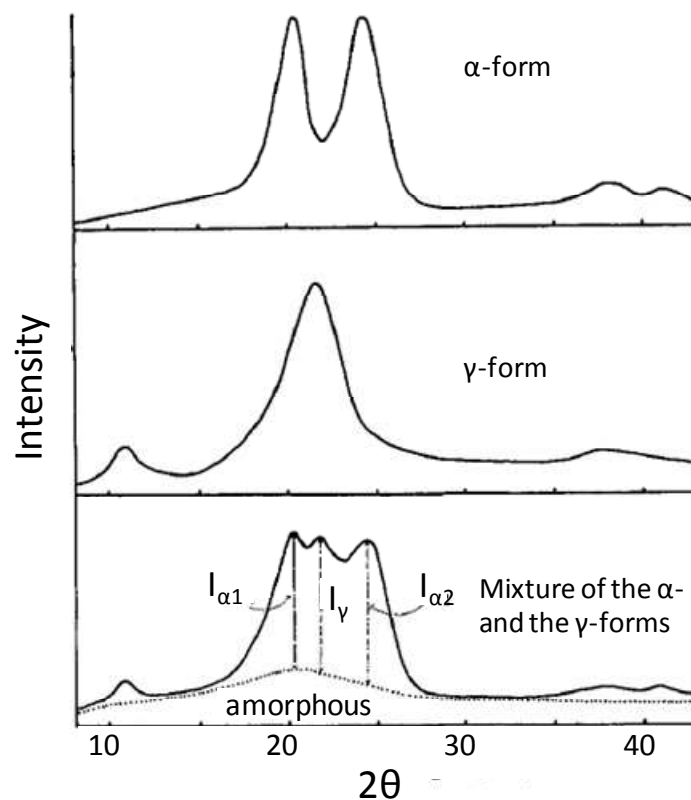


Figure 45. Wide-angle X-ray diffraction pattern of the α - and γ -phase of PA6, and a mixture of both forms. Image reprinted from Kyotani et al.^[86]

Nucleating agents for polyamides usually include inorganic particles, organic salts and polymeric nucleating agents, all being insoluble in the polymer melt and hence have to be finely dispersed during processing.^[1, 82] For example, Hitch et al. reported on a mixture of PA66 including fumed alumina, talc, graphite or calcium fluoride. Calcium fluoride showed remarkable nucleation behavior, but decreased impact strength.^[87] In contrast, organic salts like zinc phenylphosphinate and zinc phenylphosphonate showed nucleation ability in PA66 bypassing the issue of brittleness.^[88] Several publications describe polymeric materials as nucleating agents for polyamides. PA4.6 was found to efficiently nucleate both PA6 and PA66.^[89] Du et al. described the use of maleated poly(ethylene-co-vinyl acetate) as nucleating agent for PA6.^[90]

5.2. 1,3,5-Benzenetrisamides as nucleating agents for polyamides

It is worth mentioning that large proportion of the research on nucleating agents, besides following some general trends, still mainly relies on trial and error. If lead structures evolve, still a fine-tuning of the molecular structure in detail is necessary to find the best suited nucleating agent. Therefore a screening of a large number of potential candidates with respect to their nucleation ability in the particular polymer which has to be nucleated is indispensable.

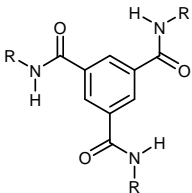
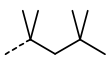
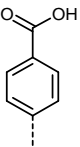
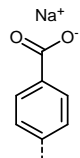
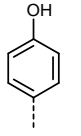
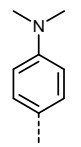
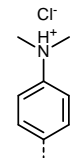
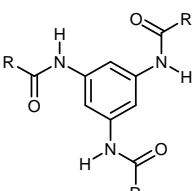
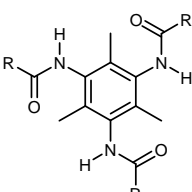
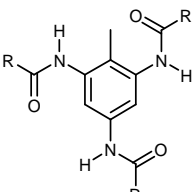
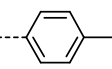
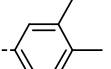
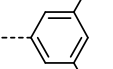
In this thesis 1,3,5-benzentrisamide derivatives were investigated for the first time as potential nucleating agents for PA6 and PA66. As polyamides exhibit both hydrophobic aliphatic chain segments as well as hydrophilic amid groups, both can either interact with a polar or nonpolar surface of the nucleating agent. On this account 1,3,5-benzentrisamide derivatives bearing nonpolar and polar peripheral substituents were investigated.

The chemical structures of the 1,3,5-benzenetrisamides screened in PA6 and PA66 by polarized optical microscopy are summarized in Table 6. The additives are based on four different cores:

- 1,3,5-Benzenetricarboxylic acid (**1-15**)
- 1,3,5-Triaminobenzene (**16-19**)
- 2,4,6-Trimethyl-1,3,5-triaminobenzene (**20-24**)
- 1,3,5-Triaminotoluene (**25-27**)

The peripheral substituents include short aliphatic, cycloaliphatic and aromatic moieties as well as polar substituents. The thermal properties of most of the screened 1,3,5-benzenetrisamide derivatives have already been discussed in detail in chapter 4.2.1.

Table 6. Chemical structures of the 1,3,5-benzenetrisamides screened in PA6 and PA66, their melting temperatures T_m (DTA) and temperatures at 10 % weight loss $T_{-10\text{wt}\%}$ (TGA, N_2 atmosphere).

	Abbr.	1	2	3	4	5
	Substituent (R)					
	T_m [°C]	subl. ^{a)}	subl.	subl.	subl.	subl.
	$T_{-10\text{wt}\%}$ [°C]	353	380	358	350	362
	Abbr.	6	7	8	9	10
	Substituent (R)					
	T_m [°C]	315	349	371	419	403
	$T_{-10\text{wt}\%}$ [°C]	342	375	380	420	418
	Abbr.	11	12	13	14	15
	Substituent (R)					
	T_m [°C]	329	394	395	374	390
	$T_{-10\text{wt}\%}$ [°C]	n.d. ^{b)}	n.d.	n.d.	n.d.	n.d.
	Abbr.	16	17	18	19	
	Substituent (R)					
	T_m [°C]	290	subl.	subl.	286	
	$T_{-10\text{wt}\%}$ [°C]	320	374	372	402	
	Abbr.	20	21	22	23	24
	Substituent (R)					
	T_m [°C]	subl.	subl.	subl.	subl.	377
	$T_{-10\text{wt}\%}$ [°C]	418	430	429	438	418
	Abbr.	25	26	27		
	Substituent (R)					
	T_m [°C]	337	353	332		
	$T_{-10\text{wt}\%}$ [°C]	408	423	421		

a) subl.: sublimation. b) n.d.: not determined due to hygroscopicity of the compound;

In contrast to the nucleation experiments in polybutylene terephthalate all screened 1,3,5-benzenetrisamides showed in the screening experiments *no indication of nucleation of PA6 and PA66*.

The typical results of the screening experiments are exemplarily shown for compound **9** in Figure 46. With compound **9** an additive was selected that showed a distinct nucleation ability in PBT. The screening results are illustrated by the micrographs recorded between crossed polarizers at different temperatures for PA6 (left) and PA66 (right). The first micrograph of PA6 at 230°C presents on the right the birefringent undissolved additive in the polymer melt. The black area corresponds to the optical isotropic polymer melt. Upon heating to 270°C, the additive dissolves and diffuses into the surrounding polymer melt. The needles partially disappear. Upon cooling with a rate of 10 K/min to again 230°C the additive crystallizes in the polymer melt into fine needles, starting from the region of the non-dissolved additive. Upon further cooling at 190°C the polymer starts to crystallize independently and not influenced by the supramolecular needles or the additive residuals. This clearly shows that no nucleation of PA6 occurs at the surface of the additive. These screening results demonstrate that even though supramolecular aggregations of the trisamides are present in the polyamide melt, the surface of the 1,3,5-benzenetrisamide derivative exhibit no epitaxial matching with the polymer and consequently no nucleation takes place.

In case of PA66 upon heating from 260°C to 290°C the additive dissolves in the melt and partially disappears. Upon cooling to again 260°C the additive remains in the dissolved state and does not crystallize in the polymer melt. At 240°C first polymer crystallites are formed independent from the dissolved or non-dissolved additive. Consequently no nucleation is induced by the additive.

Compounds **11**, **13**, and **14** bearing polar carboxylic acid- or amino-groups are too good soluble in the melt and hence did not crystallize from the polymer melt upon cooling. The sodium salt **12** or hydrochloride salt **15** of these derivatives however are nearly insoluble, but also not capable to nucleate PA6 or PA66.

Due to the absence of epitaxial matching with the polymer combined with their excellent solubility in the melt, 1,3,5-benzenetrisamides are an inappropriate class of additives for the nucleation of polyamides.

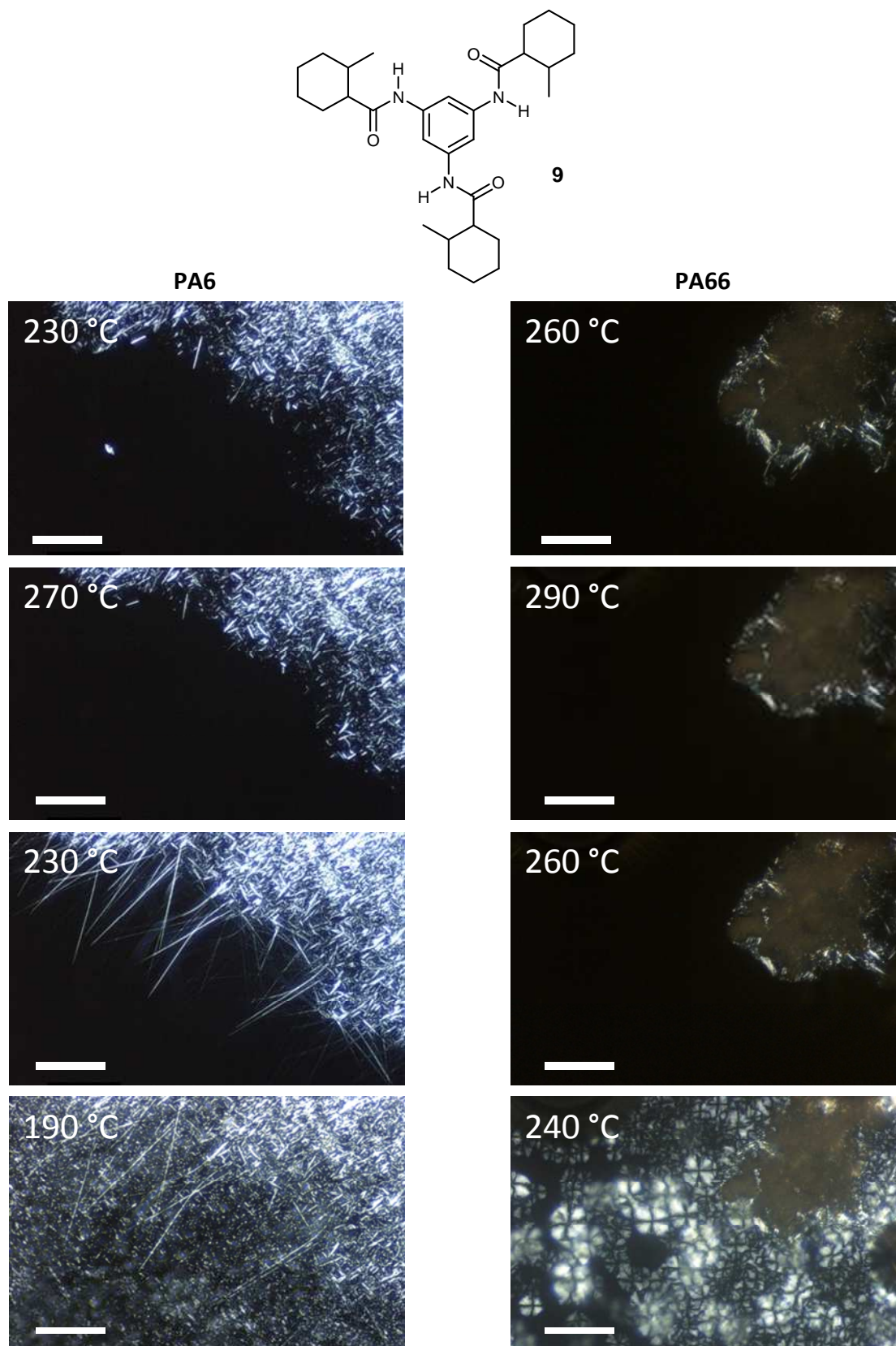


Figure 46. Optical micrographs from polarized light microscopy of the 1,3,5-benzenetrisamide **9** in PA6 (left) and PA66 (right) (scale bar 100 μm). The samples were heated, kept at 270 °C (PA6) and 290 °C (PA66) for 5 min, cooled with a rate of 10 K/min and observed at different temperatures. The additive is visible as birefringent structures in the isotropic polyamide melt (black). The non-dissolved additive diffuses into the melt and crystallizes in the case of PA6 upon cooling into fine needles, whereas in the case of PA66 the additive remains dissolved. Compound **9** is not capable to nucleate PA6 and PA66.

5.3. Bisamides as nucleating agents for polyamides

Polyamides tend to crystallize in a planar zig-zag structure as shown in chapter 5.1.^[82] Accordingly as potential nucleating agents, molecules that favor a sheet-like self assembly, similar to the schematic structure shown in Figure 47, were tested. These linear compounds consist of a central unit with hydrogen bonding units and are substituted symmetrically with aliphatic moieties.

Based on the work of Mohmeyer et al.^[55] on the nucleation of iPP with 1,4-phenylene-bisamides, two symmetrically substituted bisamides **0a** and **0b** were evaluated with respect to their nucleation potential in PA6. Both compounds were investigated in a concentration range reaching from 1.0 wt% (10000 ppm) to 0.025 wt% (250 ppm). The chemical structures of the additives and crystallization temperatures of the polymer as function of the additive concentration are shown in Figure 48. The average crystallization temperature of melt processed neat PA6 (10 samples) was at 186.5°C and is indicated by the dashed horizontal lines in Figure 48.

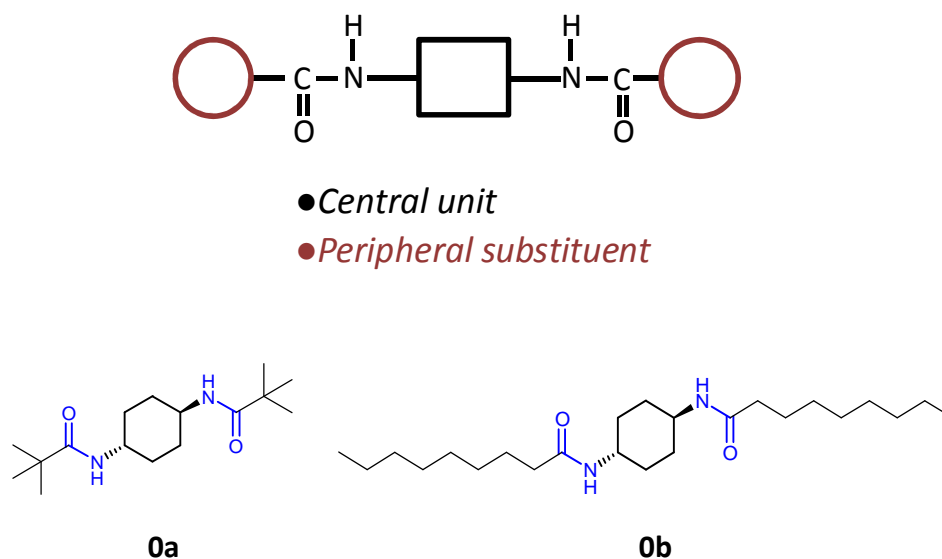


Figure 47. Schematic structure of linear bisamides consisting of a central unit, two amide linkages, and peripheral substituents (top). The bisamides **0a** and **0b** were tested as potential nucleating agents in PA6 (bottom).

As revealed in Figure 48 the bisamide derivatives **0a** and **0b** were not capable to nucleate PA6. Similar to the class of 1,3,5-benzenetrisamides, linear bisamides exhibit excellent solubility in the melt preventing the formation of supramolecular structures upon cooling. Consequently bisamides of this type are inappropriate for nucleating polyamides.

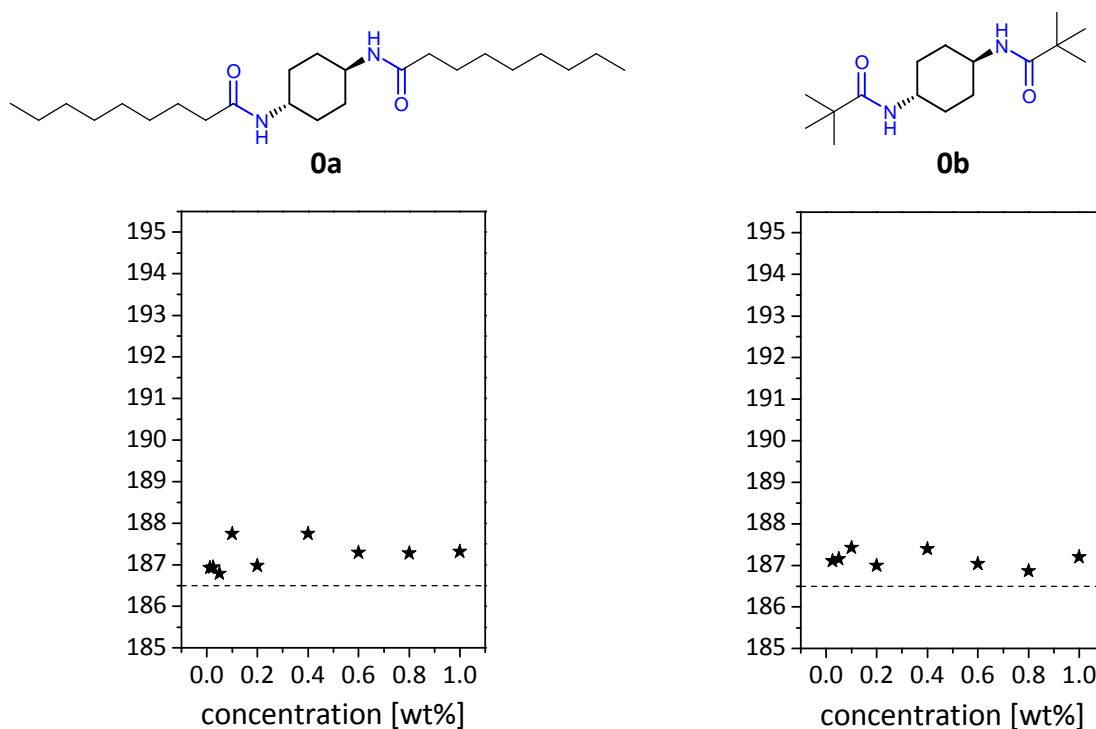


Figure 48. Crystallization temperatures of PA6 comprising the bisamide derivatives **0a** and **0b** as function of the additive concentration. The dashed lines indicate the crystallization temperature of neat PA6.

To favor supramolecular aggregation in polar ambience such as a polyamide melt the strength of the intermolecular hydrogen bonds has to be increased. Therefore in the following chapter bisurea derivatives will be discussed.

5.4. Bisureas as nucleating agents and clarifiers for polyamides

It is well known that, in contrast to the weaker amide or urethane moieties urea groups are capable to establish two hydrogen bonds between the hydrogens of the nitrogen atoms and the carbonyl oxygen.^[52, 91] This association via so-called bifurcated hydrogen bonds is schematically shown in Figure 49. Due to the strong intermolecular interactions, urea compounds combine excellent aggregation properties with high thermal stability and therefore have the potential to be applied in high melting thermoplastics.

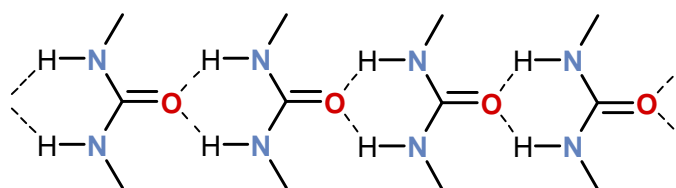


Figure 49. Schematic illustration of bifurcated hydrogen bonds formed between adjacent urea groups.

Low molecular weight compounds based on the bisurea motif have extensively been studied in the literature.^[51, 92–98] Most the work conducted on supramolecular structures through hydrogen bonding interactions of urea groups focused on the formation of organo- and hydrogels^[93, 96, 97, 99]. Also the formation of polymeric assemblies has been reported.^[92, 95, 98, 100] However, the use of bisurea molecules as supramolecular polymer additives and nucleating agents has not been investigated yet.

Therefore we synthesized a new class of C2 symmetric bisurea derivatives schematically illustrated in Figure 50 for the use as supramolecular nucleating agents in semi-crystalline polyamides.

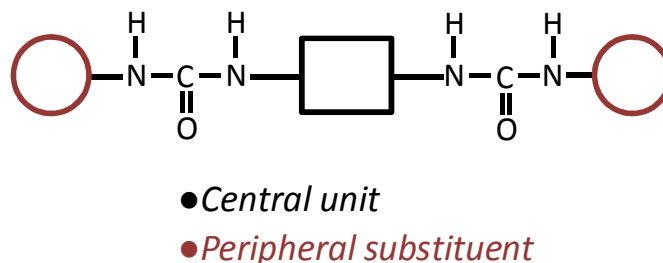


Figure 50. Schematic structure of linear bisureas consisting of a central unit, two urea linkages, and peripheral substituents.

In the following the influence of the bisurea derivatives on the crystallization behavior of PA6 and additional semi-crystalline polyamide homopolymers and copolymers will be

discussed. To establish structure property relations the structural units of the additives were systematically varied. The compounds were investigated in a concentration range from 1.5 wt% (15000 ppm) to 0.025 wt% (250 ppm) and compared with respect to their nucleation efficiency and their influence on the crystal morphology. Furthermore the influence of nucleation on the optical properties was evaluated.

5.4.1. Synthesis and Characterization

In the frame of this work, C2 symmetric bisurea derivatives were synthesized based on 1,4-substituted trans- and cis-cyclohexane central units. The synthesis can be carried out by two different synthetic routes, either starting from 1,4-diaminocyclohexane or from 1,4-cyclohexane diisocyanate. The central units were reacted to the bisurea derivatives by the addition of the corresponding isocyanates or amines under dry and inert conditions.

The synthesized compounds were characterized using $^1\text{H-NMR}$ -spectroscopy, mass spectroscopy, differential scanning calorimetry, and thermo gravimetric analysis. A summary of the characterization data for each compound is given in the Experimental Section in chapter 8.3 of this thesis.

Synthesis of trans-1,4-cyclohexyl-bisurea derivatives

The trans-1,4-cyclohexyl-bisurea derivatives were synthesized by two synthetic routes (Figure 51) employing commercially available starting materials. Route **A** comprised the reaction of a isocyanate with trans-1,4-diaminocyclohexane in dry THF. The reaction of an amine with trans-1,4-cyclohexane diisocyanate is denoted route **B**. In this case the cyclohexane core was first dissolved in THF and an equimolar amount of the corresponding substituent was slowly added under heavy stirring.

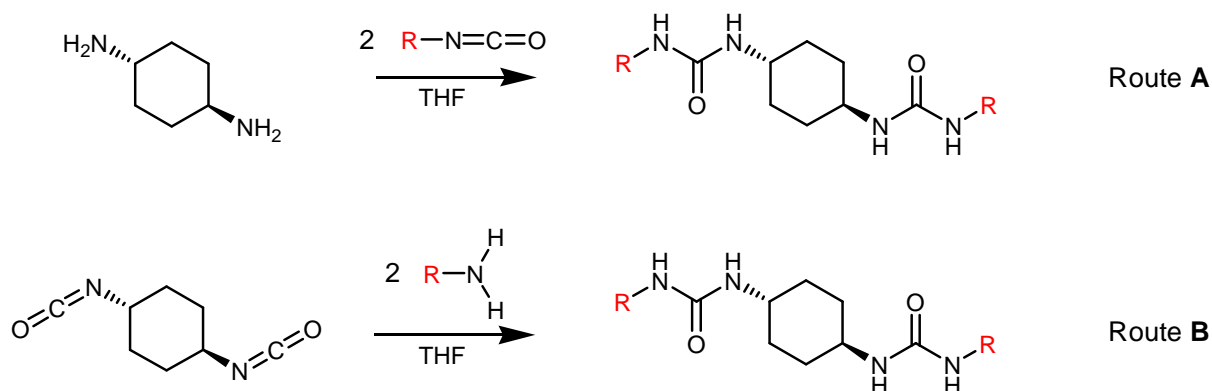
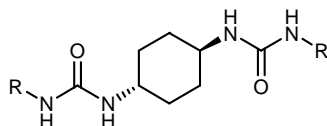


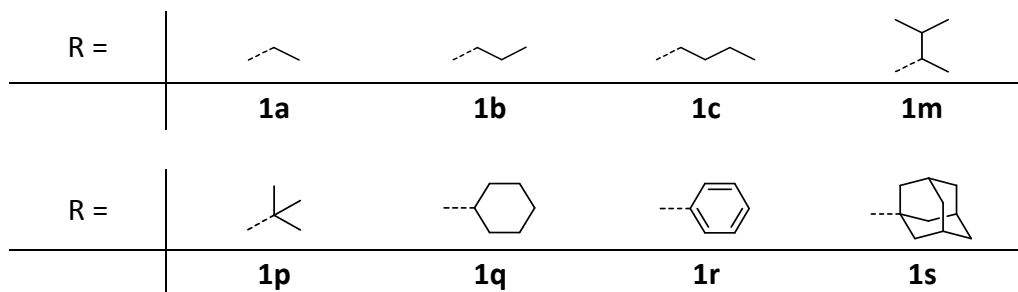
Figure 51. Synthetic routes **A** and **B** to trans-1,4-cyclohexyl-bisurea derivatives starting from trans-1,4-diaminocyclohexane and trans-1,4-cyclohexane diisocyanate.

The purification was carried out by recrystallization from organic solvents. The presence of water should be avoided as the isocyanate group reacts with traces of water to form CO₂ and the corresponding amine decreasing the total reaction yield.

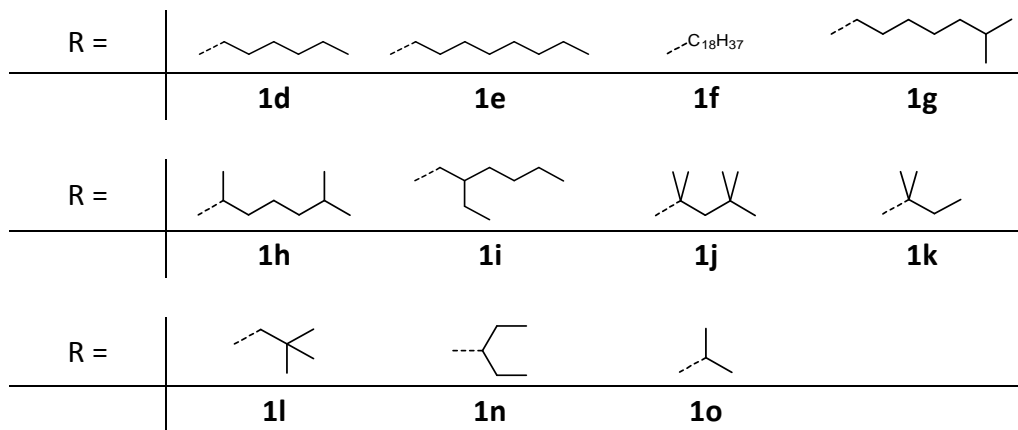
The following symmetrically substituted trans-1,4-cyclohexyl-bisurea derivatives were synthesized. As substituents linear, branched aliphatic and cycloaliphatic substituents were employed. For comparison also the phenyl substituted bisurea derivative was synthesized.



Synthetic route A:



Synthetic route B:



Synthesis of cis-1,4-cyclohexyl-bisurea derivatives

The synthesis of the cis-1,4-cyclohexyl-bisurea derivatives involved the reaction of cis-1,4-diaminocyclohexane with the corresponding substituted isocyanate, (Figure 52) similar to the synthetic route **A**, described for the trans-1,4-cyclohexyl-bisurea compounds. As cis-1,4-cyclohexane diisocyanate is not commercial available, a similar reaction via route **B** could not be realized. The purification was carried out similar to the trans-bisureas by recrystallization.

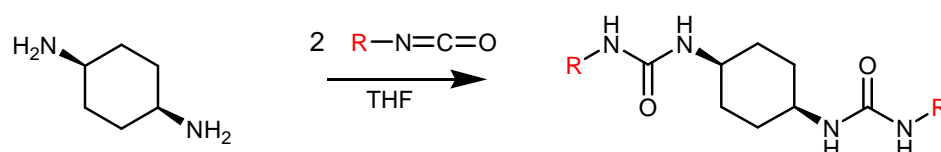
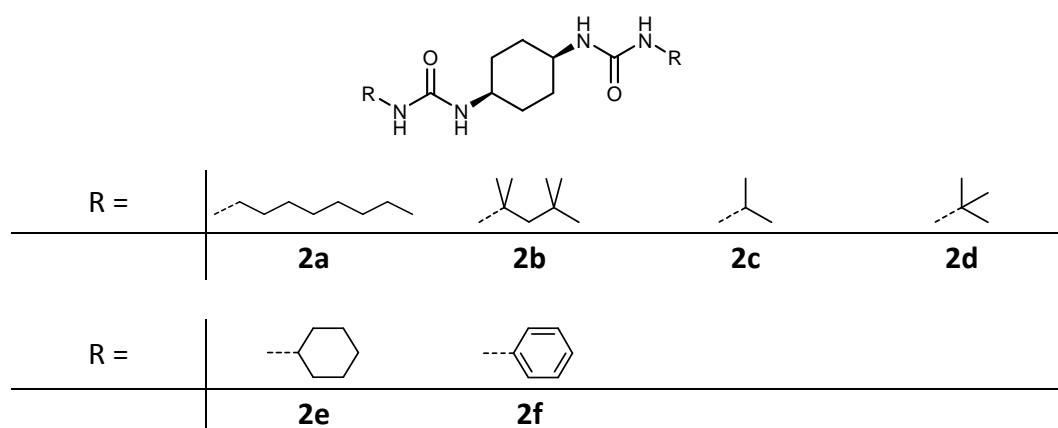


Figure 52. Synthetic route to cis-1,4-cyclohexyl-bisurea derivatives based on cis-1,4-diaminocyclohexane.

The following cis-1,4-cyclohexyl-bisurea derivatives were synthesized:

*Synthesis of asymmetrically substituted trans-1,4-cyclohexyl-bisurea derivatives*

The synthesis of the asymmetric substituted bisurea compounds was carried out in two steps (Figure 53). The first step involved the mono substitution of trans-1,4-diaminocyclohexane with cyclohexyl isocyanate yielding trans-1-(4-aminocyclohexyl)-3-cyclohexylurea, followed by an addition reaction with the second isocyanate. The synthesis of the mono-substituted compound was the more complicated reaction step. Therefore trans-1,4-diaminocyclohexane was dissolved in dried THF. The mixture was cooled in a cooling bath (isopropyl alcohol/ dry ice) and an equimolar amount of cyclohexyl isocyanate, strongly diluted in THF, was slowly added under heavy stirring. The precipitated white solid was suspended in water and acidified with HCl whereupon trans-1-(4-aminocyclohexyl)-3-

cyclohexylurea hydrochloride dissolves immediately. After filtration, the filtrate was brought to pH>8 by slowly adding NaOH and the trans-1-(4-aminocyclohexyl)-3-cyclohexylurea precipitated and could be used without further purification. The second step involved the reaction of trans-1-(4-aminocyclohexyl)-3-cyclohexylurea with the respective isocyanates in dry NMP similar to the synthesis of the symmetric substituted 4-cyclohexyl-bisurea derivatives. The purification was carried out by precipitating the solution in 1M HCl and recrystallization of the obtained solid from organic solvents.

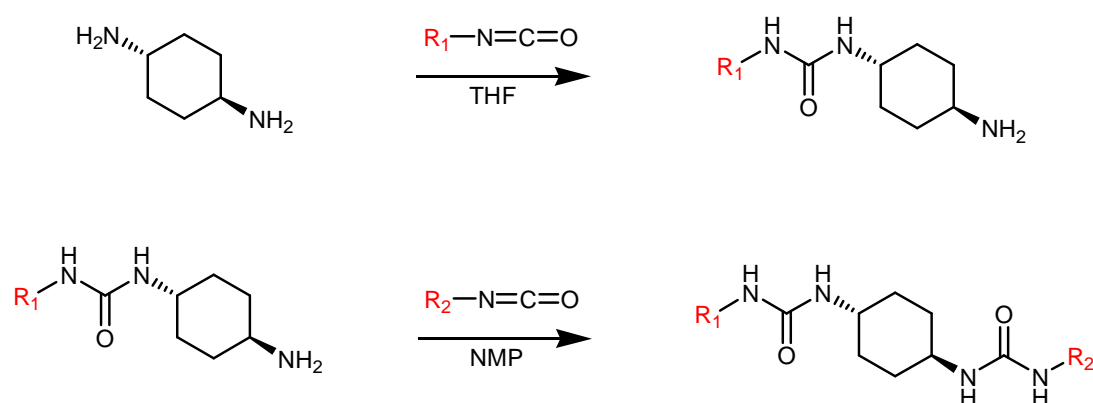
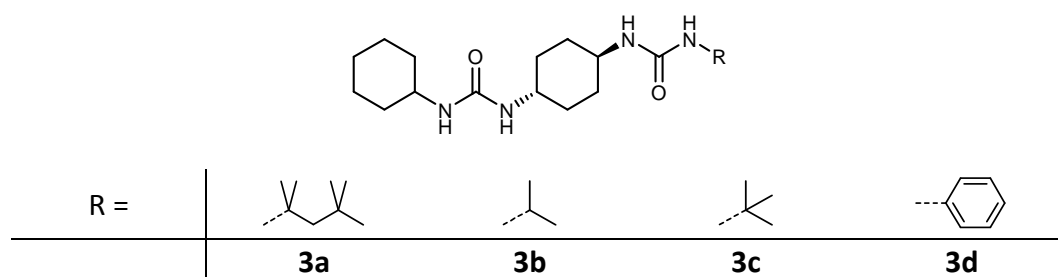


Figure 53. Synthetic route to asymmetric substituted trans-1,4-cyclohexyl-bisurea derivatives based on trans-1,4-diaminocyclohexane.

The following asymmetrically substituted trans-1,4-cyclohexyl-bisurea derivatives were synthesized. As fixed substituent for all asymmetric derivatives, cyclohexane was employed. As variable substituent branched aliphatic and phenyl substituents were employed.



NMR characterization

The spectroscopic data of all synthesized bisurea compounds is summarized in the experimental section. In the following as an example, the results of the spectroscopic characterization of the trans-bisurea derivative **1b**, the cis-bisurea **2d**, as well as the asymmetric substituted compound **3d** will be discussed in detail.

1,1'-(trans-1,4-cyclohexylene)bis(3-n-propylurea) (1b)

The $^1\text{H-NMR}$ spectrum of 1,1'-(trans-1,4-cyclohexylene)bis(3-n-propylurea) **1b** measured in $\text{CDCl}_3/\text{CF}_3\text{COOD}$ is shown in Figure 54. The N-H protons of the urea groups are not visible, due to exchange processes with the solvent. Also the signal for trifluoroacetic acid at 10.6 ppm is not presented in the spectrum. With exception of the equatorial and axial Hs of the cyclohexane core all signals could be clearly assigned to the corresponding protons. The signals of the CH-group **2** and methylene groups **3** are shifted towards higher ppm values due to their spatial proximity to the urea groups and can be found at 3.46 ppm and 3.24 ppm, respectively. The methylene group **4** can be assigned to a sextet between the signals of the equatorial and axial protons of cyclohexane core. The methyl group **5** could be assigned to the triplet at 0.96 ppm. Full substitution of trans-1,4-diaminocyclohexane was confirmed by the integration ratio of **2** and **5**.

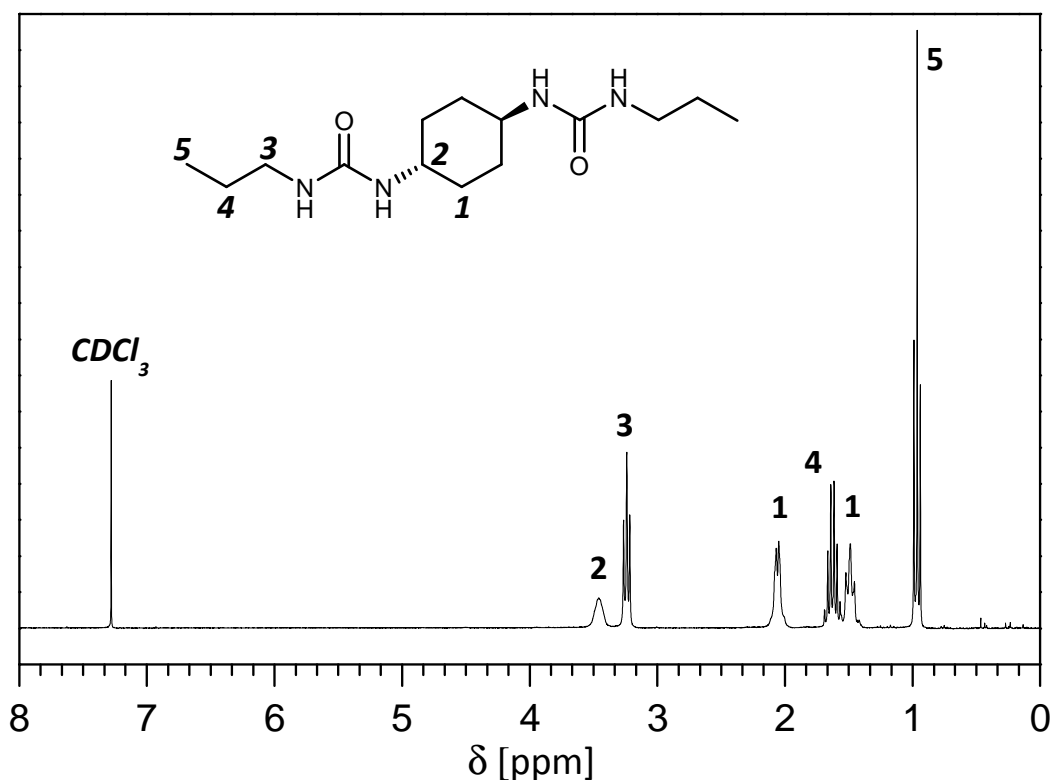


Figure 54. $^1\text{H-NMR}$ spectrum of 1,1'-(trans-1,4-cyclohexylene)bis(3-n-propylurea) **1b** ($\text{CDCl}_3/\text{CF}_3\text{COOD}$).

1,1'-(cis-1,4-cyclohexylene)bis(3-isopropylurea) (2d)

As the *cis*-1,4-cyclohexylene-bisureas are more better than their corresponding *trans*-derivatives, $^1\text{H-NMR}$ spectra of these compounds were recorded in DMSO. Figure 55 shows the spectra of compound **2d**. The N-H protons of the urea groups do not exchange with the solvent, thus being visible in the range of 5.50-5.72 ppm. Similar to **1b** the signals of the equatorial and axial protons of the cyclohexane core are not distinguishable. A duplet for the two methyl groups **6** of the isopropyl substituents can be found at 1.00 ppm. The two CH-groups **2** and **5** are again shifted to higher ppm values due to their proximity to the urea protons but can be clearly distinguished owing to their splitting.

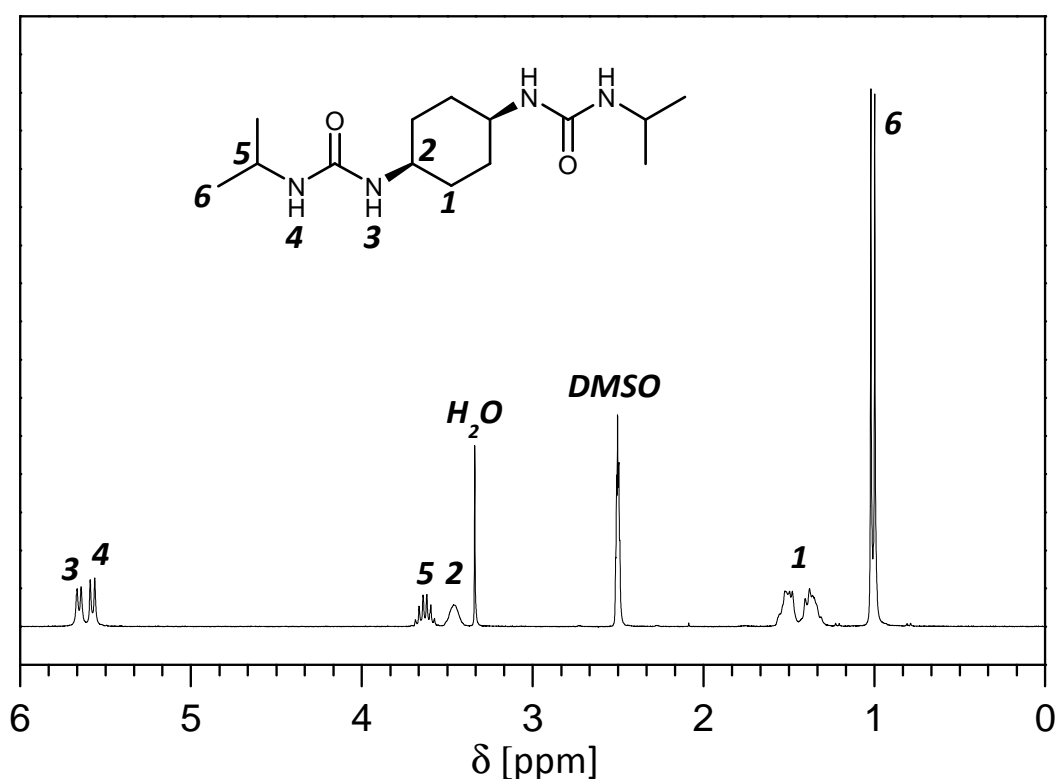


Figure 55. $^1\text{H-NMR}$ spectrum of 1,1'-(*cis*-1,4-cyclohexylene)bis(3-isopropylurea) **2d** (DMSO).

1-phenyl-3-[4-(cyclohexylcarbamoylamino)cyclohexyl]urea (3d)

The $^1\text{H-NMR}$ spectrum of 1-phenyl-3-[4-(cyclohexylcarbamoylamino)cyclohexyl]urea **3d** recorded in DMSO is shown in Figure 56. The protons of the aromatic substituent can be assigned to the signals at 6.86, 7.2, and 7.35 ppm. Due to the proximity of the phenyl-substituent to the N-H proton of the urea group **4**, the signal is shifted towards higher ppm values and can be found as a singlet at 8.29 ppm. The remaining three urea protons can be clearly distinguished owing to their integrals. The signal for the N-H protons of **5** is splitted into two duplets at 5.59 ppm because of the asymmetry of the bisurea molecule. The remaining protons of the cyclohexane core and substituent can be found as a multiplet in the range of 0.9-1.9 ppm.

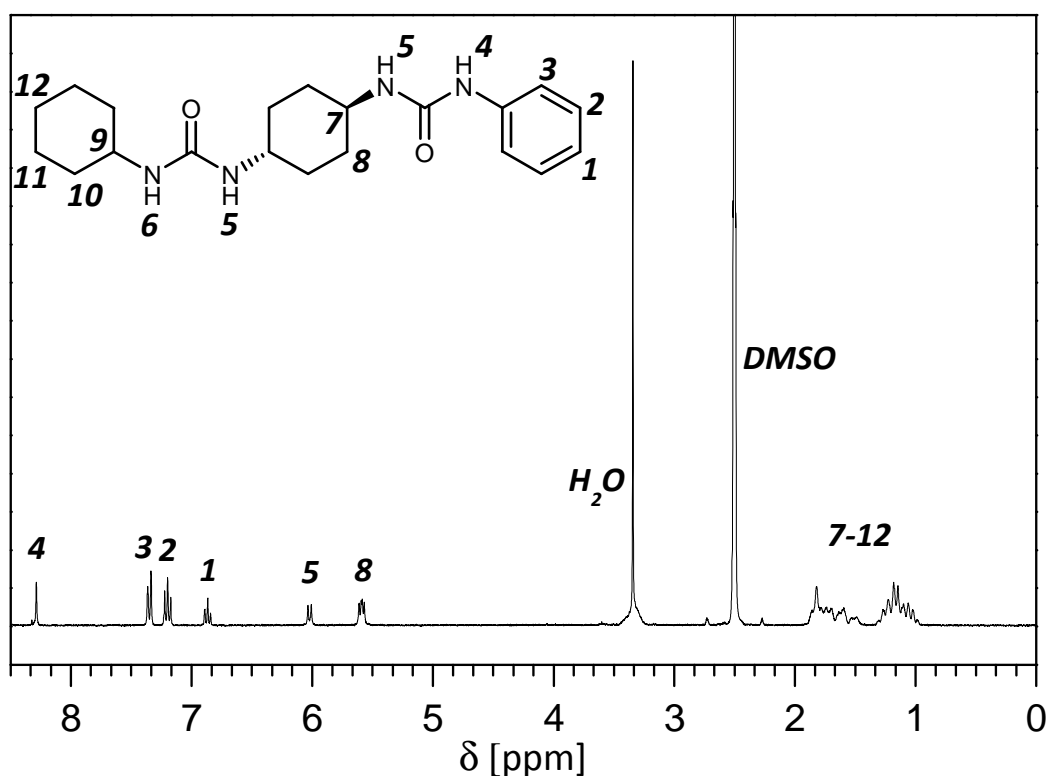


Figure 56. $^1\text{H-NMR}$ spectrum of 1-phenyl-3-[4-(cyclohexylcarbamoylamino)cyclohexyl]urea **3d** (DMSO).

5.4.2. Thermal properties

The thermal properties of the bisurea derivatives were simultaneously determined using combined thermogravimetric (TGA) and differential thermal analysis (DTA). With respect to the thermal properties the synthesized bisureas can be categorized into three categories that will be described in detail in the following.

Compounds in category **A** show a melting transition followed by the evaporation from the liquid phase. In the TGA/DTA diagram a typical melting transition can be clearly detected directly followed by a sharp and continuous weight loss. Complete evaporation is indicated by a weight loss of 100 % upon further heating. Figure 57 shows the TGA/DTA diagram of **2f**, which had a melting transition at 239°C. The 10 percent weight loss ($T_{-10 \text{ wt\%}}$) is at 256°C. The endotherm at 150°C corresponds to a solid state phase transition which could be observed by polarized optical microscopy. Similar thermal behavior was only observed for compound **2e** ($T_m = 252^\circ\text{C}$; $T_{-10 \text{ wt\%}} = 266^\circ\text{C}$).

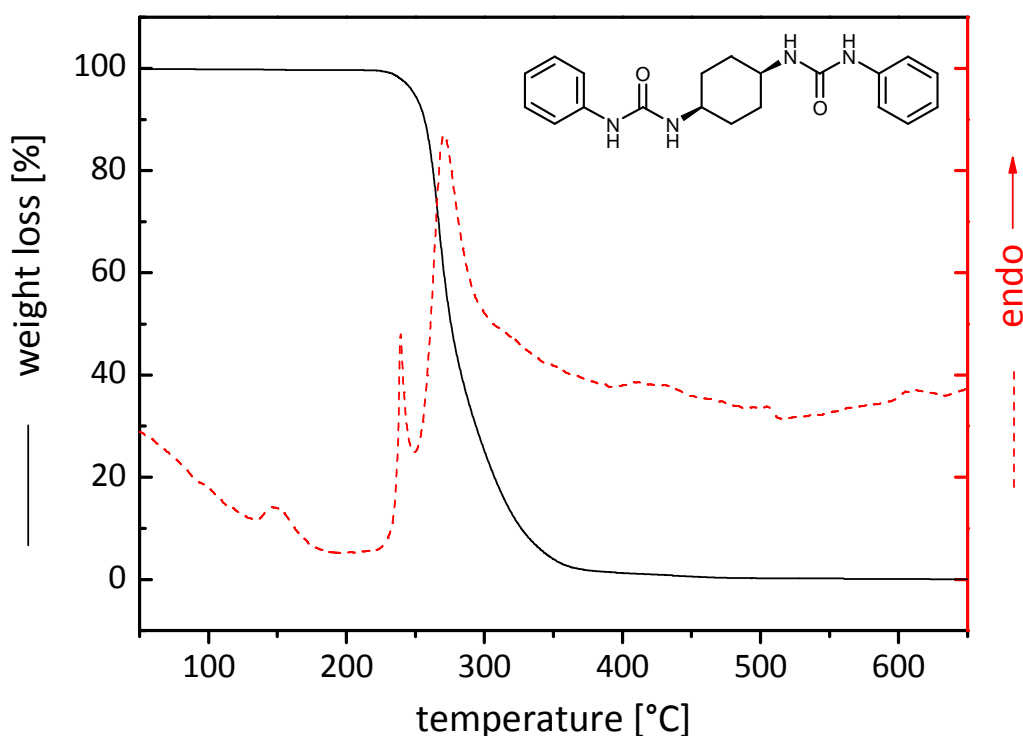


Figure 57. Thermogravimetric (solid line) and simultaneous differential thermal analysis (dashed line) analysis of **2f**, measured under nitrogen atmosphere at a heating rate of 10 K/min.

In the second category **B**, the bisurea derivatives exhibit higher melting temperatures, but melting occurs after initial sublimation. Figure 58 shows the TGA/DTA of **2d**. The first endothermic peak of the DTA curve represents the sublimation of the compound, followed by a melting transition at 319°C and subsequent evaporation from the liquid phase. The melting transition was confirmed by the disappearance of birefringent structures of the additive in polarized optical microscopy and is also indicated by a bend in the TGA curve. Similar sublimation and melting behavior was found for **1e**, **1f**, **1h**, **2a**, **2b**, **2c**, and **3c**. Their melting temperatures were in the range from 309 (**2a**) to 379°C (**3c**).

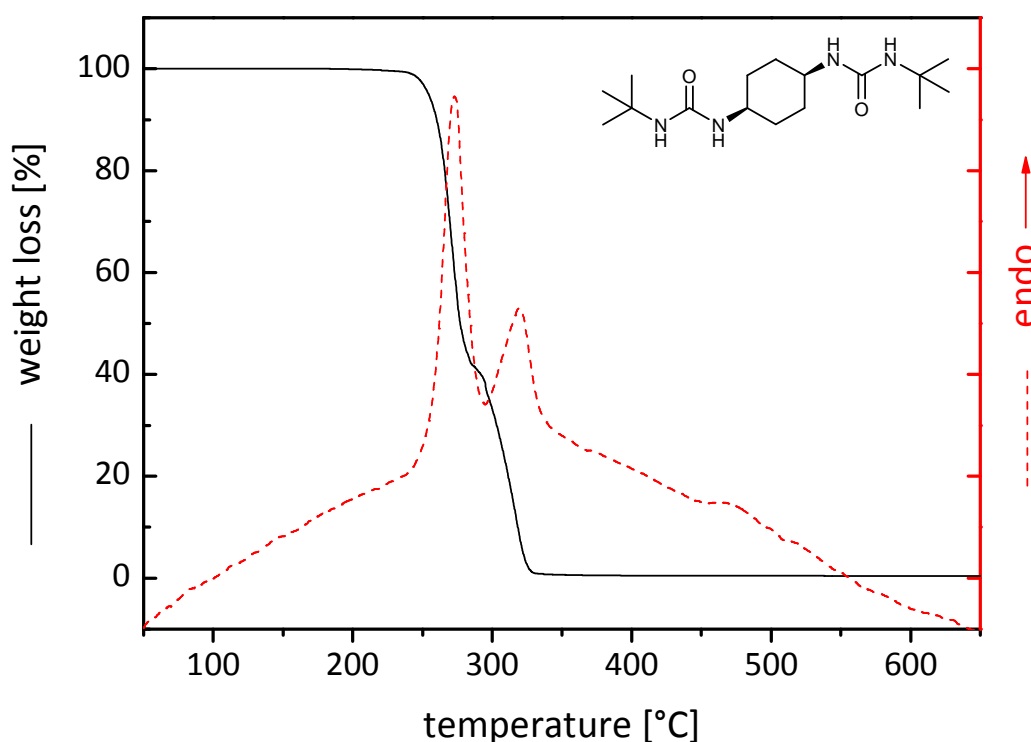


Figure 58. Thermogravimetric (solid line) and simultaneous differential thermal analysis (dashed line) analysis of **2d**, measured under nitrogen atmosphere at a heating rate of 10 K/min.

In category **C** no melting endotherm, but sublimation of the bisureas can be detected followed by thermal decomposition at elevated temperatures. Thermal decomposition was confirmed by polarized optical microscopy and is indicated by the bend in the TGA curve. Figure 59 shows the TGA/DTA diagram of **1l** which starts to sublime at around 250°C and thermal decomposition occurs above 365°C. The endotherm at 210°C corresponds to a solid state phase transition. As sublimation and thermal degradation coincide, a total weight loss of nearly 100 % is observed. The same trend was found for the compounds **1a**, **1b**, **1c**, **1d**, **1g**, **1i**, **1j**, **1k**, **1m**, **1n**, **1o**, **1p**, **1q**, **1r**, **1s**, **3a**, **3b** and **3d**.

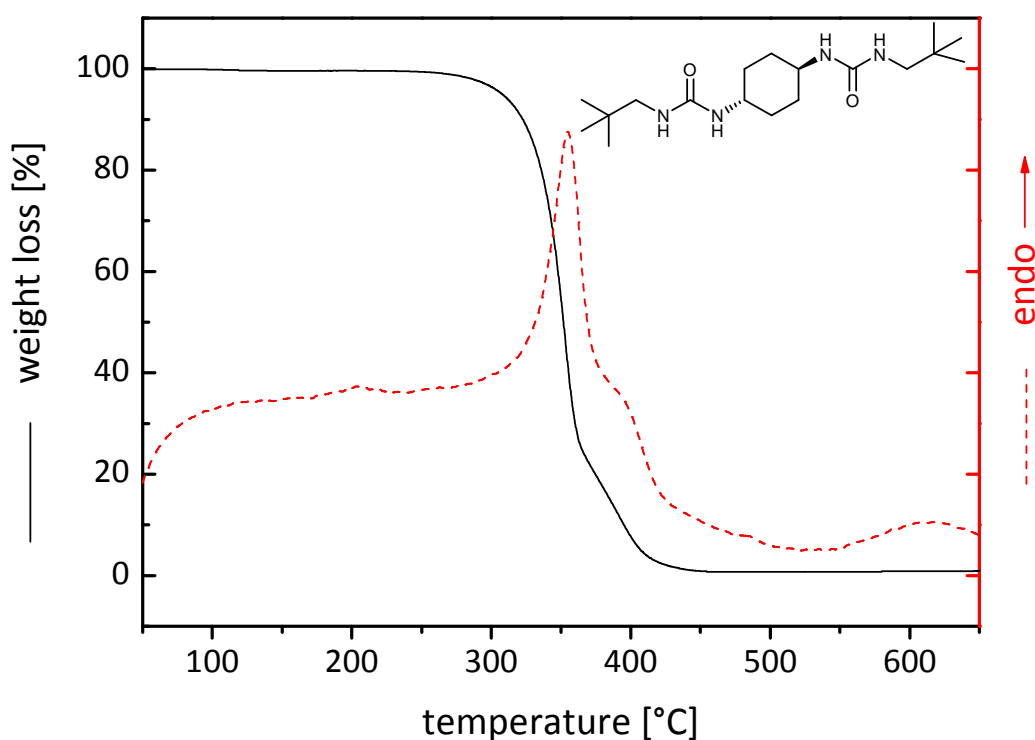
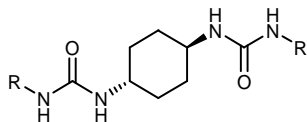


Figure 59. Thermogravimetric (solid line) and simultaneous differential thermal analysis (dashed line) analysis of **1l**, measured under nitrogen atmosphere at a heating rate of 10 K/min.

In order to establish structure property relations a short comparison of the thermal properties of the three bisurea types (symmetric trans-, cis-, and asymmetric trans-bisureas) will be given in the following.

The chemical structures of the symmetric substituted trans-bisureas, their melting temperatures and temperatures at 10 % weight loss are listed in Table 7. The investigated substituents ranged from linear and branched aliphatic to cycloaliphatic moieties. Due to the thermally stable urea linkage, all investigated compounds exhibit excellent stability reflected by high melting and weight loss temperatures. Owing to the formation of strong intermolecular hydrogen bonds, a large number of the investigated trans-bisureas sublime completely without melting, indicated by a weight loss of 100 %. Out of 16 symmetric trans-bisureas, 13 sublimed without melting. In contrast the compounds with more flexible long linear (**1e**, **1f**) or long branched aliphatic substituents (**1h**), melted at high temperatures. The highest melting transition was observed for **1e** with a T_m of 370°C.

Table 7. Chemical structures of the symmetric substituted trans-bisureas, their melting temperatures T_m (DTA) and temperatures at 10 % weight loss $T_{-10\text{wt}\%}$ (TGA, N_2 atmosphere).


Abbr.	1a	1b	1c	1d
Substituent (R)				
T_m [°C]	subl. ^{a)}	subl.	subl.	subl.
$T_{-10\text{wt}\%}$ [°C]	316	328	329	306
Abbr.	1e	1f	1g	1h
Substituent (R)		$C_{18}H_{37}$		
T_m [°C]	370	345	subl.	355
$T_{-10\text{wt}\%}$ [°C]	315	278	286	299
Abbr.	1i	1j	1k	1l
Substituent (R)				
T_m [°C]	subl.	subl.	subl.	subl.
$T_{-10\text{wt}\%}$ [°C]	290	312	319	323
Abbr.	1m	1n	1o	1p
Substituent (R)				
T_m [°C]	subl.	subl.	subl.	subl.
$T_{-10\text{wt}\%}$ [°C]	317	310	319	303
Abbr.	1q	1r	1s	
Substituent (R)				
T_m [°C]	subl.	subl.	subl.	
$T_{-10\text{wt}\%}$ [°C]	332	309	339	

a) subl.: sublimation.

The thermal properties of the symmetric substituted cis-bisureas are shown in Table 8. Due to the cis-configuration of the cyclohexane core, the urea groups are either oriented in axial or equatorial position (chair conformation) or both in axial position (boat conformation). In both conformations the molecules are less symmetric than their trans-analogues, leading to a weakening of the intermolecular hydrogen bonds. Therefore all cis-bisureas undergo a melting transition independent from their substituent. The lowest melting temperatures were found for the cyclohexyl- and phenyl-substituted compounds **2e** and **2f** with a T_m of 252 and 236°C. All cis-bisureas showed comparably low thermal stability ($T_{-10 \text{ wt\%}}$) between 243 and 266°C, whereas their corresponding trans-derivatives exhibit $T_{-10 \text{ wt\%}}$ between 290 and 339°C.

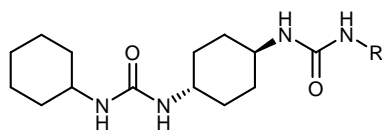
Table 8. Chemical structures of the symmetric substituted cis-bisureas, their melting temperatures T_m (DTA) and temperatures at 10 % weight loss $T_{-10 \text{ wt\%}}$ (TGA, N_2 atmosphere).

Abbr.	2a	2b	2c	2d
Substituent (R)				
T_m [°C]	308	325	309	319
$T_{-10 \text{ wt\%}}$ [°C]	254	243	265	264

Abbr.	2e	2f
Substituent (R)		
T_m [°C]	252	236
$T_{-10 \text{ wt\%}}$ [°C]	266	258

The asymmetric substituted trans-bisurea derivatives **3a-3d** showed similar thermal stability as the symmetric substituted derivatives **1a-1s** (Table 9). With exception of **3c** all bisureas sublimed directly without melting. **3c** exhibits the highest melting temperature of all investigated bisureas with 379°C. In all cases $T_{-10 \text{ wt\%}}$ was above 300°C.

Table 9. Chemical structures of asymmetric substituted trans-bisureas, their melting temperatures T_m (DTA) and temperatures at 10 % weight loss $T_{-10\text{wt}\%}$ (TGA, N_2 atmosphere).



Abbr.	3a	3b	3c	3d
Substituent (R)				
T_m [°C]	subl. ^{a)}	subl.	379	subl.
$T_{-10\text{wt}\%}$ [°C]	302	346	308	323

a) subl.: sublimation.

5.4.3. Nucleation and optical properties of PA6

As described before the nucleation ability of a supramolecular polymer additive depends on the individual chemical structure. In the self-assembled structure the surface induces nucleation via epitaxial matching. In addition the additive concentration and the solubility of the additive in the polymer melt has an influence. The optical properties are usually governed by scattering due to differences in refractive index of the crystalline and amorphous phase or anisotropic structures. A reduction in spherulite size by the addition of a nucleating agent usually leads to a certain decreased scattering enhancing the transmission and clarity of a polymeric material to some degree. In some cases special compounds are capable to improve transmission, clarity and in particular haze to a very large extent. These additives are called “clarifiers”.

In the following the influence of the chemical structure on the polymer crystallization temperature and the optical properties of PA6 will be investigated in detail. Structure property relations will be systematically discussed. The additives were investigated in a concentration range from 1.5 wt% (15000 ppm) to 0.025 wt% (250 ppm). The different concentrations were prepared by diluting the initial additive concentration of 1.5 wt% in the melt with a mixture of the initial PA6/additive powder blend and neat PA6, yielding the following dilution series: 1.3 wt%, 1.0 wt%, 0.8 wt%, 0.6 wt%, 0.4 wt%, 0.2 wt%, 0.1 wt%, 0.05 wt%, and 0.025 wt%. Optical properties were measured on injection molded platelets with a thickness of 1.1 mm.

In order to explore possible effects of transamidification or decomposition reactions of the polyamide under processing conditions on the crystallization behavior, a blank “concentration” series with neat PA6 was compounded. As shown in Figure 60 the crystallization temperatures for all ten processing runs are mainly within 1°C. The increased crystallization temperature of the first run can originate from impurities in the miniextruder. Therefore cleaning runs were conducted. The calculated mean value for the $T_{c,p}$ of neat PA6 is $186.5^{\circ}\text{C} \pm 0.5^{\circ}\text{C}$. The degree of crystallinity of PA6 was determined from the enthalpy of the first melting endotherm and is $25.2 \% \pm 0.5^{\circ}\text{C}$.^[13]

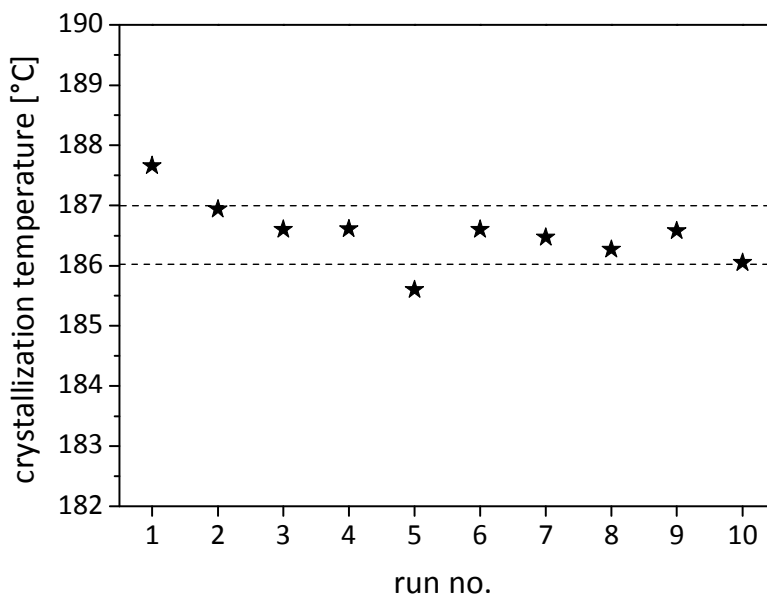


Figure 60. Crystallization temperature of neat PA6 versus the number of processing runs. For each run the samples were compounded for 4 min at 250°C.

It is well-known that the processing conditions, such as melt temperature, undercooling and shear stress have a strong influence on the crystallization kinetics of semi-crystalline polymers and particular polyamides.^[82, 101] The effect of melt processing, as described in the experimental section, on the crystallization temperature of PA6 is shown in Figure 61. The peak polymer crystallization temperature of the PA6 granulate at 174.1°C is considerably lower compared to the compounded material. The compounded PA6 has a $T_{c,p}$ at 186.5°C. In addition the crystallization exotherm was found to be broader. This result can be attributed to the formation of orientation induced chain alignment in the polyamide melt during processing.^[102] This so-called “memory effect” is particularly marked in polyamides due to the formation of H-bonds between the functional amide groups that even in the melt remain fixed to some extent.^[82, 102, 103] Consequently, as the crystallization kinetics are very sensitive towards the processing history, all samples have to be prepared under identical processing conditions, also the reference

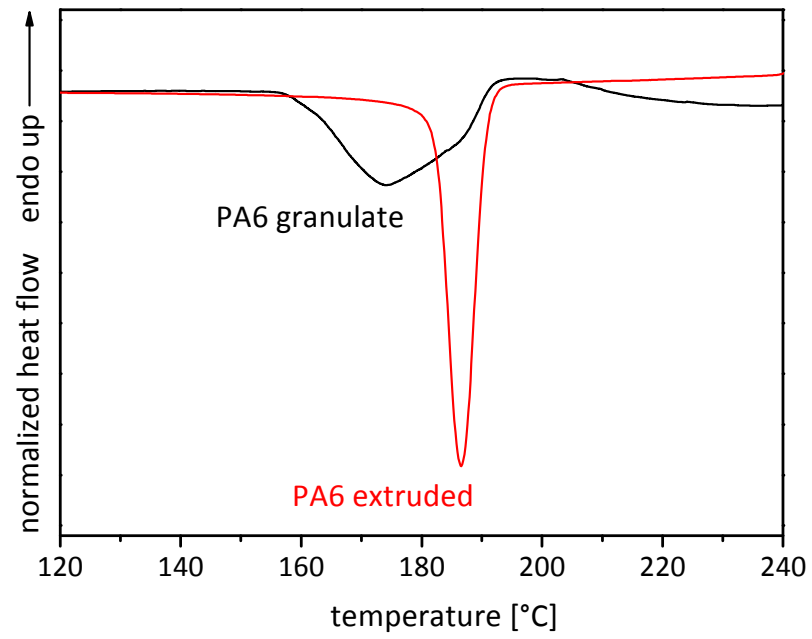


Figure 61. Differential scanning exotherms of PA6 granulate (black) and melt processed PA6 (red) at a cooling rate of 10 K/min.

In the following, the synthesized bisurea compounds will be compared systematically in sets to reveal structure property relations with respect to the nucleation and optical properties of PA6. These properties will be discussed as function of the additive concentration. The first set compares *symmetrical trans-bisureas with linear aliphatic substituents* that vary in chain length from C2 to C18. The second to the fourth set compares *symmetrical trans-bisureas with branched substituents*. The fifth set discusses *symmetrical trans-bisureas with cycloaliphatic substituents*. The sixth set compares *asymmetrically substituted trans-bisureas* and the seventh set *symmetrically substituted cis-bisurea* derivatives.

5.4.3.1. Symmetrical trans-1,4-cyclohexane bisurea derivatives with linear substituents

In this chapter the nucleation and optical properties of the bisurea derivatives **1a** – **1f** with linear substituents in PA6 will be discussed. The polymer crystallization temperature ($T_{c,p}$) was obtained from DSC measurements, reported as the temperature at the exothermic minimum upon cooling from the melt. Exemplary DSC cooling traces of neat PA6 and PA6 comprising different concentrations of the n-octyl substituted bisurea **1e** are presented in Figure 62. Upon addition of **1e** the crystallization temperature of PA6 is distinctly increased. At a high concentration of 1.0 wt% the polymer crystallization temperature is at 192.1°C. At lower additive concentrations the $T_{c,p}$ decreases. At a concentration of 0.1 wt% $T_{c,p}$ is at 191.5°C.

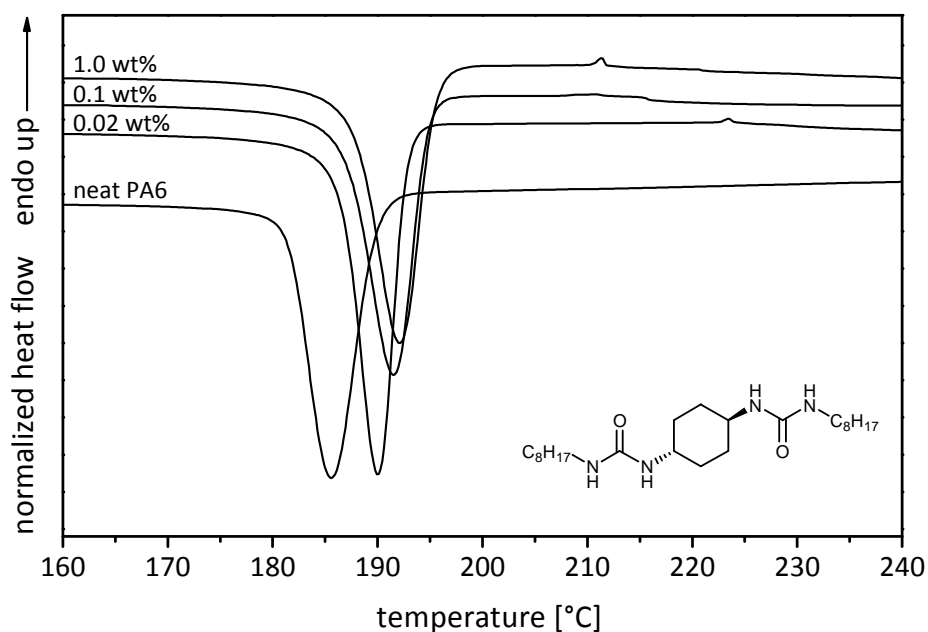


Figure 62. Differential scanning exotherms of neat PA6 and PA6 comprising different concentrations of **1e** as indicated.

The optical properties clarity and haze were determined according to ASTM D-1003 on injection molded platelets with a thickness of 1.1 mm. Figure 63 illustrates the effect of the addition of the propyl-substituted bisurea derivative **1b** on the visual appearance of injection molded PA6 platelets. On the left is neat PA6 for comparison with a clarity of 68 % and a haze of 98 %, in the middle PA6 containing 0.2 wt% of **1b** with a clarity of 96% and a haze of 79 % and on the right PA6 containing 1.3 wt% of **1b** with a clarity of 96 % and a haze of 44 %.



Figure 63. Effect of the addition of **1b** on the visual appearance of injection molded PA6 platelets. Left: neat PA6; middle: PA6 comprising 0.2 wt% of **1b**; right: PA6 comprising 1.3 wt% of **1b**.

The chemical structures of the bisurea derivatives **1a** – **1f** with linear substituents, their nucleation and optical properties are compared in detail in Figure 64 A and B. The additives are presented with increasing length of the aliphatic moieties. The substituents were varied from ethyl **1a**, n-propyl **1b**, n-butyl **1c**, n-hexyl **1d**, n-octyl **1e**, to n-octadecyl **1f**. The top row of Figure 64 shows the polymer crystallization temperature ($T_{c,p}$) of PA6 as function of the additive concentration. Remarkably with all trans-bisureas the crystallization temperature of PA6 could be distinctly increased.

For example the $T_{c,p}$ values for PA6 steeply increases by the addition of the ethyl substituted bisurea derivative **1a**. At a concentration of 0.02 wt% the crystallization temperature of PA6 is increased by 6.3°C from 186.5°C to 192.8°C. At higher additive concentrations the $T_{c,p}$ further increases to a maximum of 194.6°C at 0.4 wt%. Above 0.4 wt% the polymer crystallization temperature only varies marginally with the amount of additive. A plateau is reached with a mean $T_{c,p}$ value of 194.2°C indicated by the dashed horizontal line in Figure 64. Increasing the chain length from C2 to C18 has a noticeable influence on the nucleating ability of the bisurea derivatives. The small change in the chemical structure of the peripheral substituents from ethyl to n-propyl results in a decrease of the mean $T_{c,p}$ plateau value to 193.5°C. However **1b** is capable to efficiently nucleate PA6 at a concentration as low

as 0.02 wt% with a $T_{c,p}$ of 191.9°C. Additive **1c** with n-butyl substituents is a less efficient nucleating agent for PA6 indicated by a lower mean $T_{c,p}$ plateau value of 192.5°C. With further increasing the chain length and flexibility of the linear aliphatic substituents the mean plateau values for the polymer crystallization temperature decrease in the series from n-hexyl **1d** (192.5°C) over n-octyl **1e** (192.3°C) to n-octadecyl **1f** (191.5°C).

The optical properties clarity and haze of injection molded samples with a thickness of 1.1 mm are presented in the bottom graphs of Figure 64. In the case of the ethyl substituted derivative **1a** the clarity increases dramatically upon addition of already slight amounts of additive. The clarity reaches a plateau at around 97 % for concentrations exceeding 0.5 wt%. The change in length and flexibility of the peripheral substituent to n-propyl, n-butyl or n-hexyl does not result in a noticeable change in clarity. The values remain remarkably high. Upon further increasing the length of the substituent to n-octyl or n-octadecyl the clarity slightly decreases. For the n-octyl substituted derivative **1e** the values deteriorate from 96.1 % to 90.1 % with increasing additive concentration which can be attributed to scattering on nondissolved additive particles due to an insufficient mixing during the powder blending and processing steps. For **1f** the highest clarity is 92.4 % at a concentration of 1.5 wt%.

The haze values are presented in the bottom row of Figure 64. In the case of iPP in these kind of diagrams usually an “optimum” concentration for minimum haze is observed.^[6, 9] At very low concentrations the optical properties deteriorate due to less available nucleation sites. However if the amount of additive exceeds the “optimum” concentration, scattering occurs on undissolved additive particles and the haze increases. Regarding the bisureas investigated in this thesis, a deviant behavior was found. For **1a** the values for haze steadily decrease with increasing additive concentration in agreement with the excellent solubility of the bisureas in the polyamide melt. The lowest haze was 47 % at a concentration of 1.5 wt%. Compound **1b** with n-propyl substituent displayed an even lower haze with 41 % at 1.5 wt%. If the haze values at 1.0 wt% are compared with increasing length of the peripheral substituents an increase of the haze values is observed. The haze values increase from n-propyl < ethyl < n-butyl < n-hexyl < n-octyl < n-octadecyl. It is interesting to note that although **1e** and **1f** are still efficient nucleating agents for PA6 the haze remains at a very high value.

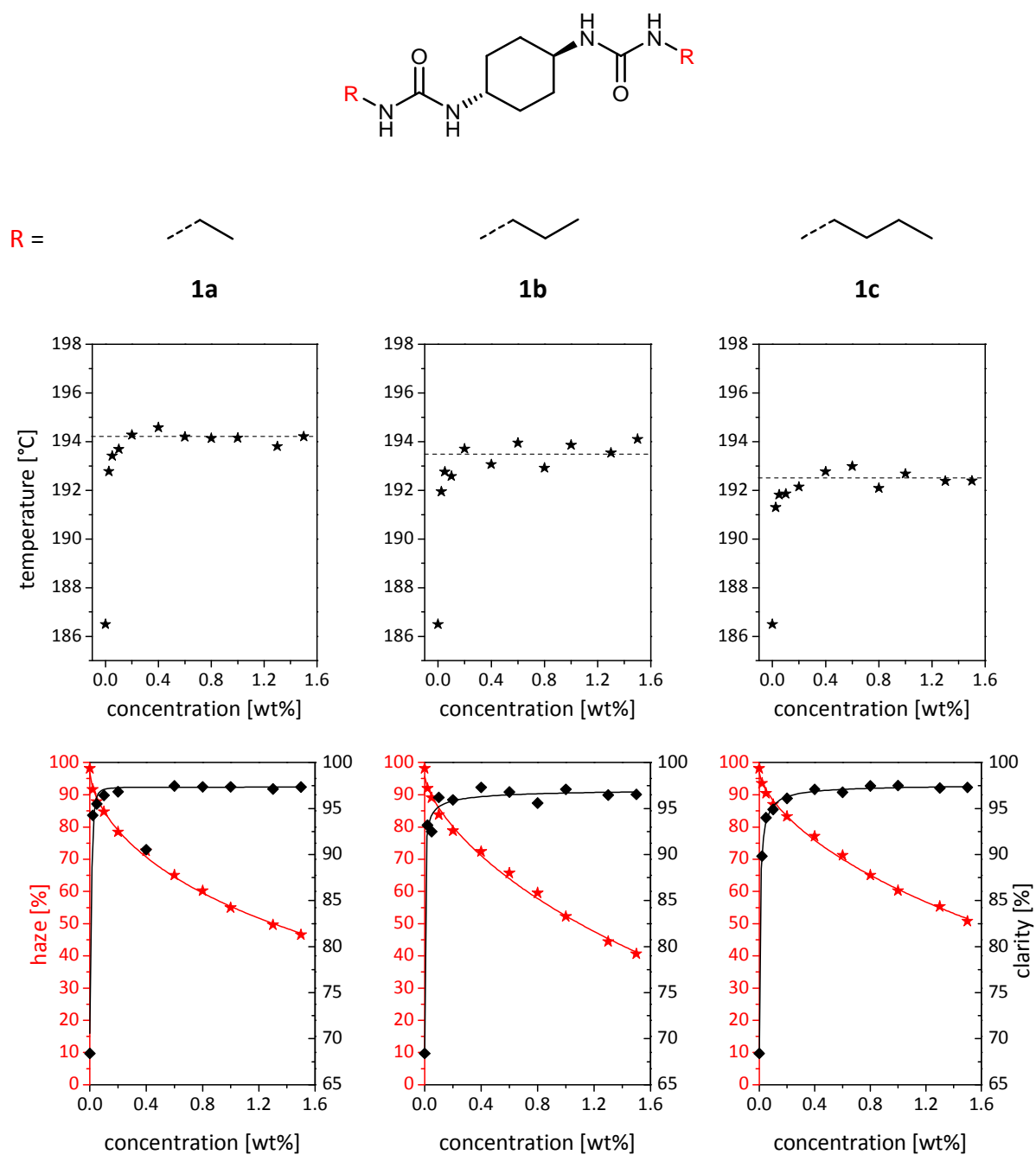


Figure 64A. Polymer crystallization temperatures ($T_{c,p}$ ★) (top graphs) and the optical properties haze (★) and clarity (◆) (bottom graphs) of PA6 comprising the trans-bisureas **1a** – **1c** as function of the additive concentration. The dashed lines indicate the plateau in the polymer crystallization temperature PA6.

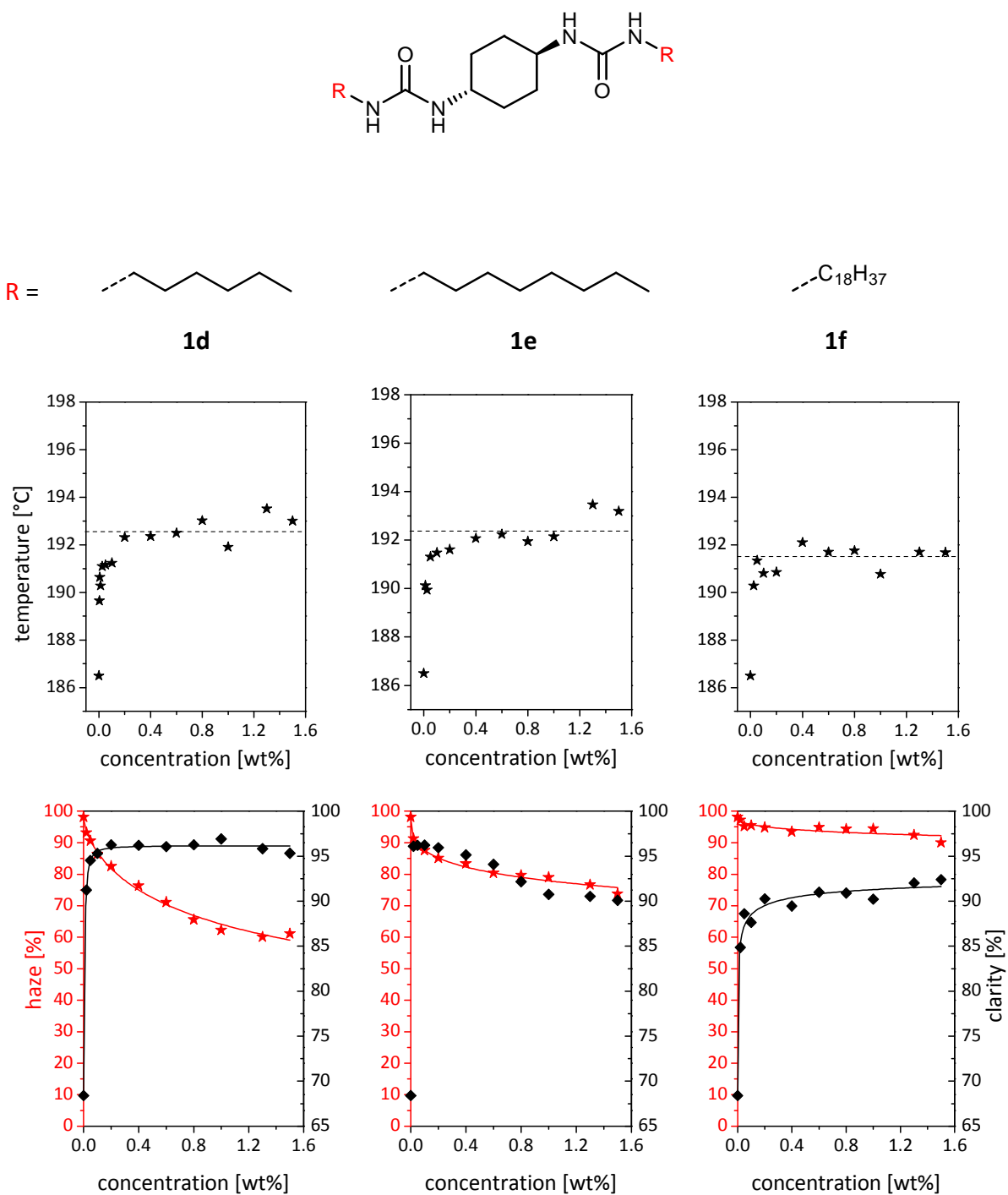


Figure 64B. Polymer crystallization temperatures ($T_{c,p}$ ★) (top graphs) and the optical properties haze (★) and clarity (◆) (bottom graphs) of PA6 comprising the trans-bisureas **1d** – **1f** as function of the additive concentration. The dashed lines indicate the plateau in the polymer crystallization temperature PA6.

5.4.3.2. Symmetrical trans-1,4-cyclohexane bisurea derivatives with branched substituents

The second set of additives compares longer branched substituents that are structural isomers of the n-octyl derivative **1e** described before. The chemical structures and their nucleation and optical properties are presented in Figure 65. For **1g** with 6-methylheptane substituents the mean $T_{c,p}$ plateau value was 192.9°C and thus in the range of the n-butyl or the n-hexyl substituted derivatives from the above discussed series of additives. However the values for the polymer crystallization temperature deteriorate for concentrations exceeding 1.0 wt%, which can be attributed to an insufficient distribution of the additive in the PA6 melt during processing. The change in chemical structure of the peripheral substituent from 6-methylheptane to 1,5-dimethylhexyl substituents **1h** does not result in improved nucleation properties. The mean $T_{c,p}$ plateau value for **1h** is 192.9°C. For the 2-ethylhexyl substituted derivative **1i** the mean polymer crystallization temperature at the plateau is approximately in the same range with 193.3°C. In contrast to the nucleation properties that are only little affected by the subtle changes in chemical structures, the introduction of branches has strong influence on the optical properties of PA6. The less beneficial nucleation ability of **1g** at higher additive concentrations is also reflected in lower clarity values. Similar to the n-octyl substituted derivative **1e** from the first series of additives, the clarity decreases slightly with the amount of additive due to an insufficient distribution in the polymer matrix. The clarity decreases from 95.1 % at 0.2 wt% to 89.1 % at a concentration of 1.5 wt%. For **1h** and **1i** high clarity values are obtained that are persistent throughout the investigated concentration range.

For **1g** with 6-methylheptane substituent the values for haze steadily decrease with increasing amount of additive. The lowest haze is 73 % at a concentration of 1.5 wt% and thus similar to the values obtained for **1e** (74 %) from the first series of additives. It is important to note that branching in proximity to the α -C atoms of the substituents as in **1h** and **1i** had severe effect on the optical properties of PA6. For **1h** the introduction of branches decreases the haze from 98 % of neat PA6 to 22 % at an additive concentration of 1.5 wt%, which corresponds to an overall decrease of 76 %. The introduction of an ethyl group in β -position as in **1i** results in a decrease of haze to 44 %, also at 1.5 wt%. Following these results it is likely to assume that branching of the peripheral substituents in close proximity to the urea group, especially in α -position to the nitrogen atom, strongly favors the clarification ability of the bisurea derivatives.

The third set of additives compares four bisurea derivatives with branched peripheral substituents, that were varied from 3-pentyl **1l**, 1,2-dimethylpropyl **1m**, neopentyl **1n** to iso-propyl **1o**. The derivatives **1l**, **1m** and **1n** are structural isomers with 5 C-atoms each. All compounds within this series were capable to efficiently promote the nucleation of PA6. For **1l** with 3-pentyl substituent the mean $T_{c,p}$ plateau values was about 192.1°C. The 1,2-dimethylpropyl substituted derivative **1m** at higher concentrations was less distributed in the polymer melt, thus the $T_{c,p}$ values decrease with the amount of additive. The neopentyl and iso-propyl substituted derivatives displayed the highest mean $T_{c,p}$ plateau values within the series. For **1n** the value is 193.1°C and for **1o** 192.8°C.

Within this set of additives all compounds displayed clarity values above 90 %. However the lack of distribution in the polymer matrix of **1m** is also reflected in the values for clarity. The values vary slightly between 95 and 98 % in the investigated concentration range, whereas the values remained almost constant for **1l**, **1n** and **1o**. One of the most important observations is that the introduction of branches in proximity to the urea groups strongly improves the haze values. For **1l** the values for haze steadily decrease with the additive concentration, with 30 % at a concentration of 1.5 wt%. Surprisingly, despite the missing branch in α -position to the nitrogen atom, **1l** has the most pronounced effect on the optical properties of PA6 within this series of additives. This result is even more interesting as **1l** shows lower nucleation ability compared to **1l**, **1n** and **1o**. This once more demonstrates that a direct correlation between the nucleation efficiency and clarifying of an additive cannot be drawn. Compound **1m** with 1,2-dimethylpropyl substituent displayed similar good optical properties with a haze as low as 42 %. For **1n** with neopentyl substituent the haze is higher with 57 % at 1.5 wt%, whereas **1o** featured a haze value at 1.5 wt% of around 36%.

To further corroborate the observation that the introduction of branches in close proximity to the urea groups are responsible for the good clarification ability of the bisureas, derivatives with highly branched substituents, preferably in α -position to the urea groups are discussed in the following.

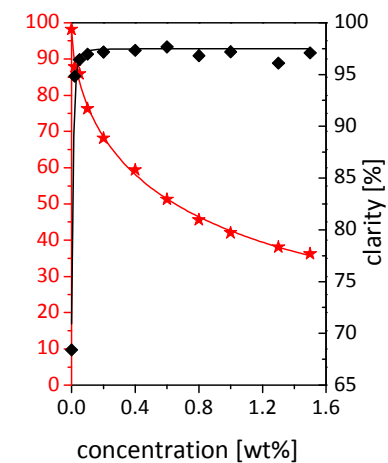
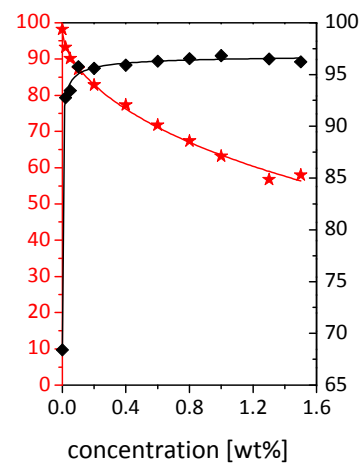
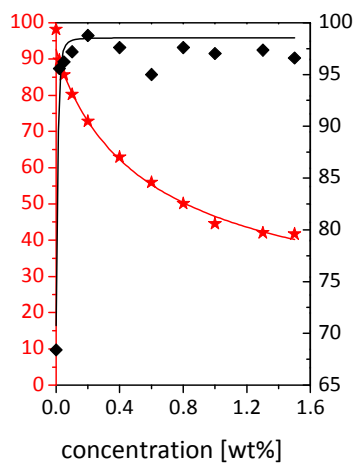
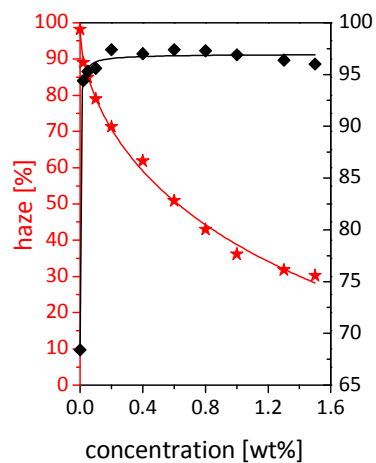
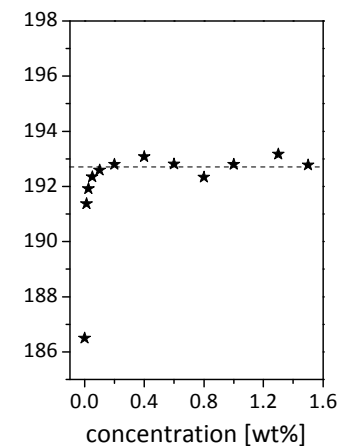
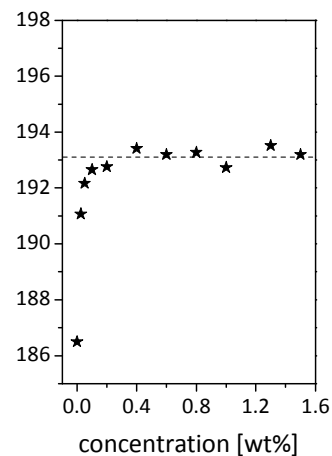
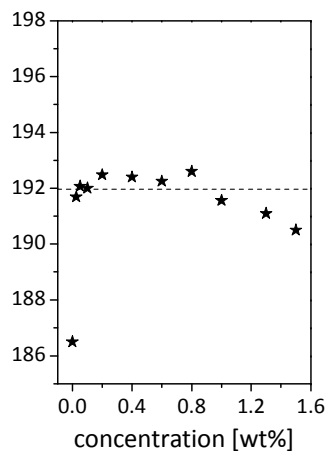
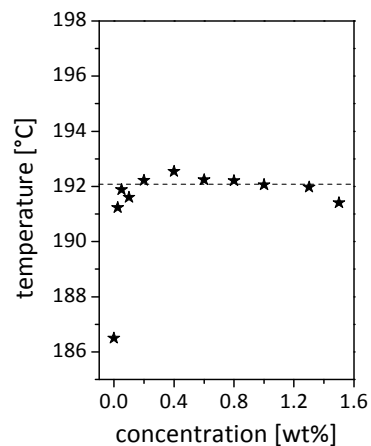
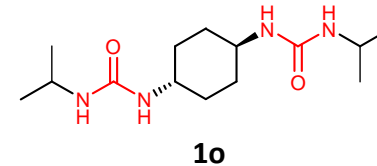
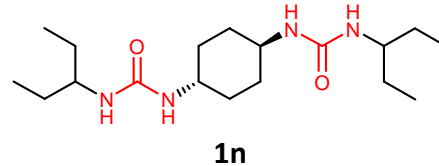
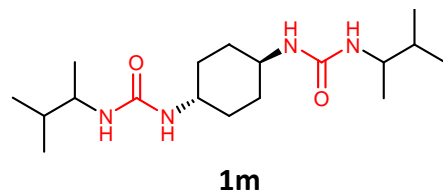
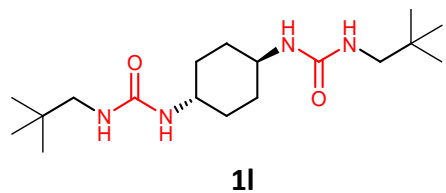


Figure 66. Polymer crystallization temperatures ($T_{c,p}$ ★) (top graphs) and the optical properties haze (★) and clarity (◆) (bottom graphs) of PA6 comprising the trans-bisureas **1l-1o** as function of the additive concentration. The dashed lines indicate the plateau in the polymer crystallization temperature of PA6.

The chemical structures, the nucleation and optical properties of the bisurea derivatives **1j**, **1k** and **1p** with quaternary α -C atoms, are presented in Figure 67. The additives are arranged with decreasing length of the peripheral substituents varied from tert-octyl **1j**, over 1,1-dimethylpropyl **1k**, to tert-butyl **1p**. All three compounds significantly increase the polymer crystallization temperatures of PA6. For **1j** the mean polymer crystallization temperature plateau value was found to be the lowest within this series of additives with 192.3°C. The one $T_{c,p}$ value at 1.3 wt% was distinctly higher than for the remaining concentrations, which seems to be an artifact with the DSC measurement. Compound **1k** with 1,1-dimethylpropyl substituent features the highest plateau in the polymer crystallization temperature at 194.3°C. This is the highest mean $T_{c,p}$ value found in this thesis. It is also interesting to note that the highest $T_{c,p}$ plateau value with 194.5°C was found for **1k** at a comparatively low concentration of 0.2 wt%. The tert-butyl substituted derivative **1p** shows similar nucleation ability with a mean $T_{c,p}$ plateau value of 193.7°C. While **1k** and **1p** displayed excellent nucleation behavior, the polymer crystallization temperatures of PA6 comprising **1j** were considerably lower, most likely due to the increased length of the peripheral substituent which slightly changes the epitaxy.

The clarity values for **1j** were found to be relatively low. They decrease also with the additive concentration. Remarkably **1k** and **1p** exhibit clarity values around 97 % even at the lowest investigated concentration of 0.02 wt%. It is important to note that despite its comparably low nucleation ability, **1j** caused a distinct reduction in haze. The lowest value is 26 % at 0.8 wt%. This again demonstrates that a direct correlation between the nucleation and clarifying ability of an additive cannot be drawn. It is interesting to note that for **1j** and **1p** the haze reaches a plateau above 0.8 wt% where the values remain constant upon further addition of additive. For **1j** the plateau is around 28 % and for **1p** 19 %. In contrast the haze for **1k** steadily decreases with the additive concentration as seen for most of the additives. As already expected from the previous series of additives these findings support strongly the assumption that an efficient clarifying agent for PA6 has to bear highly branched peripheral substituents, particular in the α -position.

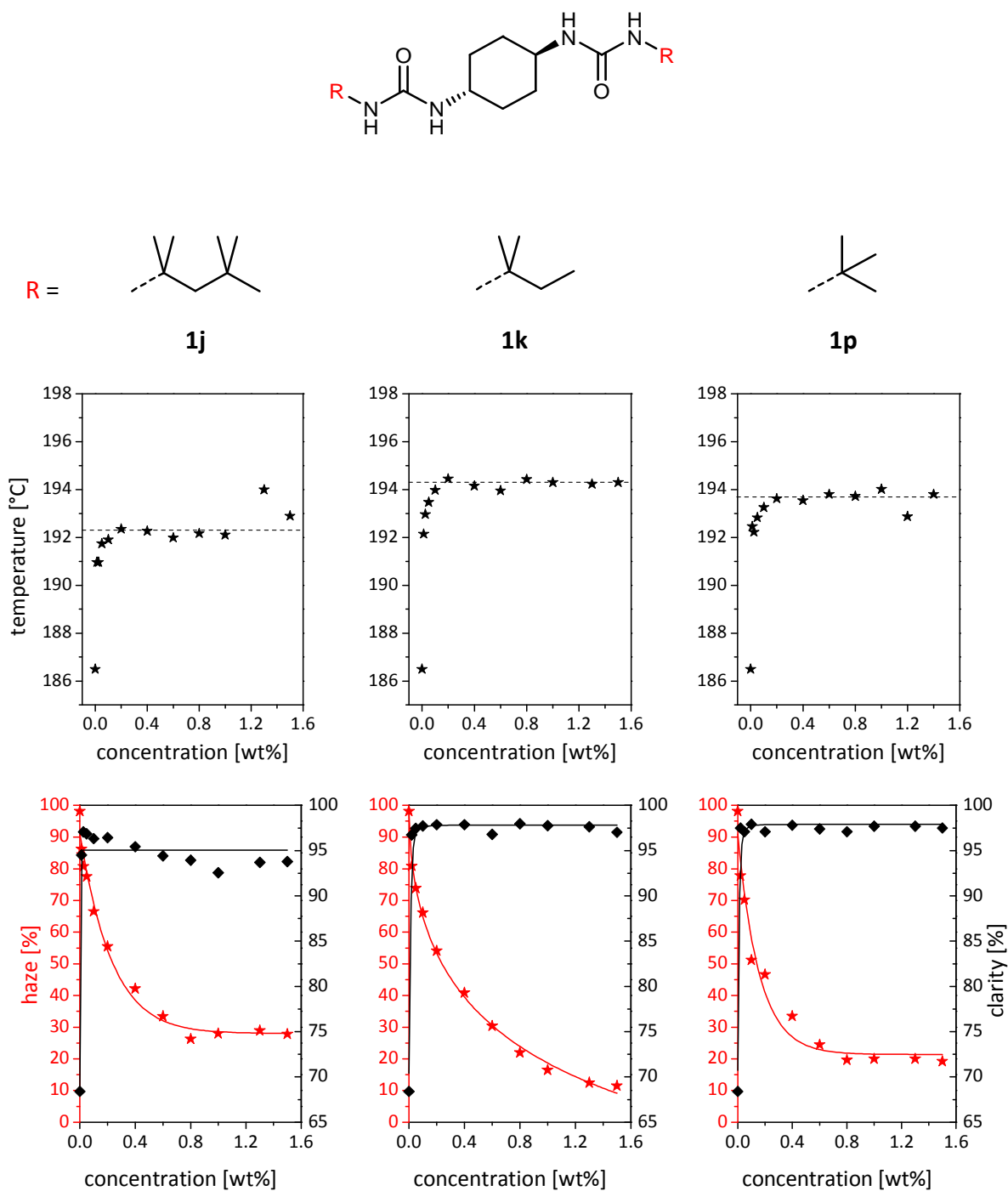


Figure 67. Polymer crystallization temperatures ($T_{c,p}$ ★) (top graphs) and the optical properties haze (★) and clarity (◆) (bottom graphs) of PA6 comprising the trans-bisureas **1j**, **1k**, and **1p** as function of the additive concentration. The dashed lines indicate the plateau in the polymer crystallization temperature of PA6.

Figure 68 illustrates the optical effect of the addition of **1p** on injection molded platelets of PA6. Already at a very low additive concentration of 0.05 wt% high clarity values of 97 % could be achieved. For concentrations exceeding 0.8 wt% the haze reaches a plateau where upon further addition of **1p** the optical properties remain unchanged. Here haze values of around 20 % and clarity values above 95 % were obtained.

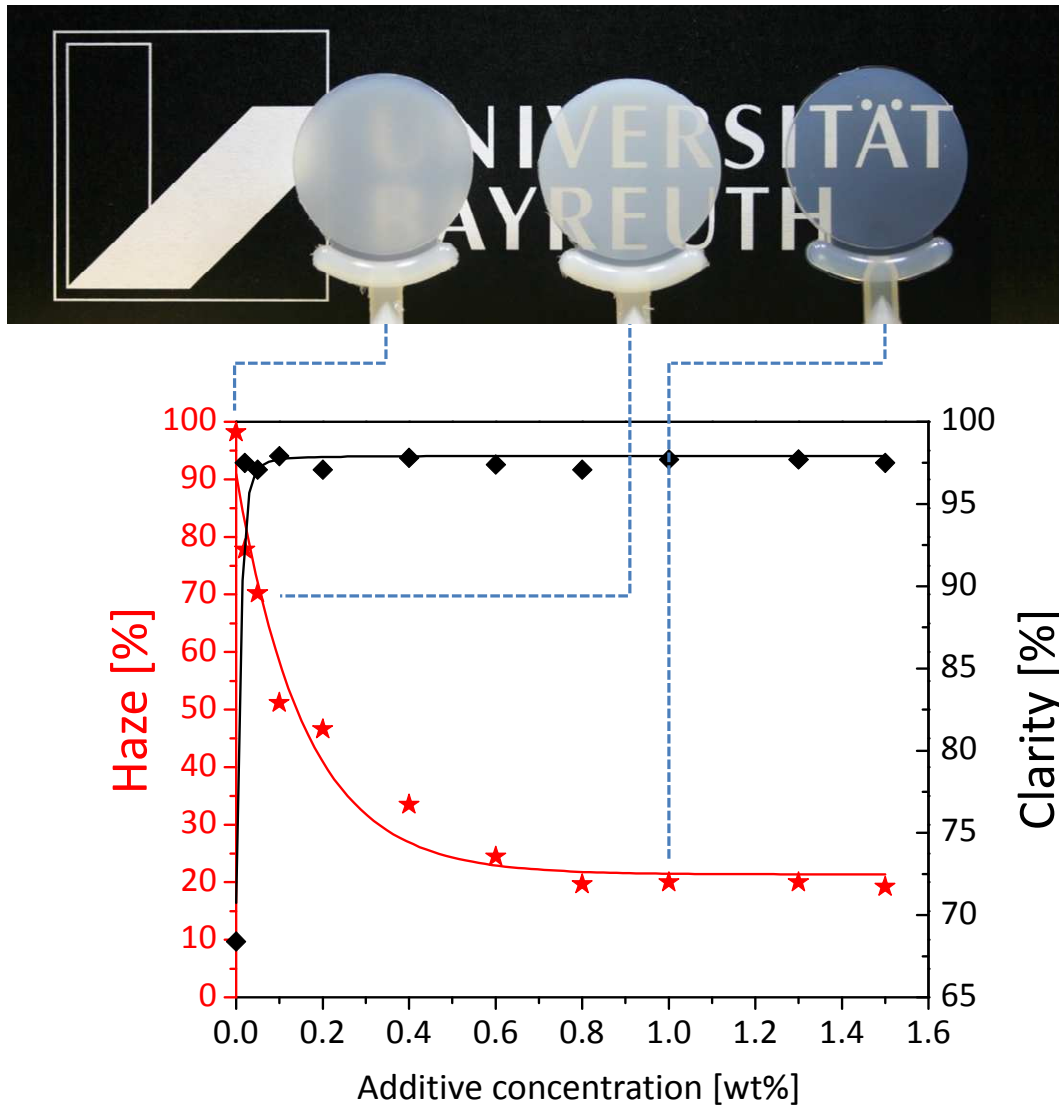


Figure 68. Emblem of the University of Bayreuth viewed through injection molded platelets of PA6 (thickness 1.1 mm) containing 0.0, 0.05 and 1.0 wt% of **1p** (top).

5.4.3.3. Symmetrical trans-bisurea derivatives with cyclic substituents

In an additional series of additives, bisurea derivatives with cycloaliphatic substituents were investigated. The peripheral substituents comprise 1-adamantyl **1s**, cyclohexyl **1q** and phenyl **1r** moieties. The chemical structures of the investigated compounds **1s-1r**, their nucleation and optical properties are presented in Figure 69. Within this series of additives all bisurea derivatives are efficient nucleating agents for PA6. The mean $T_{c,p}$ plateau value of **1s** is 192.7°C. However the crystallization temperature scatters strongly, why the assignment of a proper plateau is complicated. This can be attributed to a worse solubility in the PA6 melt. The compounds **1q** and **1r** exhibit similar plateau values at around 192.8°C.

As for all trans-bisureas the additives within this series exhibit high clarity values. For **1s** the values are above 95 % even at the lowest investigated concentration of 0.02 wt%. For **1q** the increase in clarity is less marked compared to **1s**. Here the plateau in clarity is reached for concentrations above 0.1 wt%. This effect is even more pronounced with **1r**. Regarding the haze of PA6 **1s** was found to be the most efficient clarifier with a remarkable low haze of 16 % at 1.5 wt%. Regarding the shape of the haze curve it can be assumed that further addition of **1s** leads to an even higher transparency. However, similar to the 1,1-dimethylpropyl substituted derivative **1k** from the above series of additives, the haze strongly decreases with the additive concentration due to the excellent solubility in the polymer melt. The introduction of the less branched cyclohexyl **1q** substituent yields somewhat poorer haze with 64 % at 1.5 wt%. For **1r** the lowest haze values is at 51 %, also at 1.5 wt%.

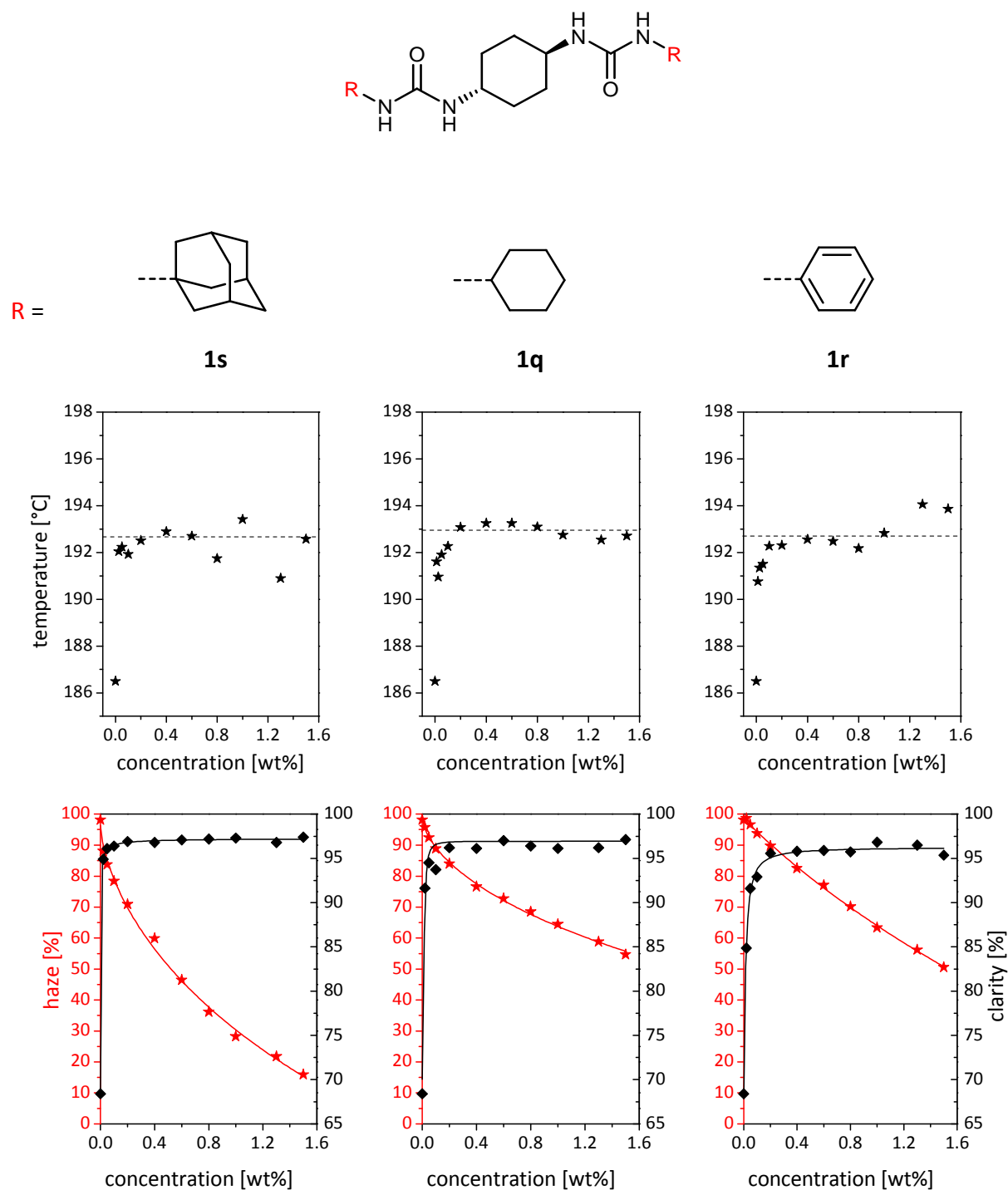


Figure 69. Polymer crystallization temperatures ($T_{c,p}$ ★) (top graphs) and the optical properties haze (★) and clarity (◆) (bottom graphs) of PA6 comprising the trans-bisureas **1s**, **1q**, and **1r** as function of the additive concentration. The dashed lines indicate the plateau in the polymer crystallization temperature of PA6.

5.4.3.4. Asymmetrically substituted trans-bisurea derivatives

In addition to the above discussed compounds, the asymmetrically substituted trans-bisureas **3a-3d** were synthesized and the properties in PA6 will be discussed in the following. All derivatives exhibit one cyclohexyl substituent and differ concerning the second peripheral substituent. The chemical structure of the asymmetric bisureas with tert-octyl **3a**, iso-propyl **3b**, tert-octyl **3c** and phenyl substituent, their nucleation and optical properties are presented in Figure 70.

In accordance with the symmetrically substituted bisureas, all derivatives in this series were capable to significantly increase the crystallization temperature of PA6. The mean $T_{c,p}$ plateau values of the asymmetric derivative **3a** is 192.6°C and thus almost similar compared to the corresponding symmetric derivative **1j** (192.3°C) with two tert-butyl substituents. For **3b** and **3d** also similar mean $T_{c,p}$ plateau values are found. In contrast the nucleation ability of **3c** is considerably lower compared to the corresponding symmetrical derivative **1p** with tert-butyl substituents. Here the $T_{c,p}$ plateau values scatter strongly why a plateau value can only be estimated.

The clarity was for all asymmetric compounds above 95 % and no distinctions between the different substituents can be made. All derivatives significantly decreased the values for haze, however this effect was less pronounced in comparison to the corresponding symmetric bisureas. For example **3a** displayed minimum haze values of 42 % at 1.5 wt% whereas the corresponding symmetric analogues **1j** featured values as low as 28 % at this concentration. This effect is likely to originate from defects in the self assembly of the bisureas due to the asymmetric structure of the additives. Despite the only minor nucleation ability **3c** is the most efficient clarifier investigated in this series. The lowest haze value is 31 % at 1.5 wt%.

It is again interesting to note that a substitution of the α -hydrogen atoms with two methyl groups resulted in a stronger decrease in haze, as already discussed before.

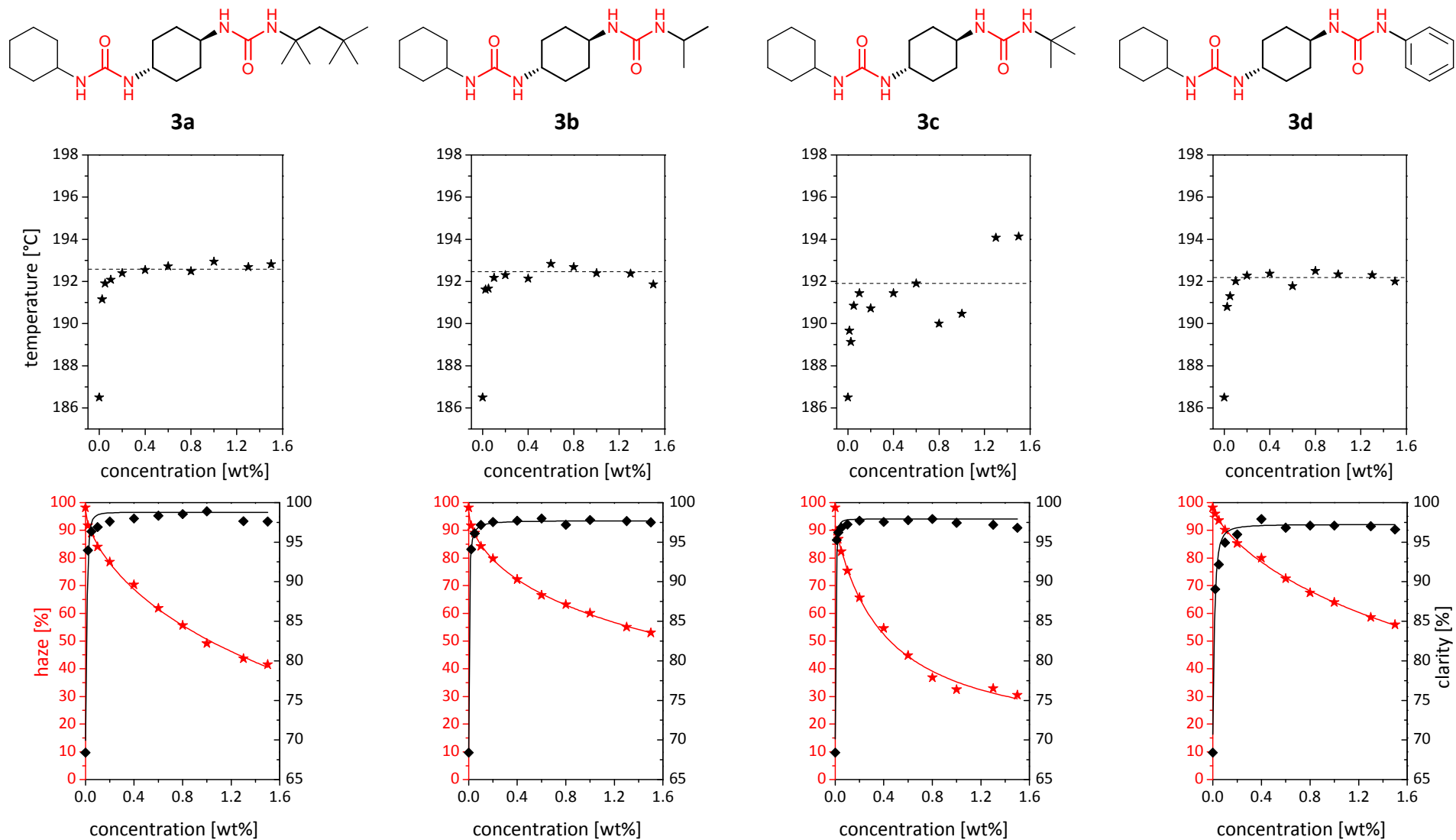


Figure 70. Polymer crystallization temperatures ($T_{c,p}$ ★) (top graphs) and the optical properties haze (★) and clarity (◆) (bottom graphs) of PA6 comprising the trans-bisureas **3a-3d** as function of the additive concentration. The dashed lines indicate the plateau in the polymer crystallization temperature of PA6.

5.4.3.5. Symmetrically substituted cis-bisurea derivatives

The chemical structures of the cis-bisurea derivatives **2a** – **2f** and their nucleation and optical properties are compared in detail in Figure 71A and B. The substituents are varied from n-octyl **2a**, tert-octyl **2b**, isopropyl **2c**, tert-butyl **2d**, cyclohexyl **2e**, to phenyl **2f**. The conformational change in the central unit from the trans- to the cis-bisureas has dramatic influence on the self-assembly and nucleation ability.

In comparison to the trans-analogues all derivatives are less efficient as nucleating agents. For **2a** with n-octyl substituents the mean $T_{c,p}$ plateau value is 190.1°C and thus considerably lower than for the corresponding trans-bisurea **1e** (192.3°C). For compound **2b** the crystallization temperature steadily increases with the additive concentration and no real plateau can be assigned. With **2b** the highest $T_{c,p}$ is 190.1°C at 1.5 wt% and thus 2.8°C lower compared to the trans-bisurea **1j** with the same substituent (192.9°C). The isopropyl substituted derivative **2c** is not capable to nucleate PA6 and no increase in $T_{c,p}$ is observed, whereas the trans analogue **1o** has a $T_{c,p}$ plateau value of 192.8°C. The compounds **2d** with tert-butyl substituents and **2e** with cyclohexyl substituents are again capable to promote nucleation of PA6. The mean $T_{c,p}$ plateau values are again distinctly lower compared to the trans-bisurea analogues **1p** and **1q**. The phenyl substituted derivative **2f** in contrast does not nucleate PA6.

It is interesting to note that for **2a** the values for clarity seem to deteriorate at lower additive concentrations compared to neat PA6. However clarity values obtained from specimens with a haze of close to 100 % are prone to errors and thus may be inaccurate. Similar behavior is observed for **2c**, **2e** and **2f**, all compounds with a haze of close to 100 %. The small nucleation ability of the cis-bisureas is also reflected in the values for haze that are distinctly higher compared to the investigated trans-bisureas. Despite the nucleation potential of **2a** no improvements in optical properties can be observed and the haze remains around the value of neat PA6 (98%) for all concentrations. Similar behavior is found for **2c**, **2e**, and **2f**. The tert-octyl substituted derivative **2b** was only capable to improve the haze by 5 % from 98 % to 93 % at 1.5 wt%. For **2d** the haze is decreased by 14 % to 84 % at 1.5 wt%. In this connection it is again apparent that derivatives with highly branched substituents are the most beneficial substituents to improve the properties of PA6.

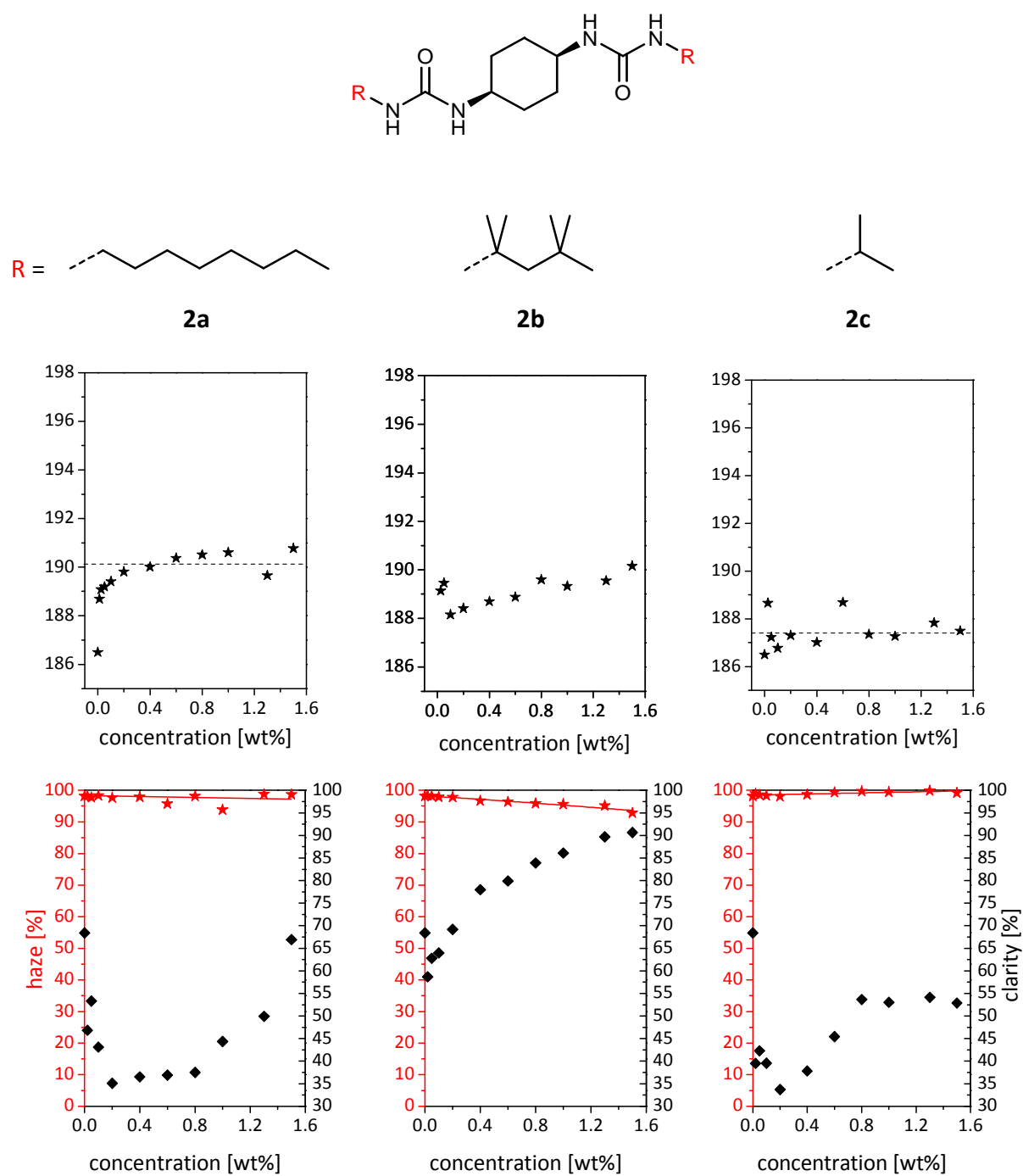


Figure 71A. Polymer crystallization temperatures ($T_{c,p}$ ★) (top graphs) and the optical properties haze (★) and clarity (◆) (bottom graphs) of PA6 comprising the cis-bisureas **2a-2c** as function of the additive concentration. The dashed lines indicate the plateau in the polymer crystallization temperature of PA6.

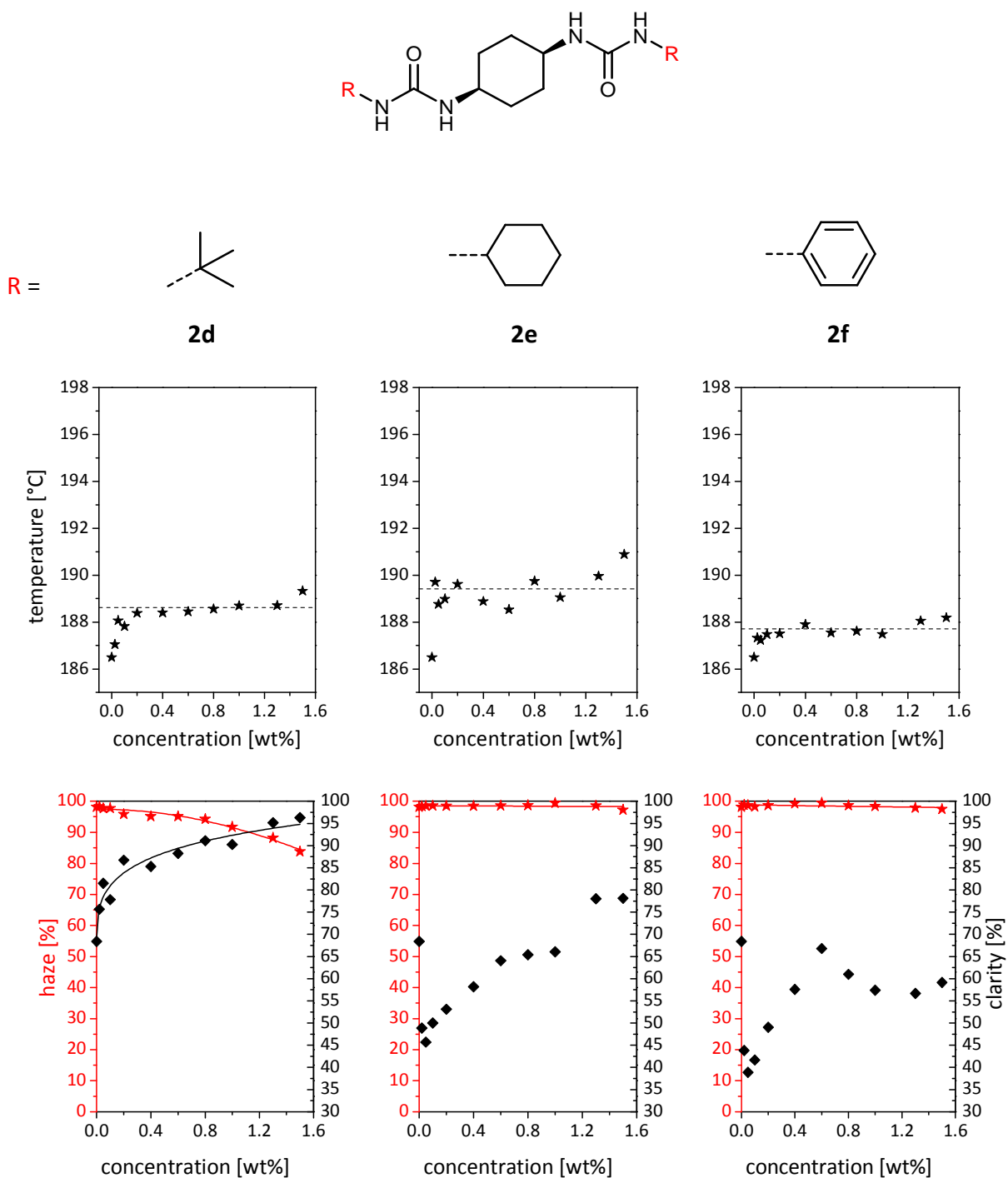


Figure 71B. Polymer crystallization temperatures ($T_{c,p}$ ★) (top graphs) and the optical properties haze (★) and clarity (◆) (bottom graphs) of PA6 comprising the cis-bisureas **2d-2e** as function of the additive concentration. The dashed lines indicate the plateau in the polymer crystallization temperature of PA6.

5.4.4. Nucleation efficiency and optical properties in comparison to talc

To determine the nucleation efficiency of the bisurea derivatives, self-seeding experiments as described by Lotz et al.^[6] for polypropylene were conducted. The self seeding procedure has already been described in chapter 4.2.3 on polybutylene terephthalate. Figure 72 shows the crystallization exotherms of melt processed neat PA6 for various self nucleation temperatures (T_s). Maximum self nucleation temperature of PA6 was induced after melting for 5 min at 220.5°C yielding a maximum achievable polymer crystallization temperature $T_{c,p\text{theo}}$ of 195.4°C.

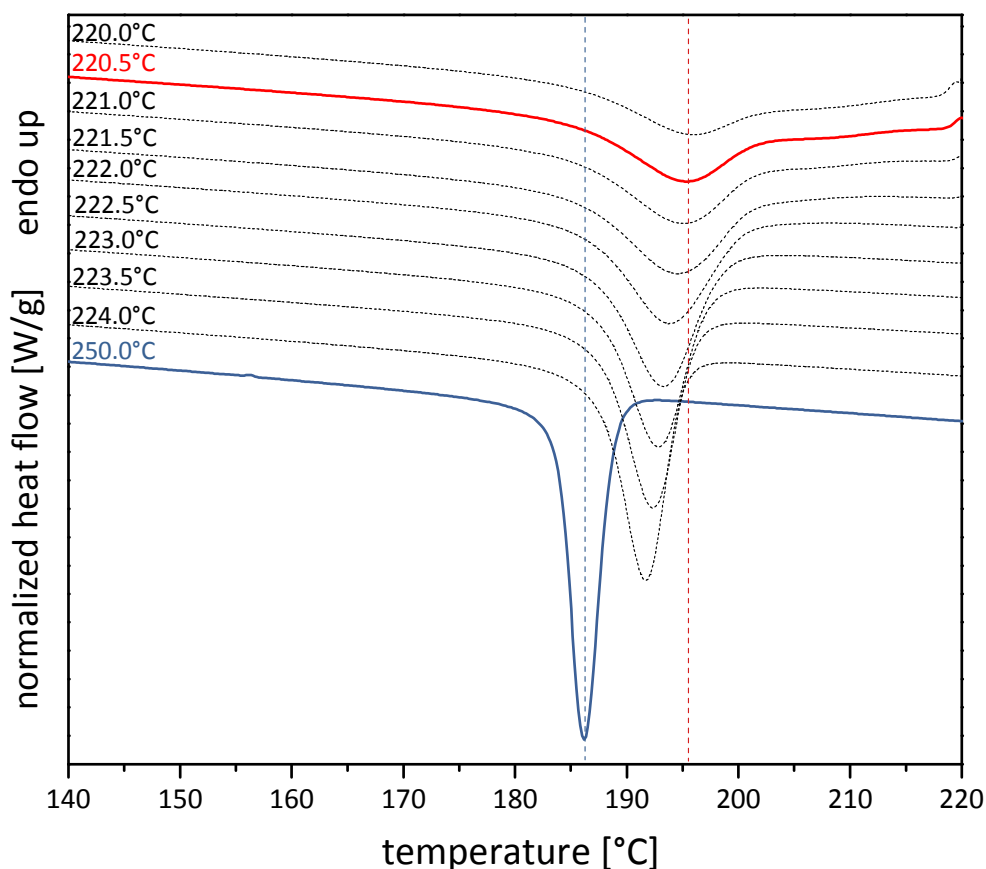


Figure 72. Crystallization exotherms of melt processed neat PA6 for different self nucleation temperatures.

In the following the nucleation behavior and optical properties of the most efficient bisureas will be compared to the literature known nucleating agent **talc**. In this study Micro-Talc IT Extra from Mondo Minerals was used.^[104] Figure 73 compares the results obtained for the crystallization temperature and the optical properties haze and clarity for **talc** in comparison to the most efficient clarifiers **1p** and **1k** discussed before. As already observed in the case of PBT, **talc** exhibits an excellent nucleation behavior in PA6. The best polymer crystallization temperature was 194.8°C at a concentration of 1.5 wt%. This corresponds to a nucleation

efficiency of 93.3 %. The values observed for talc are only slightly higher than those for the two most efficient trans-bisurea nucleating agents **1a** with ethyl ($T_{c,p} = 194.6^{\circ}\text{C}$, NE = 90.0 %, at 0.4 wt%) and **1k** with 1,1-dimethylpropyl substituent ($T_{c,p} = 194.5^{\circ}\text{C}$, NE = 88.9 %, at 0.2 wt%). It is important to note that the required concentration to reach the $T_{c,p}$ plateau is for the bisurea derivatives lower compared to **talc**. As the theoretical polymer crystallization temperature ($T_{c,p \text{ theo}}$) of PA6 is only located 9°C above the value for the equilibrium crystallization temperature, slight changes in $T_{c,p}$ strongly affect the calculated nucleating efficiencies. Besides the discussed compounds **1a** and **1k**, the n-propyl substituted derivative **1b** with a nucleation efficiency of 84.4 % at a concentration of 1.5 wt% and the tert-butyl substituted derivative **1p** with a nucleation efficiency of 83.3 % at a concentration of 1.0 wt% are the most efficient nucleating agents found in this thesis.

Regarding the optical properties the comparison with **talc** is different and very much in favor for the bisureas. In contrast to the 1,1-dimethylpropyl substituted trans-bisurea **1k** and the tert-butyl substituted trans-bisurea **1p**, **talc** improves the optical properties of PA6 only with respect to the clarity. The values for clarity show a maximum at 0.2 wt% with 93 %. With increasing additive concentration the clarity is reduced again. The haze values are only reduced to about 85 % at the highest concentration of 1.5 wt%. The comparably poor haze can be attributed to the insufficient distribution of the insoluble **talcum** particles in the polymer melt during processing and consequently increased scattering of light. This demonstrates once more the advantage of supramolecular polymer additives compared to insoluble polymer additives particular with respect to the optical properties.

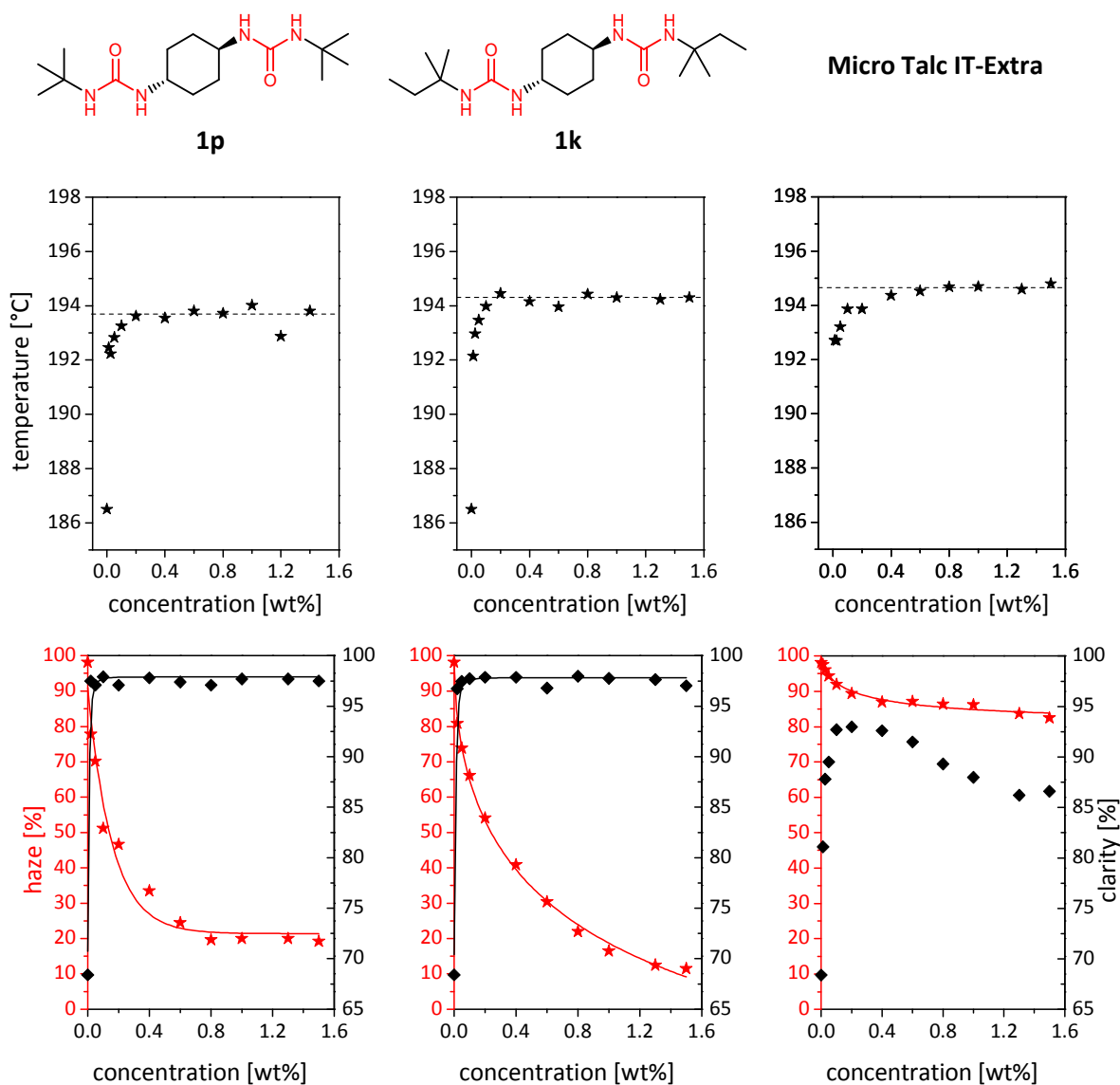


Figure 73. Polymer crystallization temperatures ($T_{c,p}$ ★) (top graphs) and the optical properties haze (★) and clarity (◆) (bottom graphs) of PA6 comprising the bisurea derivative **1p**, **1k** and **talc** as function of the additive concentration. The dashed lines indicate the plateau in the polymer crystallization temperature of PA6.

5.4.5. Stability of nucleation effect

In the literature the nucleation properties of an additive are not only determined by the increase in polymer crystallization temperature but also its stability.^[105, 26] Therefore several heating and cooling cycles are performed and the polymer crystallization temperatures are studied. In this thesis the nucleation stability was investigated by multiscanning DSC experiments according to Mai et. al.^[26] PA6 samples comprising two selected bisureas were repeatedly heated and cooled in the DSC. Samples were heated up to 250°C and held for 5 min before each cooling run to prevent self nucleation on remained non-molten crystal fragments.

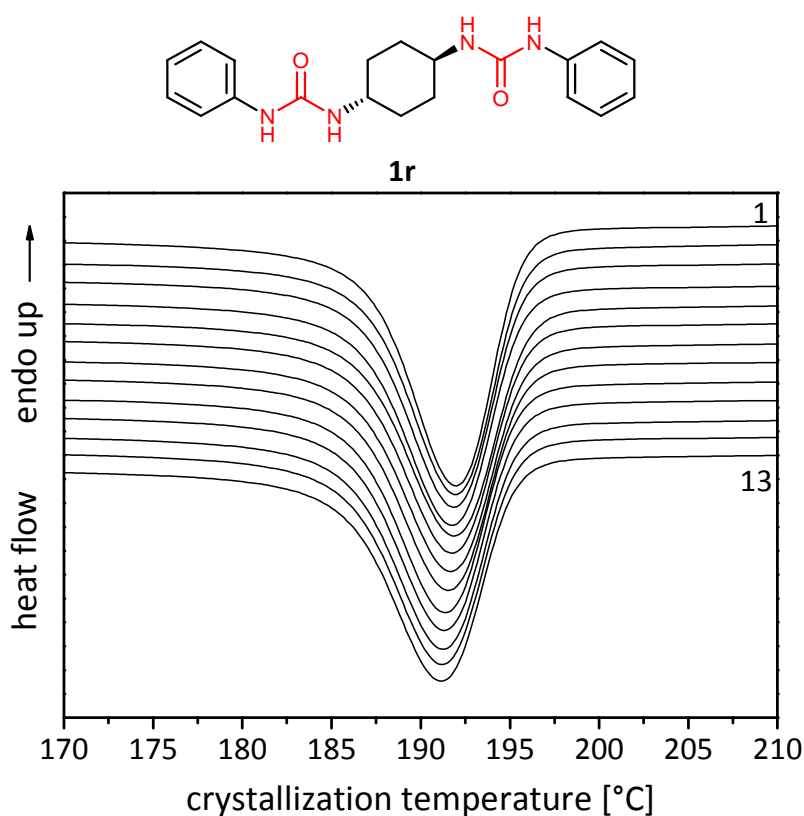


Figure 74. Cooling curves of PA6 comprising 0.4 wt% of **1r** for 13 heating and cooling cycles in a multiscanning DSC experiment. Samples were held at 250°C for 5 min before each cooling run.

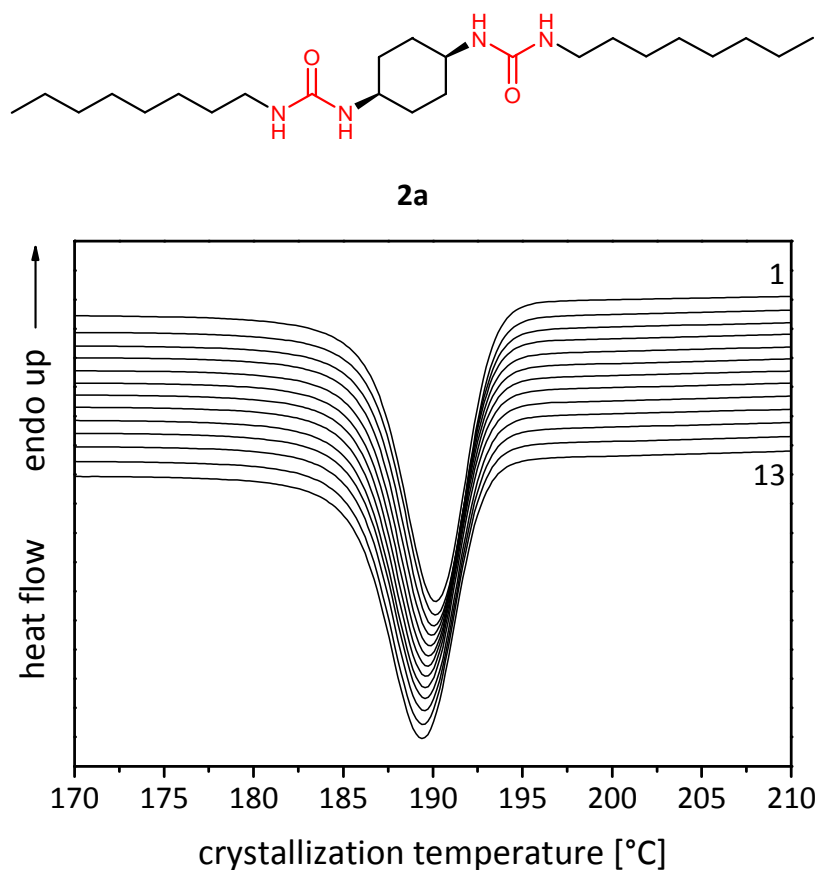


Figure 75. Cooling curves of PA6 comprising 0.4 wt% of **2a** for 13 heating and cooling cycles in a multiscanning DSC experiment. Samples were held at 250°C for 5 min before each cooling run.

The nucleation efficiencies were calculated from the polymer crystallization temperatures of the polymer for each cooling run and are shown in Figure 76. The crystallization temperature of PA6 comprising **1r** is nearly unaffected by the number of measuring cycles confirming the reversibility of the supramolecular self assembly process and demonstrating that no degradation occurred. The $T_{c,p}$ of neat PA6 is increased by the additive from 186.5°C to 191.9°C (first run). After 13 runs the $T_{c,p}$ decreases from 191.9°C to 191.1°C. This is a decrease of only 0.8°C. Despite its lower thermal stability the nucleation ability of the cis-derivative **2a** exhibits similar behavior (Figure 75). From the first DSC run to the 13th run the $T_{c,p}$ decreases from 190.1°C to 189.4°C. This corresponds to a decrease of only 0.7°C.

This becomes more visible if the nucleation efficiency depending on the number of measuring cycles is plotted (see Figure 76). Both bisureas are nearly unaffected by the number of heating and cooling scans if taken into account the thermal stress after 1 h in the melt. As already mentioned, slight changes in $T_{c,p}$ strongly affect the calculated nucleating efficiencies due to the small temperature range between $T_{c,p}$ and the theoretical crystallization temperature of PA6. After 13 cycles the values for nucleation efficiency

decreased by only 9 % for **1r** and 8 % for **2a**. In contrast sorbitol derivatives such as bis(3,4-dimethylbenzylidene)sorbitol (Millard 3988) only exhibit less thermal stability even in iPP of the heterogeneous nucleation, the latter losing most of its nucleation ability already after the 5th scan in a similar experiment.^[26]

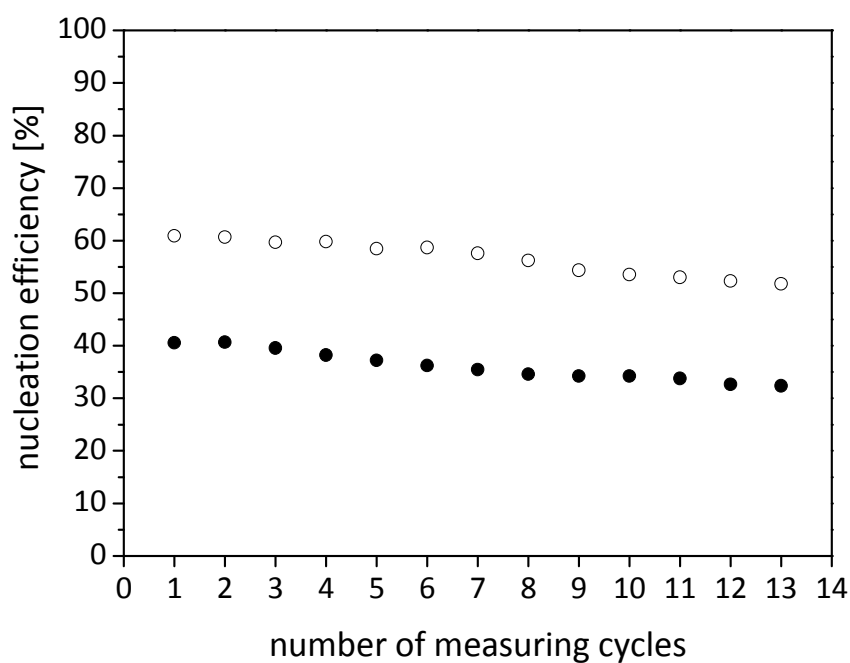


Figure 76. Nucleation efficiencies of **1p** (o) and **2a** (●) in PA6 as function of the number of measuring cycles in a multiscanning DSC experiment.

5.4.6. Influence of the mold temperature on optical properties

The macroscopic properties of semi-crystalline polymers are strongly dependent on the spherulite size and can also be influenced by the processing conditions. As it is evident from Figure 77 that upon fast cooling from the melt a higher nuclei density occurs and smaller spherulites are formed. That in turn leads to less scattering increasing the total transmission of visible light. When a polymer is cooled rather slowly, nucleation only occurs sporadically and fast crystal growth of individual particles leads to larger spherulites.^[1]

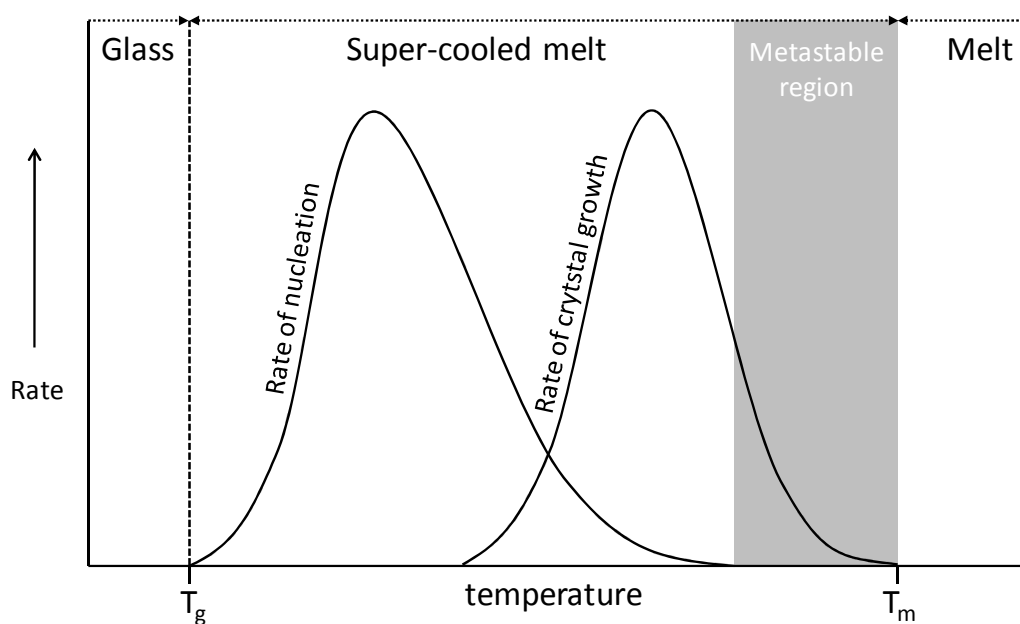


Figure 77. Schematic representation of the rate of nucleation and the rate of crystal growth as function of the temperature.^[1]

The influence of the cooling rate on the optical properties of PA6 was investigated at different mold temperatures during injection molding. The mold temperatures were varied from 40°C to 120°C. The haze values of the injection-molded specimens (1.1 mm thickness) are presented in the top graph of Figure 78. The open stars represent the values for neat PA6 and the solid squares the haze values for PA6 comprising 0.8 wt% of the tert-butyl substituted trans-bisurea **1p**. As expected the haze value decreases as faster cooling is applied, both for neat and clarified PA6. At a mold temperature of 40°C the haze values are about 12 % lower compared to the specimens injected in a mold at 120°C. Over the whole investigated temperature range **1p** acts as efficient clarifying agent and distinctly improves the haze compared to the neat PA6. Upon faster cooling, the bisureas self assemble into supramolecular nano-objects in the polyamide melt capable to nucleate and clarify. The

values for clarity are presented in the bottom graph of Figure 78. Increasing the mold temperature from 40°C to 120°C resulted for neat PA6 in a strong decrease in clarity from 90 % to only 29.2 %. Regarding the clarified samples no improvements were observed upon faster cooling.

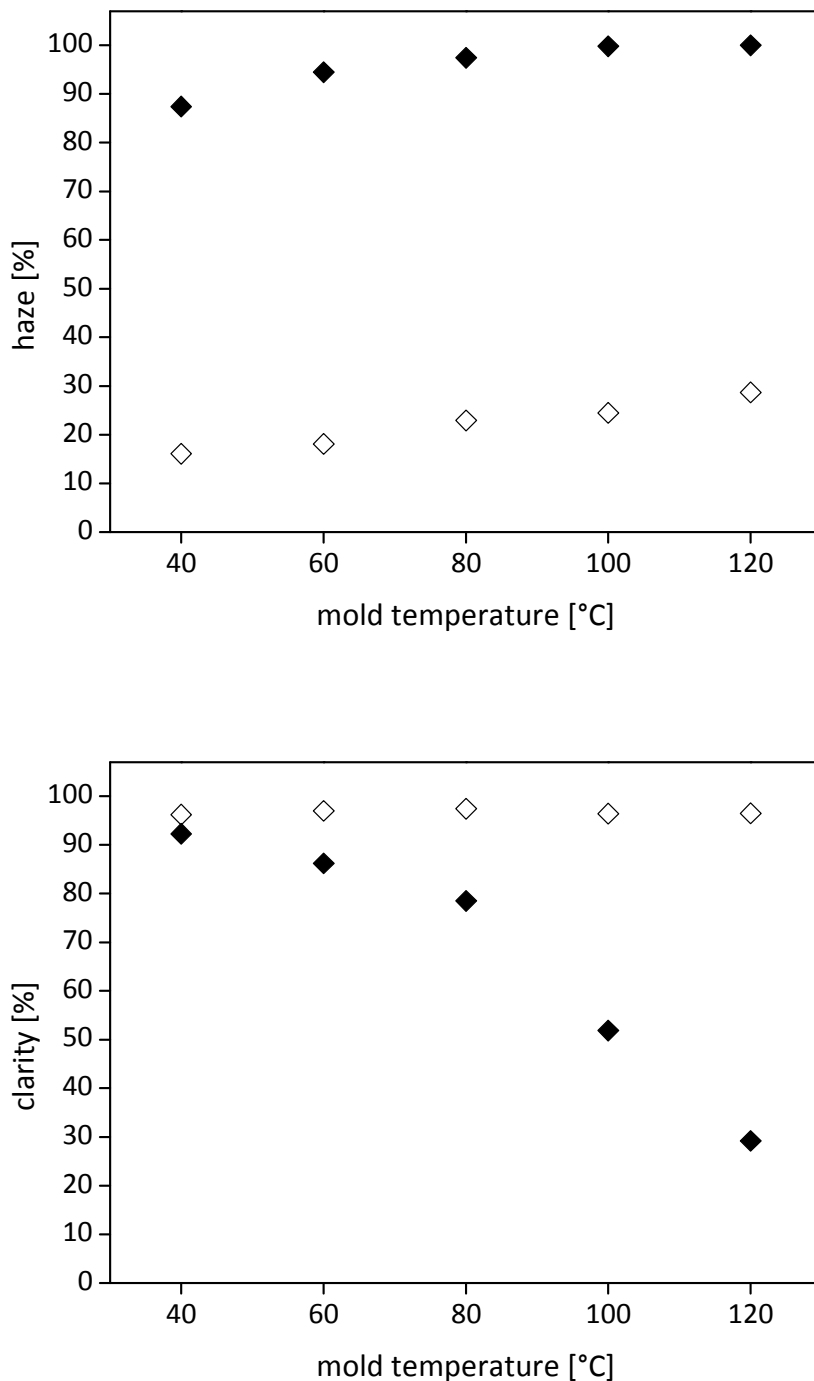


Figure 78. Values for haze (top graph) and clarity (bottom graph) for neat PA6 (solid squares) and PA6 comprising 0.8 wt% of the tert-butyl substituted trans-bisurea **1p** (open squares) as function of the mold temperature.

5.4.7. Influence of sample thickness on optical properties

Variations in sample thickness have an impact on the morphology of injection molded specimens. Fewer but larger spherulites are formed where the melt cools slowly, whereas faster cooling leads to more but small crystalline entities.^[106] As a result of the temperature gradient from the outside to the inside of the specimens the spherulite size increases from the skin to the core and is on average larger for higher mold thicknesses.^[107] As the transparency of objects is mainly determined by the amount of transmitted light, values for haze increase with thickness. The influence of the mold thickness on haze of PA6 comprising the 1,1-dimethylpropyl substituted bisurea **1k**, the tert-butyl substituted bisurea **1p** and **talc** is compared in Figure 79. As usual the haze values increase with the sample thickness.

As discussed in chapter 5.4.4 **talc** caused only a very modest reduction in haze. At a thickness of 0.5 mm a plateau in haze was reached at around 55 % for concentrations above 0.1 wt%. For 1.1 mm the haze values steadily decrease with higher additive concentrations to a value of only 85 % at the highest concentration of 1.5 wt%. For specimens thicker than 1.1 mm the haze values remained at 100 % independent of the additive concentration.

In contrast both bisurea derivatives **1k** and **1p** were capable to enhance the optical properties of PA6 for all thicknesses. For a mold thickness of 0.5 mm both additives showed minimum haze values of around 8 % at a concentration of 1.3 wt%. In thicker samples, further addition of **1k** resulted in a steady decrease in the haze values, whereas for **1p** a plateau was reached for 1.1 mm and 2.0 mm samples. Thus it can be assumed an increase of the **1k** concentration would even lead to lower haze values. In platelets with a thickness of 1.1 and 2.0 mm, **1p** with tert-butyl substituent was found to be the more efficient clarifier for PA6 up to a concentration of 0.8 wt%. This trend is reversed for concentrations exceeding 1.0 wt%. Here **1k** featured lowest haze values of 11 % at 1.1 mm and 21 % at 2.0 mm, whereas **1p** displayed values at 19 % and 30 % respectively. At a mold thickness of 3.0 mm the lowest haze achieved is 44 % for **1p** (1.5 wt%) and 53 % for **1k** (1.3 wt%). Remarkably even for very thick samples (5.0 mm), the lowest haze value obtained with **1k** was 77 % (1.5 wt%) whereas **1p** caused only a modest reduction in haze (93 %, 1.5 wt%).

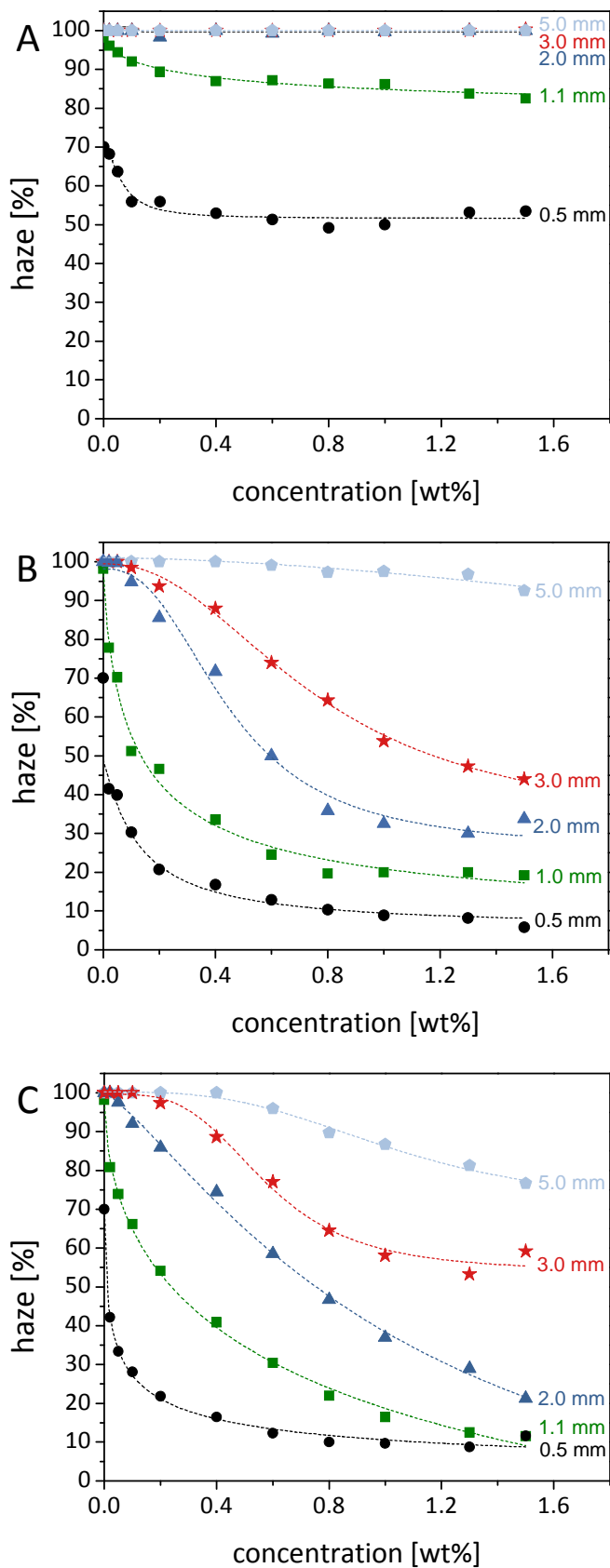


Figure 79. Haze values of PA6 comprising A: **talC**, B: the tert-butyl substituted bisurea **1p** and C: the 1,1-dimethylpropyl substituted bisurea **1k** for different mold thicknesses (0.5 mm, ●; 1.1 mm, ■; 2.0 mm, ▲; 3.0 mm, ★ and 5.0 mm, ◆) as function of the additive concentration.

5.4.8. Laser transparency

Laser transmittance of PA6 comprising the tert-butyl substituted trans-bisurea **1p** and **tal** was determined at a wavelength of 1064 nm on injection molded plaques. The investigated thickness is varied from 1.1 mm, 2.0 mm, to 3.0 mm. In Figure 80 the values for laser transparency are plotted as function of the additive concentration. The LT values for *neat* PA6 were found to be 82 % for a thickness of 1.1 mm, 72 % for a thickness of 2.0 mm and 59 % for a thickness of 3.0 mm.

Similar to the values for haze presented in chapter 5.4.3.2 one would expect steady improvements in laser transparency with increasing amounts of additive. Surprisingly for all thicknesses at low concentrations in the range from 0.02 – 0.1 wt% the LT-values are lower compared to the neat material. For a thickness of 1.1 mm at a concentration of 0.02 wt% the LT-value is only 78 % and thus 4 % lower compared to the neat PA6. At concentrations exceeding 0.2 wt% **1p** is capable to enhance the laser transparency of PA6. Here the transmittance is increased by 3 % to 86 % for a thickness of 1.1 mm at a concentration of 1.5 wt%. A very similar trend is observed for the 2.0 mm and 3.0 mm thick specimens. The lowest LT-values were 63% for a thickness of 2.0 mm at 0.02 wt% and thus 9 % lower compared to the neat PA6. For a thickness of 3.0 mm at an additive concentration of 0.02 wt% the LT-value is 53 %, 6 % lower as the neat polymer. Similar to 1.1 mm above 0.2 wt% the LT increases. The increase for 2.0 mm is 10 % to a LT-value of 82 % at a concentration of 1 wt%. For 3.0 mm the LT increases by 13 % to 72 % at a concentration of 0.8 wt%. These results demonstrate that **1p** is capable to distinctly increase the LT in PA6 especially in thick parts.

The different shapes of the curves for haze and laser transparency at low additive concentrations can be explained by the different measurement procedures for haze and laser transmittance. Haze is determined using an integrating sphere that collects the total hemispheric transmittance when the sample is placed directly on the entrance port of the sphere. Values for haze are obtained by dividing the diffuse by the total transmittance.^[59] In contrast, laser transparency is determined by a sensor located 1.1 mm below the polymer specimen and calculated as the ratio of the reference and the measurement beam.^[66] While haze is calculated with regard to the total transmittance the former can improve while the total transmittance decreases compared to the neat material.

While **talc** caused only modest improvements in haze as already shown in chapter 5.4.4 laser transmittance is reduced throughout the whole investigated concentration range and for all mold thicknesses. It is interesting to note that the transmittance values reach a plateau above an additive concentration of 0.1 wt%. For a thickness of 1.1 mm the LT-value decreases by 2 % to values of 80 %. For a thickness of 2.0 mm the LT-plateau value is at 65 % and 12 % lower than the neat PA6. For 3.0 mm the plateau value is at 50 % and 9 % lower than neat PA6. The origin of the poor laser transparency of **talc** is irregular and due to insufficient distribution in the polyamide melt causing additional scattering of the irradiating laser.

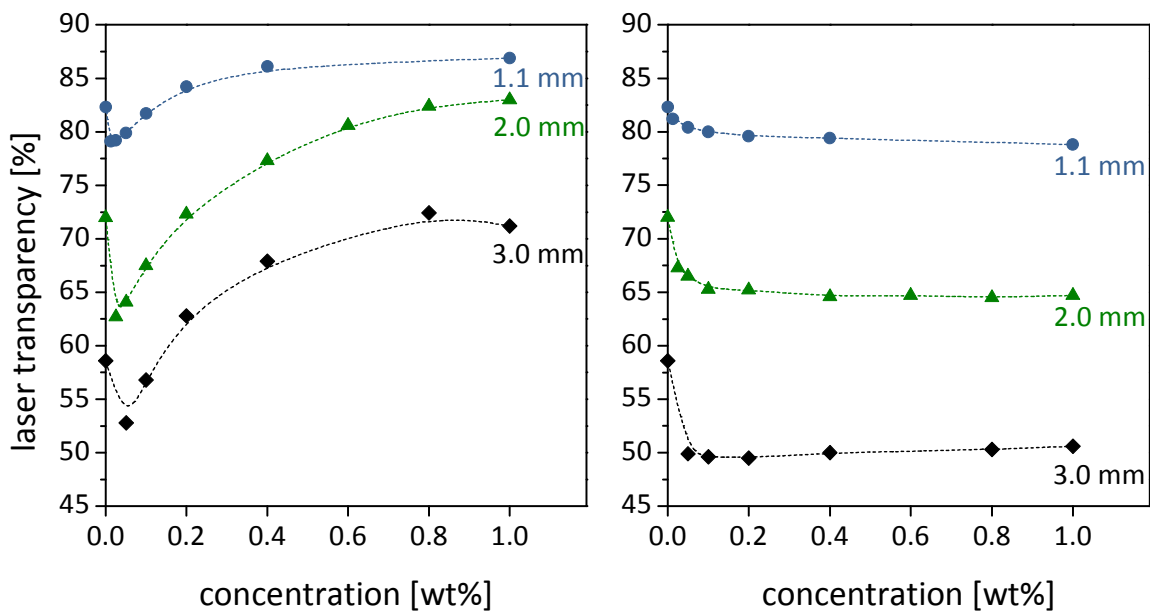


Figure 80. Laser transparency values of PA6 comprising **1p** (left) and **talc** (right) for different mold thicknesses (1 mm, ●; 2 mm, ▲ and 3 mm, ◆) as function of the additive concentration.

5.4.9. Morphology of injection molded samples

In the following the influence of nucleation on the spherulitic morphology is investigated on injection molded samples of a 1.1 mm thickness. A comparison of neat PA6 and PA6 comprising the tert-butyl substituted trans-bisurea **1p** and the reference nucleating agent **talc** will be made. Figure 81 and Figure 82 present thin sections cut parallel to the flow direction and investigated in an optical microscope between crossed polarizers. The images were merged from two separate micrographs in order to present the complete cross section of the injection molded parts. The haze values for the respective concentrations are reported in the top left of each image.

Polyamides tend to crystallize rather fast exhibiting a usually relatively fine and homogeneous spherulitic morphology. This effect is even amplified in injection molding due to the extremely fast cooling rates. A determination of concrete values for the crystallite size is at this level not possible. Figure 81 presents in the top left micrograph the spherulite structure of neat PA6. Resulting from the temperature gradient from the outside to the inside of the specimens during solidification the specimens are composed of highly oriented skin layers and a less oriented spherulitic core region.^[107, 108] The black stripe in the middle of the specimens is found for all samples and is a consequence of the injection molding process. The spherulitic morphology of PA6 was significantly influenced by the addition of 1.0 wt% of **1p**. Here single crystallites are so small to be resolved separately in polarized optical microscopy. The haze in this sample is reduced from 98 % of neat PA6 to 20 %. The thin stripes oriented parallel to the cutting direction originate from the cutting process. Upon lowering the concentration of **1p** from 1.0 wt% to 0.2 wt% the crystallite size remains relatively unaffected. The haze value increases to 47 %. Still at a concentration as low as 0.02 wt% the morphology of the injection molded specimens is significantly affected. However, the spherulites are slightly larger compared to a concentration of 0.2 wt%. As expected, the modifications in morphology are also accompanied by drastic changes regarding the optical properties. Scattering is reduced with decreasing spherulite size thus lowering the values for haze even at very low concentrations.

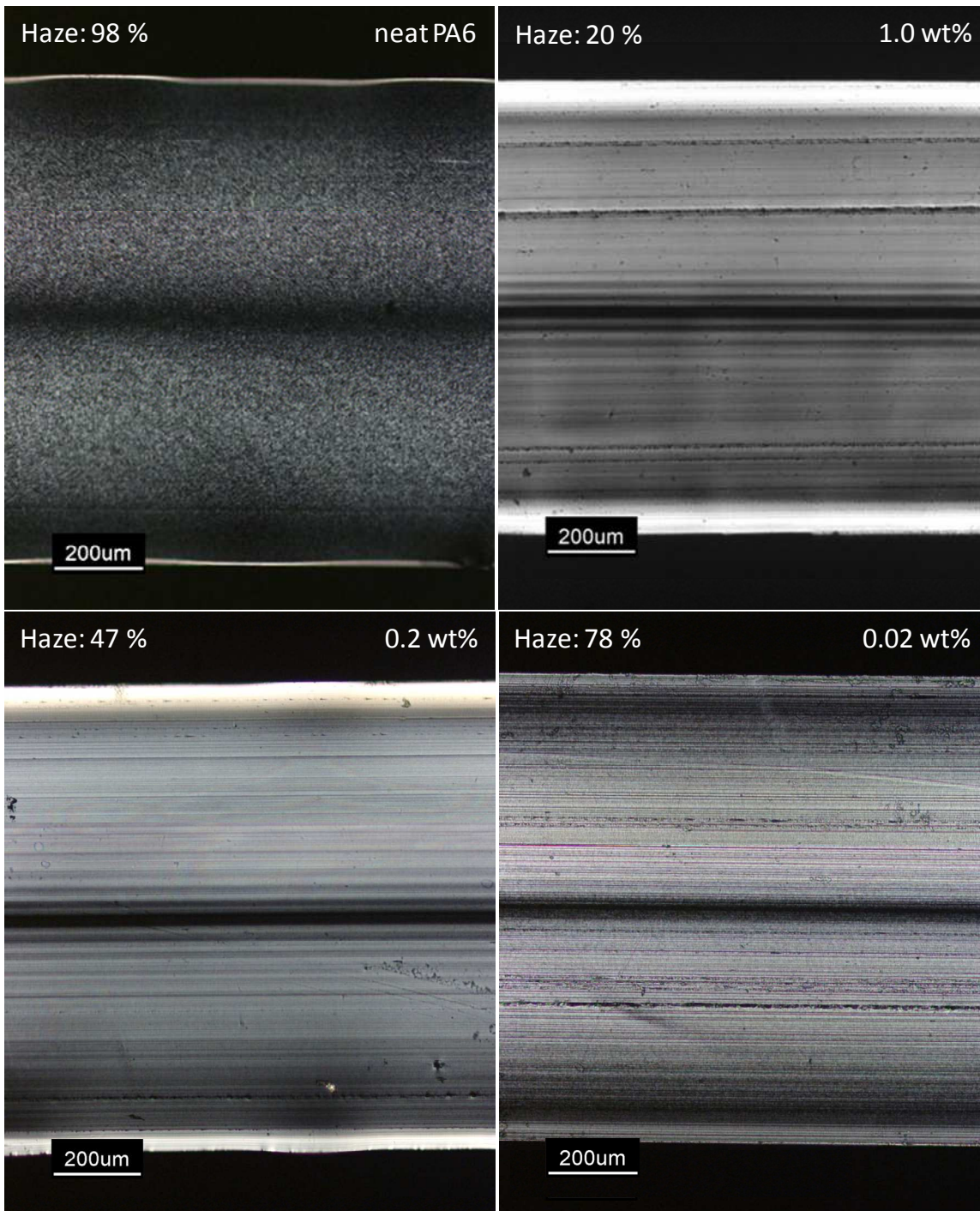


Figure 81. Thin sections of injection molded samples (thickness 1.1 mm) parallel to the flow direction and the corresponding haze values of neat PA6 (top left) and PA6 comprising **1p** at different concentrations. The images presented consist of two separate pictures taken between crossed polarizers.

Talc displays a remarkable nucleation ability in PA6, exceeding even slightly the polymer crystallization temperature values of the most efficient bisurea compounds. The effect of **talc** on the spherulitic morphology in injection molded specimens is considerably different. In contrast to the tert-butyl substituted bisurea **1p** nucleation with **talc** has less influence on the crystallite size. At a concentration 1.0 wt% and 0.6 wt% the spherulitic morphology is less homogeneous compared to **1p**. Here agglomerates of **talcum** particles are visible in optical microscopy that originate from the not ideal distribution of **talc** in the PA6 matrix. At a concentration of 0.2 wt% less agglomerated particles are visible in optical microscopy. However larger spherulites were formed compared to **1p** at the same concentration. The less homogeneous morphology and the larger spherulites are also reflected in the haze values of PA6. As already described in chapter 5.4.4 the values for haze are considerably lower compared to **1p**, which is a clarifier for PA6.

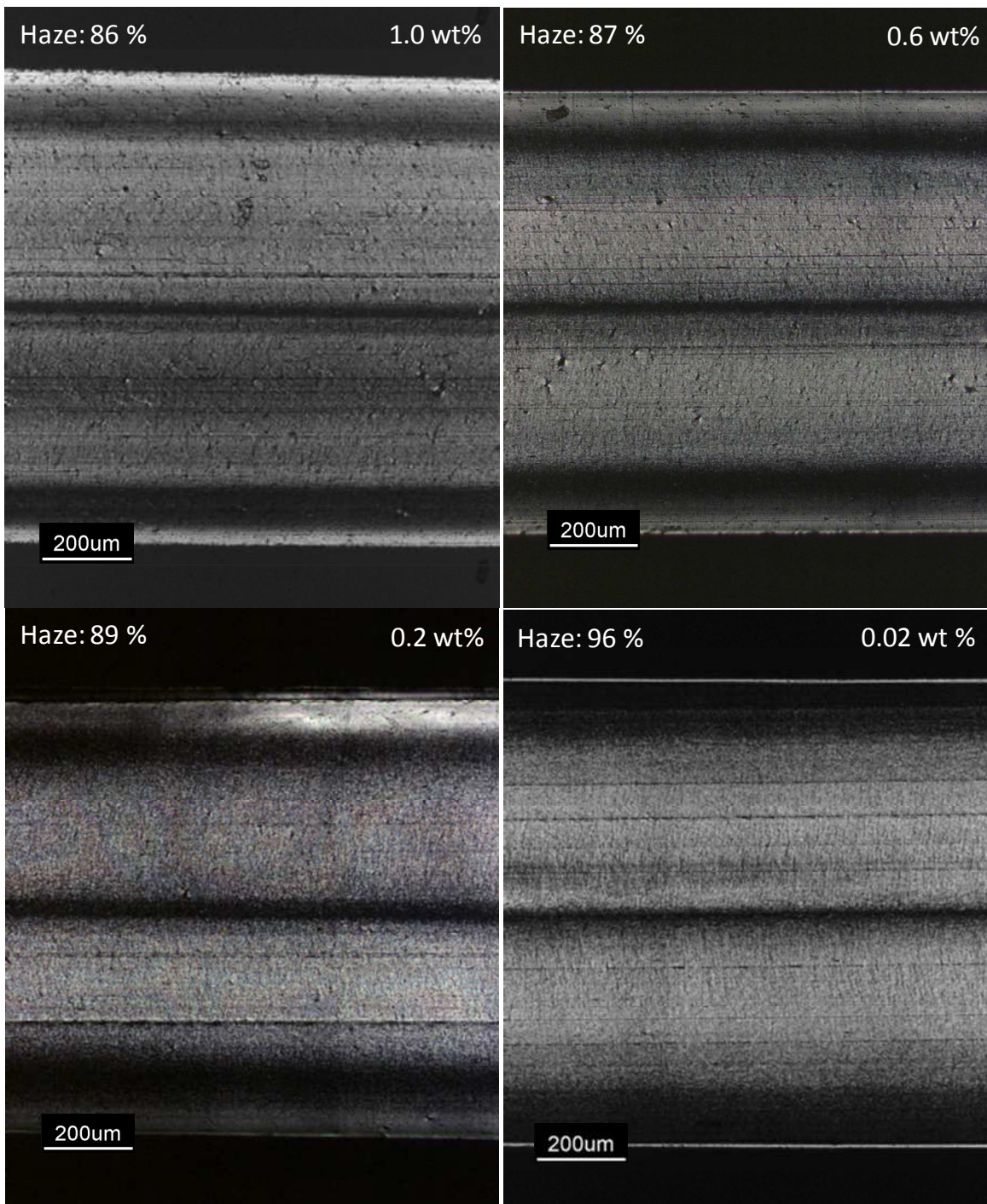


Figure 82. Thin sections of injection molded samples (thickness 1.1 mm) parallel to the flow direction and the corresponding haze values of PA6 comprising talc at different concentrations. The images presented consist of two separate pictures taken between crossed polarizers.

5.4.10. Crystal modification of PA6

PA6 crystallizes, depending on the processing conditions, into three main polymorphs, the α -, γ - and the metastable β -phase, with the α - and γ -form being the most prominent modifications. Both polymorphs differ concerning their mechanical properties as well as their thermal properties and can be detected by DSC measurements. Figure 83 shows the DSC diagram of a PA6 sample comprising 0.1 wt% talc revealing a mixture of both the α and γ form. In the heating scan two melting transitions are observed for the γ -phase at 218°C and for the α -phase at 223°C.

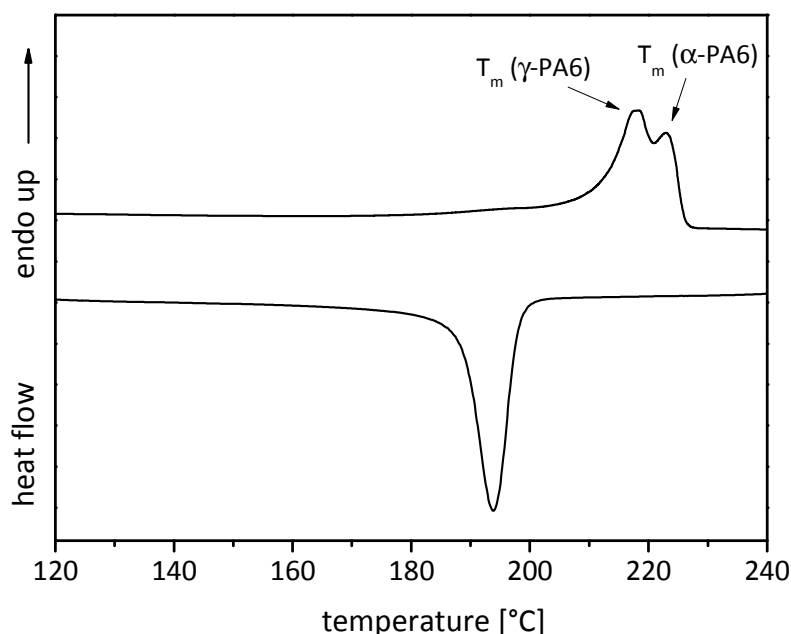


Figure 83. DSC diagram of PA6 comprising 0.1 wt% of talc.

Wide-angle X-ray diffractometry is a more accurate way to characterize the different phases and their relative amounts. The most difficult step in determining the phase content from a WAXD scan is the separation of the amorphous halo from the crystalline peaks.^[82] Other than for PE or iPP, PA6 does not show well pronounced crystalline peaks, making it more difficult to resolve the diffraction pattern especially for poorly crystallized samples. In order to bypass these difficulties a method described by Murthy et. al.^[67] using amorphous templates was used. The use of an amorphous film as template material must be discarded due to post-crystallization of the polyamide at ambient conditions. Alternatively the amorphous template was obtained by subtracting the crystalline peaks from a diffraction scan of a highly crystalline sample, enriched in α -phase. Furthermore the starting values for the positions of the crystalline diffraction peaks as well as their full width at half maximum

(FWHM) were estimated from enriched patterns. The so obtained values were used for profile fitting of the injection molded specimens using Origin8G software. To simplify the fitting routine all profiles were considered to be Gaussian.^[109]

In order to separate the contribution of the crystalline peaks from the diffraction pattern of PA6, a highly crystalline sample enriched in the α -phase was obtained by heating an injection molded specimen in water at 180°C for 3h. The so obtained diffraction pattern and the corresponding deconvolution curves are shown in Figure 84. The relevant peak positions are labeled with the designation of the lattice planes in brackets. The profile parameters are summarized in Table 10. From the integrals of the deconvolution curves the percentage of the α - and γ -form and the degree of crystallinity can be calculated using the following formulae:

$$CI_{\alpha}(\%) = \frac{\sum A_{\alpha\text{-form}}}{\sum (A_{\alpha\text{-form}} + A_{\gamma\text{-form}}) + A_{\delta\text{-form}}} \quad (3)$$

$$CI_{\gamma}(\%) = \frac{\sum A_{\gamma\text{-form}}}{\sum (A_{\alpha\text{-form}} + A_{\gamma\text{-form}}) + A_{\delta\text{-form}}} \quad (4)$$

$$CI(\%) = CI_{\alpha} + CI_{\gamma} \quad (5)$$

with $A_{\alpha\text{-form}}$ and $A_{\gamma\text{-form}}$ being the area under the crystalline peaks of the α - and γ -modification, respectively and $A_{\delta\text{-form}}$ being the area under the amorphous halo.

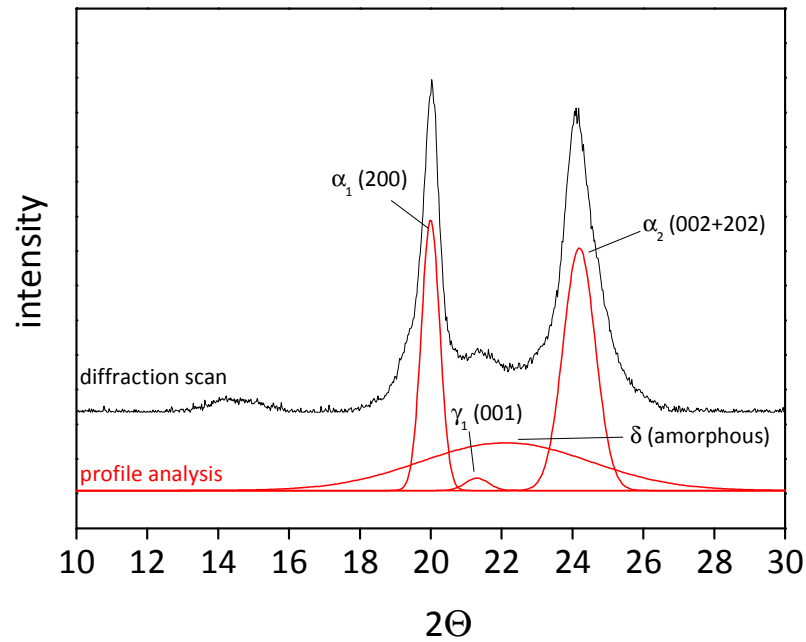


Figure 84. Diffractometer scan and corresponding profile analysis of a highly crystalline PA6 sample enriched in the α -phase.

Table 10. Profile parameters for PA6.

	α_1 (200)	α_2 (002+202)	γ_1 (001)	δ (amorphous)
Peak position [°]	19.99	24.19	21.30	22.11
FWHM [°]	0.61	0.91	0.77	5.63
Area	5054	7948	290	8241

The value for the FWHM of the amorphous halo was used in the following to analyze the crystal morphology of the injection molded specimens. As proposed by Murthy et. al.^[67] the full width of δ was allowed to vary in a small range of 0.5°. The diffraction scan of neat PA6 is shown in Figure 85. Due to the only less pronounced crystalline peaks an exact profile analysis for the neat polymer could not be drawn. However it appears clearly that PA6 crystallizes predominantly in the γ -phase under the given processing conditions.

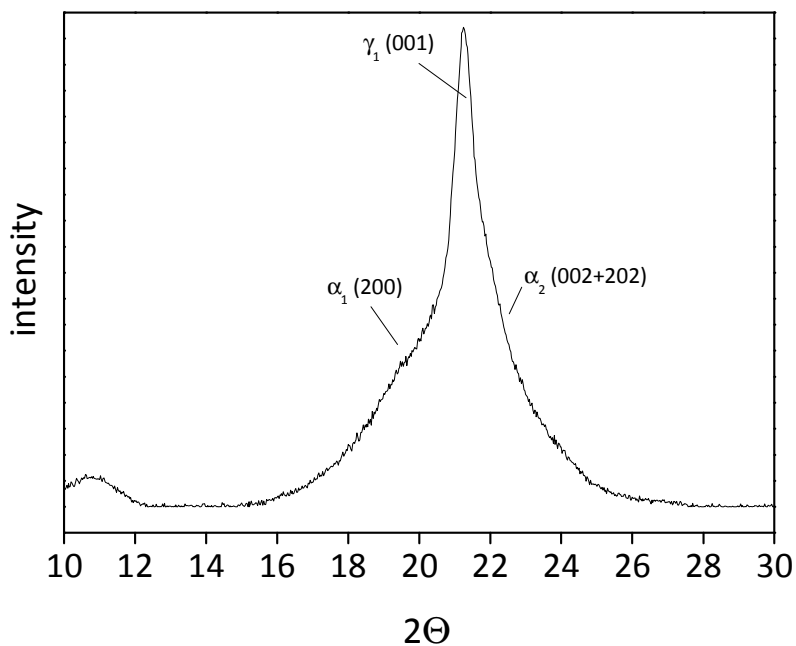


Figure 85. Diffraction scan of an injection molded specimen of PA6.

The effect of nucleation with bisurea derivatives on the crystal structure of PA6 is exemplarily shown for different concentrations of **1r** in Figure 86. The so obtained crystal phase composition is summarized in Table 11. The results of the XRD patterns significantly differ from the neat polymer. Remarkably the addition of **1r** had significant influence on the phase content of PA6. In contrast to the neat polymer, nucleation predominantly promotes the formation of α -phase crystals under equal processing conditions. An increase in the fractions of the γ -polymorph was detected at lower additive concentrations, however the values associated with the γ -form are still distinctly lower compared to the neat polymer Figure 85.

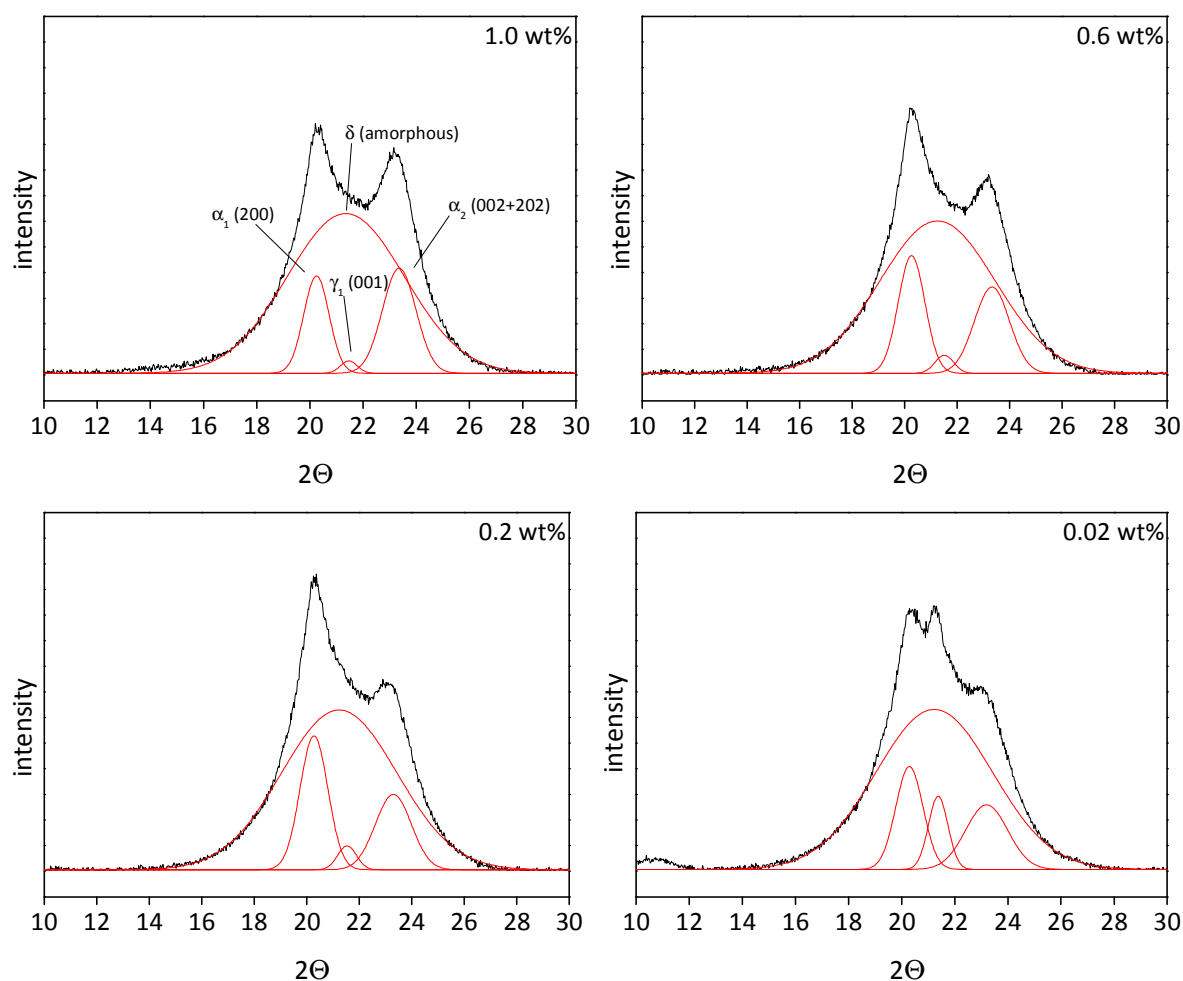


Figure 86. Diffractometer scans and corresponding profile analysis of PA6 comprising different concentrations of **1r**.

Table 11. Content of the different crystal phases of PA6 comprising different concentrations of **1r** obtained from profile analysis shown in Figure 86.

Concentration [wt%]	Cl_{α} [%]	Cl_{γ} [%]	Cl_{total} [%]	Cl_{δ} [%]
1.0 wt%	24.1	0.8	24.9	75.1
0.6 wt%	25.6	1.4	27.0	73.0
0.2 wt%	25.4	1.8	27.2	72.8
0.02 wt%	21.6	5.6	27.2	72.8

Additionally, all bisureas from the three additive series (symmetric trans-, symmetric cis- and asymmetric trans-bisureas derivatives) were investigated regarding their influence on the crystal modification of PA6 at a concentration of 0.2 wt%. The diffraction patterns for eight selected symmetrically substituted trans-bisureas and two asymmetrically substituted trans-bisureas are summarized in Figure 87 arranged with increasing haze values from bottom to top. Consistent with the observations for **1r** all trans-bisureas promoted the

formation of α -phase crystals, even at low concentrations and can thus be regarded as efficient α -phase nucleators for PA6. A correlation between the chemical structure of the trans-additives and the ability to induce the α -polymorph in PA6 could not be drawn as the diffraction patterns only differ slightly. The same applies for the optical characteristics. As example for **1f** and **1r** haze values above 90 % are observed at a concentration of 0.2 wt%. For **1p** the haze is 47 % at the same concentration. However the α -phase content of the three additives is relatively the same. In conclusion fractions of the γ -form cannot solely account for the higher haze values observed for several additives.

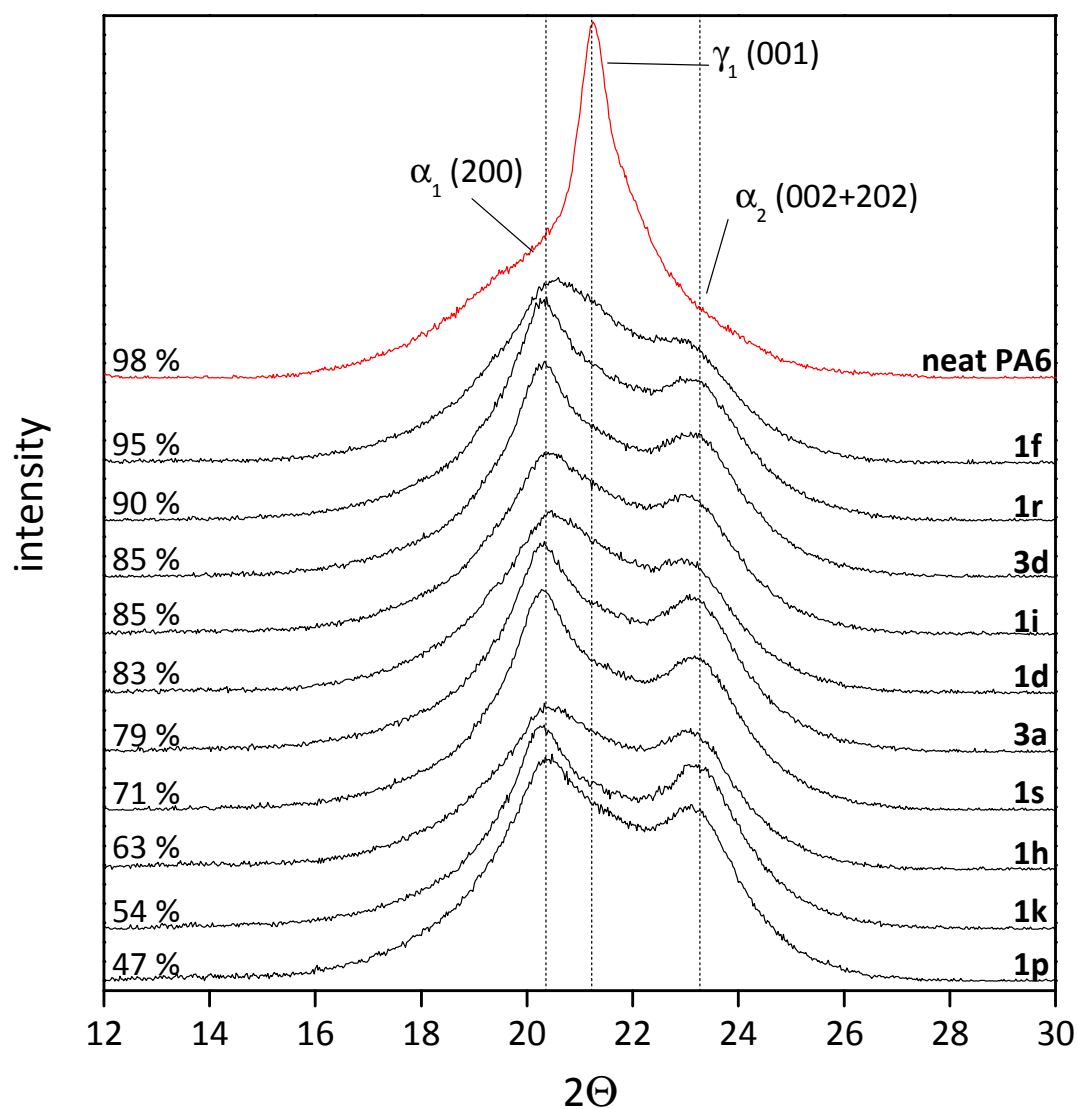


Figure 87. Diffractometer scans of neat PA6 and PA6 comprising different symmetric trans-bisurea additives at 0.2 wt% arranged from top to bottom with decreasing haze values. The haze values for plaques of 1.1 mm are presented close to the left margin.

The lower nucleation ability of the cis-bisurea derivatives is also reflected in the crystal phase composition of PA6. Only the compounds **2d**, **2b** and **2e** were capable to promote the formation of a larger amount of the α -polymorph. However in spite of the modest increase in α -phase content, the values for haze have not changed. With **2a**, **2c** and **2f** the diffraction patterns resemble those of neat PA6, with mainly γ -crystals formed.

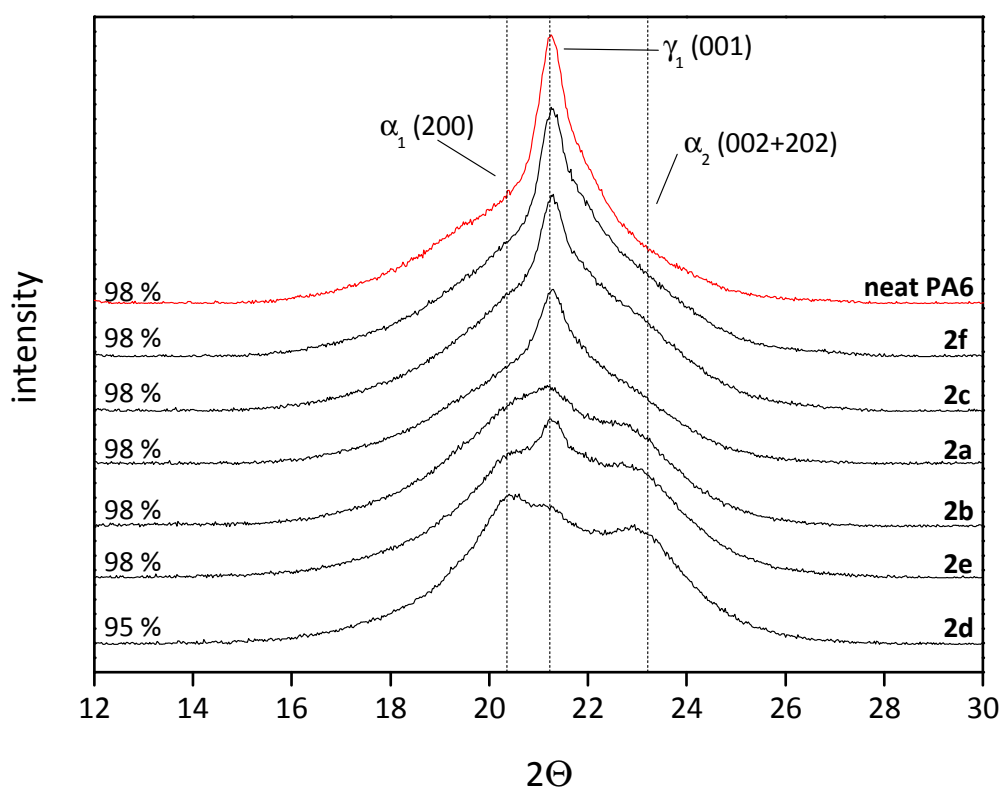


Figure 88. Diffractometer scans of neat PA6 and PA6 comprising different symmetric cis-bisureas and the corresponding haze values, arranged with increasing γ -phase content from bottom to top. The haze values for plaques of 1.1 mm are presented close to the left margin.

5.4.11. Nucleation and optical properties of PA66 and PA12 homopolymers and polyamide copolymers

In the following the influence of the most efficient bisurea derivative **1p** on the crystallization behavior and the optical properties of PA66, PA12 and polyamide copolymers is discussed. The additive concentration was varied from 1.5 wt% (15000 ppm) to 0.025 wt% (250 ppm) in the following semi-crystalline polyamides:

- Polyamide 66 (PA66), Ultramid[®] A27 E 01
- Copolyamide 6/66 (PA6/66), Ultramid[®] C33
- Copolyamide 66/6 (PA66/6), Ultramid[®] 9A E 01
- Copolyamide 6/12 (PA6/12), Zytel[®] 1512
- Polyamide 12 (PA12), Vestamid[®] L2101F

Self-seeding experiments to determine the nucleation efficiency as described for PA6 in 5.4.4 were performed for each polyamide. Figure 89 to Figure 93 show the crystallization exotherms of the above polyamides for various T_s values.

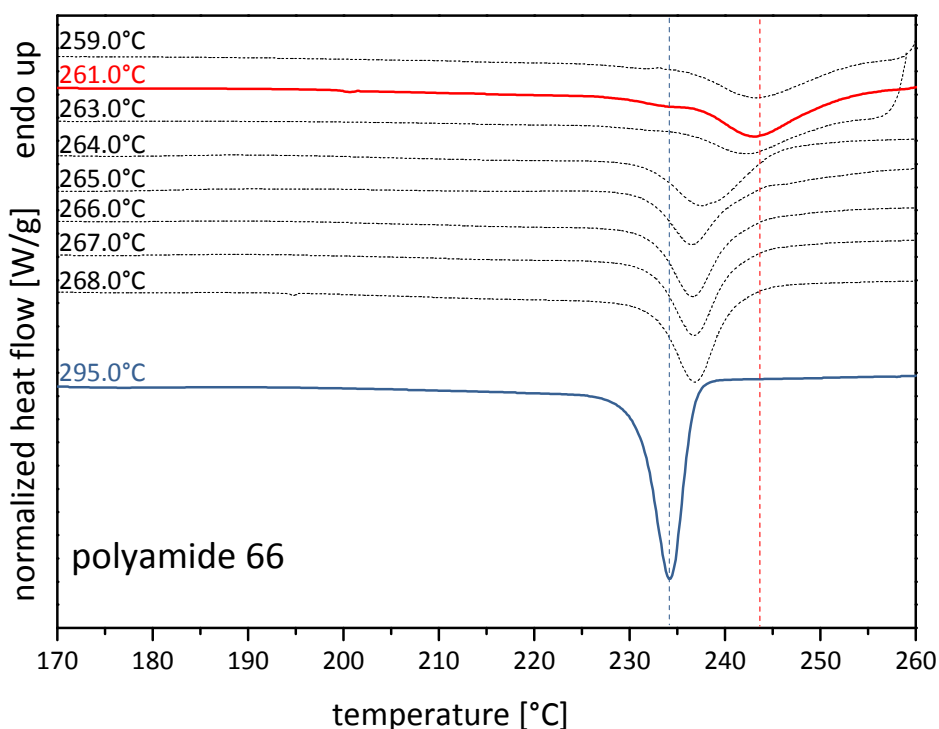


Figure 89. Crystallization exotherms of neat PA66 for different self nucleation temperatures (T_s). $T_{c,p\ theo}$ is at 243.5°C indicated by the dashed red vertical line. The $T_{c,p}$ of the neat resin heated above the equilibrium melting temperature is at 234.2°C indicated by the dashed blue vertical line.

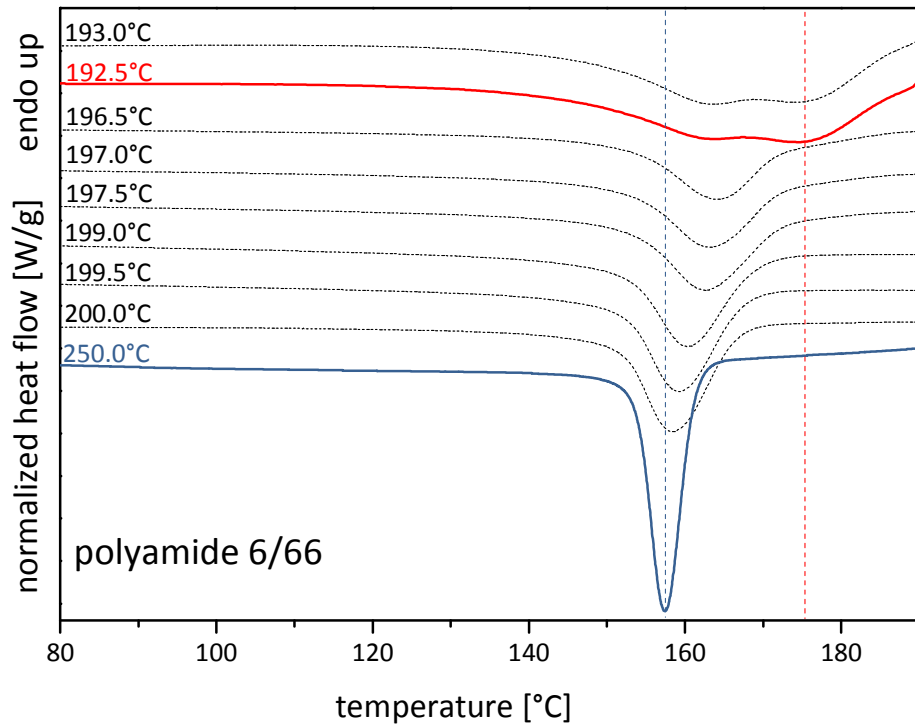


Figure 90. Crystallization exotherms of neat PA6/66 for different self nucleation temperatures (T_s). $T_{c,p \text{ theo}}$ is at 175.3°C indicated by the dashed red vertical line. The $T_{c,p}$ of the neat resin heated above the equilibrium melting temperature is at 157.5°C indicated by the dashed blue vertical line.

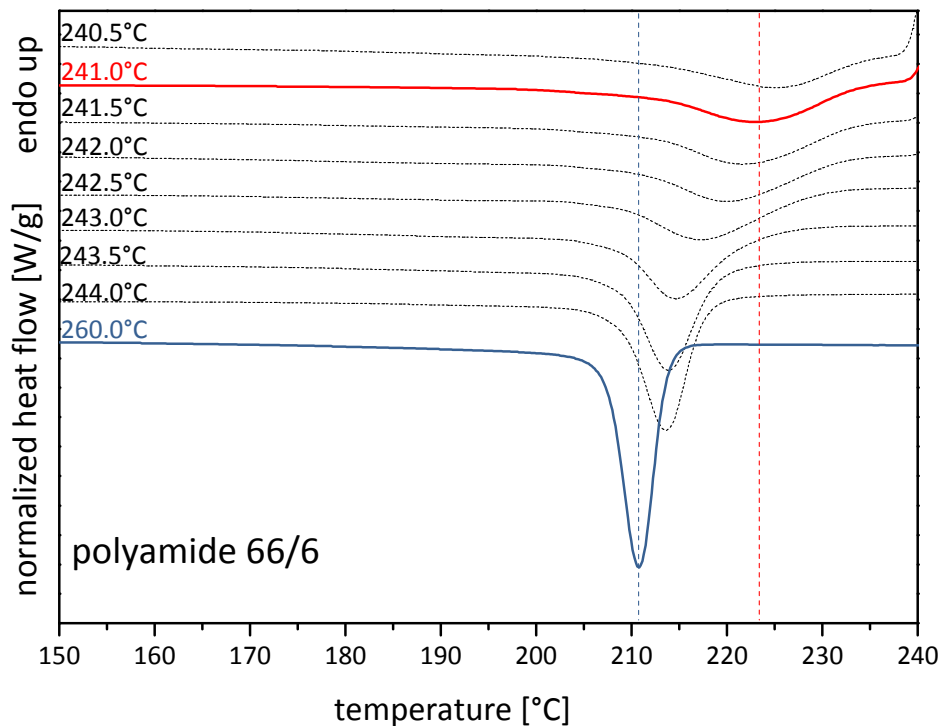


Figure 91. Crystallization exotherms of neat PA66/6 for different self nucleation temperatures (T_s). $T_{c,p \text{ theo}}$ is at 223.3°C indicated by the dashed red vertical line. The $T_{c,p}$ of the neat resin heated above the equilibrium melting temperature is at 210.7°C indicated by the dashed blue vertical line.

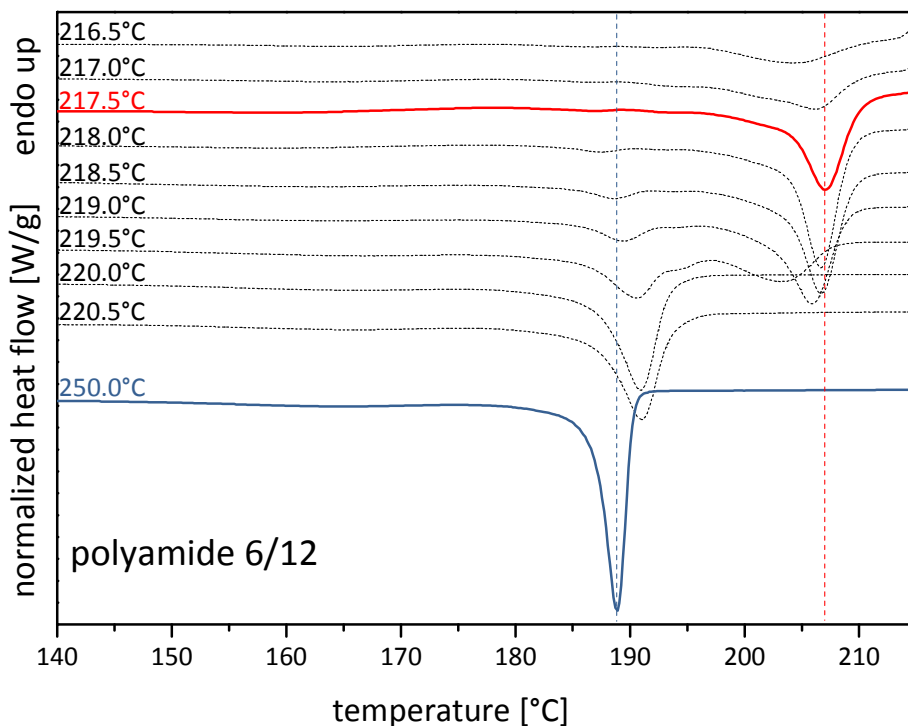


Figure 92. Crystallization exotherms of neat PA6/12 for different self nucleation temperatures (T_s). $T_{c,p \text{ theo}}$ is at 207.0°C indicated by the dashed red vertical line. The $T_{c,p}$ of the neat resin heated above the equilibrium melting temperature is at 188.8°C indicated by the dashed blue vertical line.

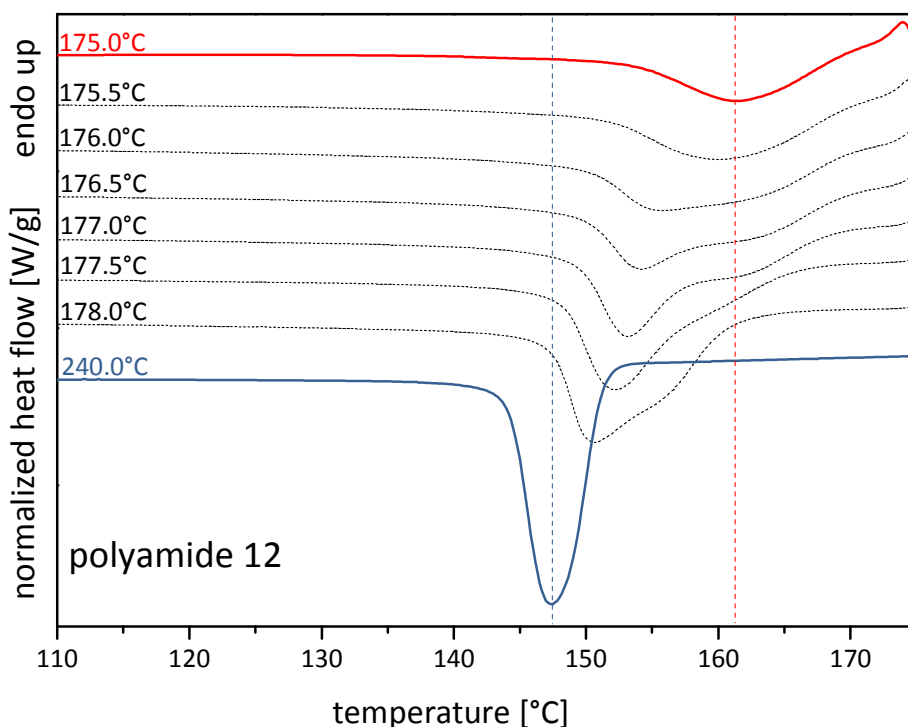


Figure 93. Crystallization exotherms of neat PA12 for different self nucleation temperatures (T_s). $T_{c,p \text{ theo}}$ is at 147.5°C indicated by the dashed red vertical line. The $T_{c,p}$ of the neat resin heated above the equilibrium melting temperature is at 161.3°C indicated by the dashed blue vertical line.

The self nucleation temperature (T_s), the polymer crystallization temperature ($T_{c,p}$), the maximum polymer crystallization temperature ($T_{c,p \text{ theo}}$) and the maximum crystallization temperature gain ($\Delta T_{c,p}$) for each polymer are summarized in Table 12.

Table 12. Self-nucleation temperature (T_s), polymer crystallization temperature ($T_{c,p}$), maximum polymer crystallization temperature ($T_{c,p \text{ theo}}$) and maximum polymer crystallization temperature gain ($\Delta T_{c,p}$) for each polymer.

Polymer	T_s [°C]	$T_{c,p}$ [°C]	$T_{c,p \text{ theo}}$ [°C]	$\Delta T_{c,p}$ [°C]
PA66	261.0	234.2	243.5	9.3
PA6/66	196.5	157.5	175.3	17.8
PA66/6	241.0	210.7	223.3	12.6
PA6/12	217.5	188.8	207.0	18.2
PA12	175.0	147.5	161.3	13.8

PA12 and the copolyamides PA6/12 and PA6/66 exhibit multiple crystallization exotherms in the self-seeding experiments as both polymers crystallize into separate polymorphs showing two melting transitions upon heating. An exact determination of the self-nucleation temperature T_s is therefore complicated. Heating above the second melting endotherm yields to an only minor raise in polymer crystallization temperature as the first phase is in the fully molten state. However, if T_s is selected too low the crystals of the second phase do not melt. Thus for the determination of the maximum theoretical polymer crystallization temperature, the polymer has to be carefully heated to a temperature T_s located between the first and second melting endotherm. The values for $T_{c,p \text{ theo}}$ of these two polymers were determined at the exothermic minimum of the first peak occurring upon cooling from T_s . Considering this, the highest values for the temperature gain are obtained for PA6/66 and PA6/12 with 17.8°C and 18.2°C respectively. In contrast, due to its very fast crystal growth rates, the lowest $\Delta T_{c,p}$ values were found for PA66, making this polymer much more difficult to nucleate.^[19]

The concentration dependence of the nucleation properties (top graphs) and the optical properties (bottom graphs) of **1p** in the polyamide copolymers PA6/66, PA66/6 and PA6/12 are presented in Figure 94. Consistent with the observation for PA6 in chapter 5.4.3.2, **1p** shows remarkable nucleation behavior in the investigated copolyamides.

For PA6/66 (Ultramid® C33) the $T_{c,p}$ values steeply increase by the addition of **1p**. At a concentration of as low as 0.02 wt% the polymer crystallization temperature increases by 7.1°C to 164,6°C. At higher amounts of additive the $T_{c,p}$ values further increase to a maximum of 173.9°C at 1.3 wt%. This corresponds to a nucleation efficiency of 92 %. The leap in $T_{c,p}$ from 1.0 to 1.3 wt% can be explained by the formation of two exothermic crystallization peaks in the DSC measurements. For the two highest concentrations an additional peak at higher temperatures evolves and was used to determine the $T_{c,p}$ values.

For PA66/6 (Ultramid® 9A) the $T_{c,p}$ also increases with increasing additive concentration. Above 0.4 wt% the polymer crystallization temperature only varies marginally with the additive concentration. A plateau with a mean $T_{c,p}$ value of 219.2 °C is reached, what corresponds to a nucleation efficiency of 67 %.

For PA6/12 (Zytel® 1512) the mean $T_{c,p}$ plateau value is at 192.1°C and also a pronounced nucleation effect is observed. It is interesting to note that the plateau is already reached at concentrations above 0.1 wt%. Here the nucleation efficiency is considerably low with only 20 %.

In addition to the crystallization kinetics, **1p** has strong influence on the optical properties of injection molded specimens. For PA6/66 the clarity values remain at the very high initial values of around 96 %. For PA66/6 clarity increases from 60 % to over 95 % with very low additive amounts. For PA6/12 the clarity values increase from 78% of the neat resin to also over 95 %. The values remain at these high values for all investigated concentrations. The values for haze steadily decrease with further addition of **1p** demonstrating the excellent solubility of the additive at the processing conditions. For PA6/66 the haze decreases to values as low as 6 % for a concentration of 1.3 wt%. For the neat resin no haze value could be obtained, due to the limited processability of neat PA6/66.

For PA66/6 the haze values decrease by 67 % from 90 % of the neat polymer to 23 % at a concentration of 1.0 wt%.

For the copolymer PA6/12 the haze values decrease from 75 % to 37 % at 0.6 wt%. For higher amounts of additive the haze increases again slightly, most likely to insufficient solubility or

liquid phase separation in the polymer melt at higher concentrations. This phenomenon was also observed for iPP with trisamide additives.^[6, 110]

As expected at lower additive concentrations the crystallization temperatures were found to decrease for all polymers, approaching the values for the corresponding neat melt processed polyamides. For PA66/6 and PA6/12 at high amounts of additive a plateau was reached where further addition of **1p** showed no influence on the T_c . Interestingly, for PA6/66 a sharp increase in crystallization temperature of around 5°C was observed for concentrations exceeding 1.0 wt%. The highest nucleation efficiencies were found for PA6/66 with 92 % at a concentration of 1.3 wt%. For this polymer, **1p** represents an almost ideal nucleating agent. For PA66/6 and PA 6/12 the highest efficiencies were found to be 74 % at 0.8 wt% and 20 % at 1.3 wt% respectively.

In addition to the crystallization kinetics, **1p** had significant influence on the optical properties of injection molded specimens (Figure 94, bottom graphs). The values for haze steadily decreased with further addition of **1p** demonstrating the excellent solubility of the additive at the processing conditions. Values for clarity maintained on a very high level, even at the lowest additive concentrations. However, the results obtained for PA6/66 are rather different. Here the optical properties deteriorate compared to the neat reference material for concentrations below 0.2 wt%.

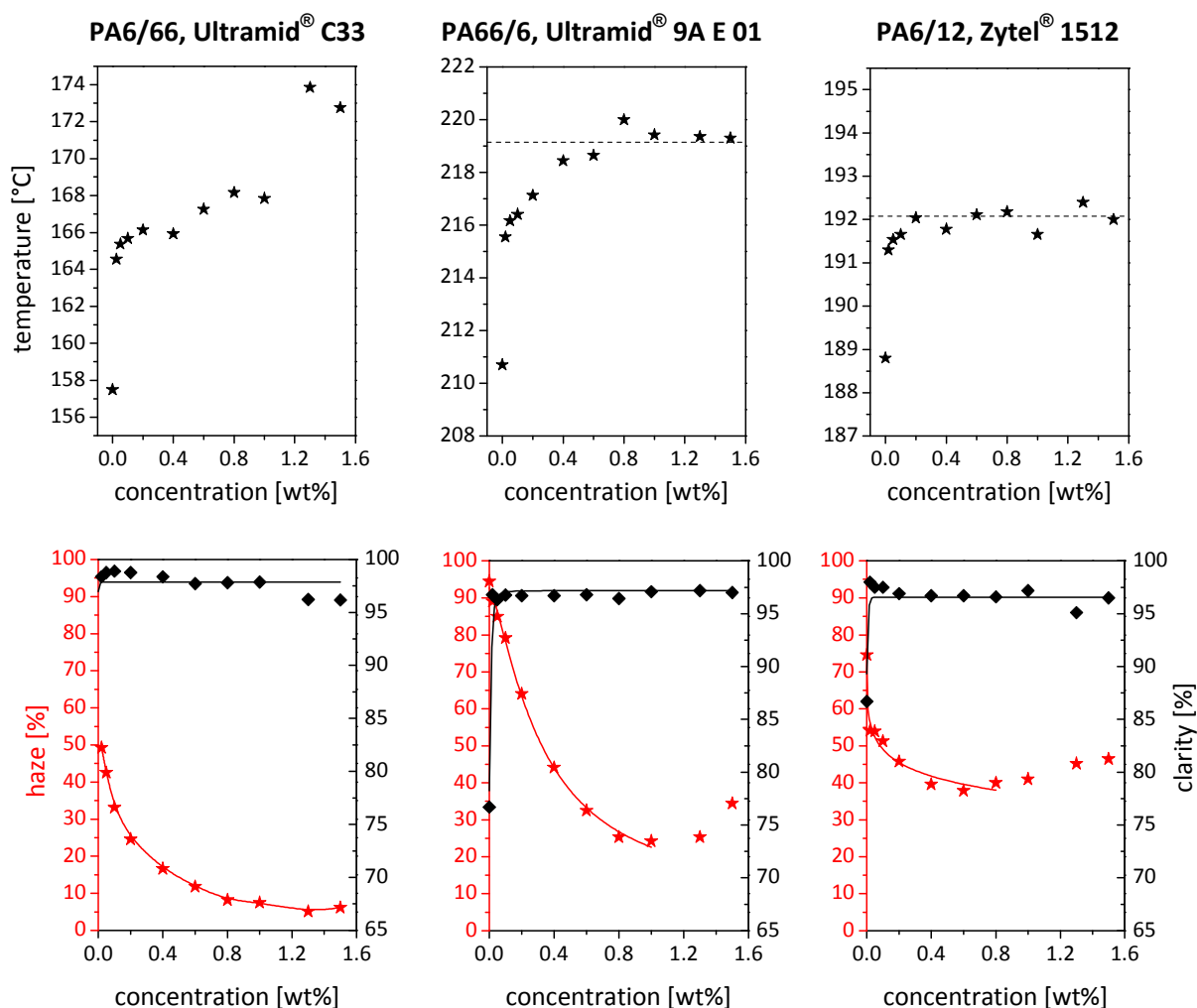


Figure 94. Crystallization temperatures ($T_{c,p}$ ★) (top graphs) and the optical properties haze (★) and clarity (◆) (bottom graphs) of the polyamide copolymers PA6/66 (Ultramid® C33), PA66/6 (Ultramid® 9A) and PA6/12 (Zytel® 1512) comprising the tert-butyl substituted trans-bisurea **1p** as function of the additive concentration. The dashed lines indicate the plateau in the polymer crystallization temperature.

The nucleation behavior of the tert-butyl substituted bisurea **1p** in PA66 (Ultramid® A27) and PA12 (Vestamid® L2101F) is shown in Figure 95. Despite the higher processing temperatures, **1p** is capable to considerably promote the nucleation of PA66 without degradation. Derivative **1p** increases the $T_{c,p}$ value from 234.2°C of neat PA66 to 240.8°C at 1.3 wt%. This corresponds to a nucleation efficiency of 71 %. However, the NE values rapidly decrease with less amount of additive most likely due to the enhanced solubility at the higher temperatures. At a concentration of 0.02 wt% the $T_{c,p}$ is only slightly increased to 235.7°C. For PA12 again a plateau was reached at concentrations above 0.4 wt%. The mean $T_{c,p}$ plateau value is at 154.0°C. This is a nucleation efficiency of 47 %. It is interesting to note that for PA6/12 and PA12 the lowest nucleation efficiencies of **1p** in the investigated

polymers were obtained. This indicates that the length of the repeating unit is essential in determining whether the additive is capable to significantly promote the nucleation of the polymer. The bisureas in this study are mainly of advantage if PA6 repeating units are present.

Nucleation with **1p** also has an influence on the optical properties of PA66 and PA12. In case of PA66 the clarity increases dramatically upon addition of already small amounts of additive. The clarity reaches a plateau for concentrations above 0.2 wt% at 95 %. For PA12 the clarity values remain at the initially high values of 95 %. Despite the excellent nucleation behavior in PA66, **1p** has only minor effects on haze at first glance. However, considering the complete opaque appearance of neat PA66 with a haze of 100 % the values obtained for haze (52 %) at 1.3 wt% are not as bad as one might initially believe. Even though **1p** is only capable to nucleate PA12 with comparably low efficiencies, the optical properties of the specimens are still improved. The lowest haze value is 27 % at 1.5 wt% and thus 43 % lower than for neat PA12. It is interesting to note that the values for haze reach a plateau for concentrations above 0.4 wt%, which most likely seems to be a result of the minor solubility in the polymer matrix due to the lower processing temperature of PA12. In conclusion, the tert-butyl substituted trans-bisurea **1p** is capable to effectively nucleate and clarify PA6. In addition a transfer was possible to further semi-crystalline polyamides. Here, the additive is most beneficial in polyamides with PA6 repeating units.

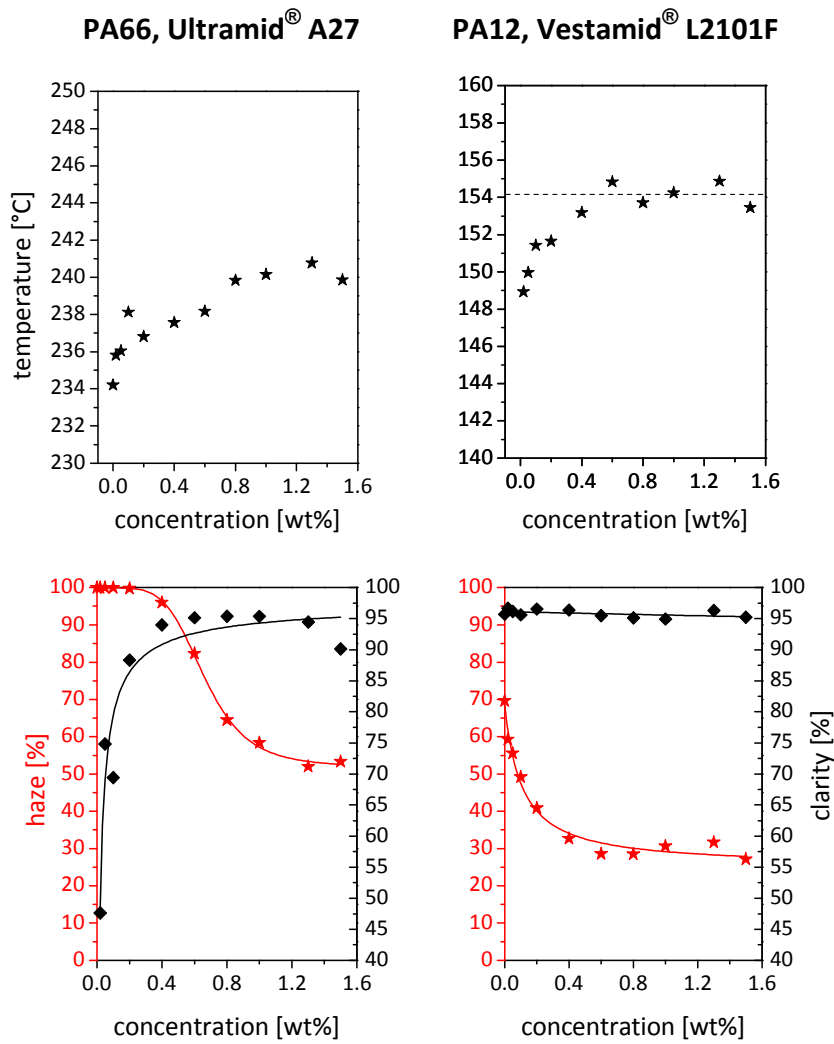


Figure 95. Crystallization temperatures (T_{cp} ★) (top) and the optical properties haze (★) and clarity (◆) (bottom) of PA66 and PA12 comprising **1p** as function of the additive concentration.

6. Summary

The use of additives to enhance the processability and end properties is one of the main measures to enlarge the property profile of commercial thermoplastic polymers. The physicochemical properties of semi crystalline polymers depend to a large extent on the crystal structure and spherulite size, which can be controlled by nucleating agents. These additives can increase the crystallization temperature and thus reduce cycle times during melt processing, affect the physical properties and can in some cases improve the optical properties (clarity and haze). This thesis describes the use of supramolecular nucleating agents to increase the polymer crystallization behavior and to improve the optical properties of polybutylene terephthalate and polyamides.

In the first chapter the influence of the molecular structure of ***1,3,5-benzenetrisamides on the nucleation behavior of polybutylene terephthalate*** was investigated. In order to explore structure property relations, 43 derivatives based on the 1,3,5-benzenetricarboxylic acid core, 1,3,5-triamino benzene core, 2,4,6-trimethyl-1,3,5-benzenetrisamide core and 1,3,5-trisaminotoluene core were screened with regard to their nucleation ability of PBT. For promising compounds the additive dissolution and crystallization behavior in the polymer melt and crystallization temperature of the polymer were investigated in the concentration range from 0.8 wt% down to 0.006 wt%. It was revealed that certain 1,3,5-benzenetrisamides are capable to nucleate PBT. The 1,3,5-benzenetrisamides feature outstanding high temperature stability and chemical resistance to be processed under the commonly applied conditions for PBT. They can act as supramolecular polymer additives, are soluble in the PBT melt under the processing conditions and upon cooling self-assemble into fine fibrillar supramolecular nano-objects inducing the nucleation of PBT. The investigated 1,3,5-benzenetrisamide additives are much more soluble in PBT compared to the same additives in isotactic polypropylene and polyvinylidene fluoride. It was found that particularly the trisamide derivatives based on the 1,3,5-triaminobenzene core are much better soluble than the derivatives based on the 1,3,5-benzenetricarboxylic acid core and 2,4,6-trimethyl-1,3,5-trisaminobenzene core. As a result additives featuring too good solubility do not self-assemble prior to the polymer crystallization and hence do not induce nucleation.

This demonstrates that the nucleation efficiency strongly depends on the individual chemical structure of the additives and slight structural changes have large impact. However a prediction of the nucleation ability based on the molecular structure is not possible. We found that the most efficient additive, namely 1,3,5-tris(2,2-dimethylbutyrylamino)benzene, was capable to increase the crystallization temperature of PBT by 10.6°C from 188.5°C to 199.1°C. In addition for the first time it was possible to visualize the supramolecular structures within the PBT matrix by selectively hydrolyzing PBT. The morphology of the formed supramolecular nano-objects is determined by cooling rate and additive concentration. Faster cooling and lower additive concentrations leads to the formation of needle-like structures with smaller lateral dimensions and a narrower size distribution. In case of the concentration of 0.2 wt% and a cooling rate of 110 K/min supramolecular nano-objects with a diameter of 37 ± 6 nm were observed. An attempt to increase the laser transparency of PBT by nucleation with 1,3,5-benzenetrisamides was not successful.

In the second chapter a ***new class of supramolecular nucleating agents*** on the structural motif of ***1,4-cyclohexane bisureas*** was synthesized specifically for ***semi-crystalline polyamides***. These compounds combine excellent aggregation behavior with high thermal stability, due to the strong intermolecular interactions between the urea groups. The bisureas are temperature stable enough to be applied in high melting polyamides. In total, 29 derivatives were synthesized and investigated with respect to their nucleation and clarification behavior in PA6. The chemical structure of the additives was systematically varied by changing the conformation of the central unit and the length and degree of branching within the peripheral substituents. Bisureas based on the trans-conformation of 1,4-cyclohexane are capable to efficiently nucleate the α -form of PA6 even at concentrations below 200 ppm, with extremely high nucleation efficiencies of around 90 %. In addition, selected derivatives were found to distinctly improve the optical properties haze and clarity, as well as the laser transparency, in injection molded samples. This is the first time semi-crystalline polyamides were clarified. The most efficient clarifiers for PA6, namely ***1,1'-(trans-1,4-cyclohexylene)bis(3-tert-butylurea)*** and ***1,1'-(trans-1,4-cyclohexylene)bis(1,1-dimethylpropylurea)*** were found to decrease the values for haze from nearly 100 % (1.1 mm thick samples) for neat PA6 to 19 % and 11 % at a concentration of 1.5 wt%. Cis-bisureas exhibit limited nucleation and no clarification ability. By varying the peripheral substituents of the trans-bisureas interesting structure-property relations could be revealed. The

investigated derivatives with longer flexible substituents were efficient nucleating agents for PA6, but displayed only modest improvements in optical properties. Short, highly branched substituents, preferably in α -position to the urea groups, were found to be a key segment for the clarification of PA6. Additionally we demonstrated that the process conditions, namely cooling rate and mold thickness, strongly determine the final optical properties. The use of trans-1,4-cyclohexane bisureas could also be expanded to other semi-crystalline polyamide homo- and copolymers. Here, *1,1'-(trans-1,4-cyclohexylene)bis(3-tert-butylurea)* was capable to efficiently nucleate PA66, PA12, PA6/66, PA66/6 and PA6/12. For PA66/6 and PA12 haze values of about 30 % were observed. The effect on the optical properties was more pronounced if PA6 repeating units are present. For PA6/66 haze values below 10 % could be achieved. For PA66 and PA6/12 the haze was between 40 and 50 %.

For the first time the concept of supramolecular nucleating and clarifying agents was successfully transferred to semi-crystalline polyamides. With the new class of compounds it could be demonstrated that trans-1,4-cyclohexane bisurea derivatives are capable to increase the crystallization behavior and improve the optical properties, particularly the haze values, remarkably.

7. Zusammenfassung

Der Einsatz von Additiven zur Verbesserung von Verarbeitbarkeit und Endigenschaften ist eine der wichtigsten Maßnahmen das Eigenschaftsprofil von kommerziellen thermoplastischen Polymeren zu erweitern. Die physikochemischen Eigenschaften von teilkristallinen Polymeren hängen im großen Maße von der Kristallstruktur und der Spherulitgröße ab, welche durch den Einsatz von Nukleierungsmitteln kontrolliert werden können. Diese Additive erhöhen die Kristallisationstemperatur des Polymers und können insbesondere beim Spritzguss die Zykluszeiten verkürzen, die physikalischen Eigenschaften beeinflussen und in einigen Fällen die optischen Eigenschaften (Clarity und Haze) des Polymerfestkörpers beeinflussen. Die vorliegende Arbeit beschreibt supramolekulare Nukleierungsmittel zur Verbesserung des Kristallisationsverhaltens und der optischen Eigenschaften von Polybutylenterephthalat und Polyamiden.

Im ersten Kapitel wurde der Einfluss der molekularen Struktur von **1,3,5-Benzoltrisamiden auf die Nukleierung von Polybutylenterephthalat** untersucht. Um Struktur Eigenschaftsbeziehungen aufzuzeigen wurden 43 Derivate basierend auf 1,3,5-Benzoltricarbonsäure, 1,3,5-Triaminobenzol, 2,4,6-Trimethyl-1,3,5-triaminobenzol und 1,3,5-Triaminotoluol hinsichtlich ihres Vermögens PBT zu nukleieren gescreent. Die Löslichkeits- sowie die Kristallisationstemperatur ausgewählter Additive in der Polymerschmelze und die Kristallisationstemperatur des Polymers wurden in einem Konzentrationsbereich von 0.8 bis zu 0.006 Gew.-% untersucht. Es wurde gefunden, dass bestimmte 1,3,5-Benzoltrisamide in der Lage sind PBT zu nukleieren. Diese Verbindungen zeigen außergewöhnliche thermische Stabilität und Chemikalienbeständigkeit und können somit bei den für PBT üblichen Bedingungen verarbeitet werden. Ausgewählte Verbindungen sind in der PBT Schmelze löslich und kristallisieren beim Abkühlen bereits über der Kristallisationstemperatur des Polymers zu homogen verteilten Nanoobjekten aus, welche die Nukleierung des Polymers induzieren. Die untersuchten 1,3,5-Benzoltrisamide sind in der PBT Schmelze löslicher verglichen mit denselben Verbindungen in isotaktischem Polypropylen oder Polyvinylidenfluorid. Insbesondere die Derivate basierend auf dem 1,3,5-Triaminobenzolkern zeigten eine erhöhte Löslichkeit. Demzufolge findet der Selbstorganisationsprozess bei zu gut löslichen Verbindungen nicht vor der Kristallisation des Polymers statt, wodurch keine Nukleierung induziert wird.

Dies zeigt deutlich dass die individuelle chemische Struktur des Additivs die Nukleierungseffizienz maßgeblich beeinflusst und schon kleine strukturelle Variationen des Additivs einen großen Einfluss ausüben. Eine Vorhersage der endgültigen Eigenschaften basierend auf der molekularen Struktur der Additive ist deshalb nicht möglich. Mit 1,3,5-Tris(2,2-dimethylbutyrylamino)benzol wurde eine Verbindung gefunden welche in der Lage ist die Kristallisationstemperatur von PBT um 10.6°C von 188.5°C auf 199.1°C anzuheben. Zudem ist es zum ersten Mal gelungen die supramolekularen Strukturen in PBT durch selektive Hydrolyse der Polymermatrix sichtbar zu machen. Die Morphologie der supramolekularen Strukturen, der über mehrere Hierarchieebenen und Längenskalen ablaufenden Selbstorganisationsprozesse, wird im Wesentlichen über die Abkühlrate und die Additivkonzentration bestimmt. Beim schnellen Abkühlen und niedrigen Konzentrationen bilden sich nadelförmige Strukturen mit kleiner lateraler Abmessung und einer engen Größenverteilung aus. Bei einer Konzentration von 0.2 Gew.-% und einer Abkühlrate von 110 K/min wurden supramolekulare Nanoobjekte mit einem Durchmesser von 37 ± 6 nm beobachtet. Der Versuch die Lasertransparenz von PBT durch die Nukleierung mit 1,3,5-Benzoltrisamiden zu steigern war nicht erfolgreich.

Im zweiten Kapitel wurde eine neue Klasse von **supramolekularen Nukleierungsmitteln** basierend auf **1,4-Cyclohexan-Bisharnstoffen**, zur Verwendung in **teilkristallinen Polyamiden**, synthetisiert. Aufgrund der starken intermolekularen Wechselwirkungen zwischen den Harnstoffgruppen zeigt diese Verbindungsklasse ein exzellentes Aggregationsverhalten und hohe thermische Stabilität, weshalb sie auch in hochschmelzenden Polyamiden eingesetzt werden können. Insgesamt wurden 29 Derivate synthetisiert und hinsichtlich der Nukleierung und Klarmodifizierung von PA6 untersucht. Die chemische Struktur der Additive wurde systematisch durch Veränderung der Konformation der zentralen Einheit und der Länge und dem Verzweigungsgrad der peripheren Substituenten, variiert. Bisharnstoffe basierend auf trans-1,4-Cyclohexan waren in der Lage die α -Form von PA6 bei sehr niedrigen Konzentrationen von 200 ppm mit extrem hohen Nukleierungseffizienzen von 90 % zu nukleieren. Ausgewählte Verbindungen verbesserten die optischen Eigenschaften Haze und Clarity, sowie die Lasertransparenz von spritzgegossenen Probekörpern deutlich. Somit war es zum ersten Mal gelungen die Transparenz von teilkristallinen Polyamiden zu verbessern. Mit 1,1'-(trans-1,4-Cyclohexan)bis(3-tert-butylurea) und 1,1'-(trans-1,4-Cyclohexan)bis(1,1-di-methylpropylurea)

wurden zwei Verbindungen gefunden welche den Haze von PA6 von fast 100 % (1.1 mm Probendicke) auf 19 % und 11 % bei einer Konzentration von 1.5 Gew.-% senken. Cis-Bisharnstoffe sind hingegen nur geringfügig in der Lage die Kristallisation von PA6 zu induzieren und verbessern nicht die optischen Eigenschaften des Polymers. Durch systematische Variation der peripheren Substituenten konnten interessante Struktur Eigenschaftsbeziehungen aufgedeckt werden. Die untersuchten Verbindungen mit längeren beweglichen Resten stellten effiziente Nukleierungsmittel für PA6 dar, waren aber nur im geringen Maße in der Lage die optischen Eigenschaften zu verbessern. Derivate mit kurzen, hochverzweigten Substituenten, bevorzugt in α -position zu den Harnstoffgruppen, verbesserten den Haze hingegen deutlich. Es konnte zudem gezeigt werden, dass die Verarbeitungsbedingungen, insbesondere die Abkühlrate und die Probendicke, starken Einfluss auf die Endigenschaften des Polymerfestkörpers ausüben. Trans-1,4-Cyclohexan-Bisharnstoffe wurden ebenfalls in anderen teilkristallinen Polyamid Homo- und Copolymeren untersucht. 1,1'-(trans-1,4-Cyclohexan)bis(3-tert-butylurea) war in der Lage effizient PA66, PA12, PA6/66, PA66/6 und PA6/12 zu nukleieren. Für PA66/6 und PA12 wurden Hazewerte von etwa 30 % erreicht. Eine größere Klaromodifizierung war in Gegenwart von PA6 Wiederholeinheiten möglich. Für PA6/66 konnte der Haze unter 10 % gesenkt werden. Bei PA66 und PA6/12 lagen die besten Hazewerte zwischen 40 und 50 %.

Zum ersten Mal konnte somit das Konzept der supramolekularen Nukleierungsmittel auf teilkristalline Polyamide übertragen werden. Mit der neu entwickelten Verbindungsklasse konnte gezeigt werden, dass trans-1,4,-Cyclohexan-Bisharnstoffe in der Lage sind das Kristallisationsverhalten zu beschleunigen und die optischen Eigenschaften, insbesondere den Haze, deutlich zu verbessern.

8. Experimental part

8.1. Materials and equipment

Chemicals and solvents

cis-1,4-diaminocyclohexane	TCI Europe 98 %, used as received
Dimethylformamide	Grüssing 99.5 %, used as received
Methanol	Technical grade, purification by distillation
N-methyl-2-pyrrolidinone	BASF, dried over CaH ₂ , distilled under vacuum
Talc Micro-Talc IT Extra	Mondo Minerals, used as received
Tetrahydrofurane	Acros 99.9 %, used as received
trans-1,4-cyclohexane diisocyanate	ABCR 97 %, used as received
trans-1,4-diaminocyclohexane	Aldrich 98 %, used as received

All solvents used for recrystallization (except DMF) were purified by distillation. All other chemicals were commercially available and used without further purification.

Equipment

Compounding	Co-rotating twin-screw compounder DSM Xplore 15 mL
DSC	Perkin Elmer Diamond DSC and Mettler Toledo DSC/SDTA 821e; Standard heating and cooling rates of 10 K/min
Haze-Meter	BYK Gardener Haze Gard plus Calibration by clarity and haze standard
Injection molding	Micro-injection molding machine DSM Xplore 12 mL
Laser transparency	FOBA DP50 Nd:YAG laser marking system Wave length: 1064 nm
Mass spectroscopy	Finnigan Mat 112S (70 eV)
Microtome	Leica RM 2255 rotary microtome
¹ H-NMR-spectroscopy	Bruker AC 300 (300 MHz)
Polarized light microscopy	Nikon, DIAPHOT 300 (microscope) Mettler, FP82HT (hot stage)

Experimental part

	Nikon, DMX1200 (digital camera)
Powder mill	Retsch ZM100, freezer mill, Schieritz & Hauenstein AG
SEM	Zeiss 1530 FESEM Cressington Sputter Coater 208HR
TGA	Mettler Toledo TGA/SDTA851e Standard heating and cooling rates of 10 K/min
WAXD	Bruker D8 Advance CuK α radiation ($\lambda = 1.54\text{\AA}$)

8.2. Polymers

In the frame of this work the influence of supramolecular additives on the crystallization behavior of semi-crystalline polymers was studied based on a thermoplastic polyester (polybutylene terephthalate) and semi-crystalline polyamides.

The following polymers were investigated:

- Polybutylene terephthalate (PBT), Ultradur[®] B4500, an intermediate-viscosity, extrusion grade for the production of flat films and thin-walled profiles.
- Polyamide 6 (PA6), Ultramid[®] B27 E, a low-viscosity grade for compounding and the production of monofilaments.
- Polyamide 66 (PA66), Ultramid[®] A27 E 01, a low-viscosity grade for compounding and the production of monofilaments and bristles.
- Co-polyamide 6/66 (PA6/66), Ultramid[®] C33, an intermediate-viscosity grade for the production of multilayer films and monofilaments.
- Co-polyamide 66/6 (PA66/6), Ultramid[®] 9A E 01, a low-viscosity grade suitable for film, monofilament, extrusion, and molding applications.
- Co-polyamide 6/12 (PA6/12), Zytel[®] 1512, suitable for molding applications.
- Polyamide 12 (PA12), Vestamid[®] L2101F, a high-viscosity film grade used for packaging applications

With exception of PA12, supplied by Evonik Industries AG, all polymer resins were provided by BASF SE. Except for PA6/12 and PA12 where no information about the specific additivation was available, all polymer grades contained no further additives. The polymer granulate was pulverized in a freezer mill (Retsch ZM100, Schieritz & Hauenstein AG) prior to use through a 1 mm sieve.

8.3. Synthesis and characterization

Synthesis and characterization of bisurea derivatives

All solvents were purified and dried prior to use according to standard procedures. The starting materials were purchased from ABCR, Acros, Aldrich, and TCI Europe and used as received. $^1\text{H-NMR}$ spectra were recorded on a Bruker Avance 300 spectrometer. The chemical shifts are reported in ppm (δ) with the coupling constant values J given in Hz. Mass spectra were recorded on a Finnigan Mat 112S instrument (70 eV) with direct probe inlet at the central analytic laboratory of the University of Bayreuth. All spectra were recorded at 298 K.

8.3.1. General synthetic route to trans-1,4-cyclohexyl-bisurea derivatives

Synthesis of trans-1,4-cyclohexyl-bisurea derivatives from trans-1,4-diaminocyclohexane

Trans-1,4-diaminocyclohexane was added in a flame-dried Schlenk flask and dissolved in THF under argon atmosphere. The solution was cooled to 0°C in an ice bath and the corresponding isocyanate, diluted in THF, was added slowly under heavy stirring. The reaction mixture was heated to reflux and, unless indicated otherwise, maintained at this temperature for 12 h. After cooling the precipitated white solid was filtered off, dried under vacuum for 2 h (70°C, 100 mbar) and recrystallized.

1,1'-(trans-1,4-cyclohexylene)bis(3-ethylurea) 1aMolecular formula: C₁₂H₂₄N₄O₂; M = 256.19 g/mol

Internal notebook number: JF262

Reaction batch:

1.78 g (16 mmol) trans-1,4-diaminocyclohexane

2.22 g (32 mmol) ethylisocyanate

150 mL THF

Purification: Recrystallization from MeOH

*Characterization:*¹H-NMR (300 MHz, DMSO d₆): δ [ppm] = 5.6 (m, 4H), 3.26 (m, 2H), 2.97 (qi, J = 6.5 Hz, 4H), 1.76 (m, 4H), 1.09 (m, 4H), 0.96 (t, J = 7.1 Hz, 6H)

MS (70 eV), m/z (%): 256 (35); 212 (21); 184 (81); 168 (93); 139 (27); 96 (59); 89 (100); 68 (35); 56 (41); 44 (45)

Schmelzpunkt: T_m = subl.Zersetzungspunkt: T_{-10 wt%} = 316°C**1,1'-(trans-1,4-cyclohexylene)bis(3-n-propylurea) 1b**Molecular formula: C₁₄H₂₈N₄O₂; M = 284.22 g/mol

Internal notebook number: JF274

Reaction batch:

1.50 g (13 mmol) trans-1,4-diaminocyclohexane

2.40 g (28 mmol) propylisocyanate

200 mL THF

Purification: Recrystallization from DMF

*Characterization:*¹H NMR (300 MHz, CDCl₃/CF₃COOD): δ [ppm] = 3.45 (s, 2H), 3.24 (t, J = ,7.3 Hz, 4H), 2.06 (d, J = 6.3 Hz, 4H), 1.38-1.72 (m, 8H), 0.96 (t, J = 7.4 Hz, 6H)

MS (70 eV), m/z (%): 284 (27); 226 (39); 198 (68); 183 (93); 182 (73); 139 (25); 113 (10); 103 (100); 97 (52); 96 (54); 59 (44); 44 (52)

Schmelzpunkt: T_m = subl.Zersetzungspunkt: T_{-10 wt%} = 328°C**1,1'-(trans-1,4-cyclohexylene)bis(3-n-butylurea) 1c**Molecular formula: C₁₆H₃₂N₄O₂; M = 312.25 g/mol

Internal notebook number: JF269

Reaction batch:

1.50 g (13 mmol) trans-1,4-diaminocyclohexane

2.90 g (29 mmol) butylisocyanate

500 mL THF

Purification: Recrystallization from DMF

*Characterization:*¹H NMR (300 MHz, CDCl₃/CF₃COOD): δ [ppm] = 3.45 (s, 2H), 3.28 (t, J = ,7.3 Hz, 4H), 2.06 (d, J = 6.3 Hz, 4H), 1.28-1.65 (m, 12H), 0.95 (t, J = 7.3 Hz, 6H)

MS (70 eV), m/z (%): 312 (28); 240 (38); 212 (72); 197 (100); 139 (26); 117 (97); 96 (46); 74 (31); 57 (30)

Schmelzpunkt: T_m = subl.Zersetzungspunkt: T_{-10 wt%} = 329°C

1,1'-(trans-1,4-cyclohexylene)bis(3-(1,2-dimethylpropyl)urea) 1m

Molecular formula: C₁₈H₃₆N₄O₂; M = 440.28 g/mol

Internal notebook number: TH01

Reaction batch:

1.46 g (9 mmol) trans-1,4-diaminocyclohexane

1.54 g (18 mmol) 1,2-dimethylpropylisocyanate

200 mL THF

Purification: Recrystallization from DMF

Characterization:

¹H NMR (300 MHz, CDCl₃/CF₃COOD): δ [ppm] = 3.61 (m, 2H), 3.42 (m, 2H), 2.06 (m, 4H), 1.76 (q, J = 6.7 Hz, 2H), 1.50 (m, 4H), 1.20 (d, J = 6.6 Hz, 6H), 0.94 (d, J = 6.6 Hz, 12H)

MS (70 eV), m/z (%): 340 (4); 297 (26); 254 (100); 211 (6); 141 (4); 93 (12); 45 (54)

Schmelzpunkt: T_m = subl.

Zersetzungspunkt: T_{-10 wt%} = 317°C

1,1'-(trans-1,4-cyclohexylene)bis(3-tert-butylurea) 1p

Molecular formula: C₁₆H₃₂N₄O₂; M = 312.25 g/mol

Internal notebook number: HH7, JF272, JF277

Reaction batch:

5.00 g (44 mmol) trans-1,4-diaminocyclohexane

9.90 g (100 mmol) tert-butylisocyanate

500 mL THF

Purification: Recrystallization from MeOH

Characterization:

¹H-NMR (300 MHz, DMSO d₆): δ [ppm] = 5.44-5.54 (m, 4H), 3.23 (m, 2H), 1.75 (m, 4H), 1.19 (s, 18H), 1.04 (m, 4H)

MS (70 eV), m/z (%): 312 (18); 240 (7); 212 (44); 197 (32); 156 (5); 139 (10); 97 (25); 61 (15); 58 (100)

Schmelzpunkt: T_m = subl.

Zersetzungspunkt: T_{-10 wt%} = 303°C

1,1'-(trans-1,4-cyclohexylene)bis(3-cyclohexylurea) 1q

Molecular formula: C₂₀H₃₆N₄O₂; M = 364.28 g/mol

Internal notebook number: JF246

Reaction batch:

2.51 g (22 mmol) trans-1,4-diaminocyclohexane

4.49 g (44 mmol) cyclohexyl isocyanate

300 mL THF

Purification: Recrystallization from DMF

Characterization:

¹H NMR (300 MHz, CDCl₃/CF₃COOD): δ [ppm] 3.56 (s, 2H), 3.4 (s, 2H), 2.33-0.9 (m, 28H)

MS (70 eV), m/z (%): 364 (11); 266 (8); 238 (46); 223 (55); 143 (38); 98 (45); 57 (100); 44 (29);

Schmelzpunkt: T_m = subl.

Zersetzungspunkt: T_{-10 wt%} = 332°C

1,1'-(trans-1,4-cyclohexylene)bis(3-phenylurea) 1rMolecular formula: $C_{20}H_{24}N_4O_2$; M = 352.19 g/mol

Internal notebook number: JF247

Reaction batch:

1.50 g (13 mmol) trans-1,4-diaminocyclohexane

2.90 g (26 mmol) phenylisocyanate

300 mL THF

Purification: Recrystallization from MeOH

Characterization: 1H -NMR (300 MHz, DMSO d_6): δ [ppm] = 8.3 (s, 2H), 7.4 (m, 4H), 7.18 (t, J = 7.8 Hz, 4H), 6.9 (t, J = 7.3 Hz, 2H), 6.06 (d, J = 7.9 Hz, 2H), 3.4 (m, 2H), 1.88 (m, 4H) 1.25 (m, 4H)

MS (70 eV), m/z (%): 352 (3); 259 (8); 232 (4); 141 (5); 99 (10); 93 (100); 66 (6); 44 (6)

Schmelzpunkt: T_m = subl.Zersetzungspunkt: $T_{-10 \text{ wt\%}}$ = 309°C**1,1'-(trans-1,4-cyclohexylene)bis(3-(1-adamantyl)urea) 1s**Molecular formula: $C_{28}H_{44}N_4O_2$; M = 468.70 g/mol

Internal notebook number: JF268

Reaction batch:

1.50 g (13 mmol) trans-1,4-diaminocyclohexane

3.40 g (29 mmol) 1-adamantyl isocyanate

200 mL THF

Purification: Extraction with DMF

Characterization: 1H -NMR (300 MHz, DMSO d_6): δ [ppm] = 5.52 (d, J = 7.9 Hz, 2H), 5.37 (s, 2H), 3.26 (m, 2H), 1.97 (s, 6H), 1.45-2.08 (m, 34H), 1.03 (m, 4H)

MS (70 eV), m/z (%): 468 (18); 290 (65); 275 (29); 177 (30); 135 (74); 113 (50); 94 (100); 58 (25)

Schmelzpunkt: T_m = subl.Zersetzungspunkt: $T_{-10 \text{ wt\%}}$ = 339°C

Synthesis of trans-1,4-cyclohexyl-bisurea derivatives from trans-1,4-cyclohexane diisocyanate

Trans-1,4-cyclohexane diisocyanate was added in a flame-dried Schlenk flask and dissolved in THF under argon atmosphere. The solution was cooled to 0°C in an ice bath and the corresponding amine, diluted in THF, was added slowly under heavy stirring. The reaction mixture was heated to reflux and, unless indicated otherwise, maintained at this temperature for 12 h. After cooling the precipitated white solid was filtered off, dried under vacuum for 2 h (70°C, 100 mbar) and recrystallized.

1,1'-(trans-1,4-cyclohexylene)bis(3-n-hexylurea) 1d

Molecular formula: C₂₀H₄₀N₄O₂; M = 368.32 g/mol

Internal notebook number: FR84

Reaction batch:

1.35 g (8 mmol) trans-1,4-cyclohexane diisocyanate

1.46 g (16 mmol) hexylamine

200 mL THF

Purification: Recrystallization from DMF

Characterization:

¹H NMR (300 MHz, CDCl₃/CF₃COOD): δ [ppm] = 3.44 (s, 2H), 3.24 (m, 4H), 2.05 (m, 4H), 1.18-1.65 (m, 20H), 0.90 (t, J = 7.0 Hz, 6H)

MS (70 eV), m/z (%): 368 (23); 268 (30); 240 (78); 225 (100); 145 (76); 102 (27); 97 (41); 57 (28); 44 (37)

Schmelzpunkt: T_m = 370°C

Zersetzungspunkt: T_{-10 wt%} = 306°C

1,1'-(trans-1,4-cyclohexylene)bis(3-n-octylurea) 1e

Molecular formula: C₂₄H₄₈N₄O₂; M = 424.38 g/mol

Internal notebook number: SG460

Reaction batch:

3.30 g (20 mmol) trans-1,4-cyclohexane diisocyanate

5.69 g (44 mmol) octylamine

200 mL THF

Purification: Recrystallization from DMF

Characterization:

¹H NMR (300 MHz, CDCl₃/CF₃COOD): δ [ppm] = 3.56 (m, 2H), 3.30 (t, J = 7.3 Hz, 4H), 2.12 (m, 4H), 1.64 (m, 4H), 1.52 (m, 4H), 1.33 (m, 20H), 0.91 (m, 6H)

MS (70 eV), m/z (%): 424 (21); 296 (30); 268 (66); 263 (100); 173 (58); 130 (27); 97 (36); 44 (27)

Schmelzpunkt: T_m = 370°C

Zersetzungspunkt: T_{-10 wt%} = 315°C

1,1'-(trans-1,4-cyclohexylene)bis(3-n-octadecylurea) 1fMolecular formula: C₄₄H₈₈N₄O₂; M = 705.20 g/mol

Internal notebook number: FR79

Reaction batch:

0.71 g (4 mmol) trans-1,4-cyclohexane diisocyanate

2.29 g (9 mmol) octadecylamine

200 mL THF

Purification: Recrystallization from DMF

*Characterization:*¹H NMR (300 MHz, CDCl₃/CF₃COOD): δ [ppm] = 3.45 (s, 2H), 3.25 (m, 4H), 2.06 (m, 4H), 1.17-1.68 (m, 68H), 0.90 (t, J = 7.0 Hz, 6H)

MS (70 eV), m/z (%): 704 (4); 546 (34); 501 (6); 437 (4); 409 (10); 367 (12); 313 (10); 270 (16); 238 (4); 170 (4); 141 (15); 99 (40); 44 (100)

Schmelzpunkt: T_m = 345°CZersetzungspunkt: T_{-10 wt%} = 278°C**1,1'-(trans-1,4-cyclohexylene)bis(3-(6-methylheptane)urea) 1g**Molecular formula: C₂₄H₄₈N₄O₂; M = 424.38 g/mol

Internal notebook number: JF285

Reaction batch:

3.09 g (18 mmol) trans-1,4-cyclohexane diisocyanate

5.29 g (40 mmol) 1-amino-6-methylheptane

150 mL THF

Purification: Recrystallization from DMF

*Characterization:*¹H NMR (300 MHz, CDCl₃/CF₃COOD): δ [ppm] = 3.52 (s, 2H), 3.19 (d, J = 6.5 Hz, 4H), 2.09 (m, 4H), 1.17-1.62 (m, 22H), 0.91 (m, 12H)

MS (70 eV), m/z (%): 424 (29); 313 (8); 296 (91); 268 (95); 253 (100); 173 (52); 130 (39); 96 (35); 58 (39); 44 (31)

Schmelzpunkt: T_m = subl.Zersetzungspunkt: T_{-10 wt%} = 286°C**1,1'-(trans-1,4-cyclohexylene)bis(3-(1,5-dimethylhexyl)urea) 1h**Molecular formula: C₂₄H₄₈N₄O₂; M = 424.38 g/mol

Internal notebook number: JF113

Reaction batch:

3.30 g (20 mmol) trans-1,4-cyclohexane diisocyanate

5.65 g (44 mmol) 1,5-dimethylhexylamine

200 mL THF

Purification: Recrystallization from DMF

*Characterization:*¹H NMR (300 MHz, CDCl₃/CF₃COOD): δ [ppm] = 3.80 (sx, J = 6.6 Hz, 2H), 3.46 (s, 2H), 2.08 (m, 4H), 1.11-1.69 (m, 24H), 0.88 (d, J = 6.6 Hz, 12H)

MS (70 eV), m/z (%): 425 (18); 340 (15); 297 (90); 269 (44); 254 (52); 211 (18); 174 (19); 128 (26); 97 (22); 44 (100)

Schmelzpunkt: T_m = 355°CZersetzungspunkt: T_{-10 wt%} = 299°C

1,1'-(trans-1,4-cyclohexylene)bis(3-(2-ethylhexyl)urea) 1i

Molecular formula: C₂₄H₄₈N₄O₂; M = 424.38 g/mol

Internal notebook number: JF112

Reaction batch:

3.30 g (20 mmol) trans-1,4-cyclohexane diisocyanate

5.65 g (44 mmol) 2-ethylhexylamine

200 mL THF

Purification: Recrystallization from MeOH/*i*-PrOH (2:1)

Characterization:

¹H NMR (300 MHz, CDCl₃/CF₃COOD): δ [ppm] = 3.53 (s, 2H), 3.21 (d, J = 6.5 Hz, 4H), 2.10 (m, 4H), 1.17-1.62 (m, 22H), 0.91 (t, J = 7.2 Hz, 12H)

MS (70 eV), m/z (%): 425 (39); 314 (18); 297 (96); 269 (92); 254 (100); 174 (34); 131 (18); 97 (14); 57 (13)

Schmelzpunkt: T_m = subl.

Zersetzungspunkt: T_{-10 wt%} = 290°C

1,1'-(trans-1,4-cyclohexylene)bis(3-(tert-octyl)urea) 1j

Molecular formula: C₂₄H₄₈N₄O₂; M = 424.38 g/mol

Internal notebook number: JF124

Reaction batch:

3.23 g (19 mmol) trans-1,4-cyclohexane diisocyanate

5.53 g (43 mmol) tert-octylamine

300 mL THF

Purification: Recrystallization from DMF

Characterization:

¹H-NMR (300 MHz, DMSO d₆): δ [ppm] = 5.48 (d, J = 7.9 Hz, 2H), 5.39 (s, 2H), 1.75 (m, 4H), 1.64 (s, 4H), 1.22 (s, 12H), 1.04 (m, 4H), 0.93 (s, 18H)

MS (70 eV), m/z (%): 425 (2); 354 (34); 314 (3); 397 (15); 241 (5); 225 (4); 184 (10); 114 (14); 97 (6); 58 (100)

Schmelzpunkt: T_m = subl.

Zersetzungspunkt: T_{-10 wt%} = 312°C

1,1'-(trans-1,4-cyclohexylene)bis(3-(1,1-dimethylpropyl)urea) 1k

Molecular formula: C₁₈H₃₆N₄O₂; M = 340.5 g/mol

Internal notebook number: JF283

Reaction batch:

2.80 g (17 mmol) trans-1,4-cyclohexane diisocyanate

3.40 g (38 mmol) 1,1-dimethylpropylamine

400 mL THF

Purification: Recrystallization from DMF

Characterization:

¹H-NMR (300 MHz, DMSO d₆): δ [ppm] = 5.53 (d, J = 7.9 Hz, 2H), 5.36 (s, 2H), 3.23 (m, 2H), 1.75 (m, 4H), 1.54 (m, 4H), 1.13 (s, 12H), 1.04 (m, 4H), 0.75 (t, J = 7.3 Hz, 6H)

MS (70 eV), m/z (%): 340 (6); 311 (9); 254 (9); 226 (11); 211 (7); 184 (6); 96 (8); 72 (24); 59 (100); 44 (11)

Schmelzpunkt: T_m = subl.

Zersetzungspunkt: T_{-10 wt%} = 319°C

1,1'-(trans-1,4-cyclohexylene)bis(3-(3-pentyl)urea) 1lMolecular formula: C₁₈H₃₆N₄O₂; M = 340.5 g/mol

Internal notebook number: JF273

Reaction batch:

2.00 g (12 mmol) trans-1,4-cyclohexane diisocyanate

2.20 g (25 mmol) 3-pentylamine

200 mL THF

Purification: Recrystallization from DMF

*Characterization:*¹H NMR (300 MHz, CDCl₃/CF₃COOD): δ [ppm] = 3.57 (m, 2H), 3.44 (m, 2H), 2.07 (m, 4H), 1.66 (m, 4H), 1.50 (m 8H), 0.94 (t, J = 7.4 Hz, 12H)

MS (70 eV), m/z (%): 340 (19); 311 (26); 254 (100); 226 (38); 211 (46); 131 (22); 96 (19); 86 (21); 59 (99)

Schmelzpunkt: T_m = subl.Zersetzungspunkt: T_{-10 wt%} = 310°C**1,1'-(trans-1,4-cyclohexylene)bis(3-neopentylurea) 1n**Molecular formula: C₁₈H₃₆N₄O₂; M = 340.5 g/mol

Internal notebook number: JF267

Reaction batch:

2.00 g (12 mmol) trans-1,4-cyclohexane diisocyanate

2.30 g (26 mmol) neopentylamine

200 mL THF

Purification: Recrystallization from DMF

*Characterization:*¹H-NMR (300 MHz, DMSO d₆): δ [ppm] = 5.68 (m, 4H), 2.78 (m, 4H), 1.78 (m, 4H), 1.09 (m, 4H), 0.8 (s, 18H)

MS (70 eV), m/z (%): 340 (16); 283 (8); 254 (100); 226 (33); 211 (65); 139 (15); 131 (41); 96 (26); 88 (23); 58 (17)

Schmelzpunkt: T_m = subl.Zersetzungspunkt: T_{-10 wt%} = 323°C**1,1'-(trans-1,4-cyclohexylene)bis(3-isopropylurea) 1o**Molecular formula: C₁₄H₂₈N₄O₂; M = 284.4 g/mol

Internal notebook number: HH6

Reaction batch:

1.75 g (11 mmol) trans-1,4-cyclohexane diisocyanate

1.25 g (21 mmol) isopropylamine

400 mL THF

Purification: Recrystallization from DMF

*Characterization:*¹H-NMR:

MS (70 eV), m/z (%): 284 (13); 226 (35); 198 (48); 183 (63); 139 (18); 113 (13); 103 (70); 97 (48); 96 (50); 58 (70); 45 (100)

Schmelzpunkt: T_m = subl.Zersetzungspunkt: T_{-10 wt%} = 319°C

8.3.2. General synthetic route to cis-1,4-cyclohexyl-bisurea derivatives

Cis-1,4-diaminocyclohexane was added in a flame-dried Schlenk flask and dissolved in THF under argon atmosphere. The solution was cooled to 0°C in an ice bath and the corresponding isocyanate, diluted in THF, was added slowly under heavy stirring. The reaction mixture was heated to reflux and, unless indicated otherwise, maintained at this temperature for 12 h. After cooling the precipitated white solid was filtered off, dried under vacuum for 2 h (70°C, 100 mbar) and recrystallized.

1,1'-(cis-1,4-cyclohexylene)bis(3-n-octylurea) 2a

Molecular formula: C₂₄H₄₈N₄O₂; M = 424.38 g/mol

Internal notebook number: SG462

Reaction batch:

3.30 g (28 mmol) cis-1,4-diaminocyclohexane

9.89 g (64 mmol) octylisocyanate

200 mL THF

Purification: Recrystallization from MeOH

Characterization:

¹H-NMR (300 MHz, DMSO d₆): δ [ppm] = 5.73 (m, 4H), 2.95 (q, J = 6.4 Hz, 4H), 1.08-1.65 (m, 34H), 0.85 (m, 6H)

MS (70 eV), m/z (%): 424 (21); 296 (39); 252 (82); 213 (28); 173 (81); 141 (45); 97 (100); 59 (58); 57 (61); 44 (57)

Schmelzpunkt: T_m = 308°C

Zersetzungspunkt: T_{-10 wt%} = 254°C

1,1'-(cis-1,4-cyclohexylene)bis(3-tert-octylurea) 2b

Molecular formula: C₂₄H₄₈N₄O₂; M = 424.38 g/mol

Internal notebook number: JF286

Reaction batch:

0.66 g (5 mmol) cis-1,4-diaminocyclohexane

2.0 g (12 mmol) tert-octylisocyanate

100 mL THF

Purification: Recrystallization from Cyclohexane

Characterization:

¹H-NMR (300 MHz, DMSO d₆): δ [ppm] = 5.60 (d, J = 7.5 Hz, 2H), 5.52 (s, 2H), 1.64 (s, 6H), 1.27-1.57 (m, 8H), 1.23 (s, 12H), 0.93 (s, 18H)

MS (70 eV), m/z (%): 426 (11); 354 (34); 297 (44); 184 (20); 141 (15); 114 (5); 58 (100)

Schmelzpunkt: T_m = 325°C

Zersetzungspunkt: T_{-10 wt%} = 243°C

1,1'-(cis-1,4-cyclohexylene)bis(3-isopropylurea) 2cMolecular formula: C₂₀H₂₄N₄O₂; M = 352.40 g/mol

Internal notebook number: JF254

Reaction batch:

1.50 g (13 mmol) cis-1,4-diaminocyclohexane

2.21 g (26 mmol) isopropyl isocyanate

150 mL THF

Purification: Recrystallization from MeOH

*Characterization:*¹H-NMR (300 MHz, DMSO d₆): δ [ppm] = 5.65 (d, J = 7.5 Hz, 2H) 5.57 (d, J = 7.6 Hz, 2H), 3.63 (m, 2H), 3.46 (m, 2H), 1.00 (d, J = 6.5 Hz, 12H)

MS (70 eV), m/z (%): 284 (8); 226 (23); 198 (12); 182 (100); 141 (39); 113 (8); 103 (75); 97 (67); 68 (36); 59 (88); 45 (81); 44 (59);

Schmelzpunkt: T_m = 309°CZersetzungspunkt: T_{-10 wt%} = 265°C**1,1'-(cis-1,4-cyclohexylene)bis(3-tert-butylurea) 2d**Molecular formula: C₁₆H₃₂N₄O₂; M = 312.50 g/mol

Internal notebook number: JF248

Reaction batch:

1.50 g (13 mmol) cis-1,4-diaminocyclohexane

2.57 g (26 mmol) tert-butylisocyanate

150 mL THF

Purification: Recrystallization from MeOH

*Characterization:*¹H-NMR (300 MHz, DMSO d₆): δ [ppm] = 5.53 (m, 2H), 5.68 (s, 2H), 3.43 (bm, 2H), 1.49 (m, 4H), 1.35 (m, 4H), 1.20 (s, 18H)

MS (70 eV), m/z (%): 297 (3); 240 (9); 196 (24); 184 (2); 141 (28); 117 (14); 97 (27); 59 (100); 42 (11);

Schmelzpunkt: T_m = 319°CZersetzungspunkt: T_{-10 wt%} = 264°C**1,1'-(cis-1,4-cyclohexylene)bis(3-cyclohexylurea) 2e**Molecular formula: C₂₀H₃₆N₄O₂; M = 364.53 g/mol

Internal notebook number: JF249

Reaction batch:

1.50 g (13 mmol) cis-1,4-diaminocyclohexane

3.25 g (26 mmol) cyclohexylisocyanate

150 mL THF

Purification: Recrystallization from MeOH

*Characterization:*¹H NMR (300 MHz, DMSO d₆): δ [ppm] 5.66 (m, 4H), 3.45 (s, 2H), 1.82-0.89 (m, 28H)

MS (70 eV), m/z (%): 364 (5); 266 (13); 238 (8); 222 (30); 192 (8); 143 (29); 98 (39); 57 (100); 44 (62); 42 (42)

Schmelzpunkt: T_m = 252°CZersetzungspunkt: T_{-10 wt%} = 266°C

1,1'-(cis-1,4-cyclohexylene)bis(3-phenylurea) 2f

Molecular formula: $C_{20}H_{24}N_4O_2$; M = 352.43 g/mol

Internal notebook number: JF250

Reaction batch:

1.50 g (13 mmol) cis-1,4-diaminocyclohexane

3.1 g (26 mmol) phenylisocyanate

150 mL THF

Purification: Recrystallization from MeOH

Characterization:

$^1\text{H-NMR}$ (300 MHz, DMSO d_6): δ [ppm] = 8.33 (s, 2H), 7.37 (m, 4H), 7.22 (t, J = 7.8 Hz, 4H), 6.88 (t, J = 7.3 Hz, 2H), 6.20 (d, J = 7.9 Hz, 2H), 3.61 (m, 2H), 1.66 (m, 4H) 1.51 (m, 4H)

MS (70 eV), m/z (%): 352 (9); 260 (15); 141 (10); 94 (13); 93 (100); 81 (6)

Schmelzpunkt: $T_m = 236^\circ\text{C}$

Zersetzungspunkt: $T_{-10 \text{ wt}\%} = 258^\circ\text{C}$

8.3.3. General synthetic route to asymmetric substituted trans-1,4-cyclohexyl-bisurea derivatives

Preparation of trans-1-(4-aminocyclohexyl)-3-cyclohexylurea

Trans-1,4-diaminocyclohexane was added in a flame-dried Schlenk flask and dissolved in THF under argon atmosphere. The solution was cooled to -40°C in a cooling bath (isopropyl alcohol/ dry ice) and isocyanatocyclohexane, diluted in THF, was added slowly under heavy stirring. The reaction mixture was stirred for 12 h at room temperature. The precipitated white solid was filtered off, suspended in water and acidified to pH 2 (HCl). The emerging clear solution was again filtrated and the filtrate was brought to pH 8 (NaOH) whereupon trans-1-(4-aminocyclohexyl)-3-cyclohexylurea precipitated as a white solid.

trans-1-(4-aminocyclohexyl)-3-cyclohexylurea

Molecular formula: C₁₃H₂₅N₃O; M = 239.63 g/mol

Internal notebook number: FR86, JF258

Reaction batch:

2.39 g (21 mmol) trans-1,4-diaminocyclohexane

2.61 g (21 mmol) cyclohexyl isocyanate

300 mL THF

Characterization:

MS (70 eV), m/z (%): 239 (26); 222 (5); 183 (6); 143 (22); 113 (18); 97 (100); 59 (44); 57 (48); 44 (27)

Schmelzpunkt: T_m = subl.

Zersetzungspunkt: T_{-10 wt%} = 229°C

Preparation of asymmetric substituted trans-1,4-cyclohexyl-bisurea derivatives

Trans-1-(4-aminocyclohexyl)-3-cyclohexylurea was added in a flame-dried Schlenk flask and dissolved in NMP under argon atmosphere. The corresponding isocyanate, diluted in NMP, was added slowly under heavy stirring. The resulting mixture was heated to 80°C and stirred for 12 h. The solution was precipitated in 1M HCl and filtered off. The resulting white solid was washed with THF, dried under vacuum for 2 h (70°C, 100 mbar) and recrystallized.

1-tert-octyl-3-[4-(cyclohexylcarbamoylamino)cyclohexyl]urea 3a

Molecular formula: C₂₂H₄₂N₄O₂; M = 394.59 g/mol

Internal notebook number: JF257

Reaction batch:

1.10 g (5 mmol) trans-1-(4-aminocyclohexyl)-3-cyclohexylurea

0.70 g (5 mmol) tert-octylisocyanate

80 mL NMP

Characterization:

¹H-NMR (300 MHz, DMSO d₆): δ [ppm] = 5.57 (d, J = 7.7 Hz, 2H), 5.47 (d, J = 7.9 Hz, 1H), 5.42 (s, 1H), 3.27 (m, 2H), 1.22 (s, 6H), 1.04 (m, 4H), 0.93 (s, 9H), 0.84-1.86 (m, 33H)

MS (70 eV), m/z (%): 394 (5); 379 (3); 323 (80); 283 (10); 266 (52); 238 (14); 223 (9); 184 (5); 141 (6); 114 (28); 98 (15); 59 (100)

Schmelzpunkt: T_m = subl.

Zersetzungspunkt: T_{-10 wt%} = 302°C

1-isopropyl-3-[4-(cyclohexylcarbamoylamino)cyclohexyl]urea 3b

Molecular formula: C₁₇H₃₂N₄O₂; M = 324.50 g/mol

Internal notebook number: JF255

Reaction batch:

2.00 g (8 mmol) trans-1-(4-aminocyclohexyl)-3-cyclohexylurea

0.70 g (8 mmol) isopropyl isocyanate

120 mL NMP

Characterization:

¹H NMR (300 MHz, CDCl₃/CF₃COOD): δ [ppm] = 3.94 (m, 1H), 3.56 (m, 1H), 3.39 (m, 2H), 1.08-2.14 (m, 24H)

MS (70 eV), m/z (%): 324 (27); 266 (21); 248 (35); 223 (47); 198 (60); 183 (55); 143 (45); 103 (46); 97 (67); 68 (26); 59 (49); 57 (100); 45 (49); 44 (50)

Schmelzpunkt: T_m = subl.

Zersetzungspunkt: T_{-10 wt%} = 346°C

1-tert-butyl-3-[4-(cyclohexylcarbamoylamino)cyclohexyl]urea 3c

Molecular formula: C₁₈H₃₄N₄O₂; M = 338.49 g/mol

Internal notebook number: FR87

Reaction batch:

2.83 g (12 mmol) trans-1-(4-aminocyclohexyl)-3-cyclohexylurea

1.17 g (12 mmol) tert-butylisocyanate

80 mL NMP

Characterization:

¹H NMR (300 MHz, CDCl₃/CF₃COOD): δ [ppm] = 3.59 (m, 1H), 3.30 (m, 2H), 1.43 (s, 9H), 1.08-2.12 (m, 18H)

MS (70 eV), m/z (%): 338 (14); 266 (11); 238 (51); 222 (31); 197 (29); 184 (7); 143 (22); 97 (39); 61 (21); 59 (100); 57 (62);

Schmelzpunkt: T_m = 379°C

Zersetzungspunkt: T_{-10 wt%} = 308°C

1-phenyl-3-[4-(cyclohexylcarbamoylamino)cyclohexyl]urea 3dMolecular formula: C₂₀H₃₀N₄O₂; M = 358.48 g/mol

Internal notebook number: JF251

Reaction batch:

3.00 g (13 mmol) trans-1-(4-aminocyclohexyl)-3-cyclohexylurea

1.50 g (13 mmol) phenylisocyanate

130 mL NMP

*Characterization:*¹H-NMR (300 MHz, DMSO d₆): δ [ppm] = 8.29 (s, 1H), 7.35 (m, 2H), 7.20 (t, J = 7.9 Hz, 2H), 6.87 (t, J = 7.2 Hz, 1H), 6.02 (d, J = 7.8 Hz, 1H), 5.59 (m, 2H), 0.93-1.94 (m, 18H)

MS (70 eV), m/z (%): 358 (21); 265 (7); 248 (15); 232 (19); 141 (10); 93 (100); 81 (9); 57 (34); 44 (13)

Schmelzpunkt: T_m = subl.Zersetzungspunkt: T_{-10 wt%} = 323°C

9. Literature

- [1] H. Zweifel, *Plastics additives handbook*, 5th edition, Hanser Gardner Publications, Cincinnati, OH. **2001**.
- [2] Y. C. Kim, C. Y. Kim, S. C. Kim, *Polym. Eng. Sci.* **1991**, *31*, 1009.
- [3] K. Hoffmann, G. Huber, D. Mäder, *Macromol. Symp.* **2001**, *176*, 83.
- [4] T. A. Shepard, C. R. Delsorbo, R. M. Louth, J. L. Walborn, D. A. Norman, N. G. Harvey, R. J. Spontak, *J. Polym. Sci. B-Polym. Phys.* **1997**, *35*, 2617.
- [5] M. Kristiansen, M. Werner, T. Tervoort, P. Smith, M. Blomenhofer, H.-W. Schmidt, *Macromolecules*. **2003**, *36*, 5150.
- [6] M. Blomenhofer, S. Ganzleben, D. Hanft, H.-W. Schmidt, M. Kristiansen, P. Smith, K. Stoll, D. Mäder, K. Hoffmann, *Macromolecules*. **2005**, *38*, 3688.
- [7] S. Fairgrieve, *Rapra Review Reports*. **2005**, *16*.
- [8] H. Wang, C.-C. Li, Y.-C. Ke, D. Zhang, Z.-Y. Li, *J. Appl. Polym. Sci.* **2006**, *99*, 1568.
- [9] F. Abraham, S. Ganzleben, D. Hanft, P. Smith, H.-W. Schmidt, *Macromol. Chem. Phys.* **2010**, *211*, 171.
- [10] G. H. Meeten, *Optical properties of polymers*, Elsevier Applied Science Publishers, London ;, New York. **1986**.
- [11] a) M. Fujiyama, T. Wakino, *J. Appl. Polym. Sci.* **1991**, *42*, 2739.
b) M. Fujiyama, T. Wakino, *J. Appl. Polym. Sci.* **1991**, *43*, 57.
c) M. Fujiyama, T. Wakino, *J. Appl. Polym. Sci.* **1991**, *42*, 2749.
- [12] M. Blomenhofer, *Dissertation, Universität Bayreuth*. **2003**.
- [13] B. Wunderlich, *Thermal analysis of polymeric materials*, Springer, Berlin. **2005**.
- [14] T. Sterzynski, M. Lambla, H. Crozier, M. Thomas, *Adv. Polym. Technol.* **1994**, *13*, 25.
- [15] C. Marco, M. A. Gomez, G. Ellis, J. M. Arribas, *J. Appl. Polym. Sci.* **2002**, *84*, 1669.
- [16] B. Fillon, J. C. Wittmann, B. Lotz, A. Thierry, *J. Polym. Sci. B Polym. Phys.* **1993**, *31*, 1383.
- [17] B. Fillon, B. Lotz, A. Thierry, J. C. Wittmann, *J. Polym. Sci. B Polym. Phys.* **1993**, *31*, 1395.
- [18] D. W. van Krevelen, *Properties of polymers: Their correlation with chemical structure ; their numerical estimation and prediction from additive group contributions*, 3rd edition, Elsevier, Amsterdam u.a. **2000**.
- [19] M. Gahleitner, C. Grein, S. Kheirandish, J. Wolfschwenger, *Intern. Polymer Processing*. **2011**, *XXVI*, 2.
- [20] a) G. C. Monroe, D. J. Vaughan, US 2991264.
b) H. N. Beck, H. D. Ledbetter, *J. Appl. Polym. Sci.* **1965**, *9*, 2131.
- [21] F. Binsbergen, *Polymer*. **1970**, *11*, 253.
- [22] J. F. Voeks, US 3367926.
- [23] a) H. Zweifel, *Plastics additives handbook*, 6th edition, Hanser, Munich, Cincinnati, Ohio. **2009**.
b) J. Menczel, J. Varga, *Journal of Thermal Analysis*. **1983**, *28*, 161.
c) P. McGenity, J. Hooper, C. Paynter, A. Riley, C. Nutbeem, N. Elton, J. Adams, *Polymer*. **1992**, *33*, 5215.
- [24] a) V. H. J. Leugering, *Makromol. Chem.* **1967**, *109*, 204.
b) J. Broda, *J. Appl. Polym. Sci.* **2003**, *90*, 3957.
c) U. Johnsen, K.-H. Moos, *Angew. Makromol. Chemie*. **1978**, *74*, 1.
- [25] a) U. Wendt, *J Mater Sci Lett*. **1988**, *7*, 643.

- b) D.-H. Lee, K.-B. Yoon, *J. Appl. Polym. Sci.* **1994**, *54*, 1507.
c) M. K. Gupta, D. J. Carlsson, D. M. Wiles, *J. Polym. Sci. Polym. Phys. Ed.* **1984**, *22*, 1011.
d) Z. Bartczak, A. Galeski, M. Pracella, *Polymer*. **1986**, *27*, 537.
- [26] K. Mai, K. Wang, Z. Han, H. Zeng, *J. Appl. Polym. Sci.* **2002**, *83*, 1643.
- [27] a) X. E. Zhao, D. L. Dotson, B. G. Morin, B. M. Burkhart, M. E. Cowan, J. R. Jones, WO 02/077092 A1.
b) R. W. J. M. Hanssen, M. B. Barker, N. A. Mehl, W. S. Wolters, WO 2007/033297 A1.
- [28] A. Thierry, C. Straupé, J.-C. Wittmann, B. Lotz, *Macromol. Symp.* **2006**, *241*, 103.
- [29] Y. P. Khanna, *Polym. Eng. Sci.* **1990**, *30*, 1615.
- [30] F. Abraham, *Dissertation, Universität Bayreuth.* **2009**.
- [31] N. Mohmeyer, *Dissertation, Universität Bayreuth.* **2006**.
- [32] a) G. Marom, A. J. Domb, D. Libster, A. Aserin, N. Garti, *Polym. Adv. Technol.* **2007**, *18*, 685.
b) R. L. Mahaffey, US 4371645.
c) K. Hamada, H. Uchiyama, US 4016118.
- [33] C. Marco, G. Ellis, M. A. Gomez, J. M. Arribas, *J. Appl. Polym. Sci.* **2002**, *84*, 2440.
- [34] a) H.-D. Phan, L. Killough, E. Santamaria, *Proceedings of the 5th European Conference on "Additives & Colors", Mondorf-les-Bains, Luxembourg, Mar. 14-15.* **2007**.
b) J. G. McDonald, C. L. Cummins, R. M. Barkley, B. M. Thompson, H. A. Lincoln, *Anal. Chem.* **2008**, *80*, 5532.
c) M. J. Mannion, US 5198484.
d) R. Schlotmann, R. Walker, *Kunststoffe.* **1996**, *86*, 1002.
- [35] H.-W. Schmidt, P. Smith, M. Blomenhofer, WO 2002046300.
- [36] H.-W. Schmidt, M. Blomenhofer, K. Stoll, H.-R. Meier, WO 2004072168.
- [37] D. Maeder, K. Hoffmann, H.-W. Schmidt, WO 2003102069.
- [38] F. Abraham, H.-W. Schmidt, *Polymer*. **2010**, *51*, 913.
- [39] a) D. P. Erhard, D. Lovera, C. Salis-Soglio, R. Giesa, V. Altstädt, H.-W. Schmidt. **2010**, *228*, 155.
b) N. Mohmeyer, N. Behrendt, X. Zhang, P. Smith, V. Altstädt, G. M. Sessler, H.-W. Schmidt, *Polymer*. **2007**, *48*, 1612.
- [40] H.-W. Schmidt, K. Stoll, K. Hoffmann, B. Rotzinger, WO 2007039471.
- [41] a) I. Tomatsu, C. F. C. Fitié, D. Byelov, W. H. de Jeu, P. C. M. M. Magusin, M. Wübbenhorst, R. P. Sijbesma, *J. Phys. Chem. B.* **2009**, *113*, 14158.
b) J. Barberá, M. A. Godoy, P. I. Hidalgo, M. L. Parra, J. A. Ulloa, J. M. Vergara, *Liquid Crystals.* **2011**, *38*, 679.
c) Y. Matsunaga, N. Miyajima, Y. Nakayasu, S. Sakai, M. Yonenaga, *Bull. Chem. Soc. Jpn.* **1988**, *61*, 207.
d) Y. Matsunaga, Y. Nakayasu, S. Sakai, M. Yonenaga, *Molecular Crystals and Liquid Crystals.* **1986**, *141*, 327.
e) Y. Harada, Y. Matsunaga, *Bull. Chem. Soc. Jpn.* **1988**, *61*, 2739.
- [42] a) K. Hanabusa, C. Koto, M. Kimura, H. Shirai, A. Kakehi, *Chem. Lett.* **1997**, 429.
b) J. J. van Gorp, J. A. J. M. Vekemans, E. W. Meijer, *J. Am. Chem. Soc.* **2002**, *124*, 14759.
c) Y. Yasuda, E. Iishi, H. Inada, Y. Shirota, *Chem. Lett.* **1996**, 575.
d) K. Hanabusa, A. Kawakami, M. Kimura, H. Shirai, *Chem. Lett.* **1997**, 191.
- [43] a) N. E. Shi, H. Dong, G. Yin, Z. Xu, S. H. Li, *Adv. Funct. Mater.* **2007**, *17*, 1837.

- b) A. Bernet, R. Q. Albuquerque, M. Behr, S. T. Hoffmann, H.-W. Schmidt, *Soft Matter*. **2011**, *8*, 66.
- c) A. Friggeri, C. van der Pol, K. J. C. van Bommel, A. Heeres, M. C. A. Stuart, B. L. Feringa, J. van Esch, *Chem. Eur. J.* **2005**, *11*, 5353.
- d) A. Heeres, C. van der Pol, M. Stuart, A. Friggeri, B. L. Feringa, J. van Esch, *J. Am. Chem. Soc.* **2003**, *125*, 14252.
- e) K. J. C. van Bommel, C. van der Pol, I. Muizebelt, A. Friggeri, A. Heeres, A. Meetsma, B. L. Feringa, J. van Esch, *Angew. Chem. Int. Ed.* **2004**, *43*, 1663.
- [44] M. Kristiansen, *PhD thesis, ETH Zürich*. **2004**.
- [45] M. Blomenhofer, *Diploma Thesis, Universität Bayreuth*. **1999**.
- [46] R. Schmitt, *Dissertation, Universität Bayreuth*. **2005**.
- [47] In, *PlasticsEurope Deutschland*. **2004**.
- [48] M. P. Lightfoot, F. S. Mair, R. G. Pritchard, J. E. Warren, *Chem. Commun.* **1999**, 1945.
- [49] M. Kristiansen, P. Smith, H. Chanzy, C. Baerlocher, V. Gramlich, L. McCusker, T. Weber, P. Pattison, M. Blomenhofer, H.-W. Schmidt, *Crystal Growth & Design*. **2009**, *9*, 2556.
- [50] a) V. Simic, L. Bouteiller, M. Jalabert, *J. Am. Chem. Soc.* **2003**, *125*, 13148.
b) K. Hanabusa, R. Tanaka, M. Suzuki, M. Kimura, H. Shirai, *Adv. Mater.* **1997**, *9*, 1095.
c) K. Hanabusa, M. Yamada, M. Kimura, H. Shirai, *Angew. Chem.* **1996**, *108*, 2086.
- [51] J. van Esch, S. de Feyter, R. M. Kellogg, F. de Schryver, B. L. Feringa, *Chem. Eur. J.* **1997**, *3*, 1238.
- [52] R. A. Koevoets, *Proefschrift, Technische Universiteit Eindhoven*. **2005**.
- [53] a) N. Mohmeyer, H.-W. Schmidt, *Chem. Eur. J.* **2007**, *13*, 4499.
b) N. Mohmeyer, D. Kuang, P. Wang, H.-W. Schmidt, S. M. Zakeeruddin, M. Gr?tzl, *J. Mater. Chem.* **2006**, *16*, 2978.
c) N. Mohmeyer, H.-W. Schmidt, *Chem. Eur. J.* **2005**, *11*, 863.
- [54] a) C. Mathieu, A. Thierry, J. C. Wittmann, B. Lotz, *J. Polym. Sci. B Polym. Phys.* **2002**, *40*, 2504. b) W. Stocker, M. Schumacher, S. Graff, A. Thierry, J.-C. Wittmann, B. Lotz, *Macromolecules*. **1998**, *31*, 807.
- [55] N. Mohmeyer, H.-W. Schmidt, P. M. Kristiansen, V. Altstädt, *Macromolecules*. **2006**, *39*, 5760.
- [56] a) T. Sterzynski, H. Oeysaed, *Polym Eng Sci.* **2004**, *44*, 352.
b) C. Grein, C. Plummer, H.-H. Kausch, Y. Germain, P. Béguelin, *Polymer*. **2002**, *43*, 3279.
c) J. Varga, *J. of Macromolecular Sc., Part B*. **2002**, *41*, 1121.
- [57] Q. Lu, Q. Dou, *Polym. J.* **2009**, *41*, 254.
- [58] BYK, *Qualitätskontrolle für Lacke und Kunststoffe*. **2007**.
- [59] *Test Method for Haze and Luminous Transmittance of Transparent Plastics*, ASTM International, West Conshohocken, PA. **2011**.
- [60] A. G. M. Last, *J. Polym. Sci.* **1959**, *39*, 543.
- [61] K. Bernland, *PhD thesis, ETH Zürich*. **2009**.
- [62] a) R. R. Lützel, *Laserdurchstrahlschweißen von teilkristallinen Thermoplasten: Dissertation, RWTH Aachen*. **2005**.
b) D. A. Grewell, *Plastics and composites welding handbook*, Hanser, München. **2003**.
c) W. Korte, *Einfluss der Spritzgießherstellbedingungen und Möglichkeiten der prozessnahen Qualitätssicherung mittels statistischer Methoden beim Ultraschallschweißen.: Dissertation, RWTH Aachen*. **1996**.

- [63] J.-E. Schulz, *Werkstoff-, Prozess- und Bauteiluntersuchungen zum Laserdurchstrahlschweißen von Kunststoffen: Dissertation, RWTH Aachen*. **2002**.
- [64] D. Hänsch, *Die optischen Eigenschaften von Polymeren und ihre Bedeutung für das Durchstrahlschweißen mit Diodenlaser*, Shaker, Aachen. **2001**.
- [65] T. Frick, M. Hopfner, *Laserstrahlschweißen von Kunststoffen*, 2nd edition, BLZ, Erlangen. **2005**.
- [66] R. von Benten, P. Eibeck, US 20110288220.
- [67] N. Murthy, H. Minor, *Polymer*. **1990**, 31, 996.
- [68] J. Scheirs, T. E. Long, *Modern polyesters: Chemistry and technology of polyesters and copolyesters*, John Wiley & Sons, Hoboken, NJ. **2003**.
- [69] G. W. Becker, D. Braun, L. Bottenbruch, *Kunststoff Handbuch 3: Technische Thermoplaste. - 1: Polycarbonate, Polyacetale, Polyester, Celluloseester*, 2nd edition, Hanser, München. **1992**.
- [70] a) Z. Mencik, *J. Polym. Sci. Polym. Phys. Ed.* **1975**, 13, 2173.
b) R. Jakeways, I. M. Ward, M. A. Wilding, I. H. Hall, I. J. Desborough, M. G. Pass, *J. Polym. Sci. Polym. Phys. Ed.* **1975**, 13, 799.
- [71] M. Yokouchi, Y. Sakakibara, Y. Chatani, H. Tadokoro, T. Tanaka, K. Yoda, *Macromolecules*. **1976**, 9, 266.
- [72] R. S. Stein, A. Misra, *J. Polym. Sci. Polym. Phys. Ed.* **1980**, 18, 327.
- [73] C.-S. Park, K.-J. Lee, S. W. Kim, Y. K. Lee, J.-D. Nam, *J. Appl. Polym. Sci.* **2002**, 86, 478.
- [74] J. W. Heuseveldt, J. van Helmond, H. Ketels, GEN ELECTRIC [US], EP0624625 (A2) **1993**.
- [75] L. Zhang, Y. Hong, T. Zhang, C. Li, *J. of Macromolecular Sc., Part B.* **2010**, 49, 514.
- [76] I. Pillin, S. Pimbert, J.-F. Feller, G. Levesque, *Polym. Eng. Sci.* **2001**, 41, 178.
- [77] P. J. M. Stals, J. C. Everts, M.-R. R. Pilot, E. A. Pidko, A. R. A. Palmans, E. W. Meijer, *Chem. Eur. J.* **2010**, 810.
- [78] D. R. Holmes, C. W. Bunn, D. J. Smith, *J. Polym. Sci.* **1955**, 17, 159.
- [79] H. Arimoto, M. Ishibashi, M. Hirai, Y. Chatani, *J. Polym. Sci. A Gen. Pap.* **1965**, 3, 317.
- [80] a) W. H. Carothers, J. A. Arvin, *J. Am. Chem. Soc.* **1929**, 51, 2560.
b) W. H. Carothers, *J. Am. Chem. Soc.* **1929**, 51, 2548.
- [81] W. H. Carothers, U.S. Patent 2 071 250 **1937**.
- [82] Melvin I. Kohen, *Nylon Plastics Handbook*, Hanser. **1995**.
- [83] A. Ziabicki, *Kolloid-Zeitschrift*. **1959**, 167, 132.
- [84] Avramova N., Fakirov S., *Polym. Commun.* **1984**, 25, 27.
- [85] a) K. Schmieder, K. Wolf, *Kolloid-Zeitschrift*. **1952**, 127, 65.
b) K. Tashiro, H. Tadokoro, *Macromolecules*. **1981**, 14, 781.
c) S. Dasgupta, W. B. Hammond, W. A. Goddard, *J. Am. Chem. Soc.* **1996**, 118, 12291.
- [86] M. Kyotani, S. Mitsunashi, *J. Polym. Sci. A-2 Polym. Phys.* **1972**, 10, 1497.
- [87] M. J. Hitch, British Patent 1 327 341 **1973**.
- [88] P. N. Richardson, U.S. Patent 4 293 502 **1981**.
- [89] T. Brink, J. L. Cohen, T. K. Sham, PCT Int. Appl. WO 9824846.
- [90] Q. Du, R. Wang, W. Chen, L. Wang, *Gaofenzi Cailiao Kexue Yu Gongcheng*. **1991**, 7, 28.
- [91] M. C. Etter, Z. Urbanczyk-Lipkowska, M. Zia-Ebrahimi, T. W. Panunto, *J. Am. Chem. Soc.* **1990**, 112, 8415.
- [92] F. Lortie, S. Boileau, L. Bouteiller, C. Chassenieux, B. Demé, G. Ducouret, M. Jalabert, F. Lauprêtre, P. Terech, *Langmuir*. **2002**, 18, 7218.
- [93] S. van der Laan, B. L. Feringa, R. M. Kellogg, J. van Esch, *Langmuir*. **2002**, 18, 7136.

- [94] a) M. R. J. Vos, G. E. Jardí, A. L. Pallas, M. Breurken, O. L. J. van Asselen, P. H. H. Bomans, P. E. L. G. Leclère, P. M. Frederik, R. J. M. Nolte, N. A. J. M. Sommerdijk, *J. Am. Chem. Soc.* **2005**, *127*, 16768.
b) O. Colombani, L. Bouteiller, *New J. Chem.* **2004**, *28*, 1373.
- [95] R. M. Versteegen, R. P. Sijbesma, E. W. Meijer, *Macromolecules.* **2005**, *38*, 3176.
- [96] N. Zweep, *Proefschrift, Rijksuniversiteit Groningen.* **2006**.
- [97] N. Zweep, A. Hopkinson, A. Meetsma, W. R. Browne, B. L. Feringa, J. H. van Esch, *Langmuir.* **2009**, *25*, 8802.
- [98] E. Sabadini, K. R. Francisco, L. Bouteiller, *Langmuir.* **2010**, *26*, 1482.
- [99] a) K. Hanabusa, K. Shimura, K. Hirose, M. Kimura, H. Shirai, *Chem. Lett.* **1996**, 885.
b) J. van Esch, F. Schoonbeek, M. de Loos, H. Kooijman, A. Spek, R. M. Kellogg, B. L. Feringa, *Chem. Eur. J.* **1999**, *5*, 937.
c) J. J. E. Moreau, B. P. Pichon, M. Wong Chi Man, C. Bied, Pritzkow J., *Angew. Chem., Int. Ed.* **2004**, *43*, 203.
- [100] N. Chebotareva, P. H. H. Bomans, P. M. Frederik, N. A. J. M. Sommerdijk, R. P. Sijbesma, *Chem. Commun.* **2005**, 4967.
- [101] a) G. Reiter, J.-U. Sommer, *Polymer crystallization: Observations, concepts, and interpretations*, Springer, Berlin ;, New York. **2003**.
b) G. Guerra, *Flow-induced crystallization of polymers*, WILEY-VCH (NY), United States. **2003**.
- [102] V. Miri, S. Elkoun, F. Peurton, C. Vanmansart, J.-M. Lefebvre, P. Krawczak, R. Seguela, *Macromolecules.* **2008**, *41*, 9234.
- [103] D. Garcia, H. W. Starkweather, *J. Polym. Sci. Polym. Phys. Ed.* **1985**, *23*, 537.
- [104] G. Gurato, D. Gaidano, R. Zannetti, *Makromol. Chem.* **1978**, *179*, 231.
- [105] Y. Chen, M. Xu, *Gaofenzi Xuebao.* **1998**, *4*, 387.
- [106] R. Čermák, M. Obadal, P. Ponížil, M. Polášková, K. Stoklasa, A. Lengálová, *European Polymer Journal.* **2005**, *41*, 1838.
- [107] G. W. Ehrenstein, *Polymer-Werkstoffe: Struktur - Eigenschaften - Anwendung*, 3rd edition, Hanser, München. **2011**.
- [108] a) H. Domininghaus, P. Elsner, P. Eyerer, T. Hirth, *Die Kunststoffe und ihre Eigenschaften*, 6th edition, Springer, Berlin. **2005**.
b) W. Lutz, *Einfluss von Morphologie und struktureller Anisotropie auf die thermo-mechanischen Eigenschaften spritzgegossener PP- und PA6-Werkstoffe*, 1st edition, Cuvillier, Göttingen. **2007**.
- [109] G. Gurato, A. Fichera, F. Z. Grandi, R. Zannetti, P. Canal, *Makromol. Chem.* **1974**, *175*, 953.
- [110] P. M. Kristiansen, A. Gress, P. Smith, D. Hanft, H.-W. Schmidt, *Polymer.* **2006**, *47*, 249.

Erklärung:

Hiermit erkläre ich, dass ich die Arbeit selbstständig verfasst und keine als die von mir angegebenen Quellen und Hilfsmittel benutzt habe.

Ferner erkläre ich, dass ich anderweitig mit oder ohne Erfolg nicht versucht habe diese Dissertation einzureichen. Ich habe keine gleichartige Doktorprüfung an einer anderen Hochschule endgültig nicht bestanden.

Bayreuth, den

(Florian Richter)